AD_____

Award Number: DAMD17-02-1-0222

TITLE: Signal Transduction Based Mouse Models of Prostate Cancer

PRINCIPAL INVESTIGATOR: Richard G. Pestell, M.D., Ph.D.

CONTRACTING ORGANIZATION: Albert Einstein College of Medicine
of Yeshiva University
Bronx, New York 10461

REPORT DATE: January 2003

TYPE OF REPORT: Final

PREPARED FOR: U.S. Army Medical Research and Materiel Command
Fort Detrick, Maryland 21702-5012

DISTRIBUTION STATEMENT: Approved for Public Release;
Distribution Unlimited

The views, opinions and/or findings contained in this report are those of the author(s) and should not be construed as an official Department of the Army position, policy or decision unless so designated by other documentation.

# REPORT DOCUMENTATION PAGE

*Form Approved*
*OMB No. 074-0188*



| 1. AGENCY USE ONLY (Leave blank) | 2. REPORT DATE | 3. REPORT TYPE AND DATES COVERED |
|---|---|---|
| | January 2003 | Final (10 Dec 01 - 9 Dec 02) |

**4. TITLE AND SUBTITLE**
Signal Transduction Based Mouse Models of Prostate Cancer

**5. FUNDING NUMBERS**
DAMD17-02-1-0222

**6. AUTHOR(S) :**
Richard G. Pestell, M.D., Ph.D.

**7. PERFORMING ORGANIZATION NAME(S) AND ADDRESS(ES)**
Albert Einstein College of Medicine
of Yeshiva University
Bronx, New York 10461
Email: pestell@aecom.yu.edu

**8. PERFORMING ORGANIZATION REPORT NUMBER**

**9. SPONSORING / MONITORING AGENCY NAME(S) AND ADDRESS(ES)**
U.S. Army Medical Research and Materiel Command
Fort Detrick, Maryland 21702-5012

**10. SPONSORING / MONITORING AGENCY REPORT NUMBER**

**11. SUPPLEMENTARY NOTES**

**12a. DISTRIBUTION / AVAILABILITY STATEMENT**
Approved for Public Release; Distribution Unlimited

**12b. DISTRIBUTION CODE**

**13. Abstract** ***(Maximum 200 Words)*** *(abstract should contain no proprietary or confidential information)*

These studies aimed to create a prostate cancer mouse model consortium. The overall objective of this study is to determine the mechanisms governing prostate cancer genesis and progression, thereby leading to a better understanding and treatment for this disease. The studies brought together investigators at distinct institutions (Albert Einstein College of Medicine (**AECOM**), Memorial Sloan Kettering Cancer Center (**MSKCC**), Beth Israel Deaconess Medical Center-Harvard/Massachusetts Institute of Technology Health Sciences and Technology, **HMS/MIT**) and UC Davis to develop and share a) mouse models engineered through sharing distinct models generated by each program member. b) software technology that will allow for the simultaneous analysis of histopathology and genetic composition of the emerging murine prostate tumors at the different institutions. c) software technology for functional clustering of data derived from microarray analysis of tumor samples.

**14. SUBJECT TERMS:**
prostate cancer

**15. NUMBER OF PAGES**
139

**16. PRICE CODE**

| 17. SECURITY CLASSIFICATION OF REPORT | 18. SECURITY CLASSIFICATION OF THIS PAGE | 19. SECURITY CLASSIFICATION OF ABSTRACT | 20. LIMITATION OF ABSTRACT |
|---|---|---|---|
| Unclassified | Unclassified | Unclassified | Unlimited |

## Table of Contents

## INTRODUCTION

These studies aimed to create a prostate cancer mouse model consortium. The overall objective of this study is to determine the mechanisms governing prostate cancer genesis and progression, thereby leading to a better understanding and treatment for this disease. The studies brought together investigators at distinct institutions (Albert Einstein College of Medicine (**AECOM**), Memorial Sloan Kettering Cancer Center (**MSKCC**), Beth Israel Deaconess Medical Center-Harvard/Massachusetts Institute of Technology Health Sciences and Technology, **HMS/MIT**) and UC Davis to develop and share a) mouse models engineered through sharing distinct models generated by each program member. b) software technology that will allow for the simultaneous analysis of histopathology and genetic composition of the emerging murine prostate tumors at the different institutions. c) software technology for functional clustering of data derived from microarray analysis of tumor samples.

## BODY

We had originally proposed:

**Task 1- Establish a web based inter-institutional communication infrastructure conforming to firewall confidentiality standards.** This system (task) concentrated on implementing data structures/data model and the foundation for web-based access to the required information for functional analysis purposes, together with a basic prototype for analysis purposes.

A data model structuring genomic data/information for functional analysis purposes was developed, based on previously developed software and standards, including microarray and laboratory information system data models. These previous models have been extended to accommodate the needs of functional analysis. The data model has been expressed/documented as (a series of) XML Schema. A prototype system has been developed which allows data generated from microarray analysis, as well as from other programs/facilities, to be stored in a database, and searched/accessed/edited/updated using web based capabilities. Further programs can be added to this core foundation facility to accommodate more advanced analysis. A central database can be implemented which allows researchers in geographical disparate locations to access all available data, perform analysis and make such results available for others to use. Currently, login, security, menus, edit/insertion and search forms are all defined. A facility to handle comparison of data which may have been updated by another entity whilst editing has also been prototyped.

**Task 2. Evaluate "Telepath" software as a shared inter-institutional communication platform for prostate cancer analysis. (Telepath provides real-time shared evaluation of cancer pathology by investigators at the separate sites).** The white board telepathology was formally evaluated by the members of the consortium. The telepathology was used for real time discussion of each of the murine prostate cancer models developed at each of the institutions. (Probasin-ras, Pten/p27 het mice, probasin AR) The pathology was reviewed by Dr. Cardiff at UC Davis while Investigators at Albert Einstein College of Medicine, MSKCC and HMS/MIT were engaged simultaneously in the dialogue and the interpretation of the pathology. The prostate cancer specimens were scanned by Dr. Davis using Scanalyze software providing high-resolution images for the discussion of the prostate cancer samples.

**Task 3. Validate microarray fingerprints of murine models.** It was predicted that tumors induced by a specific oncogene would have a "fingerprint" of altered gene expression. Mathematical models were developed and applied to the oncogene mouse models. We now refer

to these fingerprints of altered gene expression as megacluster analysis. These analyses have been implemented in transgenic mouse models of cancer from the Pestell laboratory (1).

**Task 4. Validate EES software for functional analysis of genomic information; iterative application of software to determine functional fingerprints of tumor types based on genetic model.** We proposed developing intelligent technology for interrogating the genetic information derived from microarray analysis. This software would classify the genes, identified by chip array, by virtue of their specific function(s). The prototype system has been implemented using a variety of (open source) standards. The core of the system presents the genomic information using a presentation layer based on the Xform specification. Presentation screens are developed in the Xform language and presented using the "Xsmiles" product. The Xsmiles browser is an Xform browser based on the current Xforms Candidate Recommendation. It is similar to a normal web browser in operation, but is entirely XML based and allows for operations on repeating elements within an XML instance. Data is stored as XML documents, in Xindice – which is an XML database. Xindice is organised into collections such as /db/experiments or /db/results for example. Within each collection, XML documents can be stored. Each collection can be searched as a whole using Xpath, as if an entire collection of documents is combined. The "backend" system is written in PHP, running on a Redhat Linux machine using Apache 1.3.26 as the web server. This system serves Xforms to the Xsmiles browser (upon request) and accepts returned (being edited) forms (data). PHP scripts communicate with Xindice using XML-RPC messaging to update, add, delete or query the database.

**Task 5. Rational crossing of animals between investigators to establish functional interactions between oncogene and tumor suppressor pathways implicated in human prostate cancer.** Several publications resulted from this aim (below). In addition specific transgenic models were created in the Pestell laboratory in keeping with the proposal. The probasin ErbB2Δ mice developed prostate intraepithelial neoplasia (unpublished).

**Task 6. Analysis of human prostate cancer microarray analysis using EES software for functional gene expression correlates**. These studies will identify spectrum of genes reproducibly expressed in human prostate cancer comparing traditional expression protocols (tree view cluster analysis) and functional array structuring with EES software.

## KEY RESEARCH ACCOMPLISHMENTS

1. Implementation of white board telepathology to provide inter-institutional communication between members of the consortium
    - ongoing integration of white board technology between pathology departments in local DC hospital network.

2. Pathological analysis of several new murine models of prostate cancer and analysis of new prostate cancer androgen receptor mutation (refs 2-15)
    - Fibroblast growth factor 8 isoform B overexpression loss in PIN (2)
    - RXRα loss in the development of PIN (3)
    - NKX3.1mut- loss in the development of PIN (5)
    - Cooperativity of NKX3.1 and Pten loss in the development of PIN (6)
    - Cooperativity of p27 loss and Pten loss in the development of PIN (8)
    - probasin AR mice develop PIN (9).
    - Mutant AR escape apoptosis promoting growth (10)

3. Development and application of new models for microarray analysis (1)

## REPORTABLE OUTCOMES

1. Nine publications related to the research goals of the consortium have been published by the members of the consortium.
2. Development of new murine models as described above (publications 2-9)
3. Submitted grant – (unfunded)
   R.G. Pestell, PI, Signal Transduction Based Mouse Models Of Prostate Cancer (Prostate Cancer Consortium award, Department of Defense). (AECOM, Harvard, Memorial Sloan Kettering, UC Davis) - total $8,870,363 direct $5,539,017 over 3 years. (5 competing for 2 awards.)

## CONCLUSIONS

These studies provided strong evidence that murine models can be developed that resemble human prostate cancer. Secondly we have been able to identify function clusters of genes the expression of which is selectively altered in specific tumors (megaclusters(1)). Such an approach we believe will provide independent prognostic information in human disease. A recent publication suggests that these cluster analyses are indeed valuable in providing new prognostic information in human cancer (11).

## PUBLICATIONS

1. Huang, E., Ishida, S., Pittman, J., Dressman, H., D'Amico, M., Pestell, R.G., West, M., Nevins, J.R. Gene Expression Phenotypic Models That Predict the Activity of Oncogenic Pathways. (In review - Nature Genetics).

2. Song Z, Wu X, Powell WC, Cardiff RD, Cohen MB, Tin RT, Matusik RJ, Miller GJ, Roy-Burman P. Fibroblast growth factor 8 isoform B overexpression in prostate epithelium: a new mouse model for prostatic intraepithelial neoplasia.Cancer Res. 2002 Sep 1;62(17):5096-105.

3. Huang J, Powell WC, Khodavirdi AC, Wu J, Makita T, Cardiff RD, Cohen MB, Sucov HM, Roy-Burman P. Prostatic intraepithelial neoplasia in mice with conditional disruption of the retinoid X receptor alpha allele in the prostate epithelium. Cancer Res. 2002 Aug 15;62(16):4812-9.

4. Park JH, Walls JE, Galvez JJ, Kim M, Abate-Shen C, Shen MM, Cardiff RD. Prostatic intraepithelial neoplasia in genetically engineered mice. Am J Pathol. 2002 Aug;161(2):727-35.

5. Kim MJ, Bhatia-Gaur R, Banach-Petrosky WA, Desai N, Wang Y, Hayward SW, Cunha GR, Cardiff RD, Shen MM, Abate-Shen C. Nkx3.1 mutant mice recapitulate early stages of prostate carcinogenesis.Cancer Res. 2002 Jun 1;62(11):2999-3004.

6. Kim MJ, Cardiff RD, Desai N, Banach-Petrosky WA, Parsons R, Shen MM, Abate-Shen C. Cooperativity of Nkx3.1 and Pten loss of function in a mouse model of prostate carcinogenesis. Proc Natl Acad Sci U S A. 2002 Mar 5;99(5):2884-9.

7. Rego EM, Pandolfi PP. Reciprocal products of chromosomal translocations in human cancer pathogenesis: key players or innocent bystanders? Trends Mol Med. 2002 Aug;8(8):396-405.

8. Di Cristofano A, De Acetis M, Koff A, Cordon-Cardo C, Pandolfi PP. Pten and p27KIP1 cooperate in prostate cancer tumor suppression in the mouse. Nat Genet. 2001 Feb;27(2):222-4.

9. Stanbrough M, Leav I, Kwan PW, Bubley GJ, Balk SP. Prostatic intraepithelial neoplasia in mice expressing an androgen receptor transgene in prostate epithelium. Proc Natl Acad Sci U S A. 2001 Sep 11;98(19):10823-8.

10. Fu M, Wang C, Wang J, Zhang X, Sakamaki T, Yeung YG, Chang C, Hopp T, Fuqua SA, Jaffray E, Hay RT, Palvimo JJ, Janne OA, Pestell RG. Androgen receptor acetylation governs trans activation and MEKK1-induced apoptosis without affecting in vitro sumoylation and trans-repression function. Mol Cell Biol. 2002 May;22(10):3373-88.

# Gene Expression Phenotypic Models That Predict the Activity of Oncogenic Pathways

Erich Huang[1,2], Seiichi Ishida[1,*], Jennifer Pittman[3], Holly Dressman[1,2], Richard G. Pestell[5], Mike West[3], and Joseph R. Nevins[1,2,4]

[1] Department of Molecular Genetics and Microbiology

[2] Center for Genome Technology

Duke University Medical Center

Durham, NC 27710

[3] Institute of Statistics and Decision Sciences

Duke University

Durham, NC

[4] Howard Hughes Medical Institute

[5]

* Present address: Division of Pharmacology
National Institute of Health Sciences
1-18-1, Kamiyoga, Setagaya-Ku
Tokyo 158-8501, Japan

**Abstract**

We seek to connect structural features of gene expression data with biological hypotheses by integrating "metagene" structure in DNA microarray experiments with stochastic models of the phenotypic state of a tissue. This approach facilitates direct and quantitative tests of the quality of a model by cross-validation techniques, provides predictive as well as descriptive capability, and makes possible quantitative estimations of the contributions of individual genes in a phenotypic model. We apply these techniques to elucidate and test transcriptional phenotypes that reflect activity of Ras, Myc, and Rb-E2F pathways. The phenotypic models accurately predict the activity of these pathways in the context of normal cell proliferation. Moreover, the models also predict tumors that result from the deregulation of the Myc or Ras pathways. We suggest that these gene expression phenotypes have the potential to characterize the complex genetic alterations that typify the neoplastic state in a way that truly reflects the complexity of the regulatory pathways that are affected.

## Introduction

Traditional methods for the analysis of gene expression have relied on an ability to accurately measure levels of expression one gene at a time. The advent of genomic technologies, particularly high-density DNA microarrays, allows for the efficient measurement of very large numbers of genes in one assay. It is now possible to assess the activity of a substantial portion of the expressed genes within a given tissue using these arrays and analysis of entire genomes will soon be possible for higher eukaryotes. Nevertheless, even with technology that permits global measurement of gene expression, methods for interpreting these measurements often represent a limited view of the physiologic complexity of a tissue. It is the ability to take highly complex gene expression datasets, find underlying structure within them, and rigorously test association of that structure with biological conditions that is critical to developing a comprehensive, multi-dimensional picture of the gene activity that defines cellular phenotype.

One example of a cellular phenotype that has been the subject of study with genome-scale microarrays is the process of cell proliferation and, in particular, the transition of a cell from quiescence to the initial G1 phase of the cell cycle. This process requires the widespread mobilization of cellular resources for multiple functions ranging from the basic metabolic machinery of the cell, assembling the various components required for nucleic acid synthesis, to the generation of activities required for cell cycle progression and cell division. As such, it is clear from many studies that the stimulation of cell growth out of quiescence leads to vast changes in gene activity characterized by waves of gene induction as cells progress through the cell cycle. Time course studies of cell proliferation demonstrate that unsupervised learning procedures such as hierarchical,

K-means clustering, and self-organizing maps can render such complex data into explicable waves of gene expression [1-6]. These studies reveal gene expression exhibiting distinct patterns, representing groups of genes that are coordinately regulated during this process, and in general define "clusters" of related function during the cell cycle. Similar studies on neoplastic tissues have identified pervasive patterns of gene expression that can distinguish tumor tissue from normal cells as well as categorize tumors into sub-classes with different clinical behaviors [7-16]. While these techniques clearly identify structure in gene expression data, assessing uncertainty in that structure due to experimental variability or inherent stochastic processes presents a significant challenge. In the absence of such knowledge, it becomes problematic to ask generalizable questions about the connectivity and relative contribution of genetic regulatory networks to a disease phenotype. A comprehensive understanding of an intricately orchestrated event such as initiation of cell cycle progression, or a complex series of dysregulatory events, as in neoplastic disease, depends in part on developing methods to obtain quantitative estimates of a particular gene's relation to broader integrated transcriptional programs as well as approximations of how such programs relate to known experimental or clinical conditions.

At the opposite end of the spectrum from a global analysis of gene expression's relation to cellular phenotype is the study of discrete gene pathways thought to contribute to a given phenotype, including cell cycle and oncogenesis. When proliferative signals are supplied to a quiescent cell, effectors of this transition include the products of immediate early genes such as c-Myc and activated G1 cyclin-dependent kinases (cdks). G1 cdks subsequently phosphorylate the retinoblastoma tumor suppressor protein,

thereby allowing E2F transcription factor activity to accumulate [17,18]. In vitro, overexpression of Myc and E2F family members is known to induce entry of quiescent cells into S-phase. Previous studies have shown that Myc can transactivate a variety of genes generally related to the control of cell growth [19]. More recent studies, employing DNA microarrays to achieve a genome-scale analysis, have identified genes involved in cell cycle, cell growth, cytoskeletal organization and adhesion [20]. Comparable studies of the E2F family reveal that E2F activity triggers transcription of numerous target genes necessary for DNA replication, mitosis and cell cycle regulation [2,21,22]. These results suggest that activities such as E2F and Myc set in motion multiple distinct as well as overlapping transcriptional programs that metabolically prepare the cell for reproducing itself and for determining its fate. Despite these advances, current methodologies used to identify and categorize the global transcriptional programs activated by E2F and Myc provide only a one-dimensional view of their role in determining cellular phenotype and do not provide any means for quantifying or determining the relative importance of individual target genes or groups of target genes. Further, evaluating transcriptional programs from the perspective of fold-induction or fold-repression of individual genes ignores the fact that physiologic (and pathologic) states are manifest by the complex interrelation of both up- and down-regulated genes acting in aggregate.

Probing gene regulatory networks as aggregate processes involving multiple interconnected genes demands analytic methodologies that treat them as such. Various studies have employed statistical processes that can explore the underlying patterns or structure in complex gene expression data. Singular value decomposition for linear transformations to identify "eigengenes" or "modes" of expression in gene expression

experiments, has been shown to reveal structure within the complex datasets not rendered explicit by measurements of induction or repression alone [23-25]. Related methodologies, known as factor models, or latent variable analysis, while traditionally used in the exploration of complex financial data or marketing data for identifying subtle relationships that drive the fluctuations in currency values or buying patterns, also have the potential to identify gene expression relationships that drive a biological phenotype. Methods such as these go beyond simple gene-by-gene induction or repression patterns and begin to identify interconnections. For example, our recent analysis of gene expression patterns in human breast cancer samples, using factor models and Bayesian regression methodologies, reveals underlying factors, or groups of gene expression events, that define the estrogen receptor status of the tumors [16]. Many of the genes whose expression patterns provide this discrimination naturally represent genes known previously to interact with the ER pathway. This example suggests that statistical methodologies that can classify and discriminate biological samples based on an observed property reflect the underlying biology. Using this analytic method differs significantly from clustering because it builds a probabilistic model that can be rigorously cross-validated, provides uncertainty estimates, and establishes a framework for quantifying the activity of interconnected regulatory pathways.

These methods allow us to incorporate global expression data into testable models and facilitate treating gene expression data as aggregate groups of genes, or "metagenes". Most importantly, Bayesian predictive modeling provides procedures for scoring the impact of metagenes on our prior knowledge of experimentally-controlled cellular state. This provides a foundation for us to quantitatively explore issues such as specificity of

function among members of a conserved family such as the E2Fs, or comprehensively understand how Myc and E2F-actuated transcriptional programs relate to one another.

To understand the transcriptional programs invoked by known initiating events in cell proliferation, E2F1, E2F2, and E2F3, as well as Myc and Ras were ectopically expressed in quiescent wildtype mouse embryo fibroblasts (MEFs). Employing Affymetrix Mu11K GeneChips, gene expression data from these experiments were collected in order to create a complex data set for generating a latent factor framework that would provide insight on integrated proliferative and oncogenic metagenes, as well as for developing Bayesian regression models that could substantiate the quantitative effects and relationships of such programs.

## Results

### Experimental deregulation of oncogenic pathways for the analysis of gene expression

A variety of studies have documented the signaling pathways that contribute to cellular proliferation in response to growth factors and that are often deregulated in oncogenesis (Figure 1A). These include pathways regulated by the Ras and Myc oncoproteins as well as the Rb tumor suppressor that controls the activity of the E2F transcription factors. To establish experimental conditions that would generate a comprehensive gene expression dataset for discovering phenotypic programs that correspond to the activation of Ras, Myc, or E2F activity, we employed recombinant adenoviruses that individually express activated Ras, Myc, or the E2F-1, E2F-2, and E2F-3 proteins. Quiescent primary mouse embryo fibroblasts were infected with these viruses and RNA was harvested 18 hours after infection. Importantly, we established conditions that allowed for the deregulation of these activities in otherwise quiescent cells but not to an abnormal level of accumulation. For instance, the accumulation of E2F1 activity in this experimental setting was within a factor of two of the normal G1/S accumulation of this activity as cells are stimulated to grow. In addition, to ensure that the E2F activities were produced at equivalent levels, facilitating analysis of the differences in gene expression profiles generated by these proteins, we compared the level of activity of the E2Fs by a reporter assay, using a luciferase gene under the control of an E2F-regulated promoter. As shown in Figure 1C, under the conditions of these infections, approximately equal levels of the E2F activities were achieved as seen by equivalent levels of activation of the reporter.

Affymetrix Mu11K arrays possessing 13179 control, gene and EST sequences were used to probe fluorescently-tagged target cRNA derived from RNA isolated 18 hr after deregulation of the various pathways. The dataset comprises nine independent E2F1 experiments, eleven E2F2 experiments, eight E2F3 experiments, as well as six replicates for Myc alone, and five each for Ras alone and a combination of Myc and Ras. Ten quiescent control samples, that represent quiescent cells infected with a control adenovirus, were included as well. This provides a data collection that includes 55 independent experiments with six different treatment classes, each with 13179 sequences assayed per experiment. In each case, the Affymetrix 'Average Difference' scores, as reported by the Affymetrix Microarray Analysis Suite, were log 2 transformed and normalized and then used for statistical analyses as described below.

**Identification of oncogenic gene expression phenotypes based on metagenes**

Numerous studies have analyzed similarly produced gene expression data in the context of either E2F or Myc overexpression to identify genes induced by these regulatory activities. This includes the use of DNA microarrays to achieve a comprehensive examination of gene expression, enabling the measurement of expression of thousands of genes simultaneously. For instance, this approach has been applied to the study of E2F gene regulation and identified a number of additional targets that include not only DNA replication and cell cycle regulatory genes but also genes encoding mitotic activities [2,21,22,26,27]. Nevertheless, such analyses, that generally focus on identifying those genes that exhibit a fold-change in expression regarded to be significant, are limited in scope by examining the expression of individual genes on a gene-by-gene basis.

An alternative approach is to take advantage of the complexity of the microarray data and treat the gene expression values as quanta for identifying patterns of gene expression that typify a cellular phenotype. Since all the genes expressed in a cell ultimately do define the cellular phenotype, an analysis that takes advantage of this complexity has the potential to generate phenotypes of greater detail and clarity than what can be achieved through visual or other characteristics. We have done this using statistical methodologies that have the power to find patterns that typify a particular state, in order to characterize the distinctions between quiescent cells, cells expressing individual E2F proteins, or cells expressing Myc and Ras.

The basis for the analysis relies on the identification of latent factors or "metagenes" derived by performing singular value decomposition (SVD) on a matrix $X$ whose columns represent independent experiments and rows represent individual genes. The SVD maps expression levels of $X$ to a smaller matrix $F$ whose columns $f$ represent singular factors. With a dataset comprising 55 arrays, there is a maximum of 55 orthogonal factors. Each factor represents what we term a "metagene", a linear combination of individual gene expression values that together constitute the metagene. Therefore, each gene possesses a "weight" on each metagene in the linear combination. In this example, a 55-dimensional linear subspace describes virtually all the explicable structure in the data set. Singular value decomposition provides a method to re-map the data from the high-dimensional space defined by 13179 transcripts to the lower dimensional 55-dimensional subspace while providing the added benefit of reducing the dimensionality of the data for organizational and computational purposes. Each of the 55

re-mapped dimensions represents a "metagene" that represent ranked, weighted combinations of the contribution of individual genes.

In order to reduce noise attributable to genes that do not vary consistently across experiments, we derived objectively optimized screened subsets of transcripts based on Pearson correlations between each set of experiments versus the control set. Using pairwise comparisons between experiments and controls, genes are ranked according to a correlation scale of +1 to –1, with 0 representing non-correlated. The following pairings were used to rank genes by correlation: E2F1 vs Control, E2F2 vs Control, E2F3 vs Control, Myc vs Control, Ras vs Control, Myc+Ras vs Control, or combinations thereof. Thresholds based either on number of genes to be included, or correlation scores were employed. Initial subsets of genes were identified by setting thresholds for top-ranked genes according to the absolute values of Pearson correlation scores. Once these subsets were identified, when applying SVD, we re-mapped the experiment to $p$-dimensions where $p$ is equal to the numbers of genes included in a screened subset. It should be noted that correlations are not a measure of raw signal strength of a gene, but of a consistent relationship of signals between two compared states. Relatively low signals are sufficient so long as they are coherent across replicate experiments.

An illustration of the analysis of the quiescent versus Ras or Myc expressing cells, based on three metagenes, is shown in Figure 2A. While metagene 2 or 3 does little to discriminate between the quiescent and Ras expressing cells in this particular 3-dimensional space, metagene 1 very cleanly separates the samples. Likewise, metagenes 1 in the Myc analysis provides discrimination of the quiescent versus Myc expressing cells. Simply put, this analysis identifies a metagenes, that represents a group of genes,

whose expression patterns identify the difference between a quiescent cell and a Ras or Myc expressing cell.

The factors or metagenes that can discriminate between a quiescent cell and a Ras or Myc expressing cell are based on a group of genes that together constitute this metagene. Moreover, an analysis will typically yield multiple metagenes that have the capacity to provide some discrimination of the phenotypes in a high-dimensional space. By combining these individual metagenes using logistic regression methods, we can create a compound metagene score that defines the ability to discriminate between phenotypic states. This metagene scoring scheme represents a stochastic model comprising a collection of related gene expression values that defines the phenotype of interest. Each metagenes score is then converted to a probability scale. Figure 2B depicts the estimates of the probability r that a sample possesses Ras or Myc activity based on the Ras or Myc metagenes for each of the quiescent control samples as well as the Ras or Myc expressing samples. Ninety-percent probability intervals illustrate the degree of uncertainty. This analysis provides a useful visual assessment of how clearly the samples are classified based on the metagenes analysis.

A similar factor analysis for the E2F expressing cells is shown in Figure 3. As with the analysis of Myc and Ras, one metagene depicted in the plot of Figure 3A very clearly distinguishes the E2F expressing cell (either E2F1, E2F2, or E2F3) from the quiescent cell. In addition, combining the factors that provide the discrimination of each of the E2Fs by means of a logistic regression to create a metagene model demonstrates the classification probabilities based on the E2F1, E2F2, or E2F3 metagenes for each of

the samples. Once again, this analysis provides a clear assessment of how well the samples are classified based on the metagene analysis.

**Gene expression patterns that reflect the activity of oncogenic pathways**

The genes that constitute the metagenes providing discrimination of cells expressing Ras, Myc, or the E2Fs are ranked by the weight that the estimated regression coefficient provides to the discrimination. A list of the top 200 genes, along with estimated regression weights, for each of the Ras and Myc metagenes models can be found in Table 1 and 2, respectively, of the Supplementary Material. Figure 4A depicts the relative expression values of the genes selected in the Ras and Myc discrimination with each row representing an individual gene, ordered from top to bottom as a function of estimated regression coefficients. High expression is indicated by a white color and low expression by black as indicated in the color scale at the right. The expression values were plotted after standardization across the samples by taking the mean expression value of all samples, subtracting from the value of each sample, and then dividing by the standard deviation. Distinctions in the pattern of expression of this group of 200 genes between the quiescent cells and the Myc or Ras expressing cells are clearly evident. An examination of the list of genes reveals some similarities to previously described analyses for Myc [20] in that a number of the genes encode general growth regulatory proteins or proteins involved in metabolic process associated with cell growth. The nature of the genes in the Ras discriminating group is less clear although they do appear to include a number of genes associated with cell growth signaling events such as Rac3, TNF,

guanine nucleotide binding protein, and cyclin G2 as well as general cellular metabolism (phospholipase, polyA binding protein, dual specificity phosphatase).

A similar analysis of the genes providing the discrimination between quiescent cells and the E2F expressing cells is summarized in Tables 3, 4, and 5 of the Supplementary Material and is shown graphically in Figure 4B. In this case, the differences in the pattern of expression between the quiescent cells and the E2F-expressing cells is even more distinct and shows clear evidence of clear patterns that distinguish the quiescent cell from an E2F-expressing cell. Interestingly, the genes commonly identified as E2F targets in various past studies, including the DNA replication genes, cell cycle regulatory genes, and mitotic genes, are not highly weighted in the lists of the genes that define the E2F-expressing cell. Although these canonical E2F targets are certainly part of the E2F pathway, it would appear that other genes subject to E2F control, including those genes that might be secondary or tertiary to the canonical E2F targets, most highly correlate with the function of the E2F proteins.

**Metagenes can distinguish cells expressing individual E2F proteins**

The metagene analyses presented in Figure 3 -- as scatter plots of experiments using metagenes that clearly separate control from E2F experiments -- demonstrate the ability to identify metagenes that can distinguish an E2F-expressing cell from a quiescent cell. A number of past studies have now documented distinct functional roles for the individual E2F proteins. In particular, E2F1 exhibits an ability to induce apoptosis when expressed in a quiescent cell [28-30]. E2F1also contributes to the ability of Myc to induce apoptosis [31], and contributes in part to the induction of cell death following DNA damage

[32]. In contrast, E2F3 plays a much reduced role in the apoptotic response but is critical for cell proliferation [33,34], including in response to Myc [31]. Despite these differences in function, little distinction in gene expression profiles have been seen in past experiments examining cells expressing E2F1, E2F2, or E2F3. These studies have largely relied on measures of fold-change of gene expression levels in response to the E2F. We have determined from these analyses that no matter how high a threshold is set for fold-change in expression, the ability to conclude that a given fold-change is more meaningful than another is simply not possible.

As an alternative, we have made use of metagene analyses that distinguish E2F expressing cells from quiescent cells to determine if a distinction between the individual E2Fs can be identified. We made use of the genes identified in the E2F discriminations versus quiescent cells as the starting point in factor analysis to find metagenes that could identify and discriminate the individual E2F activities.

The amount of E2F-specific structure in the data is clear even in the absence of screening methods. When an SVD is performed on the entire unscreened complement of 13179 genes represented on the Affymetrix Mu11K arrays, while considerable noise is introduced by genes not affected by E2F activity, there is still strong separation of E2F experiments from control experiments, suggesting that structure attributed to E2F activity is robust amidst the noise contributed by the entire complement of genes.

In order to place these E2F experiments in the context of previously-published knowledge of E2F function, a set of 128 E2F target genes previously identified in published literature that are also present on the Mu11K arrays was used in an SVD. These included mouse homologs of published human E2F targets identified via the NCBI

Homologene database. It is evident that under the experimental conditions described here, metagenes derived from published E2F targets depict a reasonably clear distinction between E2F experiments and controls (Figure 5A). In comparison, an equally-sized dataset of genes derived from objective correlation screens we performed of the genes most correlated to E2F status provides much sharper distinction between the E2Fs, with less variability within replicates (Figure 5B). This suggests that correlation screening identifies genes more characteristic of E2F function than genes discovered by traditional methods. Interestingly, metagenes derived from previously published genes show lesser distinction between E2F1 and E2F2 experiments, while E2F3 replicates lie some distance away and exhibit a higher degree of variability. These data suggest that while older hypothesis-driven Northern blot experiments and earlier microarray analyses do indeed identify genes related to E2F states that consequently can characterize cells demonstrating E2F activity, they do so less effectively than the genes selected on the basis of providing optimal discrimination.

**Distinct biological processes suggested by the metagenes that predict individual E2F states**

An analysis of the top 200 genes that constitute the metagenes selected for their ability to predict the E2F1, E2F2, or E2F3 phenotype suggests biological roles that are in some cases consistent with past work but also novel. For instance, amongst the E2F1 specific metagenes are a number of genes that encode proteins involved in apoptotic pathways as might have been predicted based on past work. In addition, the E2F2 metagenes include a variety of genes shown to play a role in the control of lymphocyte

proliferation including …….. Although E2F2 function has not been well defined, two recent studies do point to a role for this protein in regulation lymphocyte proliferation and differentiation. The E2F3 genes are less clear but do suggest … Finally, the analysis of the Ras and Myc metagenes provide evidence for …..

**Cross validation demonstrates the ability to recognize and predict oncogenic phenotypes**

An important feature of the experimental analysis described here is an ability to directly develop testable probability models from the genome-scale expression data. This permits applying a model derived from one experiment to new experiments, validating its usefulness outside of the context in which it was created. It also facilitates cross-validatory testing in which a sample is held out of the data set, a model regenerated from the data set minus the held out sample, and the held out sample tested against the model. The uncertainties quantified in cross-validation testing are indicative of the uncertainties one would see in real world application of a gene expression model. That is, do these patterns of gene expression truly represent a gene expression phenotype that defines the state of a cell that is expressing an E2F protein or the Myc or Ras proteins? In this instance, one of the samples is removed from the analysis, treated as an unknown, and then the remaining samples are used to recompute a metagene model. This validation model is then used to predict the state of the removed sample, treating it as an unknown.

The results of one-at-a-time cross validation assays for predicting Ras, Myc, and each E2F are shown in Figure 6. Uncertainty intervals tend to be fairly wide for some of

the samples; this high uncertainty primarily reflects the fact that we are comparing samples of very small numbers, while also reflecting inherent variability and resulting ambiguity in the expression profiles of these cases relative to the 200 genes found to be most discriminatory among the other cases. Nevertheless, it is quite clear from these analyses that the metagenes selected for their ability to identify Ras, Myc, or E2F expressing cells also have the ability to accurately predict the state of a cell based on the expression of a group of relevant genes.

**Using gene expression phenotypes to detect the activation of signaling/oncogenic pathways**

The analyses presented here provide clear evidence for distinct gene expression phenotypes reflecting the activation of Ras, Myc, and E2Fs. Yet this has involved the use of genes expressed from recombinant adenoviruses in otherwise quiescent cells—a controlled experimental environment. Obviously, one would hope that the patterns of gene expression that typify a deregulated Ras or Myc or E2F under these synthetic circumstances would reflect the events occurring during the course of normal cell growth. To extend this work to this more general question, we have tested whether these profiles reflecting Ras, Myc, and E2Fs do indeed reflect the action of these proteins in a normal, physiological setting. Specifically, we have employed our models using the Ras, or Myc, or E2F metagenes developed in an experimental setting to predict the activity of these pathways following the stimulation of cell proliferation.

Many previous studies have documented the kinetics of activation of Ras, Myc, and E2Fs as quiescent cells are stimulated to proliferate. Both Ras and Myc activity

accumulate very early in the growth response, within 3 hr of the growth stimulation. In contrast, the accumulation of E2F activity, as represented by E2F1, E2F2, and E2F3, is much slower with peak accumulation from 16 to 18 hr following the stimulation of fibroblast growth. To test the ability of the various metagenes to predict the activation of the specific pathway, we prepared RNA from mouse embryo fibroblasts that were either quiescent or stimulated to proliferate by the addition of serum. Samples were taken at various time points after stimulation, RNA prepared, and hybridization probes generated. These probes were then hybridized to the Affymetrix mouse arrays to assay gene expression at each of these times points. Each sample was then treated as of unknown state and predicted from each of the analyses using the metagene models identified for Ras, Myc, and the E2Fs. The results of predictions from the Myc and Ras models are shown in Figure 7A. Each sample predicted in each of the Myc and Ras metagene models and the resulting probabilistic predictions are graphed; these represent the relative probabilities of the sample exhibiting a Myc or Ras pattern relative to quiescence. It can be seen from this plot that both the Ras and the Myc metagenes are evident in these cell proliferation samples in the early time points and the pattern of these probabilities over time is consistent with the known time profiles of accumulation of Myc and Ras activity.

The same approach was applied to the samples using the E2F metagene models, and reveals quite distinct patterns (Figure 7B). In each case (E2F1, E2F2, E2F3), the samples early in the stimulation course did not show significant evidence for an E2F pattern but did so later in the time course. Once again, this is entirely consistent with the time at which these activities normally accumulate following the stimulation of cell growth. Based on these results, we propose that the metagenes identified through the use

of adenovirus vectors to express the relevant proteins in quiescent cells do indeed define the signatures of these pathways in a distinct and physiologically relevant manner.

**Prediction of tumors that result from deregulation of Myc or Ras**

The analyses shown above demonstrate the ability of the Ras, Myc, and E2F metagenes to accurately predict the deregulation of these pathways in mouse embryo fibroblasts. One very important and practical application of this capacity would be the ability to predict the deregulation of these activities in tumors so as to better characterize the events leading to the oncogenic state. To address this possibility, we have made use of a series of mammary tumors that developed in transgenic mice expressing either Myc or Ras from the MMTV enhancer. In addition, tumors were also generated by expression of the neu oncogene in an MMTV-directed manner. RNA was prepared from the tumors, used to generate probe, and then hybridized to Affymetrix Mu11K GeneChips. Each of these samples was then used as a validation set for prediction by either the Myc or the Ras metagenes defined in the fibroblast experiments. The results of these analyses are shown in Figure 8.

The results of these predictions, plotted as a probability of the sample exhibiting either a Myc or a Ras expression pattern, are shown in Figure 8. It is evident for the Myc prediction that the metagene identified in the mouse embryo fibroblast analysis was indeed capable of predicting a Myc state in the tumor models. The Myc tumors were predicted with a high degree of confidence and clearly separated from most of the other samples that represent either Ras or Neu tumors (panel A). The prediction of Ras tumors was also successful but less clear than for the Myc cases (panel B). Although each of the

Ras tumors was accurately predicted and clearly separated from the Neu tumors, there was little distinction between the Ras tumors and the Myc tumors. Interestingly, recent studies have shown that a large fraction of MMTV-Myc induced tumors also develop Ras point mutations [35]. Thus, the fact that the Myc tumors are predicted by both the Myc and the Ras metagenes is consistent with the activation of Ras activity in both sets of tumors.

## Discussion

Understanding the biology revealed in gene expression data is a multistep process involving the identification of structure in data, testing the association of that structure with biological phenomena, and—critically—evaluating the robustness and meaning by testing the capacity of the identified structure to accurately *predict* biological states. Using data from in vitro ectopic expression of Ras, Myc and E2F, we have developed gene expression models of these activities that are composites of "metagene" structure within the data. These models represent complex molecular phenotypes composed of not only hundreds to thousands of gene expression features, but the inter-relation of these features. As such, the methodology we employ is focused more on distinctive combinations of multiple genes with diverse gene expression profiles than on genes that share a high degree of similarity in their regulation, or genes that exhibit dramatic changes in magnitude in experiments.

### Contrasting methods for analyzing gene expression data

Clustering of gene expression data represents an effective method for highlighting structure in data by using similarity metrics to relate genes that share similar expression profiles across experiments and experiments that share similar patterns across genes. Much identified structure is undoubtedly biologically related to gene expression experiments, but there is currently no method to explicitly and quantitatively estimate the relation of groups of genes to the biology inherent in an experimental design. Typically, such relations are based on the premise of "guilt by association" and depend on laborious literature and annotation database searches to determine the function of identified genes

and develop inferences about their role in an observed phenomenon. The strongest test of whether genes are truly implicated in a biological phenomenon is to reverse the question and apply those genes in predictions of that phenomenon. Efforts to retroactively use clustered data in class predictions have shown great promise in indicating differences between types and subtypes of neoplastic disease, suggesting that gene expression data can certainly be used in a predictive mode [7,8,11,15]. However, while representing a powerful first step in organizing inherently complex data, clustering algorithms are ill-suited for model building. Similarity metrics generated by such approaches relate gene expression values or individual experiments to one another, but not to a phenotypic state. Such relations are not modeled, but inferred.

In contrast, the metagene modeling methods we employ here to understand the transcriptional phenotypes connected to Ras, Myc, and E2F activities, relate gene expression data to one another in the context of phenotypic state and permit explicit and systematic discovery of gene expression patterns pertinent to that phenotype. They further facilitate cross-validation testing of the model that quantifies uncertainty in that model. Therefore we can identify models that inadequately reflect, i.e. inadequately predict, phenotypes in validation testing. The combination of Bayesian methods of analysis and rigorous cross-validation testing also prevents "over-fitting" in models, a common circumstance when explanatory variables far outnumber experiments. The ultimate test of a model is whether it exhibits reliable predictive capacity when applied out of the milieu in which it was trained to new contexts. We have sought to do this in the examination of the analysis of physiologic states, with evident success.

Structural features of gene expression data are not necessarily directly related to the biological questions being posed; and the model-building orientation described here allows one to predict, and thereby test, the strength of the relationship between structure and phenomena. As described above, out-of-sample cross validation procedures ensure that this relationship is statistically robust. Moreover it highlights the fact that a model is not merely descriptive, but predictive. If it fails in the predictive mode, its validity as a description of biology is questionable.

**Exploration of pathways rather than targets**

Importantly, our method of analysis makes no distinction between primary, secondary, or tertiary targets of the regulatory proteins. Though the kinetics of ectopic gene expression and our choice of an 18 hour post-infection harvest point limits the potential breadth of the signal cascade initiated by ectopically expressed Ras, Myc, and E2F, the focus has been on identifying unique transcriptional features, regardless of whether they represent direct targets or those farther downstream. Statistically rigorous association of unique gene expression features with phenotypic state is primary in this model-building approach. Our intention is for the association to be made first, and thereby inform further molecular or biochemical experimentation to understand the mechanistic basis of that association.

Careful biochemical dissection of E2F or Myc transactivation demands an understanding of their primary targets. Certainly, this is critical for studies directed at the molecular mechanisms of action of these transcription factors. But, the broader understanding of the pathways regulated by these proteins is of equal importance. The

analyses described here seek to understand the breadth and depth of expression changes idiosyncratic to a particular activity. In doing so, we do not limit ourselves just to initial direct events, but the broader cascade of transcriptional changes that denote a global cellular response to an activity and that reflect what is distinctive about that activity.

In our analysis of the molecular phenotype corresponding to Myc activity, several genes previously reported to be targets of Myc do play a role in the model. These include ornithine decarboxylase, fibrillarin, translation initiation factors, hepatoma-derived growth factor, among others. What is also clear is that many genes with no previously identified relationships to Myc activity participate in its phenotypic model as well, and that we now have a method for quantifying the role that a particular gene plays in the model. This quantification is important because traditional methods have no means to estimate the physiologic importance of a putative target gene. Here, a gene can be evaluated in light of its contribution to a phenotypic model and we believe such values will prove useful in annotating the relationship of a transcript to an observed, and modeled biological effect.

Likewise, some of the known E2F targets also contributed to the models that defined an E2F phenotype. But, like the Myc case, many genes not previously associated with E2F function were heavily weighted in the E2F discrimination. Perhaps most important in this analysis was the clear evidence for a distinction in the function of the E2F1, E2F2, and E2F3 proteins, a result not generally seen in past studies. The greatest difference between traditional techniques and the approach described in this report is that the threshold for considering genes is not restricted to an arbitrary threshold of fold-

induction or fold-repression, but by consistent, statistically-validated structure related to E2F state.

This quantification becomes important in understanding the specificity of functions that individual E2Fs actuate. In the particular E2F models described above, there are 38 transcripts that are common to E2Fs –1, -2, and –3 among the top 200 weighted genes for each model. In pair-wise comparisons, there are 100 genes held common between the top 200 E2F1 and E2F2 transcripts, 44 shared between E2F1 and E2F3, and 69 shared between E2F2 and E2F3, suggesting that E2F1 and E2F2 share more similarity to one another in the transcriptional profiles they activate than they do to E2F3. Additionally, the weights attributed to these transcripts vary from E2F to E2F, the variation in these weights, and the contributions of genes unique to individual E2F activities, demonstrates that there are robust physiologic differences between E2Fs -1, -2 and –3 that were not obvious until we applied our metagene models to understanding E2F function. Very likely, because of the high level of homology between E2Fs, a target may be common, but the power of quantifying the physiologic impact of target transcripts lies in estimating whether a putative target may be of greater or lesser importance for a particular E2F activity than another. Subtle variations such as these cannot be properly assessed by traditional methods, and may account for a proportion of the differences between E2Fs. A gene may be activated by E2F1, E2F2, and E2F3, but it is activated in the context of much broader transcriptional programs specific to each E2F.

Of course, the ultimate challenge in making use of these gene expression profiles is the daunting task of understanding how they fit into a common biological framework. This will require an informatics capability that is beyond reach at the current time – an

ability to understand where any given gene fits within a signaling pathway and how pathways intersect with one another in a logical fashion.

**Using gene expression profiles to predict the activation of regulatory pathways**

A very large body of work has documented the role of somatic genetic alterations in the genesis of tumors. Moreover, it is clear that tumors result from the alteration of not just one critical pathway, but many, and that it is likely that a variety of combinations of such events can contribute to the development of a tumor. Nevertheless, although the focused analysis of oncogenic mutations or the search for loss of heterozygosity as a basis for detection of a tumor suppressor have provided evidence for the role of such alterations in the genesis of human cancer, such studies are also limited in nature. The ability to accurately predict the activation of an oncogenic pathway such as that initiated by Ras or Myc or loss of Rb, based on the analysis of gene expression profiles reflecting these pathways, opens the possibility to a more robust analysis of cancers by detecting the consequences of the genetic alteration. Understanding these consequences leads to a sharper understanding of both the physiologic and pathologic roles of individual genes implicated in neoplasia.

This work demonstrates that experimental over-expression of effectors critical in cell proliferation and neoplasia can trigger alterations in gene expression that are characteristic of Ras, Myc, and E2F activity, and that high-dimensional models of these alterations adequately predict these activities even in a physiologic setting entirely removed from the original experimental design. Formerly, genes identified in gene expression experiments could only be classified by the magnitude of their induction or

repression in these experiments. An alternative is to directly model the relation of trancscriptional profiles to a phenotypic state, allowing genes to be assessed by the strength of their relation to that state rather than fold change. As we have determined, employing fold-change as a criterion for implicating "important" genes leads to considerable misclassification, and suggests that magnitude changes, while proving convenient as a method for assessing the impact of genes, do not completely reflect biologically important changes in gene expression.

The quantitative predictions of cell proliferation data generated by our models of Ras, Myc, and E2F status provide a method for beginning to recapitulate biology with models of complex gene expression phenotypes. In testing the models against a separate set of cell cycle experiments, we generate predictions of Ras, Myc and E2F activities in accordance with what is known about them from the published literature. Predicted Ras and Myc activities peak soon after serum stimulation while E2F activities rise and peak at the G1/S transition. This biological validation of models generated from *in vitro* training experiments suggest that the admittedly artificial milieu of ectopic expression nevertheless evokes effects that are consistent with a cell's fundamental response to a discrete activity in cell proliferation or oncogenesis. Crucial in this determination is the development of tools that identify and test models of the complex interplay of structure in data and phenotypic state.

## Experimental Procedures

**Cells and virus.** Primary wild type mouse embryo fibroblasts were prepared from day 13.5 p.c. embryos as described previously. The cells were passaged on 150 mm tissue culture dishes and maintained with DMEM supplemented with 15% heat-inactivated fetal bovine serum (HIFBS). The fibroblasts were expanded to passage 4 and plated at final density of between 140 and 200 cells per $mm^2$ as determined by trypsinization and counting with a hemacytometer. The MEFs were then rendered quiescent by starvation for 48 hours in DMEM 0.1% HIFBS. Preparation and functional validation of the recombinant adenoviruses Ad-E2F1, Ad-E2F2, Ad-E2F3, Ad-Myc, Ad-$Ras^{L61}$, and Ad-CMV-GFP have been previously described. Quiescent MEFs were counted once more for accurate multiplicities and infected at the multiplicities described in 3 ml DMEM/25 mM HEPES. After infection, 20 ml DMEM 0.1% FBS was added to each plate and incubations allowed to proceed for 18 hours.

**RNA preparation**. Upon completion of 18 hours incubation with recombinant adenoviruses, infected MEFs were harvested in 4 mL TRIZol Reagent. Total RNA was isolated according to manufacturer protocols and assessed for quality with an Agilent Gene-On-A-Chip machine.

**Luciferase promoter-reporter assays**. NIH 3T3 cells were plated in DMEM/15% HIFBS at a density of 3 X $10^5$ cells per 60 mm tissue culture plates and allowed 4h to adhere. Superfect reagent (Qiagen) was used to transiently transfect 5 ug of p68-Luc and 0.5 ug of pCMV-B-gal per 60 mm plate. Following incubation at 37°C for 3h, fresh

growth medium was added and the cells were incubated for an additional 21h. After incubation, a census plate was trypsinized and counted with a hemacytometer. Cells were consistently at a density of ~5 X $10^5$. Plates were infected in triplicate with recombinant adenoviruses Ad-CMV (MOI 500), Ad-E2F1 (MOI 500), Ad-E2F2 (MOI 500), and Ad-E2F3 (MOI 500, 1000) as above. A mock infection with no virus was also performed. After 24h incubation with recombinant adenoviruses, the MEFs were harvested in 100 uL lysis buffer (Promega) and luciferase activity was measured for transactivation of the p68 promoter by ectopic E2Fs with the Luciferase Assay System (Promega). Transfection efficiency was measured using 7.5 ?l of the same extracts by assaying ?-gal activity with chlorophenol red B-D-galactopyranoside (Sigma) as substrate Luciferase activity was normalized to B-galactosidase activity.

**Analysis of tumors.** MMTV-Myc, MMTV-Ras, and MMTV-neu transgenic mice have been described previously. **[description of time of tumor isolation, method of RNA preparation].**

**DNA microarray analysis.** All experiments utilized Affymetrix Mu11K A/B GeneChips. The targets for Affymetrix DNA microarray analysis were prepared as described by the manufacturer. Briefly, double stranded cDNA was synthesized from total RNA (10 ?g starting material) isolated from tissue culture harvests. Biotin-labeled cRNA is generated by in vitro transcription from the DNA. The cRNA is fragmented before hybridization and a hybridization cocktail is prepared, including the fragmented cRNA, probe array controls, BSA and herring sperm DNA. The cRNA is hybridized to

the oligonucleotide probes on the probe array for a 16 hour incubation at 45 C. Immediately following the hybridization, the hybridized probe array undergoes an automated washing and staining protocol on an Affymetrix fluidics station. DNA chips were scanned with the Affymetrix GeneChip scanner, and the signals were processed by the GeneChip expression analysis algorithm (v.2) (Affymetrix).

**Statistical analysis methods.** For the factor analysis of expression data, we used methods essentially as described previously for the analysis of breast cancer samples [16]. The analysis utilizes binary regression models combined with singular value decompositions (SVDs) and with stochastic regularization using Bayesian analysis. A probability model estimates a classification probability for each of the two possible states (wild type versus mutant) for each sample. This probability is structured as a probit regression model in which the expression levels of genes are scored by regression parameters in a regression vector $b$. Analysis estimates this regression vector and the resulting classification probabilities for both training and validation samples. The estimated regression vector itself is important not only in defining the predictive classification, but also in scoring genes as to their contribution to the classification.

## Figure Legends

**Figure 1. Experimental deregulation of oncogenic pathways.**

**A.** Cell signaling pathways that control cell proliferation and cell fate.

**B.** Production of E2F activity following infection with recombinant adenovirus.

Extracts from cells infected with recombinant adenoviruses were assayed for E2F activity by gel retardation as described in Methods.

**C.** Reporter transactivation assay.

A.

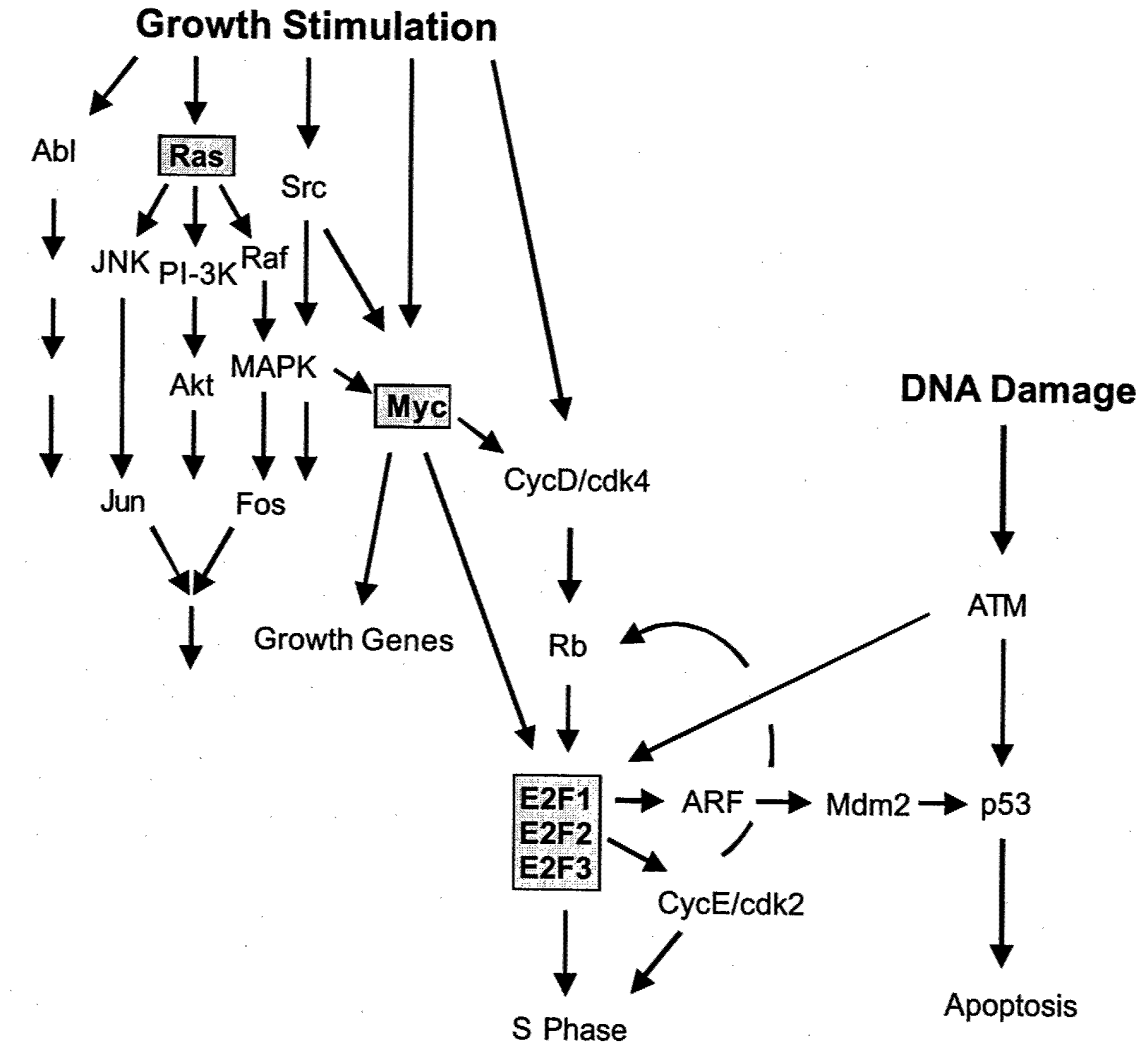
Growth Stimulation
Abl
Ras
Src
JNK
PI-3K
Raf
Akt
MAPK
Myc
Jun
Fos
CycD/cdk4
Growth Genes
Rb
DNA Damage
ATM
E2F1
E2F2
E2F3
ARF
Mdm2
p53
CycE/cdk2
S Phase
Apoptosis

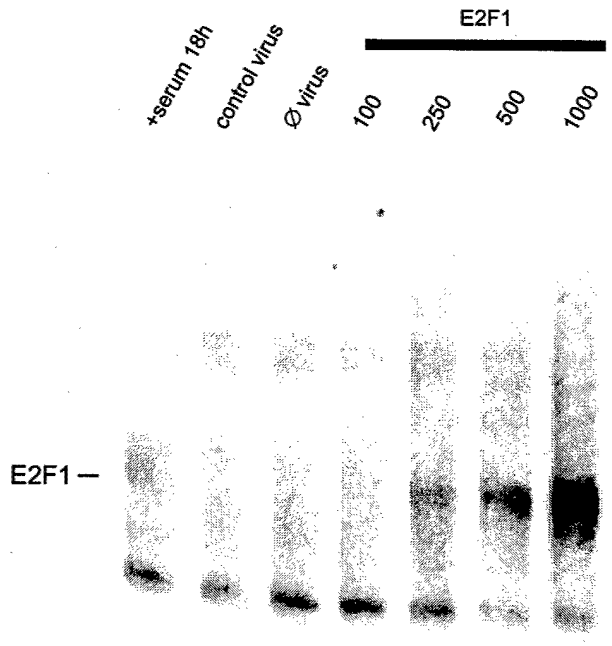
E2F1
+serum 18h
control virus
Ø virus
100
250
500
1000
E2F1

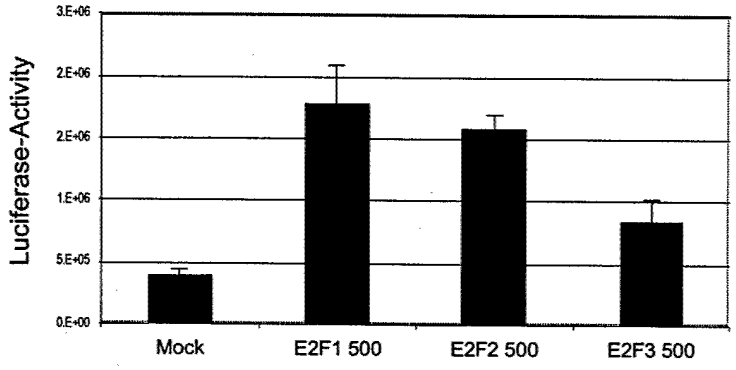
Luciferase-Activity
3.E+06
2.E+06
2.E+06
1.E+06
5.E+05
0.E+00
Mock
E2F1 500
E2F2 500
E2F3 500

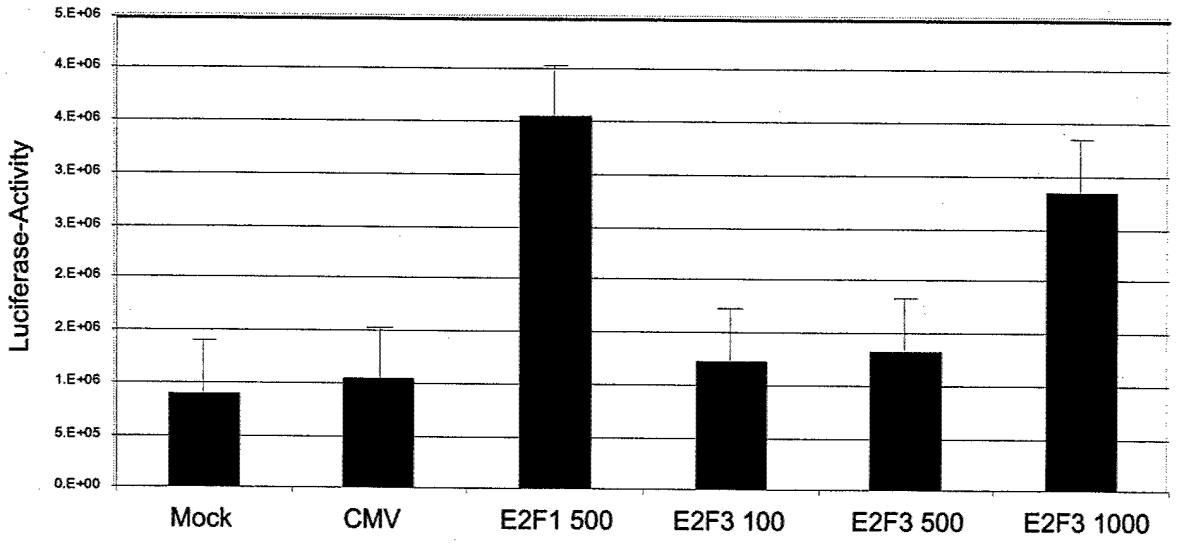
Luciferase-Activity
5.E+06
4.E+06
4.E+06
3.E+06
3.E+06
2.E+06
2.E+06
1.E+06
5.E+05
0.E+00
Mock
CMV
E2F1 500
E2F3 100
E2F3 500
E2F3 1000

**Figure 2. Factor analysis identifies gene expression differences in Myc and Ras expressing cells.**

**A.** Factor analysis. Individual samples depicted in a scatter plot on three dominant factors underlying 200 genes selected in pure discrimination of the training cases. Each sample is indicated by a simple index number and is color coded with red indicating Ras or Myc cases and blue indicating control samples.

**B.** Fitted classifications. Fitted classification probabilities for training cases from the factor regression analysis. The values on the horizontal axis are estimates of the overall factor score in the regression. The corresponding values on the vertical axis are fitted/estimated classification probabilities with corresponding 90% probability intervals marked as dashed lines to indicate uncertainty about these estimated values. Control samples are blue and Ras or Myc samples are red.

**A.**

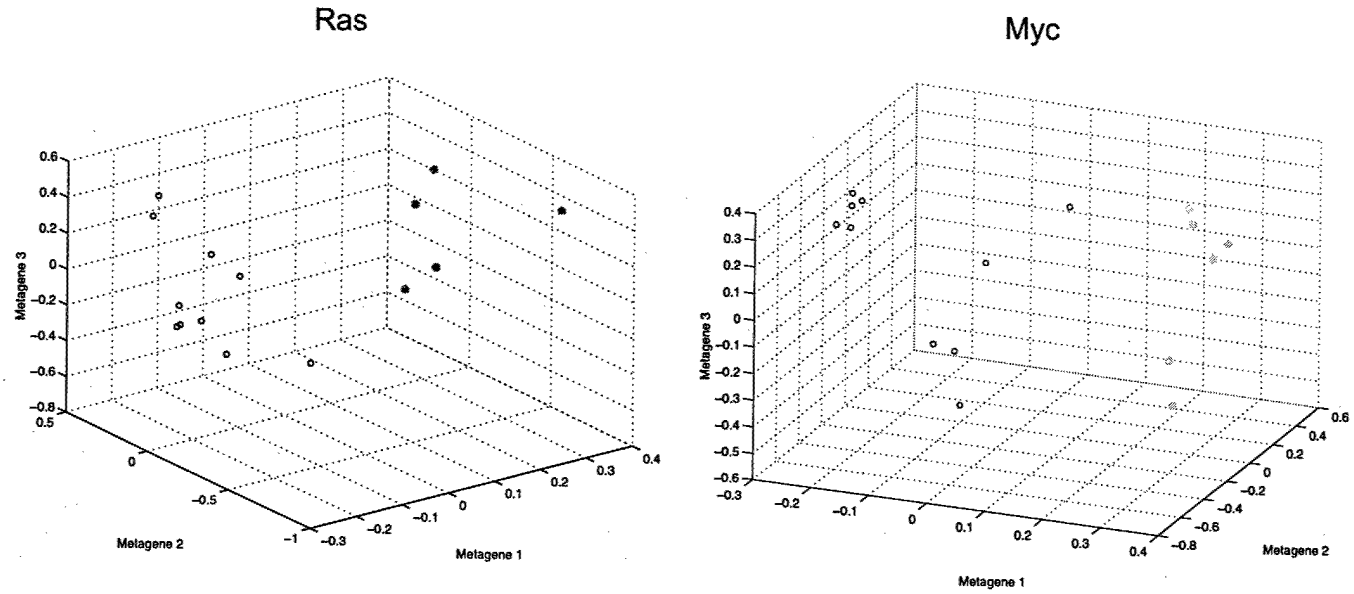
Ras
Myc
Metagene 3
Metagene 2
Metagene 1
Metagene 3
Metagene 1
Metagene 2

**B.**

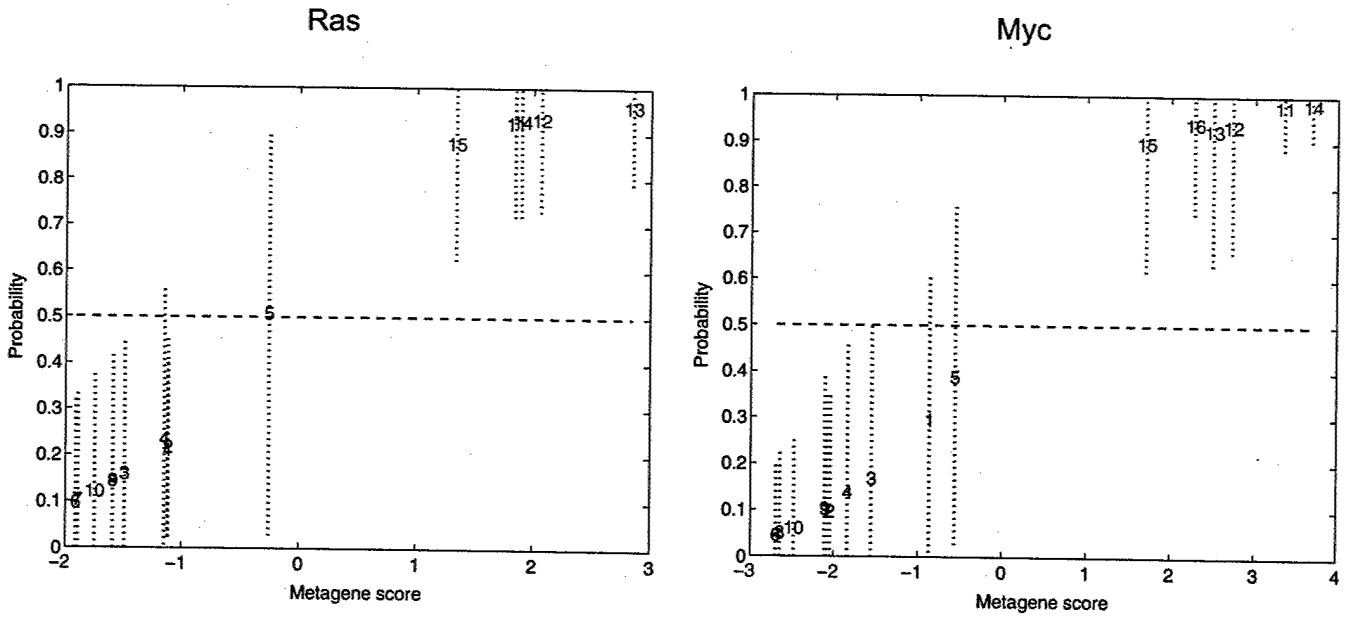
Ras
Myc
Probability
Metagene score
Probability
Metagene score

**Figure 3. Factor analysis identifies gene expression differences in E2F expressing cells.**

**A.** Factor analysis. Individual samples depicted in a scatter plot on three dominant factors underlying 200 genes selected in pure discrimination of the training cases. Each sample is indicated by a simple index number and is color coded with red, blue, or green indicating E2F1, E2F2, or E2F3 respectively, and open circles representing control samples.

**B.** Fitted classifications. Fitted classification probabilities for training cases from the factor regression analysis. The values on the horizontal axis are estimates of the overall factor score in the regression. The corresponding values on the vertical axis are fitted/estimated classification probabilities with corresponding 90% probability intervals marked as dashed lines to indicate uncertainty about these estimated values. Control samples are blue and E2F samples are red.

**A.**

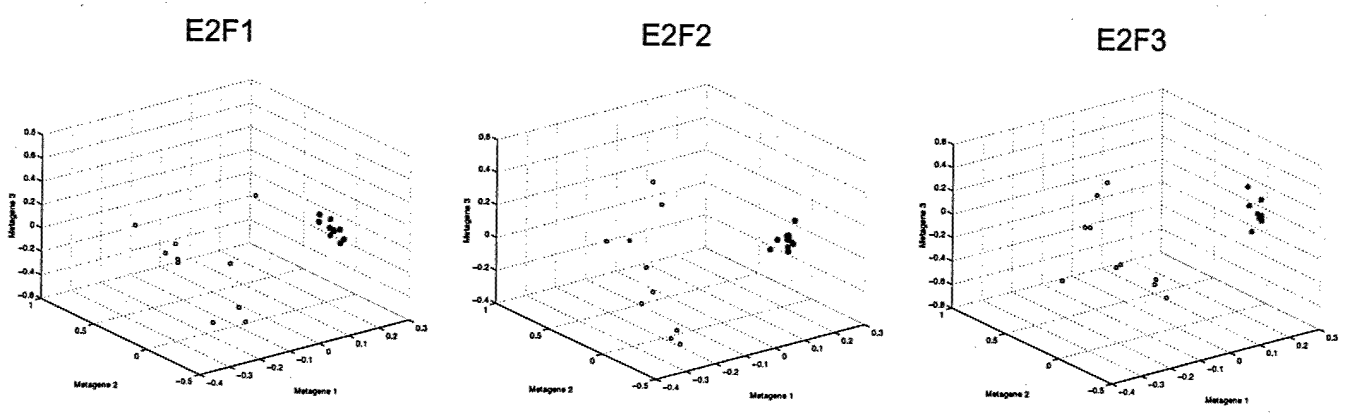
E2F1
E2F2
E2F3
Metagene 3
Metagene 2
Metagene 1

**B.**

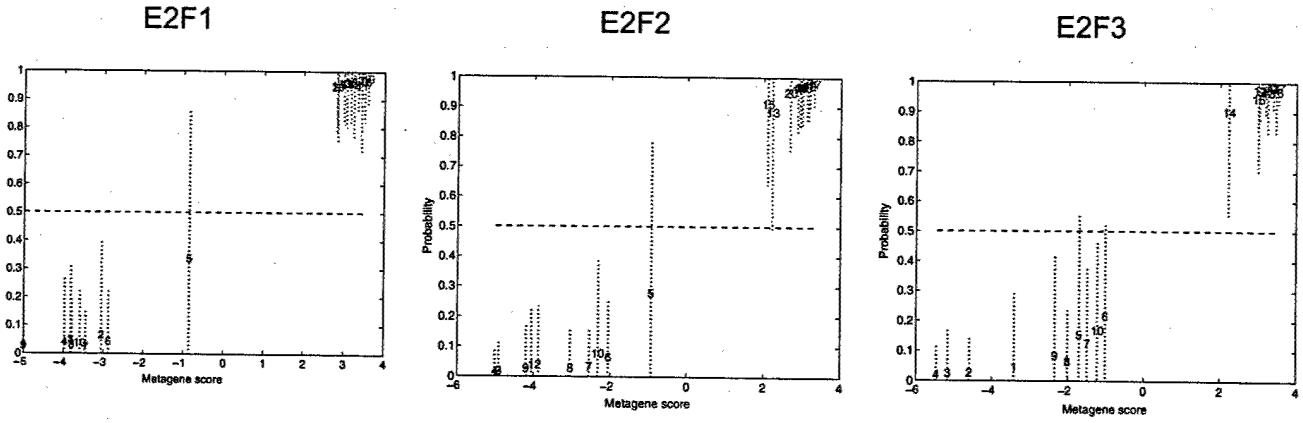
E2F1
E2F2
E2F3
Probability
Metagene score

**Figure 4. Expression patterns of discriminating genes.**

**A.** Expression levels for Ras and Myc discriminating genes. The expression values are depicted by color coding with black representing the lowest level, followed by red, orange, yellow, and then white as the highest level of expression (color scale shown on the right). Each column in the figure represents all 200 genes from an individual sample which are grouped according to control and Ras or Myc expressing cells. Each row represents an individual gene, ordered from top to bottom according to regression coefficients. The values for each gene depict standardized expression values (the mean value for each gene across all samples is subtracted from each value and then divided by the standard deviation).

**B.** Expression levels for E2F discriminating genes. The details of the plots are the same as in panel A.

**A.**

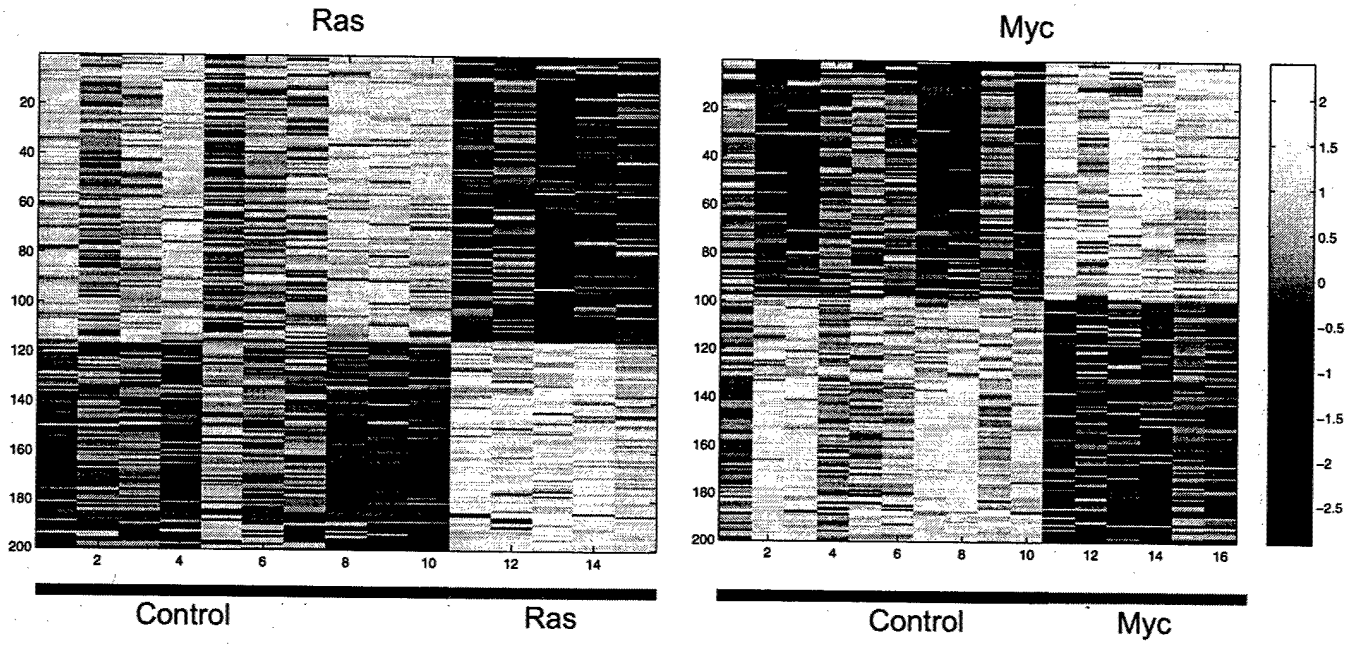
Ras
Myc
Control
Ras
Control
Myc

**B.**

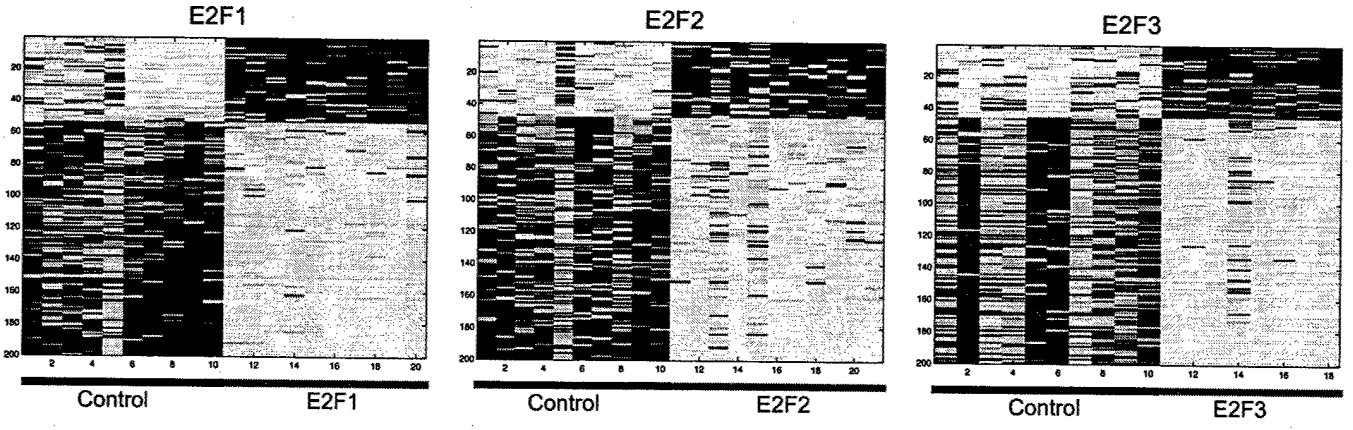
E2F1
E2F2
E2F3
Control
E2F1
Control
E2F2
Control
E2F3

**Figure 5. Gene expression profiles can discriminate E2F expressing cells.**

**A.** Metagene plot of E2F1 (red), E2F2 (blue), and E2F3 (green) experiments with metagenes derived from a gene set of 128 previously published E2F targets [2,21,22,26,27].

**B.** Metagene plot of E2F1, E2F2, and E2F3 experiments with metagenes derived from an objective correlation screen of 128 genes selected in pairwise comparisons between E2F experiments versus controls.

**A.**

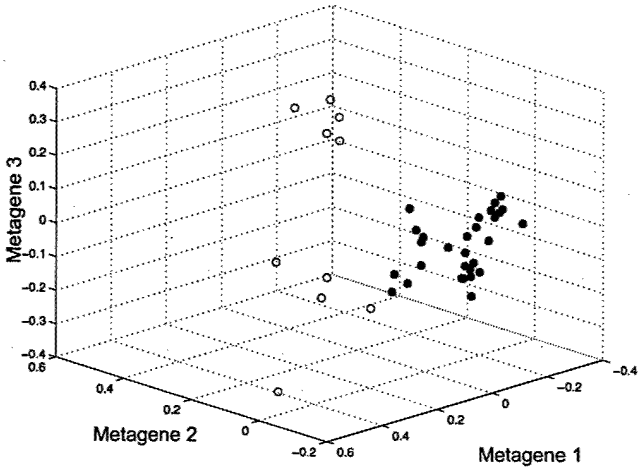
Metagene 3
0.4
0.3
0.2
0.1
0
−0.1
−0.2
−0.3
−0.4
0.6
0.4
0.2
0
−0.2
Metagene 2
0.6
0.4
0.2
0
−0.2
−0.4
Metagene 1

**B.**

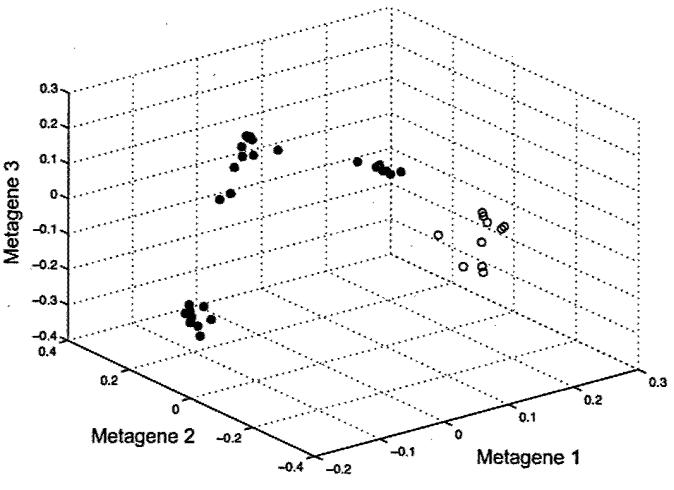
Metagene 3
0.3
0.2
0.1
0
−0.1
−0.2
−0.3
−0.4
0.4
0.2
0
−0.2
−0.4
Metagene 2
−0.2
−0.1
0
0.1
0.2
0.3
Metagene 1

**Figure 6. Gene expression profiles predict the activity of oncogenic pathways by cross-validation analysis.**

**A.** Ras and Myc prediction. One-at-a-time cross-validation predictions of classification probabilities for training cases from the factor regression analysis. The values on the horizontal axis are estimates of the overall factor scores in the regression. The corresponding values on the vertical axis are estimated classification probabilities with corresponding 90% probability intervals marked as dashed lines to indicate uncertainty about these estimated values. The analysis and predictions for each sample are based on the screened subset of 200 most discriminatory genes. The control samples are blue and the Ras or Myc samples are red.

**B.** E2F prediction. The analyses are the same as those described in panel A.

**A.**

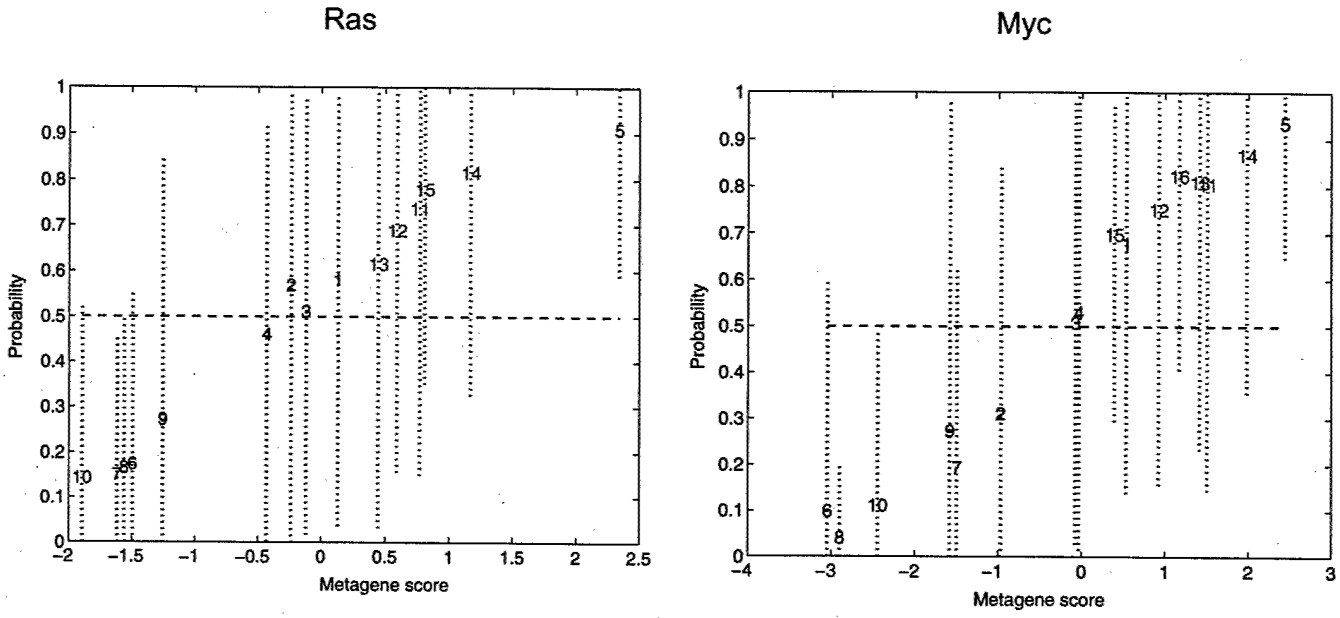
Ras
Myc
Probability
Metagene score

**B.**

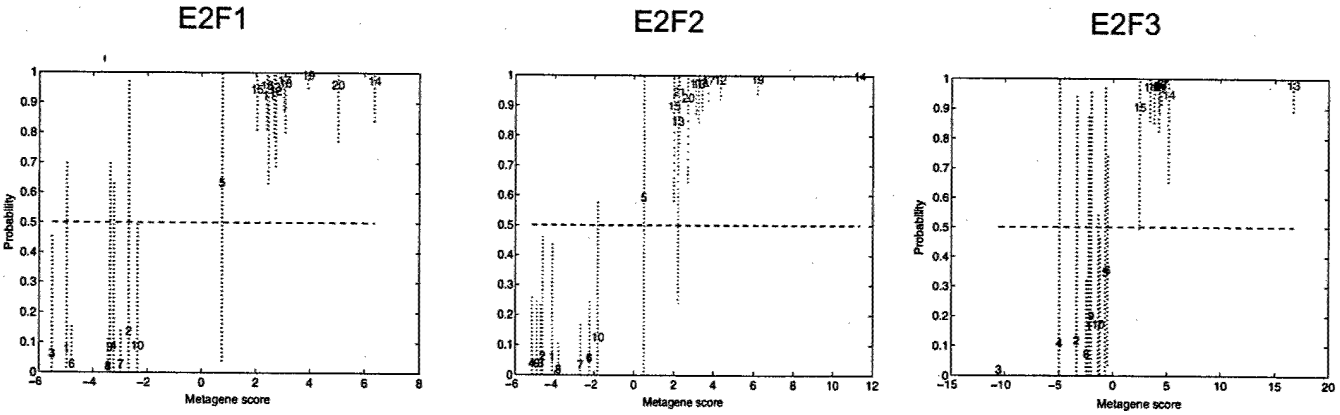
E2F1
E2F2
E2F3
Probability
Metagene score

**Figure 7. Prediction of gene activation pathways following stimulation of cell growth.**

**A.** Ras and Myc analysis. Ten traces for Ras and Myc representing 10 simulations of 34,000 Monte Carlo Markov Chain (MCMC) iterations each. Note that each predictive model represents a prediction of a distribution of possibilities. Each simulation represents a "random walk" of 34,000 steps through the distribution of possibilities for a particular model.

**B.** E2F analysis. The analyses are the same as those described in panel A.

**A.**

Ras

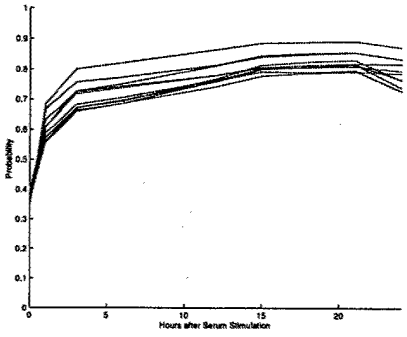


Myc

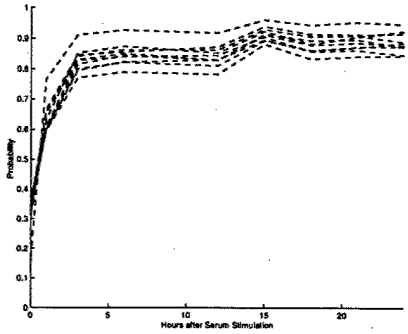


**B.**

E2F1

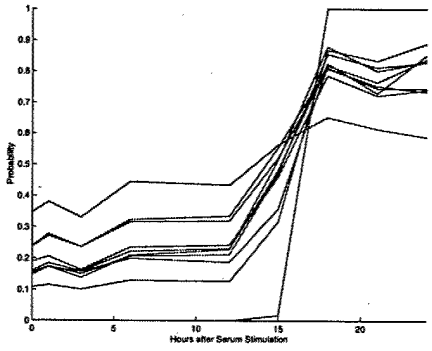


E2F2

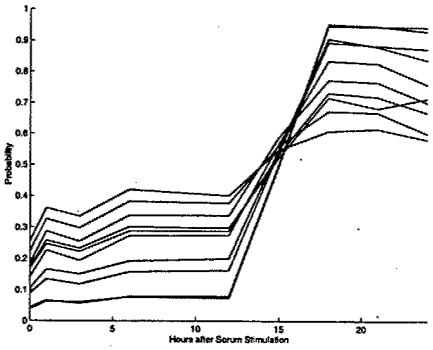


E2F3

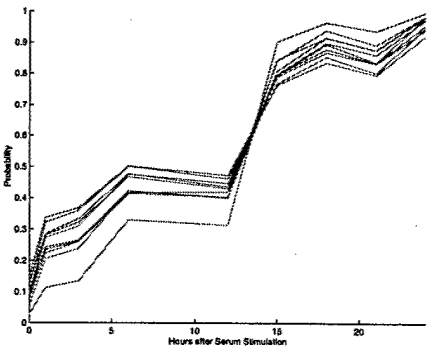

**Figure 8. Prediction of tumors that result from deregulation of Myc and Ras.**

**A.** Prediction of Myc activation in mouse tumor samples. RNA was prepared from a series of mouse mammary tumors that were derived from animals transgenic for the MMTV-Myc, MMTV-Ras, or MMTV-neu oncogenes. Hybridization was carried out the Mu11K GeneChips and analyzed as described in Methods. The results of the hybridization were then used in predictions of classification probabilities based on the trained pattern derived from the analysis of Myc expressing fibroblasts. The Myc tumors are indicated in red and the other tumors are in blue.

**B.** Prediction of Ras activation in mouse tumor samples. The results of the hybridizations described in panel A were used in predictions of classification probabilities based on the trained pattern derived from the analysis of Ras expressing fibroblasts. The Ras tumors are indicated in red and the other tumors are in blue. Tumors 34, 35, 36, and 37 are the Myc-expressing tumors.

A.

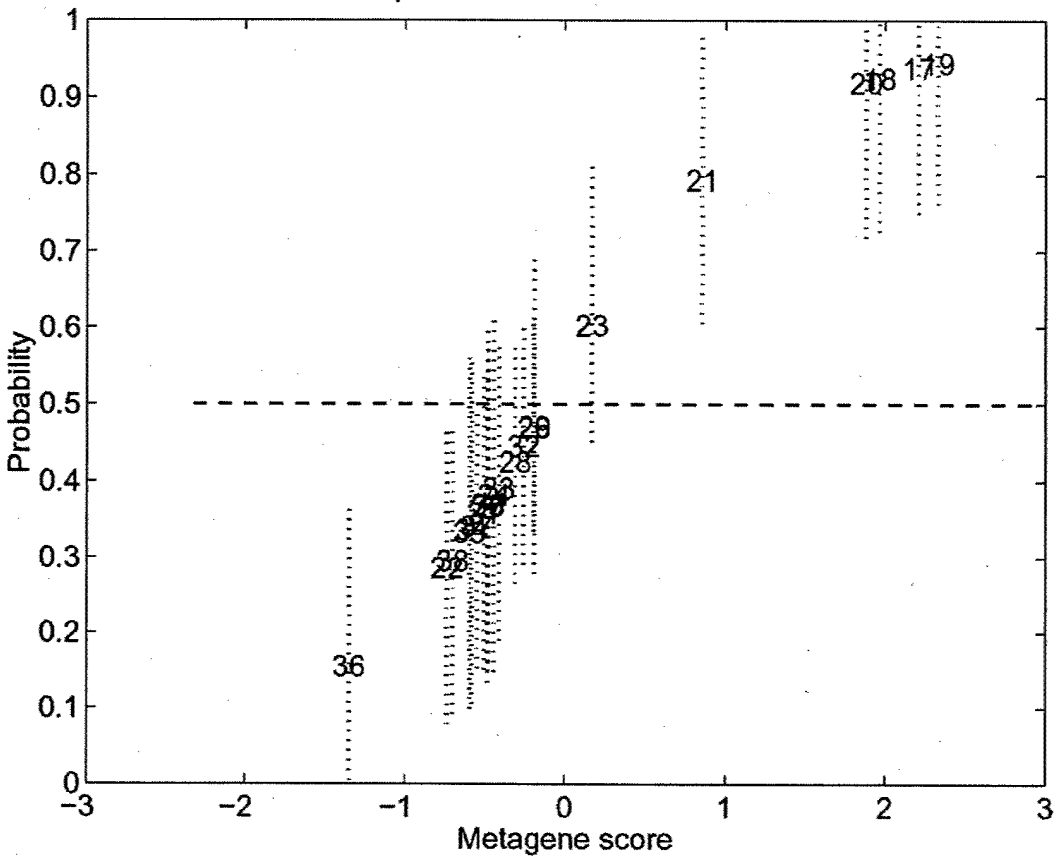
Probability
Metagene score
1
0.9
0.8
0.7
0.6
0.5
0.4
0.3
0.2
0.1
0
−3
−2
−1
0
1
2
3
21
23
36

B.

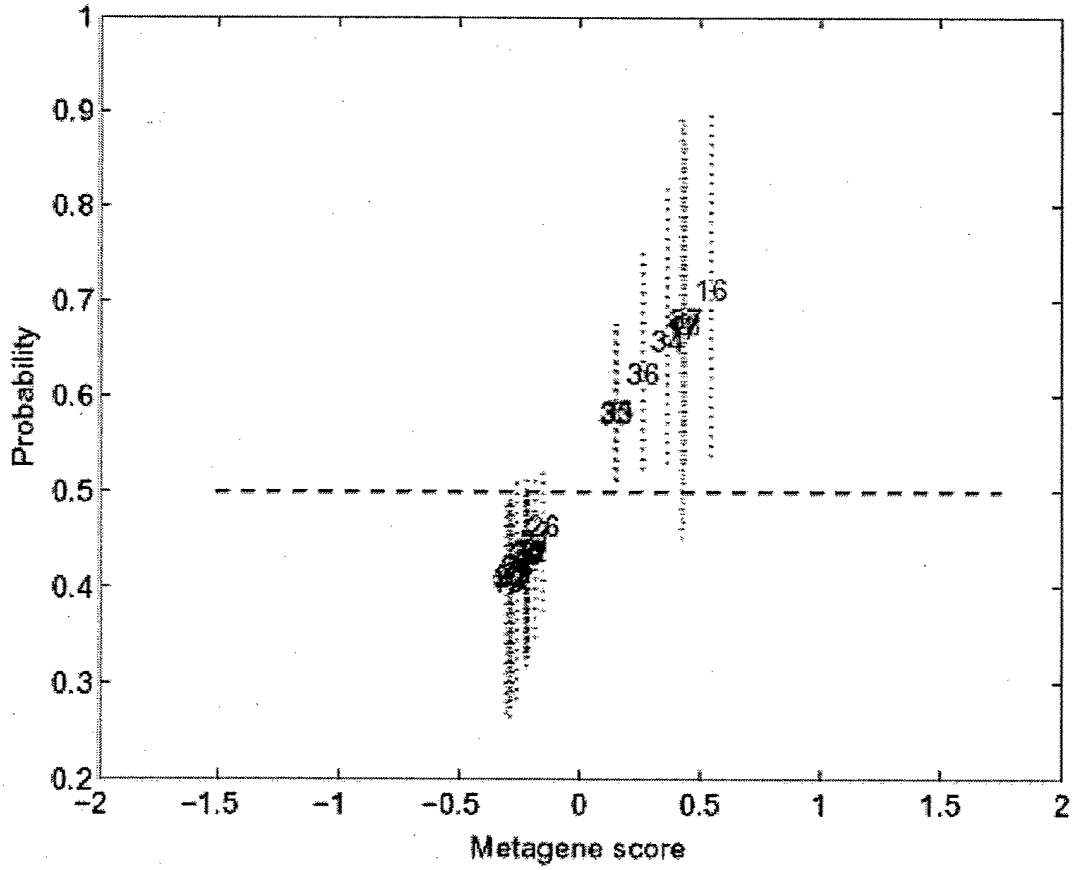
Probability
Metagene score
1
0.9
0.8
0.7
0.6
0.5
0.4
0.3
0.2
−2
−1.5
−1
−0.5
0
0.5
1
1.5
2
16
36

## Reference List


1. Cho,R.J. *et al.* A genome-wide transcriptional analysis of the mitotic cell cycle. *Mol. Cell* **2**, 65-73 (1998).

2. Ishida,S. *et al.* Role for E2F in the control of both DNA replication and mitotic functions as revealed from DNA microarray analysis. *Mol. Cell. Biol.* **21**, 4684-4699 (2001).

3. Cho,R.J. *et al.* Transcriptional regulation and function during the human cell cycle. *Nature Genetics* **27**, 48-54 (2001).

4. Iyer,V.R. *et al.* The transcriptional program in the response of human fibroblasts to serum. *Science* **283**, 83-87 (1999).

5. Spellman,P.T. *et al.* Comprehensive identification of cell cycle regulated genes of the yeast *Saccharomyces cerevisiae* by microarray hybridization. *Mol. Biol. Cell* **9**, 3273-3297 (1998).

6. Whitfield,M.L. *et al.* Identification of genes periodically expressed in the human cell cycle and their expression in tumors. *Mol. Biol. Cell* **in press**, (2002).

7. Golub,T.R. *et al.* Molecular classification of cancer: class discovery and class prediction by gene expression monitoring. *Science* **286**, 531-537 (1999).

8. Perou,C.M. *et al.* Molecular portraits of human breast tumors. *Nature* **406**, 747-752 (2000).

9. Ramaswamy,S. *et al.* Multiclass cancer diagnosis using tumor gene expression signatures. *Proc. Nat'l. Acad. Sci.* **98**, 15149-15154 (2001).

10. Su,A.I. *et al.* Molecular classification of human carcinomas by use of gene expression signatures. *Cancer Res* **61**, 7388-7393 (2001).

11. Alizadeh,A.A. *et al.* Distinct types of diffuse large B-cell lymphoma identified by gene expression profiling. *Nature* **403**, 503-511 (2000).

12. Perou,C.M. *et al.* Distinctive gene expression patterns in human mammary epithelial cells and breast cancers. *Proc. Natl. Acad. Sci. USA* **96**, 9212-9217 (1999).

13. Hedenfalk,I. *et al.* Gene expression profiles in hereditary breast cancer. *N. Engl. J. Med.* **344**, 539-548 (2001).

14. Bittner,M. *et al.* Molecular classification of cutaneous malignant melanoma by gene expression profiling. *Nature* **406**, 536-540 (2000).

15. van'T Veer,L.J. *et al.* Gene expression profiling predicts clinical outcome of breast cancer. *Nature* **415**, 530-536 (2002).

16. West,M. *et al.* Predicting the clinical status of human breast cancer by using gene expression profiles. *Proc. Natl. Acad. Sci. ,USA* **98**, 11462-11467 (2001).

17. Sherr,C.J. & Roberts,J.M. CDK inhibitors: positive and negative regulators of $G_1$-phase progression. *Genes & Dev.* **13**, 1501-1512 (1999).

18. Sherr,C.J. Cancer cell cycles. *Science* **274**, 1672-1677 (1996).

19. Dang,C.V. c-Myc target genes involved in cell growth, apoptosis, and metabolism. *Mol. Cell. Biol.* **19**, 1-11 (1999).

20. Coller,H.A. *et al.* Expression analysis with oligonucleotide microarrays reveals that MYC regulates genes involved in growth, cell cycle, signaling, and adhesion. *Proc Natl Acad Sci USA* **97**, 3260-3265 (2000).

21. Muller,H. *et al.* E2Fs regulate the expression of genes involved in differentiation, development, proliferation, and apoptosis. *Genes & Devel.* **15**, 267-285 (2001).

22. Polager,S., Kalma,Y., Berkovich,E. & Ginsberg,D. E2Fs up-regulate expression of genes involved in DNA replication, DNA repair and mitosis. *Oncogene* **21**, 437-446 (2002).

23. Alter,O., Brown,P.O. & Botstein,D. Singular value decomposition for genome-wide expression data processing and modeling. *Proc Natl Acad Sci USA* **97**, 10101-10106 (2000).

24. Holter,N.S., Cieplak,M.A., Fedoroff,N.V. & Banavar,J.R. Dynamic modeling of gene expression data. *Proc. Nat'l. Acad. Sci.* **98**, 1693-1698 (2001).

25. Holter,N.S. *et al.* Fundamental patterns underlying gene expression profiles: simplicity from complexity. *Proc Natl Acad Sci USA* **97**, 8409-8414 (2000).

26. Moroni,M.C. *et al.* Apaf-1 is a transcriptional target for E2F and p53. *Nat. Cell Biol.* **3**, 552-558 (2001).

27. Ma,Y., Croxton,R., Moorer,R.L. & Cress,W.D. Identification of novel E2F1-regulated genes by microarray. *Arch. Biochem. Biophys.* **399**, 212-224 (2002).

28. Wu,X. & Levine,A.J. p53 and E2F-1 cooperate to mediate apoptosis. *Proc. Natl. Acad. Sci. , USA* **91**, 3602-3606 (1994).

29. Kowalik,T.F., DeGregori,J., Schwarz,J.K. & Nevins,J.R. E2F1 overexpression in quiescent fibroblasts leads to induction of cellular DNA synthesis and apoptosis. *J. Virol.* **69**, 2491-2500 (1995).

30. DeGregori,J., Leone,G., Miron,A., Jakoi,L. & Nevins,J.R. Distinct roles for E2F proteins in cell growth control and apoptosis. *Proc. Natl. Acad. Sci. USA* **94**, 7245-7250 (1997).

31. Leone,G. *et al.* Myc requires distinct E2F activities to induce S phase and apoptosis. *Mol. Cell* **8**, 105-113 (2001).

32. Lin,W.-C., lin,F.-T. & Nevins,J.R. Selective induction of E2F1 in response to DNA damage, mediated by ATM-dependent phosphorylation. *Genes & Dev.* **15**, 1833-1845 (2001).

33. Leone,G. *et al.* E2F3 activity is regulated during the cell cycle and is required for the induction of S phase. *Genes & Dev.* **12**, 2120-2130 (1998).

34. Humbert,P.O. *et al.* E2f3 is critical for normal cellular proliferation. *Genes & Dev.* **14**, 690-703 (2000).

35. D'Crus,C.M. *et al.* c-MYC induces mammary tumorigenesis by means of a preferred pathway involving spontaneous Kras2 mutations. *Nature Med.* **7**, 235-239 (2001).

**Supplemental Data**

Table 1. Genes that provide Ras discrimination.

Table 2. Genes that provide Myc discrimination.

Table 3. Genes that provide E2F1 discrimination.

Table 4. Genes that provide E2F2 discrimination.

Table 5. Genes that provide E2F3 discrimination.

Huang Ms
September 25, 2002

## Table 1. Genes that provide Ras discrimination

| Weight | Acc. No. | Unigene ID | Unigene Description |
|---|---|---|---|
| 1.7064 | X16490 | Mm.5019 | serine (or cysteine) proteinase inhibitor, clade B (ovalbumin), member 2 |
| 1.5963 | X16389 | 0 | 0 |
| 1.5347 | AA057994 | Mm.23742 | nestin |
| 1.3624 | W33636 | Mm.27318 | Mus musculus mRNA for Rac3, complete cds |
| 1.2542 | AA057994 | Mm.23742 | nestin |
| 1.1897 | X02611 | Mm.1293 | tumor necrosis factor |
| -1.1625 | AA073283 | Mm.155714 | myosin heavy chain, cardiac muscle, fetal |
| -1.1611 | AA061050 | 0 | 0 |
| 1.1209 | X78545 | Mm.41979 | mast cell protease 8 |
| -1.1065 | AA142505 | Mm.27997 | RIKEN cDNA 2610020K06 gene |
| 1.0894 | M87861 | Mm.3337 | selectin, platelet |
| 1.0871 | J04423 | 0 | 0 |
| 1.0795 | M34381 | Mm.17031 | POU domain, class 5, transcription factor 1 |
| 1.0628 | AA038095 | 0 | 0 |
| -1.0366 | AA672929 | Mm.17872 | RIKEN cDNA 1110008P08 gene |
| -1.0302 | M96688 | Mm.14104 | potassium voltage-gated channel, shaker-related, subfamily, member 6 |
| 0.979 | AA060090 | 0 | 0 |
| 0.9489 | AA109910 | Mm.2779 | glycosylphosphatidylinositol specific phospholipase D1 |
| 0.8534 | AA144045 | Mm.638 | ESTs |
| 0.7811 | D44464 | Mm.4610 | uridine phosphorylase |
| -0.7752 | W54637 | 0 | 0 |
| 0.7427 | L15435 | 0 | 0 |
| 0.721 | M81445 | 0 | 0 |
| -0.7013 | Y08260 | Mm.22062 | cytoplasmic polyadenylation element binding protein |
| -0.6904 | L04961 | Mm.4095 | inactive X specific transcripts |
| -0.6652 | AA275273 | Mm.97986 | RIKEN cDNA 9130002C22 gene |
| 0.6381 | AA438003 | Mm.24581 | EST |
| 0.5795 | D30782 | Mm.4791 | epiregulin |
| 0.5476 | J04179 | Mm.4438 | high mobility group AT-hook 1 |
| 0.5079 | J04179 | Mm.4438 | high mobility group AT-hook 1 |
| 0.4971 | U39192 | 0 | 0 |
| 0.4863 | L07264 | Mm.4661 | heparin binding epidermal growth factor-like growth factor |
| 0.482 | AA673503 | Mm.21679 | RIKEN cDNA 1300002F13 gene |
| 0.4299 | Z31362 | Mm.1364 | neoplastic progression 3 |
| 0.4142 | M63658 | Mm.9336 | guanine nucleotide binding protein, beta 4 |
| 0.413 | AA673177 | Mm.195466 | EST AA673177 |
| -0.402 | AA521958 | Mm.131074 | RIKEN cDNA C030048H19 gene |
| -0.3915 | AF005885 | Mm.3527 | cyclin G2 |
| 0.3911 | AA184871 | Mm.1791 | dual specificity phosphatase 6 |
| 0.3892 | Z48043 | Mm.1614 | coagulation factor II (thrombin) receptor-like 1 |
| -0.3874 | D70842 | 0 | 0 |
| 0.3866 | L41352 | 0 | 0 |
| 0.3814 | W19040 | Mm.116819 | RIKEN cDNA 2410003M22 gene |
| 0.3754 | L39017 | Mm.3243 | protein C receptor, endothelial |
| 0.3642 | AA189300 | Mm.1911 | expressed sequence AA410048 |
| 0.3623 | AA608277 | Mm.200791 | expressed sequence AI605384 |
| 0.3549 | M64291 | Mm.3137 | prostaglandin-endoperoxide synthase 2 |
| 0.3527 | D64160 | Mm.196428 | retinoic acid early transcript 1, alpha |
| 0.3522 | X16151 | Mm.321 | secreted phosphoprotein 1 |
| 0.3475 | AA002759 | Mm.16234 | integrin alpha 5 (fibronectin receptor alpha) |
| -0.3464 | W29643 | Mm.182439 | TH1-like homolog (Drosophila) |
| 0.3406 | AA290110 | Mm.4438 | high mobility group AT-hook 1 |
| -0.3395 | D10630 | Mm.2760 | zinc finger proliferation 1 |
| 0.3356 | M73696 | Mm.16757 | solute carrier family 20, member 1 |
| 0.334 | C76481 | Mm.1359 | urokinase plasminogen activator receptor |
| -0.3339 | R74634 | Mm.214492 | DNA segment, Chr 10, Brigham & Women's Genetics 0791 expressed |
| -0.3299 | U03283 | Mm.4443 | cytochrome P450, 1b1, benz[a]anthracene inducible |
| 0.3242 | AA066782 | 0 | 0 |
| 0.3216 | AA529805 | Mm.142714 | progressive ankylosis |
| 0.3166 | AA163465 | Mm.142714 | progressive ankylosis |
| 0.3162 | M64403 | Mm.22288 | cyclin D1 |
| -0.3145 | AA238081 | Mm.24276 | complement component 1, r subcomponent |
| -0.3089 | M60523 | Mm.110 | inhibitor of DNA binding 3 |
| -0.3087 | D67076 | Mm.1421 | a disintegrin-like and metalloprotease (reprolysin type) with thrombospondin type 1 motif, 1 |
| -0.3086 | AA185999 | Mm.24003 | expressed sequence AW061234 |

| | | | |
|---|---|---|---|
| -0.3071 | AF017989 | Mm.19155 | secreted frizzled-related sequence protein 2 |
| 0.3036 | U40811 | 0 | 0 |
| -0.2987 | AA239576 | Mm.158 | expressed sequence AV253284 |
| 0.2983 | U37459 | Mm.4679 | glial cell line derived neurotrophic factor |
| -0.2963 | W71504 | 0 | 0 |
| -0.2961 | AA242620 | Mm.24276 | complement component 1, r subcomponent |
| -0.2896 | AA396006 | Mm.24441 | ESTs |
| 0.2866 | L24118 | Mm.4348 | tumor necrosis factor, alpha-induced protein 2 |
| -0.2829 | C77468 | Mm.158973 | RIKEN cDNA 3830403L08 gene |
| -0.2755 | AA138440 | Mm.28972 | expressed sequence T25534 |
| -0.2688 | AA259937 | Mm.147387 | procollagen, type III, alpha 1 |
| 0.2677 | L15443 | Mm.856 | transmembrane 4 superfamily member 1 |
| -0.2594 | X75018 | Mm.28223 | inhibitor of DNA binding 4 |
| -0.2565 | AA271049 | Mm.182194 | RIKEN cDNA 1190017B18 gene |
| 0.2555 | D89571 | Mm.3815 | syndecan 4 |
| -0.2532 | U77630 | Mm.1408 | adrenomedullin |
| 0.2511 | X69619 | Mm.8042 | inhibin beta-A |
| -0.244 | AA203807 | Mm.27168 | ESTs, Moderately similar to COTE_HUMAN COTE1 PROTEI [H.sapiens] |
| -0.2439 | AA122778 | Mm.25142 | RIKEN cDNA 5133400A03 gene |
| 0.2424 | X51834 | 0 | 0 |
| -0.2416 | U29156 | Mm.35677 | epidermal growth factor receptor pathway substrate 15, related sequence |
| -0.2364 | AF017175 | Mm.18522 | carnitine palmitoyltransferase 1, liver |
| -0.2339 | AA518955 | Mm.25306 | RAB9, member RAS oncogene family |
| 0.2335 | L42293 | Mm.28099 | sterol O-acyltransferase 1 |
| -0.2334 | C80548 | Mm.46856 | PRKC, apoptosis, WT1, regulator |
| 0.2318 | X74438 | Mm.2902 | protein tyrosine phosphatase, receptor-type, N |
| -0.229 | X57413 | Mm.18213 | transforming growth factor, beta 2 |
| 0.2282 | U07634 | Mm.2581 | Eph receptor A2 |
| 0.2265 | X65026 | Mm.33575 | guanine nucleotide binding protein, related sequence 1 |
| -0.2244 | C79593 | Mm.197970 | expressed sequence C79593 |
| -0.2243 | C78036 | Mm.21834 | origin recognition complex, subunit 4 |
| -0.2234 | AA210301 | Mm.24383 | Mus musculus, Similar to ubiquitin specific protease 20, clone IMAGE:3491447 |
| 0.2226 | X80685 | 0 | 0 |
| -0.222 | AA407796 | Mm.195194 | EST AA407796 |
| -0.222 | L39790 | 0 | 0 |
| -0.2207 | AA198370 | Mm.27579 | RIKEN cDNA 2900062L11 gene |
| 0.2161 | M63245 | Mm.19143 | aminolevulinic acid synthase 1 |
| 0.2156 | M22326 | Mm.181959 | early growth response 1 |
| -0.2135 | AA462551 | Mm.29588 | Mus musculus, Similar to mitogen-activated protein kinase kinase kinase kinase 3 |
| 0.2112 | D16497 | 0 | 0 |
| 0.2086 | D17571 | Mm.3863 | P450 (cytochrome) oxidoreductase |
| -0.2082 | L76193 | Mm.9122 | paraoxonase 3 |
| 0.2055 | AA544120 | Mm.27982 | ESTs |
| -0.2038 | AA184967 | Mm.24098 | ESTs, Weakly similar to A48830 probable transcription regulator NT fin12 - mouse |
| -0.2021 | L05439 | 0 | 0 |
| -0.201 | AA543871 | Mm.183116 | RIKEN cDNA 2310043N10 gene |
| -0.1966 | U13371 | Mm.1314 | kidney cell line derived transcript 1 |
| -0.1937 | X77557 | Mm.4525 | cadherin 11 |
| -0.1928 | U58883 | Mm.29030 | SH3 domain protein 5 |
| 0.1913 | M24843 | Mm.35692 | interleukin 1 receptor-like 1 |
| -0.1884 | AA472085 | Mm.31198 | expressed sequence AI585793 |
| 0.1877 | W44201 | Mm.190436 | RIKEN cDNA 2010012F05 gene |
| -0.1871 | AA105257 | Mm.37415 | RIKEN cDNA 1200009F10 gene |
| 0.1866 | C78306 | Mm.27454 | phosphoribosyl pyrophosphate synthetase 1 |
| -0.186 | U96441 | Mm.49224 | numb-like |
| -0.1857 | AA529994 | Mm.150686 | RIKEN cDNA 1110013J05 gene |
| -0.1849 | AA509429 | Mm.21145 | Leman coiled-coil protein |
| -0.1841 | AA271327 | Mm.28422 | expressed sequence C78339 |
| -0.1829 | M32745 | Mm.1291 | transforming growth factor, beta 3 |
| -0.1798 | AA119661 | Mm.214959 | expressed sequence C79734 |
| -0.1775 | U43512 | Mm.7524 | dystroglycan 1 |
| 0.1769 | L15447 | Mm.4633 | small nuclear ribonucleoprotein polypeptide A |
| -0.174 | AA542171 | Mm.100399 | MAD homolog 4 (Drosophila) |
| 0.174 | X66473 | Mm.5022 | matrix metalloproteinase 13 |
| 0.1725 | AA009169 | Mm.24632 | expressed sequence C76800 |
| -0.1722 | M13964 | Mm.197522 | GNAS (guanine nucleotide binding protein, alpha stimulating) complex locus |
| -0.1714 | M25825 | Mm.1948 | t-complex testis expressed 1 |
| -0.1698 | C79136 | Mm.7089 | necdin |
| -0.1687 | D37790 | Mm.182628 | RAD21 homolog (S. pombe) |

| | | | |
|---|---|---|---|
| 0.1679 | AA217614 | Mm.1196 | expressed sequence AW536703 |
| -0.1648 | U20365 | 0 | 0 |
| 0.1648 | U36277 | Mm.8884 | nuclear factor of kappa light chain gene enhancer in B-cells inhibitor, alpha |
| -0.1647 | U73039 | Mm.784 | next to the Brca1 |
| -0.1646 | AA692530 | Mm.6636 | expressed sequence C81333 |
| -0.1642 | AA170292 | Mm.27493 | expressed sequence C78303 |
| -0.1623 | AA109189 | Mm.206757 | RIKEN cDNA 4933439C20 gene |
| -0.1615 | AA600607 | Mm.6375 | glycogenin 1 |
| 0.1598 | AA163080 | Mm.24565 | translocase of inner mitochondrial membrane 23 homolog (yeast) |
| -0.1592 | AA285722 | Mm.24505 | RIKEN cDNA 1110068L01 gene |
| -0.1583 | AA645217 | Mm.171292 | RIKEN cDNA 2010200I23 gene |
| -0.1579 | AA175557 | Mm.28697 | RIKEN cDNA 2310032D16 gene |
| -0.1573 | D50463 | Mm.15125 | stromal cell derived factor receptor 1 |
| 0.1569 | AA529056 | Mm.25547 | RIKEN cDNA 0610037B21 gene |
| -0.1565 | M97636 | Mm.36894 | transcription factor 12 |
| 0.1552 | X64414 | Mm.3213 | low density lipoprotein receptor |
| -0.1535 | C76068 | 0 | 0 |
| -0.1534 | AA120290 | Mm.18048 | Mus musculus, Similar to zinc finger protein ANC_2H01, clone MGC:7348 |
| 0.1524 | AB006714 | Mm.22695 | collapsin response mediator protein 1 |
| 0.152 | D86177 | Mm.87521 | phosphatidylinositol-4-phosphate 5-kinase, type 1 beta |
| -0.1506 | U49385 | Mm.2065 | cytidine 5'-triphosphate synthase 2 |
| -0.1485 | AA032557 | Mm.21251 | deleted in polyposis 1 |
| -0.1478 | L38971 | Mm.193 | integral membrane protein 2A |
| -0.1466 | AA003541 | Mm.34218 | ESTs, Weakly similar to CHK2 MOUSE SERINE/THREONINE-PROTEIN KINASE CHK2 |
| 0.1448 | AA590060 | Mm.26973 | RIKEN cDNA 2810453H10 gene |
| -0.1419 | AA174677 | Mm.25715 | expressed sequence AW226533 |
| -0.1395 | AF033565 | Mm.147641 | CDC-like kinase 3 |
| 0.138 | AA266126 | Mm.200595 | RIKEN cDNA 5930426I11 gene |
| -0.1373 | AA217805 | Mm.26610 | RIKEN cDNA 3110027H23 gene |
| 0.136 | AA035912 | Mm.46513 | RIKEN cDNA 2610200G18 gene |
| -0.1347 | R74783 | Mm.21655 | expressed sequence R74783 |
| -0.1346 | AA254369 | Mm.7241 | solute carrier family 2, (facilitated glucose transporter), member 8 |
| -0.1343 | M60474 | Mm.30059 | myristoylated alanine rich protein kinase C substrate |
| -0.1336 | AA138853 | Mm.23222 | nuclear autoantigen |
| -0.1321 | AA119226 | Mm.21735 | RIKEN cDNA 2310043O08 gene |
| -0.1307 | AA163314 | Mm.29816 | programmed cell death 6 interacting protein |
| -0.1301 | AA467677 | Mm.10160 | expressed sequence AA960172 |
| -0.13 | AF023463 | Mm.27066 | phytanoyl-CoA hydroxylase |
| -0.1264 | AA647562 | Mm.6766 | RIKEN cDNA 5031439A09 gene |
| -0.1263 | AA177675 | Mm.140508 | tripartite motif protein 11 |
| -0.121 | AA021812 | Mm.3124 | RIKEN cDNA 3110015B12 gene |
| 0.1203 | C79315 | Mm.10665 | Mus musculus, clone IMAGE:3498496, mRNA, partial cds |
| 0.1182 | AA608073 | Mm.203905 | expressed sequence AU021838 |
| 0.1156 | C78980 | Mm.195261 | DNA segment, Chr 4, ERATO Doi 220, expressed |
| -0.1138 | AA174604 | Mm.27357 | expressed sequence AI875733 |
| -0.1105 | AA238064 | Mm.24216 | retinoblastoma binding protein 9 |
| -0.1087 | AA050769 | 0 | 0 |
| -0.1053 | D13003 | Mm.4876 | reticulocalbin |
| -0.1045 | AA571530 | Mm.102496 | Nedd4 WW binding protein 5 |
| 0.1017 | AA415044 | Mm.198690 | expressed sequence AA415044 |
| -0.1005 | W41773 | Mm.100113 | ribosomal protein 10 |
| -0.0979 | U20344 | Mm.4325 | Kruppel-like factor 4 (gut) |
| -0.0899 | AA189279 | Mm.22438 | single-stranded DNA binding protein 2 |
| -0.0871 | M85235 | Mm.37835 | ribosomal protein L7 |
| 0.0852 | AA116403 | Mm.22428 | RIKEN cDNA 3110040D16 gene |
| 0.0839 | AA415488 | Mm.199834 | expressed sequence AA415488 |
| -0.0809 | X81987 | Mm.588 | ribosomal protein L6 |
| -0.079 | AA273845 | Mm.9925 | isocitrate dehydrogenase 1 (NADP+), soluble |
| -0.0789 | AA231126 | Mm.2204 | DNA segment, Chr 11, Brigham & Women's Genetics 1349 expressed |
| -0.0783 | U29396 | Mm.1620 | annexin A5 |
| -0.0773 | C81236 | Mm.219 | RIKEN cDNA 2310010M20 gene |
| -0.0698 | D28530 | Mm.4220 | protein tyrosine phosphatase, receptor type, S |
| 0.0678 | AA060150 | Mm.5240 | EST |
| -0.0665 | U27315 | Mm.16228 | solute carrier family 25 (mitochondrial carrier; adenine nucleotide translocator), member 4 |
| -0.0628 | W41883 | Mm.142729 | thymosin, beta 4, X chromosome |
| -0.06 | X05021 | Mm.142380 | ribosomal protein L27a |

## Table 2. Genes that provide Myc discrimination

| Weight | Acc. No. | Unigene ID | Unigene Description |
|---|---|---|---|
| -2.5079 | D00466 | 0 | 0 |
| 2.4145 | AA109912 | Mm.30246 | CD151 antigen |
| -2.3723 | U04827 | 0 | 0 |
| -2.1344 | AA035870 | Mm.29658 | RIKEN cDNA 9430096L06 gene |
| -1.9986 | AA271199 | Mm.31255 | Notch gene homolog 1, (Drosophila) |
| 1.8607 | AA097203 | Mm.200406 | RIKEN cDNA 2700022N21 gene |
| -1.7896 | AA426790 | Mm.29343 | deltex 2 homolog (Drosophila) |
| 1.7886 | X63099 | Mm.90003 | gap junction membrane channel protein beta 3 |
| -1.7622 | AA386901 | Mm.22554 | hypothetical protein BC003945 |
| 1.7332 | L00039 | 0 | 0 |
| -1.7287 | AA009039 | Mm.196498 | RIKEN cDNA 1810010N17 gene |
| -1.6342 | W76686 | 0 | 0 |
| -1.6064 | C81509 | Mm.6047 | RIKEN cDNA 2410002E02 gene |
| 1.5951 | C78700 | Mm.35569 | EST C77459 |
| -1.5308 | AA562600 | Mm.66489 | DNA segment, Chr 14, ERATO Doi 114, expressed |
| -1.5013 | L04961 | Mm.4095 | inactive X specific transcripts |
| -1.4151 | AA140446 | Mm.1585 | transmembrane 7 superfamily member 1 |
| 1.3904 | W62503 | Mm.29460 | adenylate kinase 2 |
| 1.3852 | AA033369 | Mm.29391 | RIKEN cDNA 1110007F23 gene |
| -1.3669 | U78048 | Mm.7106 | bone morphogenic protein receptor, type II (serine/threonine kinase) |
| -1.3397 | D88159 | Mm.1482 | potassium inwardly-rectifying channel, subfamily J, member 8 |
| 1.2794 | L04678 | Mm.21117 | integrin beta 4 |
| -1.2701 | AA153032 | Mm.447 | expressed sequence AI447904 |
| -1.2603 | AA689927 | Mm.29321 | RIKEN cDNA 9430098E02 gene |
| 1.2548 | ET61132 | 0 | 0 |
| -1.2257 | AA409992 | Mm.213991 | ESTs, Highly similar to KIAA0713 protein [H.sapiens] |
| -1.2241 | N28086 | Mm.507 | DNA segment, Chr 8, Brigham & Women's Genetics 1414 expressed |
| 1.2209 | W29785 | 0 | 0 |
| 1.1545 | W17532 | 0 | 0 |
| 1.119 | ET63083 | 0 | 0 |
| -1.1045 | D82866 | Mm.16347 | prepronociceptin |
| 0.9959 | AA124170 | 0 | 0 |
| 0.8827 | M95525 | 0 | 0 |
| 0.8684 | C78047 | Mm.143774 | RAN guanine nucleotide release factor |
| -0.7241 | M84607 | Mm.2924 | platelet derived growth factor receptor, alpha polypeptide |
| -0.6279 | AA170668 | Mm.532 | ESTs, Weakly similar to B Chain B, Human Acyl Protein Thioesterase 1 |
| -0.6145 | W10491 | 0 | 0 |
| -0.611 | U34042 | Mm.5076 | tolloid-like |
| 0.6104 | U53546 | Mm.78861 | nucleolar and coiled-body phosphoprotein 1 |
| -0.6068 | AA274696 | Mm.2958 | expressed sequence AI843786 |
| -0.6065 | W83326 | Mm.28827 | expressed sequence AI463271 |
| 0.602 | X84789 | Mm.4742 | proliferation-associated 2G4, 38kD |
| -0.5838 | U96700 | Mm.3368 | serine protease inhibitor 6 |
| 0.5649 | AA466758 | Mm.29394 | RIKEN cDNA 2410008J01 gene |
| 0.5634 | C76683 | Mm.35801 | expressed sequence C76683 |
| 0.5511 | D87911 | Mm.2141 | proteaseome (prosome, macropain) 28 subunit, 3 |
| -0.5446 | AA462551 | Mm.29588 | Mus musculus, Similar to mitogen-activated protein kinase kinase kinase kinase 3 |
| -0.5423 | X99572 | Mm.3983 | c-fos induced growth factor |
| -0.5336 | X70398 | Mm.4919 | DNA segment, human D4S114 |
| -0.5333 | AA138440 | Mm.28972 | expressed sequence T25534 |
| 0.5264 | AA672475 | Mm.27871 | RIKEN cDNA 2610012O22 gene |
| -0.526 | X57413 | Mm.18213 | transforming growth factor, beta 2 |
| -0.5229 | AA285607 | Mm.27624 | RIKEN cDNA C530002L11 gene |
| 0.5127 | AA409134 | Mm.27853 | DNA segment, Chr 7, Wayne State University 180, expressed |
| 0.5117 | M33934 | Mm.6065 | inosine 5'-phosphate dehydrogenase 2 |
| 0.5073 | M14223 | Mm.99 | ribonucleotide reductase M2 |
| -0.505 | X75018 | Mm.28223 | inhibitor of DNA binding 4 |
| 0.5009 | L19311 | Mm.10 | spermidine synthase |
| 0.4989 | AF018262 | Mm.3294 | protein phosphatase 5, catalytic subunit |
| 0.4973 | U43918 | Mm.4742 | proliferation-associated 2G4, 38kD |
| 0.4883 | AA718288 | Mm.1643 | RIKEN cDNA 4632417K18 gene |
| 0.4873 | U85511 | Mm.1260 | expressed in non-metastatic cells 1, protein (NM23A) (nucleoside diphosphate kinase) |
| 0.486 | U64033 | Mm.18637 | teratocarcinoma expressed, serine rich |
| -0.4797 | AA271049 | Mm.182194 | RIKEN cDNA 1190017B18 gene |
| -0.4776 | M15525 | Mm.148395 | laminin B1 subunit 1 |

| | | | |
|---|---|---|---|
| -0.4757 | U22399 | Mm.168789 | cyclin-dependent kinase inhibitor 1C (P57) |
| -0.4736 | AA189487 | Mm.1927 | sushi-repeat-containing protein |
| 0.4724 | W53443 | Mm.30083 | RIKEN cDNA 2510015F01 gene |
| 0.4707 | L09192 | Mm.1845 | pyruvate decarboxylase |
| -0.469 | AA239576 | Mm.158 | expressed sequence AV253284 |
| -0.4664 | U19854 | Mm.180409 | ubiquitin-conjugating enzyme E2H |
| -0.4654 | AF004666 | Mm.4211 | solute carrier family 8 (sodium/calcium exchanger), member 1 |
| 0.4645 | D26091 | Mm.18923 | mini chromosome maintenance deficient 7 (S. cerevisiae) |
| 0.4625 | W08763 | Mm.4595 | fibrillarin |
| -0.4625 | AA475847 | Mm.7361 | RIKEN cDNA 4432411E13 gene |
| -0.4599 | D10630 | Mm.2760 | zinc finger proliferation 1 |
| 0.4574 | AA638408 | Mm.27545 | heterogeneous nuclear ribonucleoproteins methyltransferase-like 2 (S. cerevisiae) |
| -0.4544 | X53929 | Mm.1987 | decorin |
| 0.4532 | M13352 | 0 | 0 |
| -0.4501 | AA518955 | Mm.25306 | RAB9, member RAS oncogene family |
| -0.4484 | U03283 | Mm.4443 | cytochrome P450, 1b1, benz[a]anthracene inducible |
| -0.4444 | AA109109 | Mm.83615 | transient receptor protein 2 |
| -0.4406 | X70398 | Mm.4919 | DNA segment, human D4S114 |
| 0.4388 | AA470234 | Mm.203406 | expressed sequence AA470234 |
| -0.4375 | AA396006 | Mm.24441 | ESTs |
| 0.4345 | L19311 | Mm.10 | spermidine synthase |
| -0.433 | D16847 | 0 | 0 |
| 0.4321 | U85207 | 0 | 0 |
| 0.4318 | C78306 | Mm.27454 | phosphoribosyl pyrophosphate synthetase 1 |
| 0.4315 | C81007 | Mm.99 | ribonucleotide reductase M2 |
| -0.4282 | U73039 | Mm.784 | next to the Brca1 |
| 0.4222 | AA123463 | Mm.28805 | SET translocation |
| 0.4148 | L32836 | Mm.2573 | S-adenosylhomocysteine hydrolase |
| -0.4094 | AA174677 | Mm.25715 | expressed sequence AW226533 |
| -0.4046 | U33630 | Mm.4734 | myeloid ecotropic viral integration site 1 |
| 0.4016 | X78682 | Mm.2355 | prohibitin |
| 0.4002 | C81593 | Mm.99 | ribonucleotide reductase M2 |
| 0.3974 | W17411 | Mm.196607 | eukaryotic translation initiation factor 5a |
| 0.3963 | AA672939 | Mm.199839 | expressed sequence AA672939 |
| 0.3953 | U63648 | Mm.147946 | MYB binding protein (P160) 1a |
| -0.3937 | AA117532 | Mm.28258 | RIKEN cDNA 1500016L11 gene |
| 0.3912 | D13544 | Mm.2903 | DNA primase, p49 subunit |
| -0.3912 | U79523 | Mm.5121 | peptidylglycine alpha-amidating monooxygenase |
| -0.3906 | AA271327 | Mm.28422 | expressed sequence C78339 |
| -0.3891 | AF005885 | Mm.3527 | cyclin G2 |
| -0.388 | AA254520 | Mm.1568 | granulin |
| 0.385 | C79315 | Mm.10665 | Mus musculus, clone IMAGE:3498496, mRNA, partial cds |
| -0.3825 | U22399 | Mm.168789 | cyclin-dependent kinase inhibitor 1C (P57) |
| 0.3805 | U77415 | Mm.4283 | block of proliferation 1 |
| -0.3794 | AA542171 | Mm.100399 | MAD homolog 4 (Drosophila) |
| -0.3775 | D14636 | Mm.4509 | runt related transcription factor 2 |
| -0.3764 | Z30970 | Mm.4871 | tissue inhibitor of metalloproteinase 3 |
| 0.3761 | U04674 | Mm.1013 | ligase I, DNA, ATP-dependent |
| -0.3746 | U25096 | Mm.26938 | Kruppel-like factor 2 (lung) |
| 0.3732 | Z22593 | Mm.4595 | fibrillarin |
| 0.3729 | AA051298 | 0 | 0 |
| -0.3673 | U13371 | Mm.1314 | kidney cell line derived transcript 1 |
| -0.3608 | U75215 | Mm.6379 | solute carrier family 1 (glutamate/neutral amino acid transporter), member 4 |
| 0.357 | AA002550 | 0 | 0 |
| 0.3562 | AJ001101 | Mm.30049 | complement component 1, q subcomponent binding protein |
| -0.3538 | Y08135 | Mm.2379 | acid sphingomyelinase-like phosphodiesterase 3a |
| -0.3537 | C78582 | Mm.6772 | EST C78582 |
| -0.3535 | AA204042 | Mm.22704 | guanine nucleotide binding protein, alpha inhibiting 3 |
| -0.3531 | Z31326 | Mm.21396 | Mus musculus, Similar to APP-binding protein 1, clone MGC:29435 IMAGE:3711115, mRNA |
| -0.3531 | AA259937 | Mm.147387 | procollagen, type III, alpha 1 |
| -0.3507 | AA185999 | Mm.24003 | expressed sequence AW061234 |
| 0.3504 | AA638408 | Mm.27545 | heterogeneous nuclear ribonucleoproteins methyltransferase-like 2 (S. cerevisiae) |
| 0.349 | X55038 | 0 | 0 |
| -0.3481 | M38381 | Mm.1761 | CDC-like kinase |
| 0.3467 | AA408501 | Mm.202767 | expressed sequence AA408257 |
| 0.3456 | C78306 | Mm.27454 | phosphoribosyl pyrophosphate synthetase 1 |
| -0.3446 | AA416197 | Mm.70667 | Mus musculus, Similar to oxidation resistance 1, clone MGC:7295 IMAGE:3485394 |
| 0.343 | U12273 | 0 | 0 |
| -0.3405 | AA138853 | Mm.23222 | nuclear autoantigen |

| | | | |
|---|---|---|---|
| -0.3402 | AA472085 | Mm.31198 | expressed sequence AI585793 |
| 0.3396 | AA407024 | Mm.30242 | RIKEN cDNA 4930564J03 gene |
| -0.3386 | AA217805 | Mm.26610 | RIKEN cDNA 3110027H23 gene |
| 0.3366 | X62154 | Mm.4502 | mini chromosome maintenance deficient (S. cerevisiae) |
| 0.3358 | X07699 | 0 | 0 |
| -0.3353 | M31131 | Mm.14897 | cadherin 2 |
| -0.3334 | U69176 | Mm.2399 | laminin, alpha 4 |
| 0.333 | W29198 | 0 | 0 |
| -0.3315 | AA238056 | Mm.25154 | Wilms' tumour 1-associating protein |
| -0.3304 | AA145127 | Mm.46316 | serine (or cysteine) proteinase inhibitor, clade B (ovalbumin), member 1a |
| 0.3269 | AB001927 | Mm.2038 | Ras-GTPase-activating protein SH3-domain binding protein |
| -0.3269 | AA237686 | Mm.71015 | RIKEN cDNA 2700053F16 gene |
| 0.3262 | C78980 | Mm.195261 | DNA segment, Chr 4, ERATO Doi 220, expressed |
| -0.3254 | AA198370 | Mm.27579 | RIKEN cDNA 2900062L11 gene |
| -0.3251 | X96859 | Mm.1920 | ubiquitin-conjugating enzyme E2B, RAD6 homology (S. cerevisiae) |
| 0.3235 | AA008245 | Mm.12267 | Mus musculus adult male testis cDNA, RIKEN full-length enriched library, clone:4933407N23 |
| 0.3228 | U89876 | Mm.1886 | RNA and export factor binding protein 1 |
| -0.3203 | AA289470 | Mm.3350 | actin-crosslinking protein 7 |
| 0.3191 | AA563404 | Mm.205463 | ESTs, Highly similar to SL56_RAT SODIUM-DEPENDENT MULTIVITAMIN TRANSPORTER |
| 0.3176 | X72310 | Mm.925 | transcription factor Dp 1 |
| -0.3137 | AA174485 | Mm.21489 | expressed sequence AU021774 |
| 0.3135 | AA655934 | Mm.29906 | EBNA1 binding protein 2 |
| 0.3114 | Z11870 | Mm.7335 | cellular nucleic acid binding protein |
| -0.3113 | AA212898 | Mm.24383 | Mus musculus, Similar to ubiquitin specific protease 20, clone IMAGE:3491447 |
| 0.31 | AF004105 | Mm.16711 | mini chromosome maintenance deficient 2 (S. cerevisiae) |
| 0.3092 | L19737 | Mm.258 | ATP synthase, H+ transporting, mitochondrial F0 complex, subunit c (subunit 9), isoform 1 |
| -0.309 | AA174970 | Mm.2655 | quaking |
| 0.3076 | U43076 | Mm.4117 | cell division cycle 37 homolog (S. cerevisiae) |
| 0.3065 | L20509 | Mm.3576 | chaperonin subunit 3 (gamma) |
| 0.3016 | AA409164 | Mm.24506 | expressed sequence AA409164 |
| 0.2975 | X75316 | Mm.3865 | seb4-like (Xenopus laevis) |
| -0.2975 | AA231435 | Mm.200844 | expressed sequence AW557223 |
| 0.2971 | AA274628 | Mm.439 | DNA segment, Chr 9, Wayne State University 10, expressed |
| -0.2962 | AA203807 | Mm.27168 | ESTs, Moderately similar to COTE_HUMAN COTE1 PROTEI [H.sapiens] |
| 0.2955 | AA189300 | Mm.1911 | expressed sequence AA410048 |
| -0.293 | C79136 | Mm.7089 | necdin |
| -0.2924 | AA667371 | Mm.19310 | collagenous repeat-containing sequence |
| -0.2893 | AA509429 | Mm.21145 | Leman coiled-coil protein |
| -0.289 | U41765 | Mm.28908 | a disintegrin and metalloproteinase domain 9 (meltrin gamma) |
| 0.2882 | AA144078 | Mm.28420 | valyl-tRNA synthetase 2 |
| 0.2868 | AA395999 | Mm.28975 | RIKEN cDNA 2610312E17 gene |
| 0.2862 | AA408426 | Mm.209329 | EST AA408426 |
| 0.2859 | AA407116 | Mm.1248 | cell division cycle 45 homolog (S. cerevisiae)-like |
| 0.2807 | AA217614 | Mm.1196 | expressed sequence AW536703 |
| 0.2779 | AB000121 | Mm.18344 | proteasome (prosome, macropain) 26S subunit, ATPase 3, interacting protein |
| -0.2773 | U20344 | Mm.4325 | Kruppel-like factor 4 (gut) |
| -0.2744 | AA289858 | Mm.175173 | ribonuclease, RNase A family 4 |
| 0.2739 | AC002393 | 0 | 0 |
| 0.2738 | X17069 | Mm.12758 | FK506 binding protein 4 (59 kDa) |
| -0.2726 | X73230 | Mm.620 | arylsulfatase A |
| 0.2684 | D14336 | Mm.130322 | RNA polymerase I associated factor, 53 kD |
| 0.2677 | C79046 | Mm.7508 | breakpoint cluster region protein 1 |
| 0.2659 | AA038142 | 0 | 0 |
| 0.2652 | C77427 | Mm.27291 | bystin-like |
| -0.2651 | AA145471 | Mm.6710 | Rho-associated coiled-coil forming kinase 1 |
| -0.2651 | AA013647 | Mm.28463 | adaptor-related protein complex AP-3, delta subunit |
| 0.263 | AA561108 | Mm.6960 | thyroid hormone receptor interactor 13 |
| -0.263 | U05837 | 0 | 0 |
| 0.2624 | X53584 | Mm.1777 | heat shock protein, 60 kDa |
| -0.2611 | AA692530 | Mm.6636 | expressed sequence C81333 |
| 0.2601 | AA546285 | Mm.29032 | DNA segment, Chr 10, ERATO Doi 214, expressed |
| -0.2584 | AA265871 | Mm.25122 | expressed sequence AA408985 |
| 0.2582 | AA271603 | Mm.45433 | dim1 (S. pombe) |
| -0.2576 | M32486 | Mm.4992 | Mouse 19.5 mRNA |
| -0.2548 | AA387073 | Mm.202224 | expressed sequence AI159700 |
| 0.252 | C78820 | Mm.21671 | DNA segment, Chr 5, Wayne State University 45, expressed |

## Table 3. Genes that provide E2F1 discrimination

| Weight | Acc. No. | Unigene ID | Unigene Description |
|---|---|---|---|
| 0.7628 | AA039124 | Mm.16783 | phosphoglycerate mutase 1 |
| 0.7515 | AA052286 | 0 | 0 |
| -0.7408 | U48804 | 0 | 0 |
| 0.7375 | M90365 | Mm.21990 | junction plakoglobin |
| 0.7193 | AA122622 | Mm.22731 | integrin beta 4 binding protein |
| -0.6917 | AA717972 | Mm.154511 | expressed sequence C79379 |
| 0.6897 | W08455 | Mm.44240 | Mus musculus, Similar to hydroxyacyl glutathione hydrolase |
| -0.682 | AA596555 | Mm.28150 | splicing factor 3b, subunit 1, 155 kDa |
| 0.6724 | Z31238 | Mm.957 | COP9 (constitutive photomorphogenic) homolog, subunit 4 (Arabidopsis thaliana) |
| 0.6697 | AA267014 | Mm.8552 | baculoviral IAP repeat-containing 5 |
| -0.668 | U13878 | 0 | 0 |
| 0.666 | AA137667 | Mm.39046 | RIKEN cDNA 1110055E19 gene |
| 0.6633 | W99019 | Mm.30272 | RIKEN cDNA 1200003M11 gene |
| 0.6626 | U58203 | Mm.3181 | Rho guanine nucleotide exchange factor (GEF) 1 |
| 0.6553 | X17500 | Mm.3406 | transcription factor E2a |
| 0.653 | AA118363 | Mm.645 | stromal interaction molecule 1 |
| 0.6525 | X81581 | Mm.29254 | insulin-like growth factor binding protein 3 |
| 0.651 | AA727929 | Mm.196303 | RIKEN cDNA 4933413A04 gene |
| 0.6495 | D14566 | 0 | 0 |
| 0.6301 | U65735 | Mm.119162 | ELAV (embryonic lethal, abnormal vision, Drosophila)-like 1 (Hu antigen R) |
| 0.6273 | X56461 | Mm.215 | homeo box B6 |
| 0.6249 | AA137962 | Mm.196141 | RIKEN cDNA 2810475J17 gene |
| 0.6194 | W64561 | Mm.3360 | tyrosine 3-monooxygenase/tryptophan 5-monooxygenase activation protein, zeta polypeptide |
| 0.6175 | AA059517 | Mm.41787 | expressed in non-metastatic cells 4, protein (NM23-M4)(nucleoside diphosphate kinase) |
| 0.617 | W11020 | Mm.29455 | RIKEN cDNA 1810045K07 gene |
| 0.6154 | AA104912 | Mm.182563 | RIKEN cDNA 1110011F09 gene |
| 0.608 | AA008502 | 0 | 0 |
| 0.6048 | AA109912 | Mm.30246 | CD151 antigen |
| 0.5988 | AA140170 | Mm.206757 | RIKEN cDNA 4933439C20 gene |
| 0.5965 | AA137432 | Mm.15801 | lipocalin 7 |
| 0.596 | U28495 | Mm.7634 | lymphoid blast crisis-like 1 |
| -0.5924 | AA672846 | Mm.3146 | transcription factor 20 |
| 0.5884 | W75373 | Mm.29106 | RIKEN cDNA 1200017E13 gene |
| -0.5849 | AA168362 | Mm.28598 | Janus kinase 1 |
| 0.5833 | AA139094 | Mm.28984 | DNA segment, Chr 10, Johns Hopkins University 81 expressed |
| 0.583 | D89571 | Mm.3815 | syndecan 4 |
| 0.5816 | AA189586 | Mm.85892 | RIKEN cDNA 1110020A23 gene |
| 0.5764 | U37799 | Mm.4603 | scavenger receptor class B1 |
| 0.5729 | X83562 | Mm.4954 | sialyltransferase 8 (alpha-2, 8-sialytransferase) B |
| 0.5718 | X99963 | 0 | 0 |
| 0.5715 | AA014135 | 0 | 0 |
| 0.5698 | W49204 | Mm.24193 | glypican 1 |
| 0.5678 | AA103881 | Mm.10193 | G protein-coupled receptor kinase 6 |
| 0.5672 | X15666 | 0 | 0 |
| 0.5655 | U03715 | 0 | 0 |
| 0.5633 | AA008930 | Mm.18845 | superkiller viralicidic activity 2-like (S. cerevisiae ) |
| 0.5622 | AA681993 | Mm.6660 | small inducible cytokine A27 |
| 0.5616 | W50167 | 0 | 0 |
| 0.5613 | W50975 | 0 | 0 |
| -0.5596 | AA407629 | Mm.37835 | ribosomal protein L7 |
| -0.5594 | D31952 | 0 | 0 |
| 0.5582 | AA048098 | Mm.41881 | RIKEN cDNA 2900002K07 gene |
| 0.5559 | AA230396 | Mm.2478 | splicing factor, arginine/serine-rich 4 (SRp75) |
| 0.5552 | W64174 | Mm.30191 | RIKEN cDNA 2600013G09 gene |
| -0.5545 | M91243 | 0 | 0 |
| 0.5528 | AA154337 | Mm.2701 | DnaJ (Hsp40) homolog, subfamily B, member 6 |
| 0.5513 | AA217006 | Mm.2310 | open reading frame 6 |
| 0.5506 | W55419 | 0 | 0 |
| 0.5497 | AA221219 | Mm.29357 | RIKEN cDNA 1300017C10 gene |
| 0.5465 | AA105536 | Mm.25161 | sirtuin 2 (silent mating type information regulation 2, homolog) 2 (S. cerevisiae) |
| 0.5452 | AA500294 | Mm.21353 | ESTs, Weakly similar to HSJ2 MOUSE DNAJ PROTEIN HOMOLOG 2 [M.musculus] |
| -0.5451 | AA408681 | Mm.154979 | placental specific protein 1 |
| 0.5449 | AA080176 | Mm.23963 | phospholipase C, delta |
| 0.5443 | AA048413 | Mm.10154 | testis specific protein kinase 1 |
| 0.5436 | W65616 | Mm.37486 | RIKEN cDNA 2210023C10 gene |

| | | | |
|---|---|---|---|
| 0.5425 | W55211 | 0 | 0 |
| -0.5406 | U84207 | 0 | 0 |
| 0.54 | AA008831 | 0 | 0 |
| 0.5397 | AA124433 | Mm.6352 | expressed sequence AI449432 |
| -0.5387 | S80989 | 0 | 0 |
| 0.5357 | AA117227 | Mm.38450 | septin 9 |
| 0.5343 | AA002297 | Mm.16332 | ephrin A4 |
| 0.5296 | W55560 | 0 | 0 |
| 0.5294 | U22396 | Mm.4340 | zinc finger protein 100 |
| 0.5287 | M55154 | Mm.18843 | transglutaminase 2, C polypeptide |
| 0.5274 | AA184119 | Mm.27518 | Mus musculus catp mRNA for cation-transporting atpase, complete cds |
| 0.5258 | AA270586 | Mm.18561 | cysteine and histidine rich 1 |
| -0.5256 | ET61424 | 0 | 0 |
| 0.5224 | AA616577 | Mm.21884 | ESTs, Weakly similar to T14106 probable GTPase-activating protein SPA-1 - rat |
| 0.5213 | AA237297 | Mm.23869 | RIKEN cDNA 2510006M18 gene |
| -0.5191 | J04423 | 0 | 0 |
| -0.5179 | U03434 | Mm.14926 | ATPase, Cu++ transporting, alpha polypeptide |
| 0.5178 | C78700 | Mm.35569 | EST C77459 |
| 0.5176 | AA008228 | Mm.144235 | peroxisomal farnesylated protein |
| -0.5166 | L11065 | Mm.7977 | opioid receptor, kappa 1 |
| 0.515 | AA013648 | Mm.12246 | immediate early response 5 |
| 0.5145 | AA030681 | Mm.26995 | thimet oligopeptidase 1 |
| 0.514 | X13586 | Mm.22706 | 2,3-bisphosphoglycerate mutase |
| 0.5117 | AA512555 | Mm.28293 | RIKEN cDNA 2900053E13 gene |
| 0.5114 | AA219870 | Mm.143527 | RIKEN cDNA 2500002L14 gene |
| 0.5106 | AA060905 | Mm.205830 | guanosine diphosphate (GDP) dissociation ihibitor 1 |
| 0.5094 | AA015322 | Mm.27643 | secreted modular calcium binding protein 1 |
| 0.5041 | AA178252 | Mm.1648 | expressed sequence AI553596 |
| -0.5036 | W90921 | Mm.196580 | ubiquitin C, related sequence 2 |
| 0.5032 | AA072252 | Mm.108076 | phosphofructokinase, platelet |
| 0.5017 | AA023099 | Mm.29879 | RIKEN cDNA 5031412I06 gene |
| 0.5012 | AA109721 | Mm.28088 | mevalonate kinase |
| -0.5004 | W50665 | Mm.24700 | cadherin 13 |
| 0.4998 | AA107510 | Mm.19830 | a disintegrin and metalloproteinase domain 15 (metargidin) |
| 0.4982 | U60150 | Mm.28643 | vesicle-associated membrane protein 2 |
| 0.4977 | W14352 | Mm.29965 | RIKEN cDNA 2410104I19 gene |
| 0.4976 | C80271 | Mm.15801 | lipocalin 7 |
| 0.4973 | AA000817 | Mm.29549 | hairy and enhancer of split 6, (Drosophila) |
| 0.4971 | AA166191 | 0 | 0 |
| -0.4954 | M12481 | Mm.195066 | actin, beta, cytoplasmic |
| 0.4934 | AA512593 | Mm.4079 | expressed sequence AI415429 |
| 0.4918 | Z22532 | 0 | 0 |
| 0.4906 | U96687 | Mm.87804 | paired-Ig-like receptor A6 |
| 0.4904 | W48073 | 0 | 0 |
| 0.4904 | D83146 | Mm.3410 | sine oculis-related homeobox 5 homolog (Drosophila) |
| 0.4901 | W54850 | 0 | 0 |
| 0.4894 | W10994 | Mm.27467 | TC10-like Rho GTPase |
| -0.4891 | W29272 | Mm.265 | ribosomal protein S25 |
| -0.4879 | C77300 | Mm.143755 | bromodomain-containing 4 |
| 0.4866 | D13903 | Mm.89191 | protein tyrosine phosphatase, receptor type, D |
| -0.4861 | AA073154 | 0 | 0 |
| -0.4842 | AA717264 | Mm.7202 | ESTs |
| 0.4831 | AA068062 | 0 | 0 |
| 0.4825 | AA057994 | Mm.23742 | nestin |
| -0.4819 | M12813 | 0 | 0 |
| 0.4806 | W41070 | Mm.28896 | phosphatidylcholine transfer protein-like |
| 0.4805 | AA396448 | Mm.30095 | RIKEN cDNA 4930527D15 gene |
| -0.4767 | C76668 | Mm.196322 | EST X83313 |
| 0.4767 | AA059528 | Mm.28146 | expressed sequence C78718 |
| -0.4762 | W75846 | Mm.27001 | EST AI425994 |
| 0.4756 | W61431 | Mm.28230 | v-maf musculoaponeurotic fibrosarcoma oncogene family, protein G (avian) |
| -0.4744 | M34148 | Mm.6510 | zona pellucida glycoprotein 2 |
| -0.4728 | AA161979 | Mm.3380 | kinesin family member 5B |
| 0.471 | AA178722 | Mm.6803 | RIKEN cDNA 1500019G21 gene |
| 0.4708 | AA033474 | Mm.21187 | RIKEN cDNA 1110005F07 gene |
| 0.4708 | W98152 | 0 | 0 |
| 0.4707 | AA117895 | Mm.21629 | ATP-binding cassette, sub-family F (GCN20), member 2 |
| -0.4696 | W36570 | Mm.4619 | mutS homolog 2 (E. coli) |
| -0.4694 | X98369 | Mm.176369 | SRY-box containing gene 15 |

| | | | |
|---|---|---|---|
| 0.4686 | D10475 | Mm.3003 | epimorphin |
| 0.4681 | R75011 | Mm.200783 | expressed sequence R75011 |
| -0.4677 | C80249 | Mm.25065 | DNA segment, Chr 9, ERATO Doi 306, expressed |
| -0.4672 | W44228 | Mm.2718 | eukaryotic translation elongation factor 1 beta 2 |
| 0.4663 | W98100 | Mm.29381 | expressed sequence AU021460 |
| 0.4646 | W48968 | 0 | 0 |
| -0.4637 | AA118715 | Mm.182255 | CD97 antigen |
| 0.4631 | AA015118 | Mm.27577 | ESTs, Weakly similar to zinc-finger protein-37 [R.norvegicus] |
| 0.4613 | AA590212 | Mm.30232 | DNA segment, Chr 9, Brigham & Women's Genetics 1455 expressed |
| 0.461 | AA016540 | Mm.5117 | ESTs |
| 0.4606 | W13070 | Mm.28833 | RIKEN cDNA 1200010B10 gene |
| 0.4599 | W75827 | Mm.25547 | RIKEN cDNA 0610037B21 gene |
| 0.4593 | AA172719 | Mm.29804 | expressed sequence AU016300 |
| 0.4586 | AA119871 | 0 | 0 |
| -0.4586 | ET61641 | 0 | 0 |
| 0.4584 | W45951 | Mm.200674 | expressed sequence C86129 |
| -0.4577 | C80108 | Mm.25061 | ESTs |
| 0.4575 | AA139090 | Mm.28618 | RIKEN cDNA 2410004D02 gene |
| 0.4573 | AA111212 | Mm.18946 | adaptor protein complex AP-2, mu1 |
| 0.4571 | U85247 | Mm.6142 | alpha-N-acetylglucosaminidase (Sanfilippo disease IIIB) |
| -0.4566 | ET61213 | 0 | 0 |
| -0.4559 | M12481 | Mm.195066 | actin, beta, cytoplasmic |
| 0.4557 | M63659 | Mm.140610 | guanine nucleotide binding protein, alpha 12 |
| 0.4548 | X58708 | Mm.22569 | cyclin B1, related sequence 1 |
| 0.4541 | AF030178 | Mm.6354 | phosphatidylinositol glycan, class Q |
| 0.4513 | W41072 | Mm.21981 | expressed sequence AI327276 |
| 0.4511 | D11374 | Mm.3072 | signal-induced proliferation associated gene 1 |
| -0.4506 | D17920 | Mm.8688 | RIKEN cDNA 0610011B04 gene |
| 0.4504 | AA013805 | Mm.143830 | alpha actinin 4 |
| 0.4502 | AA008255 | Mm.2564 | adaptor-related protein complex AP-3, sigma 2 subunit |
| -0.4494 | W65062 | 0 | 0 |
| 0.4491 | AA015291 | Mm.41331 | RIKEN cDNA 1110012E06 gene |
| 0.449 | U88621 | Mm.43612 | 8-oxoguanine DNA-glycosylase 1 |
| -0.4474 | U14133 | Mm.16756 | silver |
| -0.447 | W13350 | Mm.28650 | RAB6, member RAS oncogene family |
| -0.4465 | AA110466 | Mm.154286 | RIKEN cDNA 4921528G01 gene |
| 0.446 | L21973 | Mm.18036 | E2F transcription factor 1 |
| 0.4457 | U95145 | Mm.2969 | A kinase anchor protein |
| 0.4453 | AA221260 | Mm.22306 | RIKEN cDNA 1810045K06 gene |
| 0.4447 | AA013581 | Mm.41568 | ESTs, Weakly similar to MFG1 MOUSE ZINC FINGER PROTEIN MFG-1 [M.musculus] |
| -0.4434 | ET62538 | 0 | 0 |
| 0.4433 | AA068094 | 0 | 0 |
| -0.443 | M20625 | Mm.4872 | cytochrome c, testis |
| 0.4416 | AF006492 | Mm.3105 | zinc finger protein, multitype 1 |
| -0.4416 | C80656 | Mm.153895 | expressed sequence C79248 |
| 0.44 | D78572 | Mm.944 | integral membrane glycoprotein |
| 0.4393 | AA003157 | Mm.28541 | RIKEN cDNA 1700012G19 gene |
| 0.4392 | AA162205 | Mm.30245 | RIKEN cDNA 2310047I15 gene |
| 0.4392 | AA066461 | 0 | 0 |
| -0.437 | AA185889 | Mm.24058 | ESTs |
| 0.4356 | AA198976 | Mm.32 | ESTs, Weakly similar to I48722 zinc finger protein - mouse [M.musculus] |
| 0.4353 | AA154786 | Mm.205422 | ESTs |
| 0.435 | U62297 | Mm.27220 | nuclear transcription factor-Y gamma |
| -0.4335 | W29537 | Mm.27664 | Unc-51 like kinase 2 (C. elegans) |
| 0.4326 | AA048950 | Mm.200760 | RIKEN cDNA 2510031P20 gene |
| -0.4318 | W10047 | 0 | 0 |
| -0.4317 | W18383 | 0 | 0 |
| -0.4304 | AA087249 | 0 | 0 |
| -0.4287 | AA118716 | Mm.20831 | eukaryotic translation initiation factor 2, subunit 3, structural gene Y-linked |
| 0.4285 | AA062247 | Mm.20415 | RIKEN cDNA 1110031C13 gene |
| 0.4282 | L15436 | Mm.689 | activin A receptor, type 1 |
| 0.4281 | AA106166 | Mm.27818 | eukaryotic translation elongation factor 2 |
| 0.4275 | AA647054 | Mm.3010 | RIKEN cDNA 2810405F18 gene |
| -0.4274 | X04405 | 0 | 0 |
| 0.427 | W57510 | 0 | 0 |
| -0.4268 | U88623 | Mm.184351 | aquaporin 4 |

## Table 4. Genes that provide E2F2 discrimination

| Weight | Acc. No. | Unigene ID | Unigene Description |
|---|---|---|---|
| 0.805 | AA137962 | Mm.196141 | RIKEN cDNA 2810475J17 gene |
| 0.7601 | X81581 | Mm.29254 | insulin-like growth factor binding protein 3 |
| 0.7416 | AA008502 | 0 | 0 |
| 0.7246 | AA039124 | Mm.16783 | phosphoglycerate mutase 1 |
| 0.7191 | AA122622 | Mm.22731 | integrin beta 4 binding protein |
| 0.6919 | W64561 | Mm.3360 | tyrosine 3-monooxygenase/tryptophan 5-monooxygenase activation protein, zeta |
| 0.6837 | D14566 | 0 | 0 |
| 0.6706 | W11020 | Mm.29455 | RIKEN cDNA 1810045K07 gene |
| 0.6647 | Z31238 | Mm.957 | COP9 (constitutive photomorphogenic) homolog, subunit 4 (Arabidopsis thaliana) |
| -0.6434 | AA066122 | 0 | 0 |
| 0.6258 | AA137667 | Mm.39046 | RIKEN cDNA 1110055E19 gene |
| 0.6183 | W55211 | 0 | 0 |
| 0.6169 | X17500 | Mm.3406 | transcription factor E2a |
| 0.6087 | W50975 | 0 | 0 |
| 0.6075 | AA104912 | Mm.182563 | RIKEN cDNA 1110011F09 gene |
| 0.607 | U28495 | Mm.7634 | lymphoid blast crisis-like 1 |
| 0.5976 | W99019 | Mm.30272 | RIKEN cDNA 1200003M11 gene |
| 0.5954 | AA727929 | Mm.196303 | RIKEN cDNA 4933413A04 gene |
| 0.592 | W98100 | Mm.29381 | expressed sequence AU021460 |
| 0.5895 | AA060905 | Mm.205830 | guanosine diphosphate (GDP) dissociation ihibitor 1 |
| 0.5829 | U65735 | Mm.119162 | ELAV (embryonic lethal, abnormal vision, Drosophila)-like 1 (Hu antigen R) |
| 0.5731 | AA154337 | Mm.2701 | DnaJ (Hsp40) homolog, subfamily B, member 6 |
| -0.5713 | R74842 | Mm.5249 | copine 6 |
| 0.5688 | X15666 | 0 | 0 |
| 0.5606 | U18996 | 0 | 0 |
| 0.5556 | AA035834 | Mm.171304 | RIKEN cDNA 4632419I22 gene |
| 0.5536 | W10994 | Mm.27467 | TC10-like Rho GTPase |
| 0.5535 | AA052286 | 0 | 0 |
| 0.5523 | W55419 | 0 | 0 |
| 0.5482 | W89475 | 0 | 0 |
| 0.548 | AA031007 | Mm.12145 | retinoblastoma binding protein 4 |
| 0.5474 | AA013648 | Mm.12246 | immediate early response 5 |
| 0.5466 | W75373 | Mm.29106 | RIKEN cDNA 1200017E13 gene |
| 0.546 | W09687 | Mm.906 | midkine |
| 0.5455 | AA219870 | Mm.143527 | RIKEN cDNA 2500002L14 gene |
| 0.5402 | AA140170 | Mm.206757 | RIKEN cDNA 4933439C20 gene |
| -0.5386 | AA118715 | Mm.182255 | CD97 antigen |
| -0.5378 | C76668 | Mm.196322 | EST X83313 |
| 0.5349 | AA015291 | Mm.41331 | RIKEN cDNA 1110012E06 gene |
| 0.5346 | W54850 | 0 | 0 |
| 0.5337 | AF014117 | Mm.88367 | glial cell line derived neurotrophic factor family receptor alpha 1 |
| 0.5318 | AA267014 | Mm.8552 | baculoviral IAP repeat-containing 5 |
| 0.5302 | AA117227 | Mm.38450 | septin 9 |
| 0.5275 | AA106166 | Mm.27818 | eukaryotic translation elongation factor 2 |
| -0.5231 | AA066391 | 0 | 0 |
| -0.523 | D31952 | 0 | 0 |
| 0.5227 | AA014135 | 0 | 0 |
| 0.5211 | W42399 | 0 | 0 |
| 0.5205 | C78700 | Mm.35569 | EST C77459 |
| 0.52 | AA068094 | 0 | 0 |
| 0.5196 | AA139094 | Mm.28984 | DNA segment, Chr 10, Johns Hopkins University 81 expressed |
| 0.5168 | W70427 | 0 | 0 |
| 0.516 | AA103881 | Mm.10193 | G protein-coupled receptor kinase 6 |
| 0.5158 | D13903 | Mm.89191 | protein tyrosine phosphatase, receptor type, D |
| 0.5127 | W49204 | Mm.24193 | glypican 1 |
| 0.51 | W55350 | 0 | 0 |
| 0.5081 | D89571 | Mm.3815 | syndecan 4 |
| 0.5081 | Z22532 | 0 | 0 |
| 0.5071 | AA013805 | Mm.143830 | alpha actinin 4 |
| 0.5057 | AA118363 | Mm.645 | stromal interaction molecule 1 |
| -0.5049 | M97013 | Mm.57242 | paired box gene 5 |
| -0.501 | S80989 | 0 | 0 |
| 0.5007 | W55368 | 0 | 0 |
| -0.4974 | ET62538 | 0 | 0 |
| 0.4963 | AA008930 | Mm.18845 | superkiller viralicidic activity 2-like (S. cerevisiae ) |

| | | | |
|---|---|---|---|
| 0.4952 | U37799 | Mm.4603 | scavenger receptor class B1 |
| -0.4925 | W34634 | Mm.24775 | expressed sequence AI324798 |
| 0.492 | AA109912 | Mm.30246 | CD151 antigen |
| -0.4918 | AA571535 | Mm.21187 | RIKEN cDNA 1110005F07 gene |
| -0.4886 | W64676 | 0 | 0 |
| 0.4876 | W48968 | 0 | 0 |
| 0.4871 | AA027669 | Mm.41531 | RIKEN cDNA 2410044K02 gene |
| 0.4859 | W45951 | Mm.200674 | expressed sequence C86129 |
| 0.4853 | AA072252 | Mm.108076 | phosphofructokinase, platelet |
| -0.4846 | AA087332 | 0 | 0 |
| 0.4838 | AA038658 | Mm.104955 | serine protease inhibitor, Kunitz type 1 |
| -0.4828 | AA050715 | 0 | 0 |
| 0.4826 | AA008831 | 0 | 0 |
| 0.4808 | AA059517 | Mm.41787 | expressed in non-metastatic cells 4, (NM23-M4)(nucleoside diphosphate kinase) |
| 0.4786 | AA109721 | Mm.28088 | mevalonate kinase |
| 0.4783 | W64174 | Mm.30191 | RIKEN cDNA 2600013G09 gene |
| -0.4767 | ET62360 | 0 | 0 |
| 0.4756 | W50461 | 0 | 0 |
| 0.4743 | AA071776 | 0 | 0 |
| 0.4739 | AA033474 | Mm.21187 | RIKEN cDNA 1110005F07 gene |
| 0.4737 | AA111212 | Mm.18946 | adaptor protein complex AP-2, mu1 |
| -0.473 | X75384 | Mm.4293 | spinal cord axial homeobox gene 1 |
| 0.4703 | AA144734 | Mm.821 | U2 small nuclear ribonucleoprotein polypeptide A' |
| 0.468 | AA041982 | Mm.542 | RNA binding motif protein 4 |
| -0.4677 | W36570 | Mm.4619 | mutS homolog 2 (E. coli) |
| 0.4675 | AA023099 | Mm.29879 | RIKEN cDNA 5031412I06 gene |
| 0.4661 | W85144 | Mm.196475 | Mus musculus F-box-WD40 repeat protein 6 (Fbxw6) mRNA, complete cds |
| 0.4659 | AA166191 | 0 | 0 |
| -0.4657 | AA118534 | 0 | 0 |
| 0.4628 | AA048098 | Mm.41881 | RIKEN cDNA 2900002K07 gene |
| 0.4616 | W84983 | 0 | 0 |
| 0.4584 | U95145 | Mm.2969 | A kinase anchor protein |
| -0.4579 | M34148 | Mm.6510 | zona pellucida glycoprotein 2 |
| 0.4573 | X81581 | Mm.29254 | insulin-like growth factor binding protein 3 |
| -0.4564 | W50665 | Mm.24700 | cadherin 13 |
| 0.456 | X99963 | 0 | 0 |
| 0.4559 | AA000455 | Mm.6834 | interferon (alpha and beta) receptor 2 |
| -0.4548 | W90921 | Mm.196580 | ubiquitin C, related sequence 2 |
| 0.4548 | D10475 | Mm.3003 | epimorphin |
| -0.4542 | W54637 | 0 | 0 |
| 0.4541 | U03715 | 0 | 0 |
| -0.4536 | U84207 | 0 | 0 |
| 0.4528 | W83068 | 0 | 0 |
| -0.4512 | ET61266 | 0 | 0 |
| -0.451 | AA073154 | 0 | 0 |
| 0.4509 | W51226 | 0 | 0 |
| -0.4498 | L11330 | Mm.4729 | dual specificity phosphatase 2 |
| 0.4488 | AA107510 | Mm.19830 | a disintegrin and metalloproteinase domain 15 (metargidin) |
| 0.4488 | AA097203 | Mm.200406 | RIKEN cDNA 2700022N21 gene |
| 0.4459 | W08472 | Mm.27955 | Williams-Beuren syndrome chromosome region 1 homolog (human) |
| 0.4454 | AA105536 | Mm.25161 | sirtuin 2 (silent mating type information regulation 2, homolog) 2 (S. cerevisiae) |
| 0.443 | AA119871 | 0 | 0 |
| 0.4422 | W66916 | Mm.144235 | peroxisomal farnesylated protein |
| -0.442 | AF026216 | Mm.3906 | mitogen activated protein kinase kinase 7 |
| 0.4407 | U22396 | Mm.4340 | zinc finger protein 100 |
| 0.4406 | U61085 | Mm.182905 | solute carrier family 12, member 3 |
| 0.4406 | X79131 | Mm.42143 | antigen identified by monoclonal antibody 2A8 |
| 0.4402 | AA178252 | Mm.1648 | expressed sequence AI553596 |
| -0.4397 | AA544897 | Mm.27792 | RIKEN cDNA 0610011C19 gene |
| 0.4372 | AA033333 | Mm.143830 | alpha actinin 4 |
| 0.4367 | W75827 | Mm.25547 | RIKEN cDNA 0610037B21 gene |
| -0.436 | AA212722 | Mm.141020 | Mus musculus, clone MGC:6279 IMAGE:2648344, mRNA, complete cds |
| -0.4341 | W12794 | 0 | 0 |
| 0.4336 | M63659 | Mm.140610 | guanine nucleotide binding protein, alpha 12 |
| 0.4327 | C78893 | Mm.43904 | expressed sequence C78893 |
| -0.4326 | AF007560 | 0 | 0 |
| -0.4316 | C76435 | Mm.27809 | expressed sequence C76435 |
| -0.43 | W82332 | Mm.3862 | insulin-like growth factor 2 |
| -0.4291 | AA110466 | Mm.154286 | RIKEN cDNA 4921528G01 gene |

| | | | |
|---|---|---|---|
| -0.4277 | ET61641 | 0 | 0 |
| 0.4275 | W50167 | 0 | 0 |
| 0.4268 | AA068062 | 0 | 0 |
| 0.4266 | W14352 | Mm.29965 | RIKEN cDNA 2410104I19 gene |
| -0.4265 | L06451 | Mm.1890 | nonagouti |
| 0.4253 | AA002297 | Mm.16332 | ephrin A4 |
| 0.421 | AA033369 | Mm.29391 | RIKEN cDNA 1110007F23 gene |
| 0.4199 | M90365 | Mm.21990 | junction plakoglobin |
| 0.4188 | AA022143 | 0 | 0 |
| 0.4187 | AA117074 | 0 | 0 |
| 0.4183 | AA072239 | 0 | 0 |
| 0.4181 | W89472 | Mm.38016 | sterol regulatory element binding factor 2 |
| 0.4165 | AA144601 | Mm.23522 | RIKEN cDNA 1700009N14 gene |
| 0.4163 | AA163771 | Mm.29383 | EST, similar to E2BE RAT TRANSLATION INITIATION FACTOR EIF-2B EPSILON |
| 0.416 | W59236 | 0 | 0 |
| 0.4153 | W51229 | 0 | 0 |
| 0.4149 | AA396448 | Mm.30095 | RIKEN cDNA 4930527D15 gene |
| 0.4147 | AA163902 | Mm.25264 | DEAD/H (Asp-Glu-Ala-Asp/His) box polypeptide 21 (RNA helicase II/Gu) |
| 0.4142 | AB004048 | Mm.140956 | neuronatin |
| 0.4138 | AA116951 | Mm.16453 | peroxisomal membrane protein 3, 35 kDa |
| -0.4135 | W29537 | Mm.27664 | Unc-51 like kinase 2 (C. elegans) |
| 0.4132 | AA110061 | Mm.20912 | cell division cycle 6 homolog (S. cerevisiae) |
| 0.4126 | U67321 | Mm.35687 | caspase 7 |
| 0.4124 | AA107615 | Mm.61206 | glucokinase activity, related sequence 2 |
| 0.4115 | AF022962 | Mm.6925 | SEC8 (S. cerevisiae) |
| -0.4107 | X54542 | Mm.1019 | interleukin 6 |
| 0.4106 | M64849 | 0 | 0 |
| 0.4101 | AA517665 | Mm.34869 | NADH dehydrogenase (ubiquinone) 1 alpha subcomplex, 1 |
| 0.409 | W71076 | 0 | 0 |
| 0.4081 | AA111277 | Mm.20937 | hippocalcin-like 1 |
| 0.4071 | AA117905 | 0 | 0 |
| 0.4071 | AA137795 | Mm.182518 | ESTs, Moderately similar to OXYB_HUMAN OXYSTEROL-BINDING PROTEIN |
| 0.4054 | AA221219 | Mm.29357 | RIKEN cDNA 1300017C10 gene |
| -0.4051 | C76739 | Mm.24920 | macrophage C-type lectin |
| 0.4041 | ET63083 | 0 | 0 |
| -0.4036 | X15684 | Mm.18443 | solute carrier family 2 (facilitated glucose transporter), member 2 |
| -0.4033 | AA168858 | 0 | 0 |
| 0.4029 | AA098332 | Mm.200912 | protein kinase, AMP-activated, beta 1 non-catalytic subunit |
| -0.4023 | AA154079 | Mm.141758 | hemoglobin X, alpha-like embryonic chain in Hba complex |
| -0.4021 | J03458 | Mm.4685 | filaggrin |
| 0.4018 | C81431 | Mm.34949 | expressed sequence C81431 |
| 0.4018 | D86081 | Mm.24245 | transcription elongation factor A (SII), 2 |
| 0.4013 | AA511380 | Mm.28797 | proline rich protein expressed in brain |
| 0.401 | U43321 | 0 | 0 |
| 0.4005 | AA172719 | Mm.29804 | expressed sequence AU016300 |
| 0.3998 | U46956 | 0 | 0 |
| 0.3983 | X95351 | Mm.4674 | maternal embryonic leucine zipper kinase |
| 0.3978 | W75644 | Mm.30250 | DNA segment, Chr 18, Wayne State University 181, expressed |
| 0.3969 | D83146 | Mm.3410 | sine oculis-related homeobox 5 homolog (Drosophila) |
| -0.3969 | AA717972 | Mm.154511 | expressed sequence C79379 |
| 0.3968 | AA063800 | Mm.42246 | phosphoenolpyruvate carboxykinase 1, cytosolic |
| -0.3965 | W13689 | Mm.30066 | ribosomal protein L8 |
| 0.3963 | AA590212 | Mm.30232 | DNA segment, Chr 9, Brigham & Women's Genetics 1455 expressed |
| 0.396 | AA087986 | Mm.24174 | expressed sequence C76919 |
| 0.3959 | X13450 | Mm.1355 | immunoglobulin-associated alpha |
| -0.3954 | AA119173 | Mm.35829 | Mus musculus, clone MGC:5764 IMAGE:3499536, mRNA, complete cds |
| 0.395 | AA008737 | Mm.22418 | peroxin 5 |
| 0.3948 | W85566 | 0 | 0 |
| 0.3947 | W49331 | Mm.26214 | RIKEN cDNA 5730502D15 gene |
| 0.3947 | U96687 | Mm.87804 | paired-Ig-like receptor A6 |
| -0.3932 | X06115 | Mm.35605 | cadherin 1 |
| 0.393 | U62297 | Mm.27220 | nuclear transcription factor-Y gamma |
| 0.3911 | AA139090 | Mm.28618 | RIKEN cDNA 2410004D02 gene |
| 0.3906 | W77035 | Mm.41196 | ESTs, Weakly similar to JQ1322 tenascin precursor - mouse [M.musculus] |
| -0.3902 | M15177 | Mm.779 | CD5 antigen |
| 0.3902 | M55154 | Mm.18843 | transglutaminase 2, C polypeptide |

## Table 5. Genes that provide E2F3 discrimination

| Weight | Acc. No. | Unigene ID | Unigene Description |
|---|---|---|---|
| 3.0645 | U18996 | 0 | 0 |
| 2.7761 | AA106166 | Mm.27818 | eukaryotic translation elongation factor 2 |
| -2.7539 | AA415898 | Mm.29008 | interferon-inducible GTPase |
| -2.6976 | AA152553 | 0 | 0 |
| 2.673 | AA052286 | 0 | 0 |
| 2.5911 | W42399 | 0 | 0 |
| 2.5576 | W44228 | Mm.2718 | eukaryotic translation elongation factor 1 beta 2 |
| 2.5557 | X81581 | Mm.29254 | insulin-like growth factor binding protein 3 |
| -2.5536 | L32973 | Mm.1676 | thymidylate kinase family LPS-inducible member |
| 2.5412 | U28495 | Mm.7634 | lymphoid blast crisis-like 1 |
| 2.5363 | AA060905 | Mm.205830 | guanosine diphosphate (GDP) dissociation ihibitor 1 |
| 2.5045 | AA071776 | 0 | 0 |
| 2.4372 | W50975 | 0 | 0 |
| 2.426 | W64561 | Mm.3360 | tyrosine 3-monooxygenase/tryptophan 5-monooxygenase activation protein, zeta |
| 2.4206 | W55211 | 0 | 0 |
| 2.3717 | AA013648 | Mm.12246 | immediate early response 5 |
| 2.363 | AA104912 | Mm.182563 | RIKEN cDNA 1110011F09 gene |
| 2.3483 | W66916 | Mm.144235 | peroxisomal farnesylated protein |
| 2.3461 | M32599 | Mm.5289 | glyceraldehyde-3-phosphate dehydrogenase |
| 2.3455 | AA140170 | Mm.206757 | RIKEN cDNA 4933439C20 gene |
| 2.3337 | AA087986 | Mm.24174 | expressed sequence C76919 |
| 2.3267 | AA137667 | Mm.39046 | RIKEN cDNA 1110055E19 gene |
| 2.3193 | M32599 | Mm.5289 | glyceraldehyde-3-phosphate dehydrogenase |
| 2.2915 | AA013805 | Mm.143830 | alpha actinin 4 |
| 2.2786 | AA039124 | Mm.16783 | phosphoglycerate mutase 1 |
| 2.271 | AF022962 | Mm.6925 | SEC8 (S. cerevisiae) |
| 2.2506 | AA109912 | Mm.30246 | CD151 antigen |
| 2.2021 | AA511380 | Mm.28797 | proline rich protein expressed in brain |
| 2.2007 | X81581 | Mm.29254 | insulin-like growth factor binding protein 3 |
| 2.1706 | W11020 | Mm.29455 | RIKEN cDNA 1810045K07 gene |
| 2.1667 | AA033333 | Mm.143830 | alpha actinin 4 |
| -2.1582 | AA109998 | 0 | 0 |
| 2.1548 | AA000574 | Mm.28095 | expressed sequence AL024016 |
| 2.151 | Z31238 | Mm.957 | COP9 (constitutive photomorphogenic) homolog, subunit 4 (Arabidopsis thaliana) |
| 2.1465 | AA692247 | Mm.196544 | lysyl-tRNA synthetase |
| -2.1398 | X61232 | Mm.31395 | carboxypeptidase E |
| 2.1396 | AA072239 | 0 | 0 |
| 2.136 | W48968 | 0 | 0 |
| 2.127 | U91511 | Mm.31308 | ectonucleoside triphosphate diphosphohydrolase 2 |
| 2.1113 | AA517665 | Mm.34869 | NADH dehydrogenase (ubiquinone) 1 alpha subcomplex, 1 |
| 2.0929 | AA116633 | 0 | 0 |
| 2.0904 | AA117227 | Mm.38450 | septin 9 |
| -2.0901 | U02298 | 0 | 0 |
| 2.0894 | X17500 | Mm.3406 | transcription factor E2a |
| -2.0874 | W76686 | 0 | 0 |
| 2.078 | AA035834 | Mm.171304 | RIKEN cDNA 4632419I22 gene |
| 2.0613 | AA066354 | Mm.28598 | Janus kinase 1 |
| 2.055 | AA671482 | Mm.27954 | expressed sequence AI551216 |
| 2.0343 | AA068094 | 0 | 0 |
| 2.0279 | W10994 | Mm.27467 | TC10-like Rho GTPase |
| -2.0171 | AA177851 | Mm.21551 | RIKEN cDNA 9130009C22 gene |
| 2.0075 | AA219870 | Mm.143527 | RIKEN cDNA 2500002L14 gene |
| 2.0048 | U46956 | 0 | 0 |
| 1.991 | W63876 | Mm.24174 | expressed sequence C76919 |
| 1.9848 | U00938 | 0 | 0 |
| 1.9804 | X99963 | 0 | 0 |
| 1.975 | AA097203 | Mm.200406 | RIKEN cDNA 2700022N21 gene |
| 1.9749 | AA105536 | Mm.25161 | sirtuin 2 (silent mating type information regulation 2, homolog) 2 (S. cerevisiae) |
| -1.9599 | AA616057 | Mm.196884 | cleavage and polyadenylation specific factor 4, 30kD subunit |
| 1.9525 | M32599 | Mm.5289 | glyceraldehyde-3-phosphate dehydrogenase |
| 1.9487 | W54638 | 0 | 0 |
| -1.9439 | C78385 | Mm.24950 | DNA segment, Chr 16, ERATO Doi 36, expressed |
| 1.9382 | W89472 | Mm.38016 | sterol regulatory element binding factor 2 |
| 1.9321 | AA073251 | 0 | 0 |
| -1.9277 | AA254016 | Mm.19080 | GTP binding protein 1 |

| | | | |
|---|---|---|---|
| 1.9235 | W84983 | 0 | 0 |
| 1.9201 | X99291 | Mm.57227 | homeo box D13 |
| 1.9072 | AA016928 | Mm.28060 | RIKEN cDNA 2310058J06 gene |
| 1.9039 | W55560 | 0 | 0 |
| -1.9019 | X87096 | Mm.4598 | brevican |
| -1.8965 | M31419 | Mm.212870 | interferon activated gene 204 |
| 1.8871 | U10325 | Mm.4316 | aryl hydrocarbon receptor nuclear translocator |
| 1.8871 | AA166440 | Mm.30245 | RIKEN cDNA 2310047I15 gene |
| -1.8861 | AA087249 | 0 | 0 |
| -1.8775 | AA118534 | 0 | 0 |
| -1.8774 | S80989 | 0 | 0 |
| 1.873 | AA050440 | Mm.7103 | pre B-cell leukemia transcription factor 2 |
| 1.8705 | W50461 | 0 | 0 |
| 1.8696 | AA049052 | Mm.147641 | CDC-like kinase 3 |
| 1.8623 | M63659 | Mm.140610 | guanine nucleotide binding protein, alpha 12 |
| 1.8584 | AA537309 | Mm.21776 | calponin 2 |
| 1.8552 | AA066700 | 0 | 0 |
| 1.8549 | AA073388 | 0 | 0 |
| -1.8414 | U44731 | Mm.1909 | guanylate nucleotide binding protein 3 |
| 1.8407 | AA111356 | Mm.29699 | adaptor protein complex AP-1, beta 1 subunit |
| 1.8374 | AA072347 | 0 | 0 |
| 1.8373 | AA041982 | Mm.542 | RNA binding motif protein 4 |
| -1.8345 | W55620 | 0 | 0 |
| -1.8327 | J03776 | Mm.3288 | tripartite motif protein 30 |
| 1.8169 | W48104 | Mm.12267 | Mus musculus adult male testis cDNA, RIKEN full-length enriched library, clone:4933407N23 |
| 1.8081 | Z22532 | 0 | 0 |
| -1.807 | M74753 | Mm.2780 | myosin, heavy polypeptide 3, skeletal muscle, embryonic |
| 1.8065 | M89798 | Mm.32207 | wingless-related MMTV integration site 5A |
| 1.8015 | U03184 | Mm.206790 | cortactin |
| 1.8015 | AA049952 | Mm.5202 | RIKEN cDNA 6330406L22 gene |
| 1.801 | AA270881 | Mm.7271 | nuclear RNA export factor 1 homolog (S. cerevisiae) |
| -1.7992 | AA009095 | 0 | 0 |
| 1.7927 | AA048650 | Mm.22505 | hydroxysteroid (17-beta) dehydrogenase 12 |
| 1.7925 | AA003323 | Mm.28044 | Mus musculus, clone IMAGE:3590270, mRNA, partial cds |
| 1.7883 | Y12783 | Mm.31512 | ring finger protein 2 |
| 1.7844 | X75926 | Mm.369 | ATP-binding cassette, sub-family A (ABC1), member 1 |
| 1.7819 | X79131 | Mm.42143 | antigen identified by monoclonal antibody 2A8 |
| 1.7791 | W75077 | 0 | 0 |
| -1.779 | AA682089 | Mm.201482 | expressed sequence AA682089 |
| 1.7774 | W50514 | 0 | 0 |
| 1.7773 | C76966 | Mm.24939 | ESTs |
| 1.7753 | AA030421 | 0 | 0 |
| 1.7749 | AA072843 | Mm.5612 | expressed sequence C85189 |
| -1.7728 | L11330 | Mm.4729 | dual specificity phosphatase 2 |
| 1.772 | AA137795 | Mm.182518 | ESTs, Moderately similar to OXYB_HUMAN OXYSTEROL-BINDING PROTEI [H.sapiens] |
| 1.7669 | W75644 | Mm.30250 | DNA segment, Chr 18, Wayne State University 181, expressed |
| 1.764 | W09791 | Mm.7729 | aldolase 3, C isoform |
| -1.7624 | Y15238 | 0 | 0 |
| 1.7619 | C75959 | Mm.28063 | expressed sequence AA409091 |
| 1.7611 | AA137822 | 0 | 0 |
| 1.7556 | AA106224 | Mm.172947 | tuftelin-interacting protein, 39 kD |
| 1.7545 | AA014135 | 0 | 0 |
| 1.7538 | AA161905 | Mm.27560 | ubiquitin-like 1 (sentrin) activating enzyme E1B |
| 1.7445 | U95145 | Mm.2969 | A kinase anchor protein |
| 1.7421 | AA274974 | Mm.22485 | RIKEN cDNA 2610311I19 gene |
| 1.7421 | AA098332 | Mm.200912 | protein kinase, AMP-activated, beta 1 non-catalytic subunit |
| 1.7384 | W61758 | 0 | 0 |
| 1.7328 | AA096813 | Mm.930 | cathepsin L |
| 1.731 | W84988 | 0 | 0 |
| 1.7228 | AA067092 | 0 | 0 |
| -1.7196 | X92590 | Mm.15694 | histone cell cycle regulation defective homolog A (S. cerevisiae) |
| 1.7181 | AA088054 | 0 | 0 |
| 1.7093 | AA061310 | Mm.29106 | RIKEN cDNA 1200017E13 gene |
| 1.7059 | W08822 | Mm.43636 | zinc finger protein 289 |
| 1.7043 | AA008737 | Mm.22418 | peroxin 5 |
| 1.7015 | W50655 | Mm.2831 | nucleosome assembly protein 1-like 4 |
| 1.7015 | AA097626 | Mm.157900 | RIKEN cDNA 1300007C21 gene |
| -1.6972 | Y11682 | Mm.364 | mitochondrial ribosomal protein S12 |
| 1.6972 | W75373 | Mm.29106 | RIKEN cDNA 1200017E13 gene |

| | | | |
|---|---|---|---|
| -1.6945 | U35370 | 0 | 0 |
| 1.6938 | AA023107 | Mm.2551 | SEC22 vesicle trafficking protein-like 1 (S. cerevisiae) |
| 1.6928 | AA068862 | Mm.24495 | RIKEN cDNA 2410015A15 gene |
| -1.6928 | J04423 | 0 | 0 |
| 1.6882 | U18996 | 0 | 0 |
| 1.6876 | W49204 | Mm.24193 | glypican 1 |
| -1.6873 | AA124352 | Mm.22246 | RIKEN cDNA 3110023K12 gene |
| 1.6868 | W98379 | Mm.14722 | tyrosine 3-monooxygenase/tryptophan 5-monooxygenase activation protein, theta |
| 1.6856 | AA571856 | Mm.24777 | ESTs |
| 1.6847 | U04379 | Mm.8038 | zeta-chain (TCR) associated protein kinase (70kD) |
| 1.6819 | W81884 | Mm.196520 | t-complex protein 1, related sequence 1 |
| -1.6799 | AA549016 | Mm.18617 | RIKEN cDNA 3830408D16 gene |
| 1.6788 | AA031007 | Mm.12145 | retinoblastoma binding protein 4 |
| -1.6764 | C76668 | Mm.196322 | EST X83313 |
| -1.676 | AA616327 | Mm.24855 | RIKEN cDNA 1110020N13 gene |
| 1.6759 | D89571 | Mm.3815 | syndecan 4 |
| 1.673 | AA014138 | Mm.103356 | ATP-binding cassette, sub-family F (GCN20), member 1 |
| 1.6704 | AA117905 | 0 | 0 |
| -1.6677 | AA616578 | Mm.6718 | interferon-induced protein with tetratricopeptide repeats 1 |
| -1.6666 | ET62761 | 0 | 0 |
| 1.6656 | AA008228 | Mm.144235 | peroxisomal farnesylated protein |
| -1.6645 | U15647 | 0 | 0 |
| 1.6635 | AA022143 | 0 | 0 |
| 1.6633 | AA058027 | Mm.29081 | zinc finger protein 263 |
| 1.6561 | W48936 | 0 | 0 |
| 1.6536 | AA013675 | 0 | 0 |
| 1.6493 | AA103881 | Mm.10193 | G protein-coupled receptor kinase 6 |
| 1.6468 | X07888 | 0 | 0 |
| 1.6453 | W82793 | Mm.20915 | topoisomerase (DNA) III beta |
| 1.6441 | AA168283 | Mm.6958 | calpain 2 |
| 1.6414 | AA674353 | Mm.29927 | expressed sequence AA408278 |
| 1.6397 | X04574 | Mm.14410 | trypsin 2 |
| 1.6363 | W46084 | Mm.154511 | expressed sequence C79379 |
| -1.6351 | M32370 | Mm.1302 | SFFV proviral integration 1 |
| 1.6334 | AA153484 | Mm.42255 | ATPase, Ca++ transporting, cardiac muscle, slow twitch 2 |
| 1.6234 | AA116951 | Mm.16453 | peroxisomal membrane protein 3, 35 kDa |
| 1.6155 | AA154734 | Mm.7214 | annexin A3 |
| -1.6131 | X85990 | Mm.4083 | sema domain, immunoglob domain (Ig), short basic domain, secreted, (semaphorin)3B |
| -1.613 | AA571535 | Mm.21187 | RIKEN cDNA 1110005F07 gene |
| -1.6031 | M16360 | Mm.197701 | major urinary protein 5 |
| 1.6029 | AA072334 | 0 | 0 |
| 1.5992 | W45951 | Mm.200674 | expressed sequence C86129 |
| -1.5963 | AA057994 | Mm.23742 | nestin |
| 1.5946 | D12713 | 0 | 0 |
| 1.5942 | AA027404 | Mm.424 | ATPase, Na+/K+ transporting, beta 3 polypeptide |
| -1.5921 | W40709 | Mm.29650 | RIKEN cDNA 2310034O17 gene |
| 1.5916 | AA166139 | Mm.29623 | damage specific DNA binding protein 1 (127 kDa) |
| 1.5909 | M32599 | Mm.5289 | glyceraldehyde-3-phosphate dehydrogenase |
| 1.5881 | X03986 | Mm.4583 | cholinergic receptor, nicotinic, alpha polypeptide 1 (muscle) |
| -1.5865 | Z36270 | Mm.4292 | TGFB inducible early growth response |
| 1.5857 | W47953 | 0 | 0 |
| -1.5841 | AA073154 | 0 | 0 |
| -1.5834 | X06115 | Mm.35605 | cadherin 1 |
| 1.581 | AA117665 | Mm.28952 | cell line NK14 derived transforming oncogene |
| 1.5776 | AA667872 | Mm.988 | RIKEN cDNA 1500004O06 gene |
| 1.5701 | W48999 | 0 | 0 |
| 1.5651 | AA154337 | Mm.2701 | DnaJ (Hsp40) homolog, subfamily B, member 6 |
| 1.5641 | AA139958 | Mm.29530 | RIKEN cDNA 5730504C04 gene |
| 1.5639 | AA541910 | Mm.140568 | RIKEN cDNA 1100001I22 gene |
| 1.5637 | AA008255 | Mm.2564 | adaptor-related protein complex AP-3, sigma 2 subunit |
| 1.5634 | AA079926 | 0 | 0 |
| 1.5572 | AA087290 | 0 | 0 |
| 1.5571 | Z31134 | Mm.3955 | eukaryotic translation initiation factor 3, subunit 7 (zeta, 66/67 kDa) |
| 1.5555 | AA015415 | Mm.20354 | kinesin light chain 1 |
| 1.5512 | W45817 | Mm.24042 | RIKEN cDNA 1210001E11 gene |
| -1.5476 | U34293 | 0 | 0 |

[CANCER RESEARCH 62, 5096–5105, September 1, 2002]

# Fibroblast Growth Factor 8 Isoform b Overexpression in Prostate Epithelium: A New Mouse Model for Prostatic Intraepithelial Neoplasia[1]

**Zhigang Song,[2] Xiantuo Wu,[2] William C. Powell, Robert D. Cardiff, Michael B. Cohen, Robert T. Tin, Robert J. Matusik, Gary J. Miller,[3] and Pradip Roy-Burman[4]**

*Departments of Pathology [Z. S., X. W., W. C. P., R. T. T., P. R-B.] and Biochemistry and Molecular Biology [P. R-B.], University of Southern California, Keck School of Medicine, Los Angeles, California 90033; Center for Comparative Medicine, University of California-Davis, Davis, California 95616 [R. D. C.]; Departments of Pathology, Urology and Epidemiology, The University of Iowa, Iowa City, Iowa 52242 [M. B. C.]; Department of Urologic Surgery, Vanderbilt Prostate Cancer Center, Nashville, Tennessee 37232 [R. J. M.]; and Department of Pathology, University of Colorado Health Sciences Center, Denver, Colorado 80262 [G. J. M.]*

## ABSTRACT

**Fibroblast growth factor 8 isoform b (FGF8b), a mitogenic and transforming polypeptide, was demonstrated to be naturally up-regulated in prostatic premalignant and malignant lesions in men. We generated four independent lines of transgenic mice with targeted overexpression of FGF8b in the prostatic epithelium using an improved rat probasin promoter, $ARR_2PB$. Transgene expression in the prostate tissue was readily demonstrated by reverse transcription-PCR and localized to the prostatic epithelium by *in situ* hybridization. The histopathology of the prostate tissues was followed in different age groups of the various lines but most extensively in one line (line 3), starting from 1 month of age up to 24 months. Prostatic hyperplasia appeared in the lateral and ventral prostates in some animals as early as 2–3 months and in other lobes between 6 and 16 months. Beginning at 5–7 months, dysplasia, akin to what may be considered low-grade prostatic intraepithelial neoplasia (LGPIN) in humans, was detected. During the first 14 months, 100% of animals exhibited multifocal epithelial hyperplasia; 35% also had areas of LGPIN. This profile changed in subsequent months (15–24 months) to a higher incidence of LGPIN (66%) along with high-grade PIN (HGPIN) lesions (51%). Similar to HGPIN, stromal proliferation and appearance of papillary hyperplasia with atypia displayed a delayed pattern. The affected stroma consisted primarily of the smooth muscle cell component. The incidence of chronic inflammation, mostly involving T cells, was higher in the prostate of the transgenic mice relative to controls; however, the presence of a direct correlation between inflammation and hyperplasia or preneoplastic lesions was not identified. These transgenic mice represent a "natural" animal model for investigating the mechanism of development and progression of prostatic diseases, such as prostatic hyperplasia and preneoplastic lesions.**

## INTRODUCTION

PIN[5] is generally considered as a preneoplastic lesion in humans (1–3). To understand mechanisms involved in the genesis and progression of prostatic preneoplastic lesions, the availability of suitable animal models for the disease process is critical. Although several mouse models for the study of prostate tumorigenesis have been described recently (4–8), there are, as yet, no good mouse models of prostate adenocarcinoma. As such, attempts to generate other animal models targeting specific genes for growth factors, oncoproteins, or tumor suppressors known to be naturally involved in this malignancy should have a high priority. Perhaps, through a logical combination of these animals, the resultant hybrid animals may more closely resemble either early or late, if not the complete histopathological and clinicophysiologic characteristics of the human prostate cancer.

Dysregulation of several growth factors has been implicated in prostate tumorigenesis (9, 10). One such factor, FGF8, was reported to be associated with the development or progression of this malignancy (11–16). The conventional knockout of the *fgf8* gene in the mouse led to early embryonic lethality (17) because FGF8 is a crucial signaling molecule for outgrowth and patterning, such as the elongating body axis, midbrain/hindbrain junction, limb, and face (18–24). Alternative splicing of the first exon of the *fgf8* gene in mouse gives rise to eight potential protein isoforms that vary in their amino termini (20, 25–27). In humans, however, only four protein isoforms (FGF8a, 8b, 8e, and 8f) are predicted because of a blocked reading frame in the exon 1B of the human gene (28, 29). Of the four possible isoforms, FGF8b has been demonstrated to possess the most transforming and tumorigenic potential (11, 26, 30, 31), it appears to be the primary species in prostate epithelial cell lines or malignant epithelium (11, 13, 15), and its expression is practically undetected in the stromal component of prostate cancer (13, 15, 32). The overexpression of FGF8b in LNCaP cells increases their growth rate, soft agar clonogenicity, and *in vitro* and *in vivo* invasion ability (16). Furthermore, it is demonstrated that the growth of stromal cells can be strongly up-regulated when cocultured with FGF8b-producing LNCaP cells (16). Down-regulation FGF8b mRNA by antisense RNA expression reduces the growth rate, inhibits the soft agar clonogenic activity, and decreases *in vivo* tumorigenicity of prostate tumor cells (14). Among the FGF receptors, the "c" splice isoform of FGFR2 or FGFR3, as well as FGFR4, is reported to be most efficiently activated by FGF8b (33, 34). Although these receptor isoforms are considered to be largely expressed in mesenchymal cells (35), there is evidence of aberrant expression of FGFR isoforms in prostate cancer cells (9, 36). It is also interesting that prostate appears to exhibit wide expression of the general classes of FGFRs. For example, a moderate level of expression of FGFR1 and FGFR2 is found in prostate epithelium and the microvasculature, whereas stromal smooth muscle cells exhibit a weak level of expression of FGFR3 (37). In another study (35) with primary cultures of human prostatic epithelial and stromal cells, FGFR3 was found to be the primary product in epithelial cells with a smaller amount of FGFR2, whereas stromal cells express primarily FGFR3 and a smaller amount of FGFR1 and FGFR2. More recently, increased expression of FGF8 isoforms and their receptors were reported in PIN lesions (32). Together, these observations indicate that FGF8-FGFR signaling plays an important role in prostate biology and cancer.

Thus, to study the *in vivo* effects of FGF8b, it was important to establish transgenic mouse lines by targeting FGF8b overexpression in the prostate epithelium. For this purpose, the small rat composite 468-bp probasin promoter $ARR_2PB$ was chosen. This promoter has been demonstrated to confer a high level of reporter transgene expression specifically in the luminal prostatic epithelium and is

Received 2/20/02; accepted 7/1/02.

The costs of publication of this article were defrayed in part by the payment of page charges. This article must therefore be hereby marked *advertisement* in accordance with 18 U.S.C. Section 1734 solely to indicate this fact.

[1] This research was supported by NIH R01 CA59705 and, in part, by a grant from the T. J. Martell Foundation and NIH R01 CA76192.

[2] These two authors contributed equally to this work.

[3] Deceased, May 25, 2001.

[4] To whom requests for reprints should be addressed, at Department of Pathology, University of Southern California, Keck School of Medicine, 2011 Zonal Avenue, Los Angeles, CA 90033. Phone: (323) 442-1184; Fax: (323) 442-3049; E-mail: royburma@usc.edu.

[5] The abbreviations used are: PIN, prostatic intraepithelial neoplasia; LGPIN, low-grade PIN; HGPIN, high-grade PIN; FGF8, fibroblast growth factor 8; RT-PCR, reverse transcription-PCR; BrdUrd, bromodeoxyuridine; SMA, smooth muscle actin; AP, anterior prostate; DLP, dorsolateral prostate; DP, dorsal prostate; LP, lateral prostate; VP, ventral prostate; DD, ductus deferens; SV, seminal vesicle.

strongly regulated by androgens (38, 39). Four independent transgenic lines, in which the FGF8b transgene expression is driven by this promoter, were generated. The specificity of expression of the transgene was confirmed by RT-PCR and *in situ* hybridization, and the transgenic animals heterozygous for the transgene were followed for study of the histopathology for up to 24 months of age.

## MATERIALS AND METHODS

**Construction of Transgene.** The *Xho*I-*Xba*I fragment of $ARR_2PB$ (38) was blunted and ligated into pSV plasmid vector containing the SV40 poly(A) sequence and splicing signal sequence. Subsequently the full-length human FGF8b cDNA fragment (11), which harbored 100% amino acid sequence identity to the mouse FGF8b sequence (11), was inserted into the *Eco*RI site after the $ARR_2PB$ promoter (Fig. 1*A*). The sequence of the FGF8b coding region and junction of each fragment were confirmed by automated DNA sequencing. The fragment containing the $ARR_2PB$ promoter, FGF8b cDNA, and SV40 poly(A) sequence was released by digestion with *Not*I and *Kpn*I, isolated by agarose gel, and purified by Qiagen spin column (Qiagen, Valencia, CA) and Elutip column according to the manufacturer's protocol.

**Generation of Transgenic Mice.** Two rounds of pronuclear injection of $ARR_2PB$ promoter-FGF8b-SV40 poly(A) fragment were performed. The (C57BL/6 × DBA2)$F_1$ hybrid fertilized eggs containing the transgene construct were placed into pseudo-pregnant females. Potential founder animals were screened by PCR and confirmed by Southern blot analysis using clipped tissue DNA samples. Four productive transgenic lines were established by mating the founder animals with nontransgenic (C57BL/6 × DBA2)$F_1$ mice. Offspring were genotyped by PCR from tail DNA at 3–4 weeks of age.

**Tissue Preparation.** An aliquot of 150–200 μl of 10 mg/ml BrdUrd (Sigma Chemical Co., St. Louis, MO) was injected i.p. 1 h before animals were sacrificed. The urogenital system was removed, and the individual prostate lobes were dissected under a dissecting microscope. Tissues for histopathological observation were fixed overnight in 10% neutral buffered formalin (Surgipath, Richmond, IL). Fixed tissues were processed and embedded in paraffin. Thin sections (5 μm) were cut and stained with H&E. Tissues for mRNA assays were frozen in liquid nitrogen at the time of dissection.

**PCR and Southern Blot Analysis.** The tissue specimens were digested with 20 mg/ml proteinase K (Life Technologies, Inc., Buffalo, NY) in 500 μl of a buffer containing 50 mM Tris-HCl (pH 8.0), 100 mM EDTA (pH 8.0), 100 mM NaCl, and 1% SDS at 50°C for overnight. After centrifugation, the supernatant containing the genomic DNA was collected. After boiling for 5 min, 2 μl of the supernatant were used as the template in 30 μl of reaction mixture containing 0.2 mM dNTP, 1.0 mM $MgCl_2$, 0.02% (w/v) DMSO, 6 pmol of each primer, and 0.3 unit of Tag polymerase (Life Technologies, Inc.). The sequences of the primers F8b-3 and SV40-a used for PCR and RT-PCR were 5′-AACTACACAGCGCTGCAGAATG-3′, which is complementary to the FGF8b cDNA sequence (11), and 5′-GTTGAGAGTCAGCAGTAGCCTC-3′, which is complementary to the SV40 poly(A) signal sequence (Fig. 1*A*). The PCR was started at 94°C for 4 min, followed by 35 cycles at 94°C for 1 min, 58°C for 90 s, and 72°C for 90 s, and ended with 72°C for 5 min. Founder animals were further confirmed by Southern blot analysis. Briefly, 10 μg of tail DNA were digested by *Bam*HI, run on a 1.5% agarose gel, and transferred to Nylon membrane. A $^{32}P$-labeled SV40 signal sequence was used to probe the Southern blot.

**RT-PCR.** The tissue RNA was extracted using RNeasy Mini kit (Qiagen, Germany). The ThermoScript RT-PCR System (Life Technologies, Inc.) was used for RT-PCR assay. A solution of 1 μg of RNA was mixed with 1 μl of random hexamer primers provided in 10 μl volume and denatured at 65°C for 5 min. After cooling on the ice, 10 μl of cDNA synthesis mixture were added. The samples were incubated at 25°C for 10 min, followed by 60 min at 50°C, and terminated at 85°C for 5 min. Aliquots of 2–4 μl of cDNA synthesis reaction mixtures were used as templates for PCR as described above.

***In Situ* Hybridization Assays.** The transgene construct was amplified by PCR using primers of F8b-T7 and F8b-T3 or primers of SV40-T7 and SV40-T3 (Fig. 1*A*). The sequence of F8b-T7 was 5′-GCGCTAATACGACTCACTATAGGGTAAGCTTGCTGCCATGGGCAGC-3′, which contained the T7 promoter sequence and a segment that was complementary to FGF8b sequence at the 5′ end (11). The sequence of F8b-T3 was 5′-GCGCAATTA-

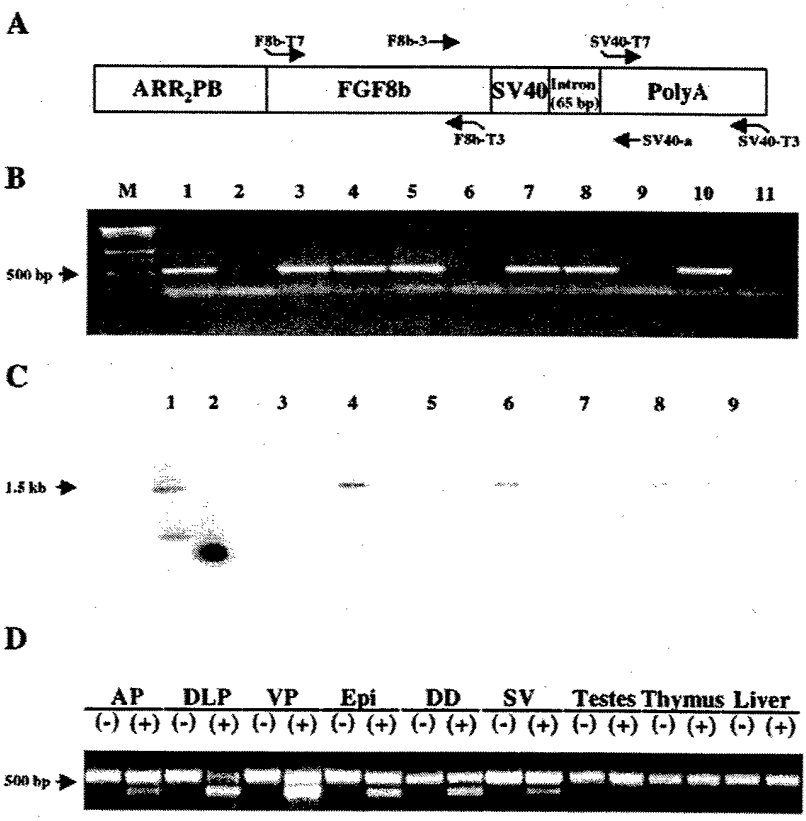


Fig. 1. Detection of transgene and its expression in transgenic animals. *A*, graphic illustration of transgene construct. The *FGF8b* gene is driven by a prostatic-specific promoter $ARR_2PB$ and followed by the SV40 poly(A) signal sequence, in which a 65-bp intron is included. Locations of the various primers are indicated by *arrows*. *B*, an example of PCR genotyping using F8b-3 and SV40-a primer set. The expected size of the amplified product is 550 bp. *M*, DNA molecular weight marker. Numbers over the lanes represent DNA samples from various PB-FGF8b transgenic progeny. *Lane 1*, positive sample; *Lane 2*, negative sample. Transgene was detected in samples of *Lanes 3, 4, 5, 7, 8,* and *10*. *C*, Southern blot analysis of genomic DNA from potential founder animals using a $^{32}P$-labeled SV40 poly(A) signal sequence probe. A band of 1.5 kb is expected. Each lane represents a putative PB-FGF8b transgenic founder animal. *Lane 1*, positive sample; *Lane 2*, negative samples. *Lanes 4, 5, 6,* and *8* (founder animal nos. 1, 3, 5, and A, respectively) were transgene positive. *D*, RT-PCR analysis of the tissue RNA from transgenic animals; the presence or absence of reverse transcriptase is indicated by (+) and (−), respectively. Transgene expression was readily detected in AP, DLP, and VP and was also detectable in DD, SV, and epididymis (*Epi*). However, transgene expression was not detected in other tissues tested, *i.e.*, testes, thymus, liver, kidney, lung, spleen, and heart.

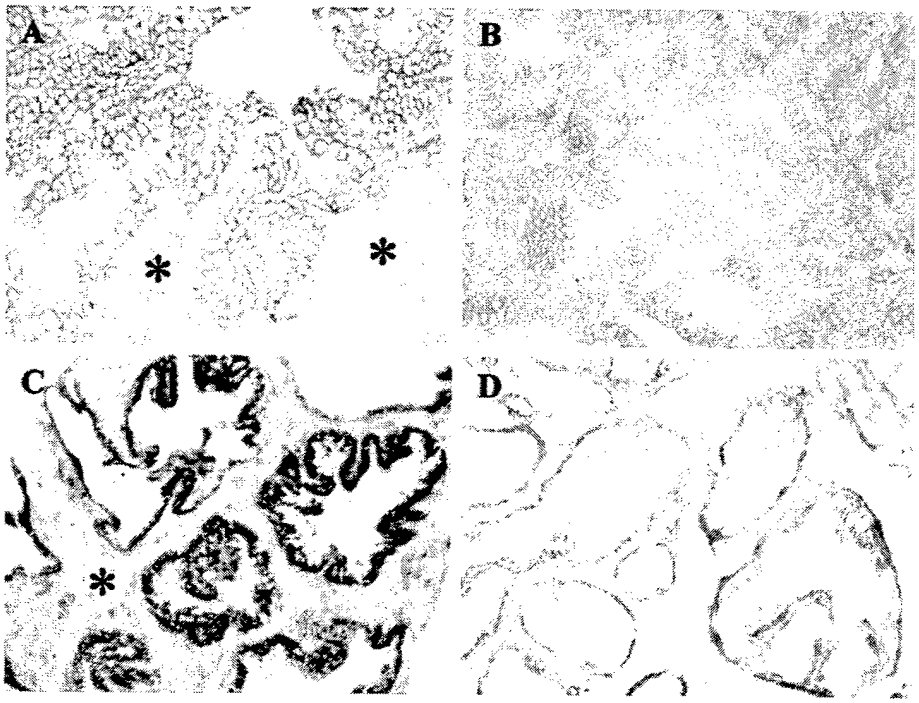


Fig. 2. *In situ* hybridization assays. Detection of *FGF8* gene expression in PIN lesions in DLP of a LPB-Tag transgenic subline, 12T-7s (*A*, X200) using a FGF8-specific antisense riboprobe, F8b-T3 (Fig. 1*A*). *FGF8* expression was mostly detected in epithelial cells, whereas there was only weak or no expression in stromal compartments. For illustration, some areas of the stroma are marked by *. Adjacent sections of the lesions were incubated with a FGF8-specific sense probe, F8b-T7, serving as the negative control (*B*, ×200). Detection of transgene expression in our PB-FGF8b transgenic animals is illustrated by a section of VP from a 6-month-old mouse using a SV40 poly(A)-specific antisense riboprobe, SV40-T3. Transgene expression was prominently detected in epithelial cells but not in the stroma (*C*, ×40); again, stromal areas are labeled with *. Section of VP from a littermate control animal using the same antisense probe served as a negative control (*D*, ×40).

ACCCTCACTAAAGGGGCTTGATATCGAATTCAGGATG-3′, which contained the T3 promoter sequence and segment that was complementary to FGF8b sequence at the 3′ end (11). The sequence of SV40-T7 was 5′-GTAATACGACTCACTATAGGGCGCAGTGGTGGAATGCCTTTAATG-3′, which contained the T7 promoter sequence and a segment that was complementary to SV40 poly(A) signal at 5′ end. The sequence of SV40-T3 is 5′-GCGCAATTAACCCTCACTAAAGGGACCTCTACAAATGTGG-TATGGCT-3′, which contained the T3 promoter sequence and segment that was complementary to SV40 poly(A) signal at 3′ end. PCR products were transcribed *in vitro* into probes that were labeled with digoxigenin using a digoxigenin labeling kit (Boehringer Mannheim, Mannheim, Germany). *In Situ* hybridization assay was performed as described by Nieto *et al.* (40) with some modifications (41). In short, frozen tissues (5 μm) were hybridized overnight at 60°C in hybridization mixture with a probe diluted to 1:100. Sections were incubated in the blocking solution containing alkaline phosphatase labeled sheep anti-digoxigenin Fab fragments (1:1500; Boehringer Mannheim) overnight at room temperature. Signals were detected with a detection solution containing 4-nitro blue tetrazolium chloride and 5-bromo-4-chloro-3-indolyl-1-phosphate (Boehringer Mannheim).

**Histological Classification.** Consistent with previously described criteria (8, 42), a similar grading system for PIN-like lesions was used to evaluate PB-FGF8b animals. Generally, PIN lesions were categorized into LGPIN and HGPIN based on their degree of cytological atypia. LGPINs showed mild cytological atypia. HGPINs were distinguished from LGPINs by more epithelial cell proliferation, nuclear stratification, and cytological atypia. Other lesions, such as papillary hyperplasia, that cannot be characterized by this grading system are described separately, based on their architecture and cytology.

**Immunohistochemistry.** BrdUrd staining was performed using the Zymed BrdUrd staining kit (Zymed, South San Francisco, CA). Sections were incubated with a biotinylated monoclonal anti-BrdUrd antibody. Signals were generated by the Streptavidin-peroxidase with diaminobenzidine as a chromogen. The slides were counterstained with methylene green (KPL Labs, Gaithersburg, MD). The staining for androgen receptor was performed in a similar manner. After antigen retrieval by microwave heating in 1 M urea, specimens were incubated with a rabbit anti-androgen receptor polyclonal antibody (Santa Cruz Technology, Santa Cruz, CA) at 0.8 μg/ml concentration. The bound antibody was detected with the biotinylated goat antirabbit immunoglobulin. Sections incubated without primary antibody served as negative controls. For SMA staining, a mouse monoclonal antibody against α-SMA (Sigma Chemical Co.) was used at 1.1 μg/ml concentration with the DAKO ARK kit (DAKO, Carpinteria, CA) to eliminate mouse background staining. A rabbit polyclonal antihuman CD3 antibody (DAKO) was used at 0.8 μg/ml concentration for T-cell staining. For B-cell staining, a rat antimouse CD45R/B220 monoclonal antibody (PharMingen, San Diego, CA) was used at 0.6 μg/ml concentration.

## RESULTS

**Status of FGF8 Expression in PIN Lesions of the Mouse Prostate in LPB-Tag Sublines.** Although an association between FGF8 overexpression and human prostate cancer was described previously, little was known about this association in mice. Thus, it was important to investigate the FGF8 expression status in prostatic lesions from mice. For this purpose, LPB-Tag sublines 12T-7f and 12T-7s were used (5). PIN lesions of these mice were analyzed for FGF8 expression by *in situ* hybridization assay in which FGF8-specific riboprobes were used. Signals were readily detected by a F8b-T3 antisense probe in the epithelial lesions of these lines. This is illustrated in Fig. 2*A* for the 12T-7s line. Weak signals were also detected in prostate tissues of wild-type control animals only after prolonged exposure (data not shown). Sections incubated with a F8b-T7 sense probe served as an internal negative control as shown in Fig. 2*B*. The major FGF8 RNA species expressed in the tumor sections was identified to be FGF8b following the same RT-PCR protocol that we reported before (11). A similar RT-PCR analysis of a tumor cell line, TRAMP-C, derived from the TRAMP model (43), also showed a single FGF8b species as the primary product (data not shown).

**Generation of Productive Transgenic Lines.** The founder animals were identified by the presence of a 550-bp PCR product amplified from tail DNA by the primers that spanned the FGF8b cDNA gene and the SV40 poly(A) signal sequence of the transgene (Fig. 1*B*). These founder animals were further confirmed by the presence of a 1.5-kb band on a Southern blot of *Bam*HI-digested genomic DNA probed with the SV40 poly(A) signal sequence probe (Fig. 1*C*). Four founder animals were identified from the first pronuclear injection and marked as 1, 3, 5, and A. Another series of five founder mice, named 6, 8, 18, 20, and 24, was obtained from the

Table 1 *Pathology of PB-FGF8b line 3 mice*

| Age (mo) | Animal no. | Histology of the prostate[a] | | | | Other notable findings |
|---|---|---|---|---|---|---|
| | | VP | LP | DP | AP | |
| 1 | 310 | normal | normal | normal | normal | |
| 2 | 289 | normal | Hy | normal | normal | |
| 3 | 272 | Hy | normal | normal | normal | |
| 4 | 268 | Hy | Hy | normal | normal | |
| | 245 | Hy | Hy | normal | normal | |
| 5 | 257 | Hy | LGPIN | In | normal | |
| 6 | 234 | Hy, In, Sp | LGPIN, In | LGPIN, In | In | |
| 7 | 223 | Hy, Sp | Hy | normal | normal | |
| | 11 | normal | LGPIN | normal | normal | |
| | 203 | LGPIN | LGPIN, In | normal | normal | |
| 8 | 37 | Hy | Hy | normal | normal | |
| 9 | 213 | Hy | normal | normal | normal | |
| | 172 | normal | normal | Hy | normal | |
| 11 | 58 | LGPIN, In | normal | LGPIN | normal | |
| | 91 | Hy | Hy, In | normal | normal | |
| 12 | 2 | Acute In | Acute In | normal | normal | |
| 13 | 128 | LGPIN, In | LGPIN | LGPIN | normal | |
| 14 | 209 | Hy | Hy, In | normal | normal | |
| 15 | 120 | LGPIN | LGPIN | HGPIN | normal | |
| 16 | 202 | Hy | LGPIN | Hy, In | In | |
| | 103 | Papillary Hy/atypia | HGPIN, Papillary Hy/atypia | LGPIN | Hy | |
| 17 | 178 | Hy | Hy | Hy | normal | |
| | 185 | LGPIN, Sp | LGPIN | Hy | Hy | |
| | 190 | Hy, In | Hy, In, Sp | LGPIN, In | LGPIN, In | a, b, c, d |
| | 191 | Hy | LGPIN, In, Sp | LGPIN | normal | |
| | 98 | HGPIN, In, Sp | HGPIN, In, Sp | HGPIN | normal | |
| 18 | 47 | LGPIN, In | HGPIN, In | LGPIN | normal | |
| | 88 | LGPIN, In, Sp | HGPIN, In, Sp | HGPIN, Sp | LGPIN, Sp | |
| | 162 | Hy | Hy | Hy | normal | |
| | 156 | Papillary Hy/atypia | LGPIN, In | Sp | Hy, Sp | |
| 19 | 82 | HGPIN, Papillary Hy/atypia, In, Sp | HGPIN | HGPIN | In | |
| | 163 | LGPIN | LGPIN | LGPIN | normal | |
| | 157 | HGPIN, Papillary Hy/atypia | HGPIN | normal | normal | |
| | 150 | LGPIN | LGPIN, Sp | HGPIN, In, Sp | normal | |
| | 151 | LGPIN, Sp | HGPIN | HGPIN | normal | |
| 20 | 90 | Acute In | HGPIN | normal | normal | |
| | 114 | Hy, In, Sp | HGPIN | HGPIN, Sp | LGPIN | |
| | 135 | HGPIN | HGPIN | HGPIN | LGPIN | |
| | 147 | LGPIN | HGPIN, In | HGPIN | normal | |
| | 99 | LGPIN | HGPIN | HGPIN | LGPIN | |
| | 97 | LGPIN | HGPIN | HGPIN | normal | |
| 21 | 101 | Papillary Hy/atypia | LGPIN, In | LGPIN | Hy, Sp | |
| | 113 | LGPIN, In, Sp | Papillary Hy/atypia, Sp | LGPIN, In, Sp | normal | |
| | 105 | HGPIN | HGPIN | HGPIN | normal | |
| | 108 | Papillary Hy/atypia, Sp | Papillary Hy/atypia, Sp | Papillary Hy/atypia | normal | |
| | 119 | LGPIN, In | LGPIN, In | In, Sp | HGPIN, In, Sp | |
| 22 | 109 | Hy | Hy, In | normal | Sp | |
| | 143 | Papillary Hy/atypia, In, Sp | Hy | LGPIN | normal | |
| | 148 | Hy | Hy | normal | normal | |
| | 131 | LGPIN, In, Sp | Papillary Hy/atypia, In, Sp | LGPIN, In, Sp | Hy | a |
| | 138 | Hy | HGPIN, In, Sp | normal | LGPIN | |
| | 141 | Hy | In | Hy | Sp | |
| 23 | 130 | LGPIN | LGPIN | Hy | In | |
| | 133 | LGPIN, In, Sp | LGPIN, In, Sp | Hy, In | normal | |
| | 126 | Hy, In, Sp | Hy, In, Sp | normal | normal | |
| | 129 | LGPIN, In, Sp | HGPIN | Hy | normal | |
| 24 | 122 | HGPIN, In, Sp | HGPIN, In, Sp | Hy, In | Sp | |

[a] Hy, hyperplasia; In, inflammation. Sp, stromal proliferation. Mild inflammation is shown in DD (a), SV (b), and epididymis (c). d, lymphocyte infiltration, mostly T cells, in stomach and small intestinal tissues.

second injection. Founder A, a male animal, was determined to be infertile. Founders 5, 6, and 8 did not transmit the transgene to the offspring, as determined by PCR screening of tail DNA, after testing of four litters of total 25 offspring. Animal 24 contained the transgene but failed to express it in the prostate tissues as determined by RT-PCR analysis using three different age groups of the offspring. Eventually, four productive lines, 1, 3, 18, and 20, that contained the transgene and expressed the mRNA in prostate tissues were established.

Because the primers for the detection of transgene expression were designed to flank an intron in SV40 poly(A) signal sequence, an additional band of 485-bp long was expected to be amplified if the transgene was transcribed and spliced (Fig. 1*D*). For all productive lines, the expression of the spliced version was detected in all prostate lobes, *i.e.*, AP, DLP, and VP. A detectable level of expression was also seen in the DD, SV, and epididymis. To determine whether there was spurious expression of the transgene, various other tissues (testes, thymus, liver, kidney, lung, spleen, and heart) from animals of different lines were examined for transgene expression by RT-PCR. There was no detectable FGF8b mRNA in these tissues. When prostates of animals of different ages (4–24 months) were assayed by RT-PCR, it was found that the transgene continued to be expressed throughout the time period of this investigation (data not shown). The transgene expression was localized by *in situ* hybridization assay using a SV40 poly(A)-specific riboprobe. In prostate tissue sections, transgene mRNA was readily detected by the SV40-T3 antisense probe, whereas the SV40-T7 sense probe served as an internal negative control. As illustrated in Fig. 2*C*, the signals for the transgene

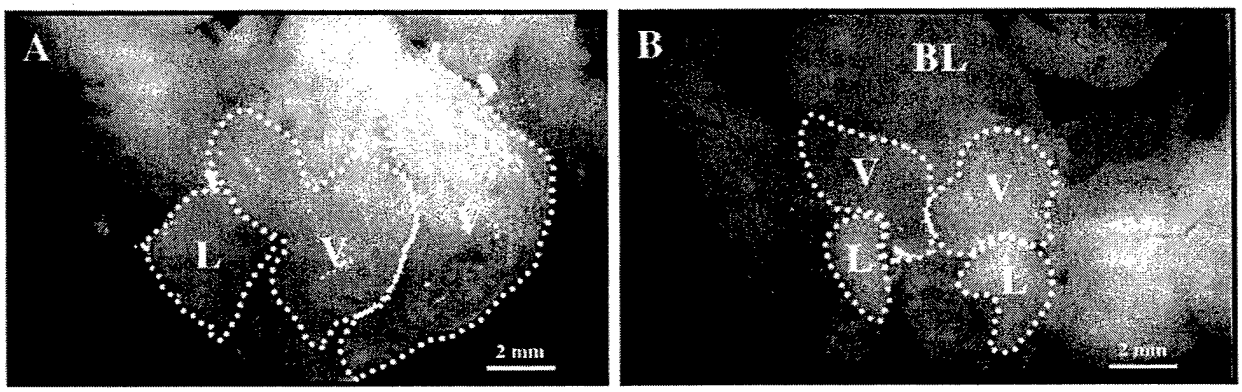


Fig. 3. Gross examination of prostate tissues. *A*, a 19-month-old transgenic animal. *B*, a littermate control animal. *BL*, bladder; *V*, VP; *L*, LP.

transcripts were strikingly confined to the epithelial cells of the prostate. No positive signals were found on the prostate tissue sections of the nontransgenic littermate control animals under identical experimental conditions (Fig. 2*D*).

**Overexpression of FGF8b Led to PIN Lesions.** Throughout the experimental period, no significant difference in gross body weight between the transgenic animals and wild-type siblings was found. Among the four productive lines, line 3 was studied most extensively (Table 1). In this line, after 2 to 3 months, the LP and VP of the transgenic animals were consistently larger in size, varying between 2 and 15 times those of the age-matched control animals (Fig. 3). Histopathologically, hyperplasia was detected in the LP and VP of some animals at time points as early as 2–3 months of age, which was consistent with the results of the gross examination. The lesions were usually multifocal in that epithelial hyperplasia was identified in many ducts of one lobe, as illustrated for VP of one transgenic in Fig. 4*A*. Fig. 4*B* represents the VP of a littermate nontransgenic animal. Generally, multifocal hyperplasia developed later in the DP and AP, with the earliest starting at 6 and 16 months, respectively. Stromal proliferation surrounding the epithelial hyperplasia (Fig. 4*A*) became prominent in older transgenic animals, generally beginning at around 17 months of age, although in two cases, stromal hypercellularity in VP was noted as early as 6–7 months of age (Table 1).

Between 5 and 7 months, LGPIN was readily detected in the DP, LP, and VP. These lesions were organized in flattened, papillary, cribriform, or tufting patterns. The atypical cells were generally larger than adjacent hyperplastic cells. Although the nuclei were larger and hyperchromatic, they were mildly pleomorphic (Fig. 4, *C* and *D*). Abundant eosinophilic cytoplasm was also readily seen. Occasionally, mitotic figures could be identified (Fig. 4*C*). Beginning at 15–17 months, HGPINs appeared in the DP, LP, and VP. In these relatively advanced lesions, atypical cells filled or almost filled the lumina (Fig. 5, *A–C*). Cellular atypia in HGPIN was much more pronounced as compared with LGPIN. This was characterized by an increased nuclear: cytoplasmic ratio, marked nuclear atypia, hyperchromasia, and prominent nucleoli. Mitotic figures were more common in HGPIN than LGPIN (Fig. 5, *A* and *D*). As shown in Fig. 5*C*, a bulging duct filled with atypical cells arranged in cribriform pattern stood out from the

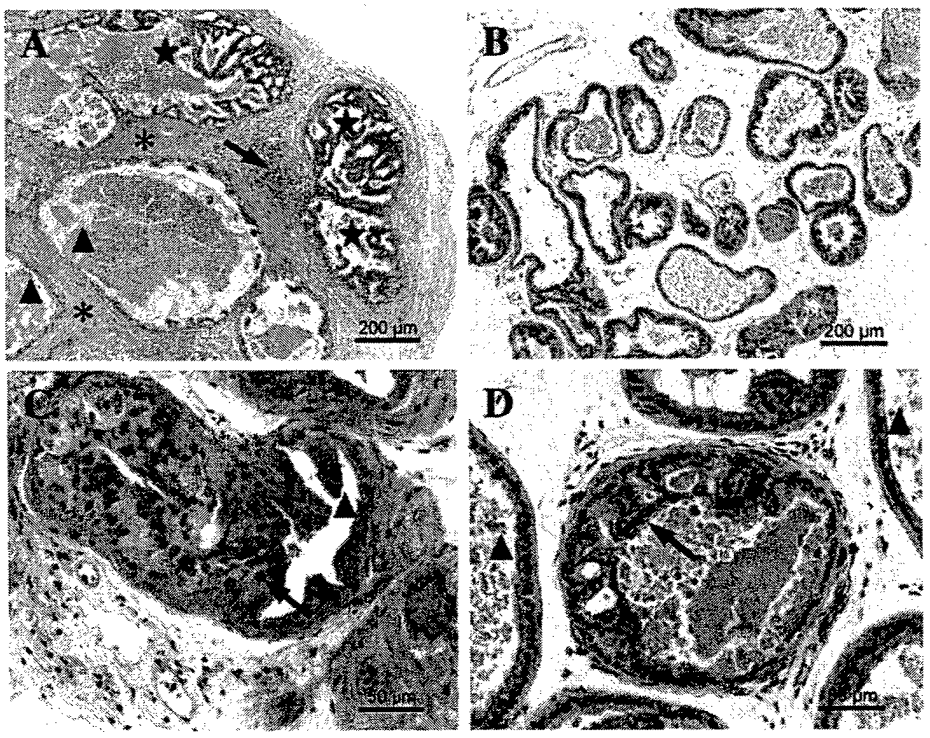


Fig. 4. Illustrations of histopathology of PB-FGF8b transgenic animals (H&E). *A*, multifocal hyperplasia (★), stromal proliferation (*), and mild chronic inflammation (*arrow*) in a VP of a 20-month-old transgenic animal are indicated. Uninvolved areas (▲) served as internal control. *B*, VP of a littermate nontransgenic animal. *C*, LGPIN in a DP of a 21-month-old transgenic animal. *Arrow*, mitotic figure. A portion of normal DP epithelium (▲) served as an internal control. *D*, LGPIN in a LP of a 5-month-old transgenic animal. *Arrow*, lumen containing the LGPIN lesion. Lumina of normal LP epithelium (▲) served as the internal control.

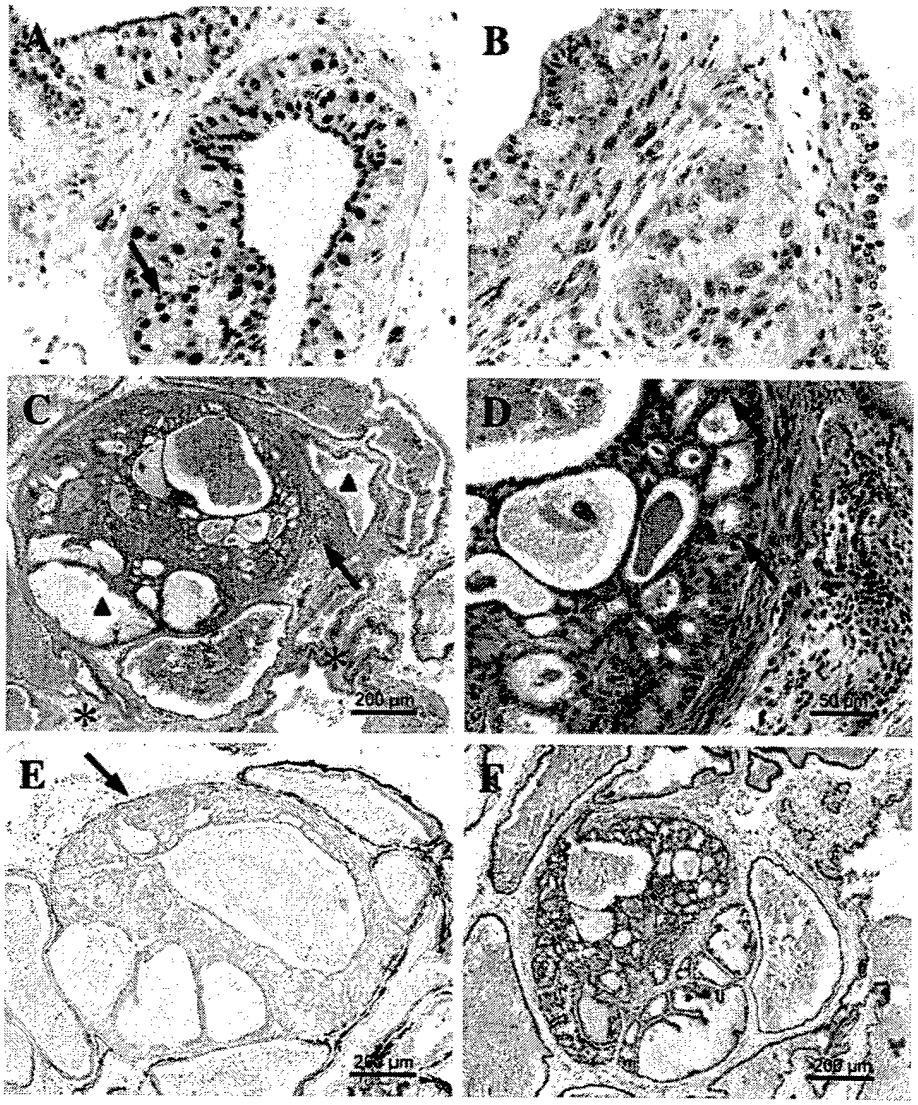


Fig. 5. HGPIN in PB-FGF8b transgenic animals. *A*, HGPIN lesion in a DP of a 16-month-old transgenic animal (H&E, ×400). *Arrow*, mitotic figure. *B*, HGPIN in a VP of the same 16-month-old transgenic animal (H&E, ×400). *C*, HGPIN in a LP of an 18-month-old transgenic animal (H&E). The bulging duct appeared filled with atypical cells arranged in the cribriform pattern. Areas of thickened stroma (*) and an inflammatory reaction (*arrow*) are also indicated. Adjacent lumina (▲), which appeared normal, served as internal control. *D*, high power examination of the HGPIN lesion in *C* (H&E). Highly pleomorphic atypical cells manifested as back-to-back glandular structures. *Arrow*, mitotic figures. Reactive inflammation was also prominent (*right side* of the *arrows*). *E*, anti-SMA immunostaining of the HGPIN lesion in *C*. A portion of the fibromuscular sheath of the affected lumen (*arrow*) was missing, in contrast to the intact lining seen surrounding the adjacent normal glands. *F*, presence of androgen receptors in these atypical cells of *C* is demonstrated by the anti-androgen receptor immunostaining.

adjacent abnormal glands. Apoptotic bodies and an inflammatory reaction were noted (Fig. 5*D*). Although the epithelium was still surrounded by a thin layer of laminin focally, a part of fibromuscular sheath appeared disrupted as revealed by anti-SMA immunostaining (Fig. 5*E*). Androgen receptor expression appeared to be intact in epithelial cells of HGPIN (Fig. 5*F*).

Papillary hyperplasia, a frequent phenotype in PB-FGF8b animals, was found around 16 months of age. It was manifested as multiple nodules bulging into and filling the lumina with a stalk connected to the basement membrane (Fig. 6*A*). Although VP, LP, and DP of some but not all animals exhibited papillary hyperplasia, these lesions were not observed in AP. Microscopically, the individual lesion presented as an exophytic papillary proliferation of epithelial cells overlying a solid fibromuscular core in which some blood vessels were readily visible (Fig. 6, *A* and *B*). Atypical epithelial cells with different degrees of cytological abnormalities, as described above, were evident. These nodules, shown in Fig. 6*C*, when examined for BrdUrd immunostaining, displayed a much higher proliferation index as compared with that of the tissue from age-matched control animals (Fig. 6*D*).

In general, as summarized in Table 1 and Fig. 7, between 2 and 14 months, 100% (17/17) of line 3 transgenic animals developed multifocal hyperplasia in at least one lobe of the prostate, and 35% (6 of 17) developed LGPIN. No papillary hyperplasia or HGPIN was detected in animals up to the age of 14 months. After 15 months, 100% (39 of 39) transgenic animals continued to display hyperplasia in increased number of lobes; 23% (9 of 39) developed papillary hyperplasia with atypia, the incidence of LGPIN increased to 66% (26 of 39), and 51% (20 of 39) developed HGPIN. Similar lesions were also identified in the transgenic animals of other lines (Table 2). Throughout the investigation period, none of the nontransgenic control animals developed PIN lesions, whereas a mild hyperplasia was noted in ~20% of aging controls.

**Overexpression of FGF8b in the Epithelial Cells Also Led to Stromal Hypercellularity and Increased Inflammation in Prostate.** In line 3, chronic inflammation was frequently noticed starting at 5 months and became more common in older animals (Table 1). Generally, the inflammation was found in the LP and VP, although AP and DP were also involved but to a lesser extent. Similar changes were also present in animals of line 1, occasionally with a higher intensity when compared with animals of other lines (Table 2). Although the earliest time points of their appearances were similar, a

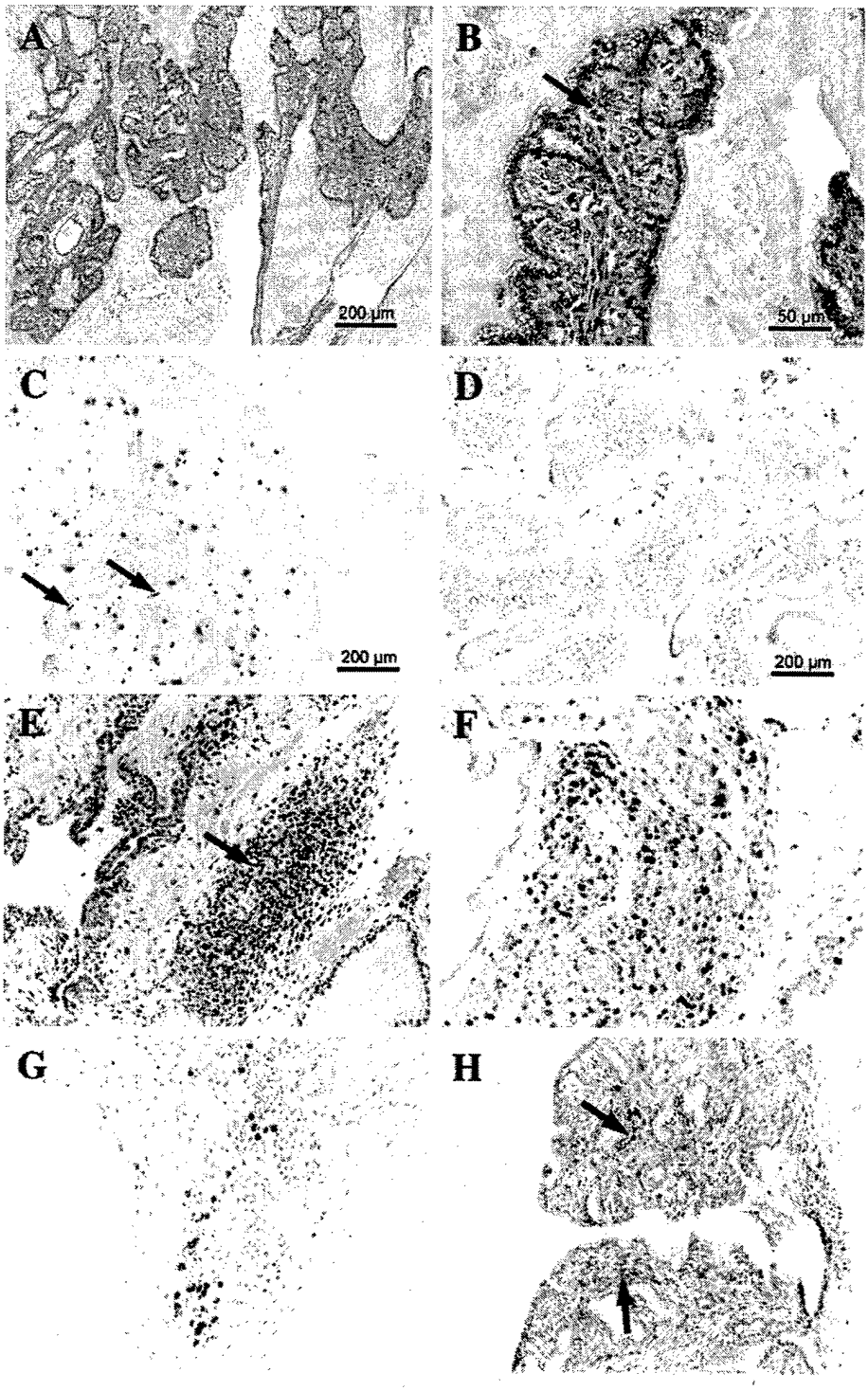


Fig. 6. Histopathology of PB-FGF8b transgenic animals. *A*, papillary hyperplasia in a LP of a 23-month-old transgenic animal (H&E). *B*, stromal cells occupied the core of papillary hyperplasia shown in *A*. Highly pleomorphic stromal cells were present with occasional mitotic figures, with one indicated by the *arrow*. *C*, increased rate of cell proliferation in papillary hyperplasia, as assessed by BrdUrd immunostaining, is illustrated by a section of LP from a 16-month-old transgenic animal as compared with its littermate control (*D*). Proliferation, which was pronounced in the epithelium, was also involved in the stroma, as indicated by *arrows*. *E*, inflammation in AP of a 23-month-old transgenic animal is indicated by the arrow (H&E, ×200). *F*, anti-CD3 immunostaining of the lymphocytes in *E* (×200). *G*, anti-CD45R/B220 immunohistochemistry of the lymphocytes in *E* (×200). *H*, anti-SMA immunostaining of the stromal cells in a section adjacent to *B*. Areas of immunoreactive cells are labeled by *arrows*.

direct correlation between the inflammation and PIN lesions could not be made, because there were specimens with PINs that lacked overt evidence of inflammation and *vice versa*. Microscopically, clusters of lymphocytes were sparsely located in the stroma (Figs. 4, 5, and 6*E*). While in close continuity with the ducts, these lymphocytes did not seem to invade the epithelial cells in most animals. Immunohistochemically, most of these lymphocytes were CD3 positive (Fig. 6*F*), whereas a small percentage was of B-cell lineage as determined by immunoreactivity to an anti-CD45R/B220 antibody (Fig. 6*G*). In rare cases (2 of 56 animals in line 3), a mixed acute and chronic inflammation was found where the glandular profile was severely disrupted. In one animal of line 3 and one of line 1 (Tables 1 and 2), the CD3-positive inflammatory cells appeared in a pattern suggestive of lymphoma within the prostate tissues, a matter that remains to be further investigated. In these animals, the inflammatory infiltration was also found in some extraprostatic tissues, such as small intestine and stomach. The stromal proliferation, which was relatively more prominent in the AP than other lobes, was another remarkable change

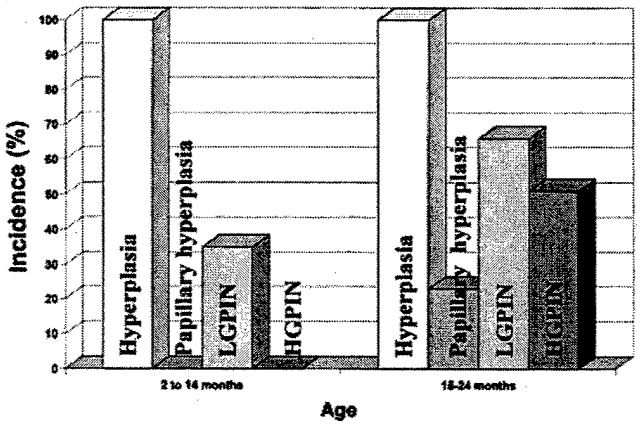


Fig. 7. Temporal incidence of appearance of prostatic lesions in PB-FGF8b transgenic animals, line 3. Between 2 and 14 months, 100% (17 of 17) of line 3 transgenic animals developed multifocal hyperplasia in at least one lobe of the prostate, and 35% (6 of 17) developed LGPIN. No papillary hyperplasia or HGPIN was detected in animals up to the age of 14 months. After 15 months, 100% (39 of 39) transgenic animals continued to display hyperplasia encompassing more lobes, 23% (9 of 39) papillary hyperplasia with atypia, 66% (26 of 39) LGPIN, and 51% (20 of 39) HGPIN.

in PB-FGF8b transgenic animals. It was characterized by significantly thick stroma with hypercellularity (Figs. 4*A* and 6, *A* and *B*). Smooth muscle cells were identified by immunohistochemistry as the major component of the stroma (Fig. 6*H*). These stromal cells also exhibited a high proliferation index (Fig. 6*C*). In some animals, proliferation of stromal cells apparently led to stromal papilloma (Fig. 6, *A* and *B*), which manifested the phyllodes-like pattern. These cells, having increased nuclear:cytoplasmic ratio, displayed pleomorphic, hyperchromatic nuclei with prominent nucleoli. A few scattered mitotic figures could also be noted (Fig. 6*B*).

The mild chronic inflammation was also found in the stroma of the DD, SV, and epididymis in some of the transgenic animals. Interestingly, these were also the nonprostatic tissues that manifested a low level of transgene expression as detected by RT-PCR assay. However, these abnormalities did not affect the fertility of the transgenic animals because all established lines could be successfully maintained. Chronic inflammation, much less severe than that identified in transgenics, was also noted in ~10% of old control animals. However, none of those control animals exhibited significant stromal hypercellularity.

## DISCUSSION

Although there is ample evidence for the up-regulation of *FGF8* gene expression in human prostatic premalignant and malignant lesions (12, 13, 15, 32), until now it was not known whether this observation is unique to the human disease or more general in nature in terms of prostate carcinogenesis. Here, we demonstrate that mouse *fgf8* transcription is also elevated in PIN lesions of SV40 Tag-driven mouse models (5). Similar to the observations in human prostate cancers, we find that *fgf8*, isoform b mRNA, whose amino acid coding sequence is 100% identical between the human and mouse species (11), is specifically up-regulated in mouse PINs. Thus, it was considered logical to develop mouse models in which the *fgf8b* is targeted for overexpression in the prostatic epithelium.

Table 2 *Pathology of other PB-FGF8b lines*

| Line no. | Age (mo) | Animal no. | Histology of the Prostate[a] | | | | Other notable findings |
|---|---|---|---|---|---|---|---|
| | | | VP | LP | DP | AP | |
| 1 | 4 | 33 | normal | normal | normal | normal | |
| | 6 | 16 | normal | normal | normal | normal | |
| | 9 | 3 | Hy | normal | normal | normal | |
| | 10 | 45 | LGPIN, Sp | normal | normal | Hy | |
| | 12 | 2 | normal | Hy | normal | normal | |
| | 13 | 18 | Hy | normal | normal | normal | |
| | 14 | 59 | In | LGPIN, In | Hy | Hy | |
| | 16 | 76 | e | e | e | e | |
| | 17 | 118 | Hy | Hy, In | In | normal | |
| | | 121 | LGPIN, Sp | Hy, In | e | normal | |
| | 18 | 47 | In, e | e | e | e | |
| | | 29 | LGPIN, In | HGPIN, In | In | In | |
| | 19 | 37 | Hy, In | LGPIN, In | e | In | |
| | | 56 | In | In | In | In | |
| | 20 | 53 | LGPIN, In, Sp | Papillary Hy/atypia | e | In, Sp | |
| | | 54 | In, Sp | Hy, In | normal | normal | |
| | | 44 | LGPIN, In, Sp | LGPIN, Sp | normal | normal | |
| | | 55 | Hy, In | normal | normal | Sp | |
| | | 60 | Hy | LGPIN, Sp | Hy | Hy | |
| | 21 | 74 | In, Sp | Hy, In, Sp | Sp | In | |
| | | 62 | LGPIN | Hy, In | normal | normal | |
| | 22 | 92 | Papillary Hy/atypia, In, Sp | LGPIN, In, Sp | e | In, Sp | a |
| | | 87 | Hy | Hy, Sp | Sp | Hy, In | a, c |
| | | 95 | Hy, In, Sp | LGPIN, In | In | Sp | |
| | | 91 | In, Sp | LGPIN, In, Sp | In, Sp | In, Sp | |
| | 23 | 72 | Hy, In, Sp | In | In, Sp | In, Sp | a, b, c |
| | | 75 | In, Sp, e | In, Sp, e | In, Sp, e | In, Sp, e | a, b, c, d |
| | | 78 | LGPIN, In, Sp | Papillary Hy/atypia, In, Sp | In, Sp | In, Sp | b |
| | | 79 | In, Sp, e | In, Sp, e | In, Sp, e | In, Sp | |
| | 24 | 83 | Hy, In, Sp | In, Sp | In | In | |
| 18 | 14 | 13 | HGPIN, Sp | HGPIN, Sp | HGPIN | normal | |
| | 16 | 16 | In | HGPIN, Sp | LGPIN | Hy | |
| | 20 | #18 | Papillary Hy/atypia, In, Sp | Hy, Sp | In, Sp | In, Sp | |
| 20 | 14 | 5 | Hy, Sp | LGPIN | HGPIN, In | In | |
| | 17 | 8 | Hy | Hy, In | Hy | Hy | |
| | 18 | 10 | LGPIN, In | Hy, Sp | Sp | normal | |
| A | 7 | #A | Hy | Hy | normal | normal | |

[a] Hy, hyperplasia, In, inflammation, Sp, stromal proliferation. Mild inflammation is shown in DD (a), SV (b), and epididymis (c). d, lymphocyte infiltration, mostly T cell, in stomach and small intestinal tissues. e, dilated glands.

We describe four productive lines of transgenic mice, in each of which the expression of FGF8b transgene is under the control of the androgen-regulated, prostate epithelium-specific $ARR_2PB$ promoter (38). These independent lines display a similar sequence of development of phenotypic changes in prostatic tissues. In general, the results point to an increased expression of FGF8b that is sufficient to drive proliferation in the prostatic epithelium preceding the development of histopathologically identifiable lesions, many of which resemble human preneoplastic prostatic lesions. A stochastic pattern of disease progression in these transgenic mice is noteworthy (Fig. 7). The prostatic abnormalities, beginning with multifocal epithelial hyperplasia, are followed by appearance of LGPIN and, subsequently, HGPIN lesions. If all of the prostatic pathology is combined, irrespective of whether one of more lobes are involved, 100% of the transgenic animals manifest prostatic hyperplasia. Although this high incidence of hyperplasia is followed by the development of LGPIN at a rate of 35% within the first 14 months, no HGPINs could be detected up to this time point. However, during further aging (15–24 months), as the incidence of LGPIN increases from 35 to 66%, there is also the first appearance of HGPIN at a remarkable high frequency of 51%. Thus, the overexpression of FGF8b appears to be a distinct initiating event in the development of hyperplasia which, in turn, is perhaps conducive to the manifestation of other genetic lesions, which may represent the rate-limiting factors responsible for a potentially temporal progression from hyperplastic changes to HGPIN lesions. These properties of the transgenic mice, which are markedly prostate restricted, also closely reflect the usual slow progression of prostatic disease in humans.

Although the specific mechanisms by which FGF8b drives tumorigenesis are not known, some of the observations made *in vivo* with this transgenic model are concordant with those reported previously in other systems. For example, *in vitro* mitogenic and transforming activity of FGF8b (11, 26, 30, 31) or tumorigenicity in mouse mammary tumor virus promoter-driven mammary or ovarian epithelium (31) are consistent with the current findings. Moreover, a delayed but fairly common development of stromal hypercellularity in the prostate of the FGF8b transgenic mice mimics the *in vitro* coculture experiments described before (16), implicating an indirect effect of FGF8b signaling in epithelial cells on the stromal cells. Thus, FGF8b is likely to act not only as an initiation factor but also, possibly, as a progression factor. Because transgene expression in our model is found to be continuous throughout the 2-year period of life investigated and considering that FGF8b overexpression in weakly tumorigenic human prostatic tumor LNCaP cells could significantly enhance their tumorigenicity and invasiveness (16), this potential should not be overlooked. However, because the model has yet to yield invasive cancer, and as described above, there are likely to be other rate-limiting factors in the progression of the lesions, FGF8b is only proven to be an etiological factor in prostate tumorigenesis in this model. Its role as a progression factor, along with other hitherto unidentified secondary factors, remains to be investigated.

In summary, transgenic mice overexpressing FGF8b in prostate epithelial cells are found to develop progressively epithelial hyperplasia, LGPIN, and ultimately HGPIN. Interestingly, abnormalities of stroma including hyperplasia and chronic inflammation are also observed in these animals. These findings are biologically significant because FGF8b expression is associated with progression of human prostate cancer, beginning with PIN lesions. The model is likely to be valuable in examining how FGF8b may be involved in influencing the autocrine and paracrine pathways in the prostate tissue. It is also important to note that the potential of the model could be greatly enhanced by seeking genetic synergy between FGF8b transgenics with mutated mice known to reflect other "natural" changes in prostate cancer, such as Nkx 3.1 (6, 44), p27 (45), and PTEN (46). With the development of an efficient prostate epithelium-specific Cre-loxP model (39), it is also now possible to generate animals with conditional alleles of genes whose disruption is otherwise embryonically lethal. One such allele, *RXRα retinoid receptor* (47, 48), has already been combined in the background of FGF8b overproduction, and there is indication of acceleration of the phenotypic changes in the prostate from this intercrossing.[6]

## ACKNOWLEDGMENTS

We thank Dr. Robert Maxon for providing us the pSV vector containing SV40 poly(A) and splicing signal sequence and for use of the transgenic facility under his direction. We are grateful to Dr. Scott Shappell of Vanderbilt University for assessment of some of the pathology slides and all members of the Roy-Burman laboratory for assistance in various aspects of the work.

## REFERENCES

1. McNeal, J. E., and Bostwick, D. G. Intraductal dysplasia: a premalignant lesion of the prostate. Hum. Pathol., *17:* 64–71, 1986.
2. Bostwick, D. G., and Brawer, M. K. Prostatic intra-epithelial neoplasia and early invasion in prostate cancer. Cancer (Phila.), *59:* 788–794, 1987.
3. Bostwick, D. G. Prostatic intraepithelial neoplasia is a risk factor for cancer. Semin. Urol. Oncol., *17:* 187–198, 1999.
4. Greenberg, N. M., DeMayo, F., Finegold, M. J., Medina, D., Tilley, W. D., Aspinall, J. O., Cunha, G. R., Donjacour, A. A., Matusik, R. J., and Rosen, J. M. Prostate cancer in a transgenic mouse. Proc. Natl. Acad. Sci. USA, *92:* 3439–3443, 1995.
5. Kasper, S., Sheppard, P. C., Yan, Y., Pettigrew, N., Borowsky, A. D., Prins, G. S., Dodd, J. G., Duckworth, M. L., and Matusik, R. J. Development, progression, and androgen-dependence of prostate tumors in probasin-large T antigen transgenic mice: a model for prostate cancer. Lab. Investig., *78:* i–xv, 1998.
6. Bhatia-Gaur, R., Donjacour, A. A., Sciavolino, P. J., Kim, M., Desai, N., Young, P., Norton, C. R., Gridley, T., Cardiff, R. D., Cunha, G. R., Abate-Shen, C., and Shen, M. M. Roles for Nkx3.1 in prostate development and cancer. Genes Dev., *13:* 966–977, 1999.
7. DiGiovanni, J., Kiguchi, K., Frijhoff, A., Wilker, E., Bol, D. K., Beltran, L., Moats, S., Ramirez, A., Jorcano, J., and Conti, C. Deregulated expression of insulin-like growth factor 1 in prostate epithelium leads to neoplasia in transgenic mice. Proc. Natl. Acad. Sci. USA, *97:* 3455–3460, 2000.
8. Masumori, N., Thomas, T. Z., Chaurand, P., Case, T., Paul, M., Kasper, S., Caprioli, R. M., Tsukamoto, T., Shappell, S. B., and Matusik, R. J. A probasin-large T antigen transgenic mouse line develops prostate adenocarcinoma and neuroendocrine carcinoma with metastatic potential. Cancer Res., *61:* 2239–2249, 2001.
9. McKeehan, W. L., Wang, F., and Kan, M. The heparan sulfate-fibroblast growth factor family: diversity of structure and function. Prog. Nucleic Acid Res. Mol. Biol., *59:* 135–176, 1998.
10. Djakiew, D. Dysregulated expression of growth factors and their receptors in the development of prostate cancer. Prostate, *42:* 150–160, 2000.
11. Ghosh, A. K., Shankar, D. B., Shackleford, G. M., Wu, K., T' Ang, A., Miller, G. J., Zheng, J., and Roy-Burman, P. Molecular cloning and characterization of human FGF8 alternative messenger RNA forms. Cell Growth Differ., *7:* 1425–1434, 1996.
12. Leung, H. Y., Dickson, C., Robson, C. N., and Neal, D. E. Over-expression of fibroblast growth factor-8 in human prostate cancer. Oncogene, *12:* 1833–1835, 1996.
13. Tanaka, A., Furuya, A., Yamasaki, M., Hanai, N., Kuriki, K., Kamiakito, T., Kobayashi, Y., Yoshida, H., Koike, M., and Fukayama, M. High frequency of fibroblast growth factor (FGF) 8 expression in clinical prostate cancers and breast tissues, immunohistochemically demonstrated by a newly established neutralizing monoclonal antibody against FGF 8. Cancer Res., *58:* 2053–2056, 1998.
14. Rudra-Ganguly, N., Zheng, J., Hoang, A. T., and Roy-Burman, P. Downregulation of human FGF8 activity by antisense constructs in murine fibroblastic and human prostatic carcinoma cell systems. Oncogene, *16:* 1487–1492, 1998.
15. Dorkin, T. J., Robinson, M. C., Marsh, C., Bjartell, A., Neal, D. E., and Leung, H. Y. FGF8 over-expression in prostate cancer is associated with decreased patient survival and persists in androgen independent disease. Oncogene, *18:* 2755–2761, 1999.
16. Song, Z., Powell, W. C., Kasahara, N., van Bokhoven, A., Miller, G. J., and Roy-Burman, P. The effect of fibroblast growth factor 8, isoform b, on the biology of prostate carcinoma cells and their interaction with stromal cells. Cancer Res., *60:* 6730–6736, 2000.
17. Meyers, E. N., Lewandoski, M., and Martin, G. R. An Fgf8 mutant allelic series generated by Cre- and Flp-mediated recombination. Nat. Genet., *18:* 136–141, 1998.
18. Heikinheimo, M., Lawshe, A., Shackleford, G. M., Wilson, D. B., and MacArthur, C. A. Fgf-8 expression in the post-gastrulation mouse suggests roles in the development of the face, limbs and central nervous system. Mech. Dev., *48:* 129–138, 1994.
19. Ohuchi, H., Yoshioka, H., Tanaka, A., Kawakami, Y., Nohno, T., and Noji, S. Involvement of androgen-induced growth factor (*FGF-8*) gene in mouse embryogenesis and morphogenesis. Biochem. Biophys. Res. Commun., *204:* 882–888, 1994.

[6] Our unpublished data.

20. Crossley, P. H., and Martin, G. R. The mouse *Fgf8* gene encodes a family of polypeptides and is expressed in regions that direct outgrowth and patterning in the developing embryo. Development (Camb.), *121:* 439–451, 1995.
21. Lorenzi, M. V., Long, J. E., Miki, T., and Aaronson, S. A. Expression cloning, developmental expression and chromosomal localization of fibroblast growth factor-8. Oncogene, *10:* 2051–2055, 1995.
22. Mahmood, R., Bresnick, J., Hornbruch, A., Mahony, C., Morton, N., Colquhoun, K., Martin, P., Lumsden, A., Dickson, C., and Mason, I. A role for FGF-8 in the initiation and maintenance of vertebrate limb bud outgrowth. Curr. Biol., *5:* 797–806, 1995.
23. Crossley, P. H., Minowada, G., MacArthur, C. A., and Martin, G. R. Roles for FGF8 in the induction, initiation, and maintenance of chick limb development. Cell, *84:* 127–136, 1996.
24. Crossley, P. H., Martinez, S., and Martin, G. R. Midbrain development induced by FGF8 in the chick embryo. Nature (Lond.), *380:* 66–68, 1996.
25. Tanaka, A., Miyamoto, K., Minamino, N., Takeda, M., Sato, B., Matsuo, H., and Matsumoto, K. Cloning and characterization of an androgen-induced growth factor essential for the androgen-dependent growth of mouse mammary carcinoma cells. Proc. Natl. Acad. Sci. USA, *89:* 8928–8932, 1992.
26. MacArthur, C. A., Lawshe, A., Shankar, D. B., Heikinheimo, M., and Shackleford, G. M. FGF-8 isoforms differ in NIH3T3 cell transforming potential. Cell Growth Differ., *6:* 817–825, 1995.
27. MacArthur, C. A., Shankar, D. B., and Shackleford, G. M. Fgf-8, activated by proviral insertion, cooperates with the Wnt-1 transgene in murine mammary tumorigenesis. J. Virol., *69:* 2501–2507, 1995.
28. Tanaka, A., Miyamoto, K., Matsuo, H., Matsumoto, K., and Yoshida, H. Human androgen-induced growth factor in prostate and breast cancer cells: its molecular cloning and growth properties. FEBS Lett., *363:* 226–230, 1995.
29. Gemel, J., Gorry, M., Ehrlich, G. D., and MacArthur, C. A. Structure and sequence of human FGF8. Genomics, *35:* 253–257, 1996.
30. Kouhara, H., Koga, M., Kasayama, S., Tanaka, A., Kishimoto, T., and Sato, B. Transforming activity of a newly cloned androgen-induced growth factor. Oncogene, *9:* 455–462, 1994.
31. Daphna-Iken, D., Shankar, D. B., Lawshe, A., Ornitz, D. M., Shackleford, G. M., and MacArthur, C. A. MMTV-Fgf8 transgenic mice develop mammary and salivary gland neoplasia and ovarian stromal hyperplasia. Oncogene, *17:* 2711–2717, 1998.
32. Valve, E. M., Nevalainen, M. T., Nurmi, M. J., Laato, M. K., Martikainen, P. M., and Harkonen, P. L. Increased expression of FGF-8 isoforms and FGF receptors in human premalignant prostatic intraepithelial neoplasia lesions and prostate cancer. Lab. Investig., *81:* 815–826, 2001.
33. MacArthur, C. A., Lawshe, A., Xu, J., Santos-Ocampo, S., Heikinheimo, M., Chellaiah, A. T., and Ornitz, D. M. FGF-8 isoforms activate receptor splice forms that are expressed in mesenchymal regions of mouse development. Development (Camb.), *121:* 3603–3613, 1995.
34. Blunt, A. G., Lawshe, A., Cunningham, M. L., Seto, M. L., Ornitz, D. M., and MacArthur, C. A. Overlapping expression and redundant activation of mesenchymal fibroblast growth factor (FGF) receptors by alternatively spliced FGF-8 ligands. J. Biol. Chem., *272:* 3733–3738, 1997.
35. Ittman, M., and Mansukhani, A. Expression of fibroblast growth factors (FGFs) and FGF receptors in human prostate. J. Urol., *157:* 351–356, 1997.
36. Klein, R. D., Maliner-Jongewaard, M. S., Udayakumar, T. S., Boyd, J. L., Nagle, R. B., and Bowden, G. T. Promatrilysin expression is induced by fibroblast growth factors in the prostatic carcinoma cell line LNCaP but not in normal primary prostate epithelial cells. Prostate, *41:* 215–223, 1999.
37. Hughes, S. E. Differential expression of the fibroblast growth factor receptor (FGFR) multigene family in normal human adult tissues. J. Histochem. Cytochem., *45:* 1005–1019, 1997.
38. Zhang, J., Thomas, T. Z., Kasper, S., and Matusik, R. J. A small composite probasin promoter confers high levels of prostate-specific gene expression through regulation by androgens and glucocorticoids *in vitro* and *in vivo*. Endocrinology, *141:* 4698–4710, 2000.
39. Wu, X., Wu, J., Huang, J., Powell, W. C., Zhang, J., Matusik, R. J., Sangiorgi, F. O., Maxson, R. E., Sucov, H. M., and Roy-Burman, P. Generation of a prostate epithelial cell-specific Cre transgenic mouse model for tissue-specific gene ablation. Mech. Dev., *101:* 61–69, 2001.
40. Nieto, M. A., Patel, K., and Wilkinson, D. G. *In situ* hybridization analysis of chick embryos in whole mount and tissue sections. Methods Cell Biol., *51:* 219–235, 1996.
41. Ting-Xin Jiang, N. S. S., Widelitz, R. B., and Chuong, C-M. Current methods in the study of avian skin appendages. *In:* C-M. Chuong (ed.), Molecular Basis of Epithelial Appendage Morphogenesis, pp. 395–408. Austin, TX: R. G. Landes Company, 1998.
42. Shibata, M. A., Ward, J. M., Devor, D. E., Liu, M. L., and Green, J. E. Progression of prostatic intraepithelial neoplasia to invasive carcinoma in C3(1)/SV40 large T antigen transgenic mice: histopathological and molecular biological alterations. Cancer Res., *56:* 4894–4903, 1996.
43. Gingrich, J. R., Barrios, R. J., Kattan, M. W., Nahm, H. S., Finegold, M. J., and Greenberg, N. M. Androgen-independent prostate cancer progression in the TRAMP model. Cancer Res., *57:* 4687–4691, 1997.
44. Tanaka, M., Komuro, I., Inagaki, H., Jenkins, N. A., Copeland, N. G., and Izumo, S. Nkx3.1, a murine homolog of *Drosophila bagpipe*, regulates epithelial ductal branching and proliferation of the prostate and palatine glands. Dev. Dyn., *219:* 248–260, 2000.
45. Di Cristofano, A., De Acetis, M., Koff, A., Cordon-Cardo, C., and Pandolfi, P. P. Pten and p27KIP1 cooperate in prostate cancer tumor suppression in the mouse [see comments]. Nat. Genet., *27:* 222–224, 2001.
46. Podsypanina, K., Ellenson, L. H., Nemes, A., Gu, J., Tamura, M., Yamada, K. M., Cordon-Cardo, C., Catoretti, G., Fisher, P. E., and Parsons, R. Mutation of Pten/Mmac1 in mice causes neoplasia in multiple organ systems. Proc. Natl. Acad. Sci. USA, *96:* 1563–1568, 1999.
47. Lohnes, D., Kastner, P., Dierich, A., Mark, M., LeMeur, M., and Chambon, P. Function of retinoic acid receptor $\gamma$ in the mouse. Cell, *73:* 643–658, 1993.
48. Krezel, W., Dupe, V., Mark, M., Dierich, A., Kastner, P., and Chambon, P. RXR$\gamma$ null mice are apparently normal and compound RXR$\alpha$ +/−/RXR$\beta$ −/−/RXR$\gamma$ −/− mutant mice are viable. Proc. Natl. Acad. Sci. USA, *93:* 9010–9014, 1996.

[CANCER RESEARCH 62, 4812–4819, August 15, 2002]

# Prostatic Intraepithelial Neoplasia in Mice with Conditional Disruption of the *Retinoid X Receptor α* Allele in the Prostate Epithelium[1]

**Jiapeng Huang, William C. Powell, Ani C. Khodavirdi, Jian Wu, Takako Makita, Robert D. Cardiff, Michael B. Cohen, Henry M. Sucov, and Pradip Roy-Burman[2]**

*Departments of Biochemistry and Molecular Biology [J. H., T. M., H. M. S., P. R-B.]. Pathology [W. C. P., A. C. K., J. W., P. R-B.], and Cell and Neurobiology [H. M. S.], Keck School of Medicine, University of Southern California, Los Angeles, California 90033; Center for Comparative Medicine, University of California-Davis, Davis, California 95616 [R. D. C.]; and Department of Pathology, The University of Iowa, Iowa City, Iowa 52242 [M. B. C.]*

## ABSTRACT

**Retinoids, which are important regulators of cell growth, differentiation, and apoptosis, have been used in treatment or chemoprevention of multiple cancers including prostate cancer. To elucidate the mechanism of action of retinoids in the context of the prostate, we used the *Cre-loxP* system to disrupt the *retinoid X receptor α* (*RXRα*) gene specifically in the prostatic epithelium of the mouse. Evidence for tissue-specific gene inactivation was obtained at DNA, RNA, and protein levels. Phenotypic changes in the prostate in the homozygous animals of different age groups ranging from 1 to 15 months were investigated. Developmentally, prostatic ductal branching appeared to be increased from the loss of *RXRα* function. There was also a significant change in the profile of secretory proteins in the *RXRα* mutant prostate relative to littermate controls with intact *RXRα* allele. Histopathologically, homozygous *RXRα*-deficient prostates showed multifocal hyperplasia as early as 4 months of age. Lesions, which could be described as low-grade prostatic intraepithelial neoplasias, were detected after 5 months. Subsequently, beginning at ~10 months, high-grade prostatic intraepithelial neoplasias developed in some animals. The incidences of low-grade prostatic intraepithelial neoplasias and high-grade prostatic intraepithelial neoplasias among the animals 10–15 months of age were 62 and 17%, respectively. The heterozygous mutant mice also developed similar prostatic phenotypes but in a delayed manner, implying a role of haploinsufficiency. Together, these results indicated for the first time that a major component of retinoid action in the prostate is mediated by a retinoid receptor, *RXRα*, the inactivation of which in the prostatic epithelium leads to the development of preneoplastic lesions.**

## INTRODUCTION

Prostate cancer is the most frequently diagnosed and the second leading cause of death from cancer in American men (1). In recent years, a few genes have been identified as critical factors during prostate cancer initiation and progression (2). Among those, disruption of Nkx3.1, a homeodomain transcription factor, showed prostatic epithelial hyperplasia and dysplasia followed by lesions of PIN[3] in both homozygous and heterozygous mutant mice (3). Heterozygous inactivation of phosphatase and tensin homologue (PTEN) also resulted in similar premalignant lesions in the prostate (4). As expected, cell cycle and apoptotic regulatory genes have been shown to participate in prostatic tumorigenesis (2). Still, in general, the mechanisms of prostate cancer remain largely unknown, and it is likely that there are many other molecular players, yet to be identified, that may explain the complexity and phenotypic heterogeneity of this common disease (5).

A role for vitamin A in prostate biology has long been appreciated (6). For prostate development, offspring of vitamin A-deficient female mice exhibit squamous metaplasia or agenesis of the prostate (7). Recent studies confirmed that exogenous RA can significantly inhibit ductal growth and branching of AP, DP, LP, and VP in mice (8, 9). In regard to carcinogenesis, prostate carcinoma tissues contain significantly less endogenous retinoids and its biologically active metabolite, RA, than normal prostate (10). Epidemiological studies also revealed an inverse trend between serum vitamin A levels and subsequent incidence of prostate cancer (11, 12). Furthermore, retinoids, as differentiation agents, have attracted much interest for prostate cancer prevention and treatment. There is evidence that retinoids could effectively inhibit tumor growth and progression in various chemical-induced mouse prostate cancer models (13–15). In studies with human prostate cancer cell lines, retinoids alone or with other chemotherapeutic agents reduced their clonal growth and tumorigenic potential (16, 17). Although clinical trials with retinoids for prostate cancer indicated only limited efficacy to date, it is, however, contended that improved pharmacokinetics and application of selective retinoid analogues might lead to a better clinical outcome (18–21).

Actions of retinoids are mediated either by its nuclear receptors or through receptor-independent mechanisms. There are two families of RA receptors, RARs (α, β, and γ) and RXRs (α, β, and γ; Refs. 22, 23). The physiological consequences of RAR and RXR inactivation were investigated via conventional knockout technology. It was reported that RARγ null mutant mice developed squamous metaplasia of the prostate (24). Because mice lacking both *RXRβ* and *RXRγ* were normal in terms of prostate morphology and function (25) and considering that the active RA receptor is indeed a heterodimer of one RAR and one RXR (26), the critical RXR in prostate biology appears to be RXRα. Moreover, to mediate multiple signaling pathways in the prostate, RXRα may partner with other nuclear receptors, such as PPARγ and vitamin D receptor, the ligands of which have been shown to inhibit prostatic cancer cell growth (26, 27).

Because conventional disruption of the *RXRα* gene is embryonic lethal (28, 29), we used our PB-Cre4 mice (30), which express a high level of Cre recombinase specifically in the prostatic epithelium, to breed with floxed *RXRα* mice (31) to selectively mutate the *RXRα* gene for a direct assessment of the role of *RXRα* in the prostate. We document here that RXRα is a critical gene function in maintaining normal phenotype of the gland because loss of RXRα function results in developmental and functional abnormalities as well as preneoplastic lesions in the prostate.

## MATERIALS AND METHODS

**Generation of Study Mice.** Production of PB-Cre4 transgenic mice (30) and conditionally floxed *RXRα* mice (31) were described previously. PB-Cre4 male mice were crossed with $RXR\alpha^{floxed/floxed}$ female mice to abolish RXRα

Received 3/29/02; accepted 6/14/02.

The costs of publication of this article were defrayed in part by the payment of page charges. This article must therefore be hereby marked *advertisement* in accordance with 18 U.S.C. Section 1734 solely to indicate this fact.

[1] This research was supported by NIH Grant R01 CA 59705 and, in part, by a grant from the T. J. Martell Foundation, NIH Grant R21 DK 59192, and NIH Predoctoral Training Grant Fellowship T32 CA 09569 (to A. C. K.).

[2] To whom requests for reprints should be addressed, at Department of Pathology, University of Southern California, Keck School of Medicine, 2011 Zonal Avenue, Los Angeles, CA 90033. Phone: (323) 442-1184; Fax: (323) 442-3049; E-mail: royburma@usc.edu.

[3] The abbreviations used are: PIN, prostatic intraepithelial neoplasia; LGPIN, low-grade PIN; HGPIN, high-grade PIN; RA, retinoic acid; RAR, RA receptor; RXR, retinoid X receptor; AP, anterior prostate; DP, dorsal prostate; LP, lateral prostate; VP, ventral prostate; PPARγ, peroxisome proliferator-activated receptor γ; RT-PCR, reverse transcription-PCR; BrdUrd, bromodeoxyuridine.

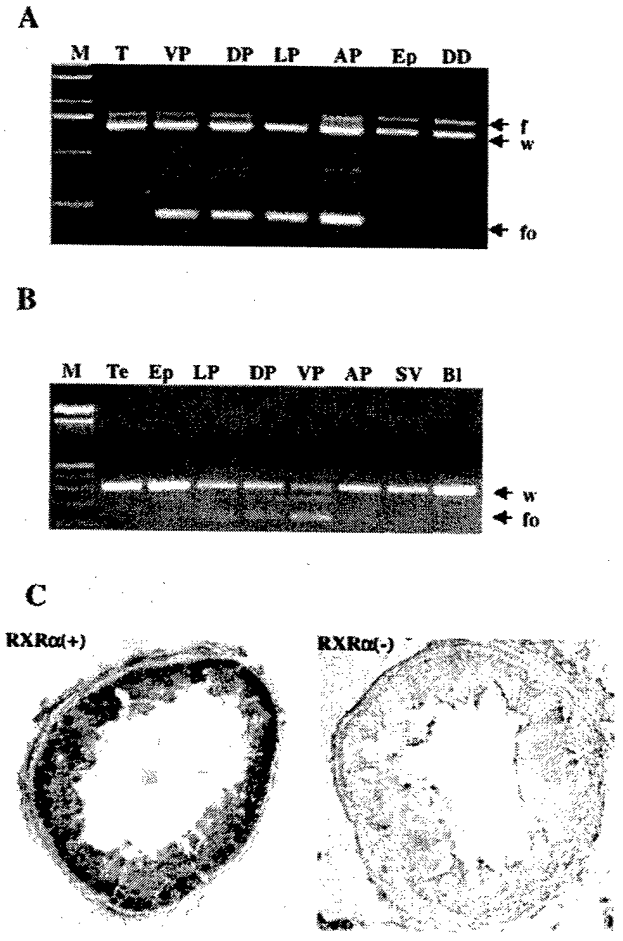


Fig. 1. Efficiency of *RXRα* disruption in prostate epithelial cells by PB-*Cre*. *A*, DNA analysis of *RXRα* allele. Genomic DNA extracted from different lobes of the prostate and other tissues of a $Cre^{+/-}RXR\alpha^{wt/floxed}$ animal 14 months of age was analyzed by PCR, and alleles were differentiated by size. *T*, tail; *VP*, ventral prostate; *DP*, dorsal prostate; *LP*, lateral prostate; *AP*, anterior prostate; *Ep*, epididymis; *DD*, ductus deferens; *f*, floxed allele; *w*, wild-type allele; *fo*, floxed-out allele. *B*, RNA analysis of *RXRα* recombination. RNA of the prostate and different tissues from a $Cre^{+/-}RXR\alpha^{floxed/floxed}$ animal 3 months of age was used to perform RT-PCR analysis for the *RXRα* transcript. *Te*, testes; *SV*, seminal vesicle; *Bl*, bladder; *w*, wild-type transcript; *fo*, deleted transcript without exon 4. *C*, RXRα immunohistochemistry. Sections of VP from a $Cre^{-/-}RXR\alpha^{floxed/floxed}$ [*(RXRα(+)*] or a $Cre^{+/-}RXR\alpha^{floxed/floxed}$ [*RXRα(−)*] mouse 10 months of age were immunostained using antibody against the $NH_2$-terminal region of RXRα.

function in the prostatic epithelium. Experimental male animals carried one allele of PB-*Cre* transgene and were either homozygous for the floxed *RXRα* allele ($RXR\alpha^{floxed/floxed}$) or heterozygous carrying one wild-type and one floxed allele ($RXR\alpha^{wt/floxed}$). Because the floxed *RXRα* allele is functionally identical to the wild-type allele, control male animals used were either $RXR\alpha^{wt/floxed}$ or $RXR\alpha^{floxed/floxed}$ or $RXR\alpha^{wt/wt}$ and did not carry the *Cre* transgene.

**PCR and RT-PCR Analysis.** Genomic DNA was extracted from mouse tissues by digestion with 20 μg/ml proteinase K (Life Technologies, Inc., Buffalo, NY) at 50°C for overnight. Aliquots (0.5 μg) of genomic DNA were used for the PCR analysis. Primers for *RXRα* amplification were 5′-ACCAAGCACATCTGTGCTATCT-3′ and 5′-ATGAAACTGCAAGTGGCCTTGA-3′. PCR products were approximately 1.5 kb, 1.7 kb, and 500 bp, corresponding to wild-type, floxed, and floxed-out *RXRα* allele, respectively. For RT-PCR, total RNA was extracted from the tissue samples using RNeasy Mini kit (Qiagen, Valencia, CA). Total RNA was converted to cDNA by random priming and then amplified for 32 cycles using primers 5′-TGCCCATCCCTCAGGAAATATGG-3′ and 5′-TGTTTGCCTCCACGTATGTCTC-3′.

**Quantitative RT-PCR.** Total RNA was extracted from individual prostatic lobes by guanidinium isothiocyanate extraction procedure. Quantitative RT-PCR was performed as described by Makita *et al.* (32). Briefly, PCR reactions including [$^{32}$P]dCTP were first run with 18S RNA primers and competimers to normalize for input between samples; subsequent reactions for retinoid receptor transcripts were done under conditions where amplification was in the linear range. PCR products were separated by acrylamide gel electrophoresis, dried, and exposed to film and also analyzed quantitatively by PhosphorImaging (Amersham Pharmacia Biotechology, Piscataway, NJ). The sequences of the primers used in this study were: *RXRβ*, 5′-GCTCATTGGCGACACCCCCA-3′ and 5′-GAAGGTAGACATAAAGTCCT-3′; and *RXRγ*, 5′-ACGGGCCATCGTGCTGTTTAAC-3′ and 5′-CAGCTGAGGAGGTTCAGGTG-3′. The primers used for *RARα* and *RARβ* were reported previously (33). The primers for *RARγ* were as described (34).

**Immunohistochemistry.** Zymed BrdUrd staining kit (Zymed, South San Francisco, CA) was used for BrdUrd staining. Briefly, sections were incubated with biotinylated anti-BrdUrd antibody and detected by the streptavidin-peroxidase with diaminobenzidine as a chromogen. Slides were then counterstained with methylene green (KPL Labs, Gaithersburg, MD). RXRα immunostaining using a rabbit polyclonal antibody against the $NH_2$ terminus of RXRα (Santa Cruz Biotechnology, Inc., Santa Cruz, CA) was performed in a similar way except for antigen retrieval by microwave heating in 1 M urea. Tissue sections, which were not incubated with primary antibody, served as negative controls.

**Tissue Preparation.** A 150-μl solution of 10 mg/ml BrdUrd (Sigma Chemical Co., St. Louis, MO) was injected i.p. 1 h before animals were sacrificed. The urogenital system was surgically isolated, and the individual prostatic lobes were dissected out under a dissecting microscope. Tissues for histopathological observation were fixed in 10% neutral buffered formalin (Surgipath, Richmond, IL) for overnight. Fixed tissues were processed and embedded in paraffin. Thin sections (5 μm) were produced and stained with H&E. Tissues for RNA assays were frozen in liquid nitrogen immediately after dissections until usage.

**Phenotypic Analysis of *RXRα* Mutant Prostates.** Experimental male mice ranging in age from 1 to 15 months for homozygous *RXRα* deletion or up to 18 months of age for the heterozygous allele were examined. For analysis of secretory proteins, individual lobes of the dissected prostates were collected in PBS containing a protease inhibitor mixture (Roche Diagnostics Corp., Indianapolis, IN), punched with a 28-gauge needle, and then centrifuged (3). Secretory proteins in the supernatant fluids were resolved on 10–20% SDS-polyacrylamide gels (Bio-Rad Laboratories, Hercules, CA). Coomassie blue staining was used for visualization.

For branching analysis, microdissection of LP, DP, VP, and AP was performed as described previously using collagenase to facilitate the process (3). The number of branch tips was quantitated by examination of the photographed specimen. A statistical analysis (ANOVA) was performed to determine the difference in branching morphogenesis between wild-type and RXRα-deficient prostates.

For analysis of histopathology, 16 control animals ranging from 1 to 18 months, which showed normal histology, along with 45 homozygous and 16 heterozygous *RXRα*-mutant mice were sacrificed and analyzed. A grading system for PIN-like lesions was used to evaluate *RXRα*-deficient animals. Generally, PIN lesions were categorized into LGPIN and HGPIN based on their architecture, differentiation pattern, and degree of cytological atypia. LGPINs showed mild cytological atypia. HGPINs were distinguished from LGPINs by the advanced degree of epithelial cell proliferation, nuclear stratification, and cytological atypia.

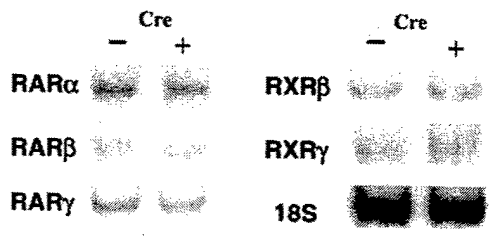


Fig. 2. Quantitative RT-PCR assay for other retinoid receptors in *RXRα*-deficient prostate. Total RNA was extracted from the LP of either $Cre^{+/-}RXR\alpha^{floxed/floxed}$ or $Cre^{-/-}RXR\alpha^{floxed/floxed}$ male animals 6 months of age. Quantitative RT-PCR for *RARs* (α, β, and γ) and *RXRs* (β and γ) were performed using 18S RNA as an internal control.

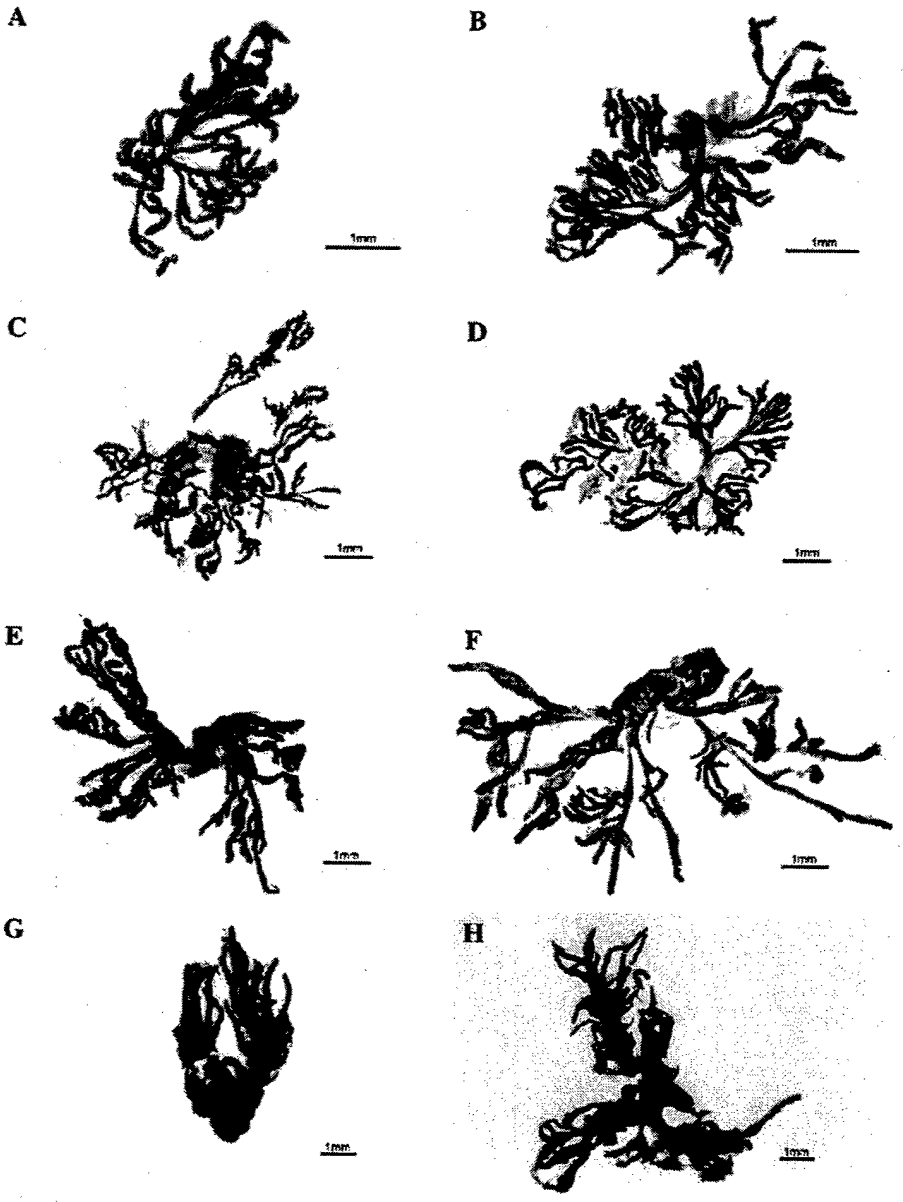


Fig. 3. Comparison of branching morphogenesis in prostate lobes from $Cre^{-/-}RXR\alpha^{floxed/floxed}$ (*A, C, E,* and *G*) and littermate $Cre^{+/-}RXR\alpha^{floxed/floxed}$ (*B, D, F,* and *H*) animals 4 months of age. *A* and *B,* LP; *C* and *D,* DP; *E* and *F,* VP; *G* and *H,* AP.

## RESULTS

**Generation of Mice with *RXRα*-deficient Prostates.** The established conditional *RXRα* allele had two *loxP* sites introduced into the introns surrounding the fourth exon of the gene, an exon that encodes an essential domain of the RXRα protein (31). When the intervening sequence (including the fourth exon) is deleted, the gene is converted into a loss-of-function allele. Before initiating breeding experiments for conditional inactivation of the *RXRα* allele in the prostate, we examined RXRα expression in the prostate of the normal mice with the *RXRα* conditional alleles by immunohistochemistry. The results, as illustrated in Fig. 1*C,* revealed that RXRα expression could be readily detected in the prostatic epithelium. It was, therefore, considered highly appropriate to cross the floxed *RXRα* mice with our PB-Cre4 mouse line (30), which expresses Cre recombinase with high specificity and penetrance in the prostatic epithelium. We crossed PB-Cre4 male mice with floxed *RXRα* female mice to recover both $Cre^{+/-}RXR\alpha^{wt/floxed}$ and $Cre^{+/-}RXR\alpha^{floxed/floxed}$ male mice for the following phenotypic studies in the prostate.

**Validation of *RXRα* Gene Disruption in Prostate Epithelial Cells.** To document specificity and extent of recombination of the conditional *RXRα* gene under the direction of the PB-*Cre* transgene, genomic DNA was isolated from various tissues of $Cre^{+/-}RXR\alpha^{wt/floxed}$ male mice and analyzed by PCR amplification. At 3 months, recombination of the conditional *RXRα* allele was prominent in VP, LP, and DP but significantly lesser in AP. No tissues other than prostate displayed strong recombination, except that epididymis, seminal vesicle, and ductus deferens showed low levels of recombination (30). However, in mice 14 months of age, prominent recombination had occurred in all prostatic lobes (Fig. 1*A*). To further demonstrate the effectiveness of *Cre*-mediated recombination of the *RXRα* gene, we isolated RNA from prostatic tissues of $Cre^{+/-}RXR\alpha^{floxed/floxed}$ mice 3 months of age and evaluated it by RT-PCR. A deleted but

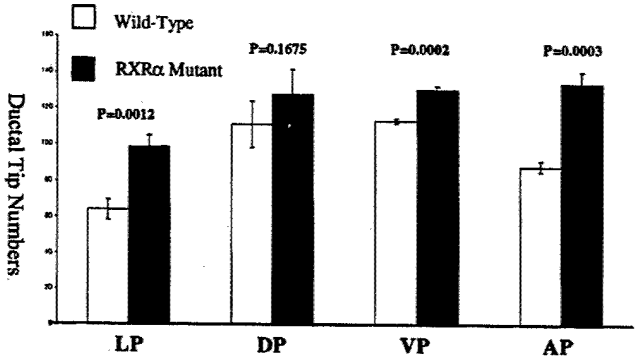


Fig. 4. Quantitation of ductal tip numbers in wild-type and *RXRα* mutant prostate. Results represent analysis of three separate experiments. *Bars*, SD. The *Ps* were significant for LP, VP, and AP but not DP.

stable transcript was detected in DP, LP, VP, and AP, indicating efficiency and specificity of our *Cre-loxP* system for *RXRα* inactivation (Fig. 1*B*). Considering the potential that a dominant-negative RXRα protein might be produced from deleted transcripts, we used immunohistochemistry technique to explore expression of RXRα using antibodies against a domain contained in both normal and the putative mutant RXRα protein. No detectable level of RXRα expression was observed in the *RXRα* mutant prostate compared with strong signals detected in the control prostate (Fig. 1*C*). It appeared that if the truncated transcript was translated, the protein product lacked stability.

**Lack of Compensatory Increase in Other Retinoid Receptors in *RXRα*-deficient Prostates.** In several mouse gene knockout models, mutation of one gene can result in compensatory expression by other members of the same gene family. To determine whether this occurs in the prostate of our hybrid model, LP tissues from $RXR\alpha^{floxed/floxed}$ mice 3 months of age, either bearing the PB-*Cre* transgene or not, were isolated to extract RNA and analyzed by quantitative RT-PCR. As shown in Fig. 2, other five members of retinoid receptors were expressed in the prostate, and expression of other retinoid receptor genes was not significantly changed as a consequence of *RXRα* gene inactivation, indicating a lack of compensatory up-regulation of RARs and other RXRs. Therefore, phenotypic changes in *RXRα*-deficient prostates, described below, were primarily attributable to *RXRα* inactivation rather than changes in expression of other retinoid receptors, at least at the level of transcripts.

***RXRα* Inactivation Results in Increased Branching Morphogenesis in the Prostate.** $Cre^{+/-}RXR\alpha^{wt/floxed}$ and $Cre^{+/-}RXR\alpha^{floxed/floxed}$ male mice were born and reared normally without exterior abnormalities up to 18 months of age, the point of maturity of this report. We first addressed the effect of *RXRα* inactivation in prostate development. In mice, development of the prostate is induced in late gestation when the epithelium of urogenital sinus grows into the surrounding mesenchyme to form prostate ductal buds. Subsequent branching morphogenesis of ductal systems occurs largely in the postnatal period by a process of concentrated mitotic activity at ductal tips, lumenalization of epithelial extensions, and branching of ducts (8). The mechanisms regulating the branching process remain unknown. Because the probasin promoter that we used to drive *Cre* expression only becomes active after birth, we circumvented the confounding effects of possible prostatic bud abnormalities on branching morphogenesis (30, 35). Gross inspection of *RXRα* mutant prostate glands did not reveal any noteworthy abnormalities. *RXRα*-deficient and *RXRα*-intact prostates did not appear to differ in size or weight to any significant extent. LP, DP, VP, and AP were microdissected to assess their branching patterns quantitatively by counting the number of distal ductal tips. In the *RXRα* conditional knockout group, all lobes appeared to show increased branching morphogenesis, as shown in Fig. 3. In LP and AP, there was a 54 and 52% increase in the number of ductal tips, respectively. For DP and VP, changes were less pronounced (Fig. 4). Several reports suggested involvement of RA in the prostate ductal morphogenesis, possibly by receptor-mediated effects on *Hox* gene clusters, which are known to control morphogenesis in a variety of systems (9, 36). Although it is difficult to address effects of *RXRα* inactivation on prostatic bud formation in our mouse model, our results suggested that RA action, at least on the prostate branching process, is mediated through RXRα.

***RXRα* Deficiency Altered Secretory Protein Profiles in the Prostate.** Because the primary function of the prostate is to contribute secretory proteins into seminal fluids in adult mice, we collected prostatic secretions from experimental $Cre^{+/-}RXR\alpha^{floxed/floxed}$ and control $Cre^{-/-}RXR\alpha^{floxed/floxed}$ animals 6 months of age and then resolved the secretions on SDS-PAGE gel. Reproducible changes of protein profiles were detected in LP, DP, and VP without significant changes in AP (Fig. 5). *RXRα* deletion caused both decreases and increases in major secretory proteins. Those results suggested that RXRα, as a transcription factor, played both positive and negative regulatory roles in prostatic gene expression. Although identities of those altered protein bands remained unknown, this finding underscored a potential role for RXRα-mediated transcription control in normal prostatic function, specifically in relation to protein secretions. However, because all conditional male animals examined to date are fertile, the significance of those changes could not be attributed to biological reproductive function.

**PIN Lesions in the *RXRα* Mutant Prostate.** Histopathological evaluation of the prostate sections led to several noteworthy observations. The most prominent phenotype in *RXRα* mutant prostate was hyperplasia, which, with advancing age, was accompanied by PIN lesions. Homozygous *RXRα* inactivation in mice older than 4 months demonstrated multifocal areas of epithelial hyperplasia with an incidence rate of 71%. Lesions became more severe and progressed to LGPINs after 5 months of age. As shown in Fig. 6, *A* and *B*, prostate glands showed abnormal configuration with nuclear stratification. Although there were abundant cytoplasms, nuclear sizes were enlarged with prominent nucleoli indicating malignant nature. Interestingly, focal areas of LGPINs were detected at multiple sites in the same animal, suggesting continuity in the progression of those lesions. After 10 months of age, HGPINs were detected in some animals. In Fig. 6, *C* and *D*, areas of normal morphology with a single-cell layer of secretory epithelium, together with areas of LGPINs and HGPINs,

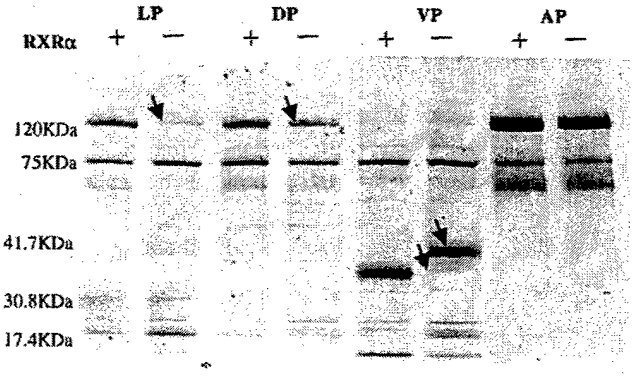


Fig. 5. Altered secretory protein profiles from *RXRα* inactivation. The same amount of prostatic secretory proteins from animals 6 months of age either with $Cre^{-/-}RXR\alpha^{floxed/floxed}$ [*RXRα*(+)] or $Cre^{+/-}RXR\alpha^{floxed/floxed}$ [*RXRα*(−)] genotype were collected and resolved on 10–20% SDS-PAGE gel. *Arrows*, protein bands showing reproducible changes.

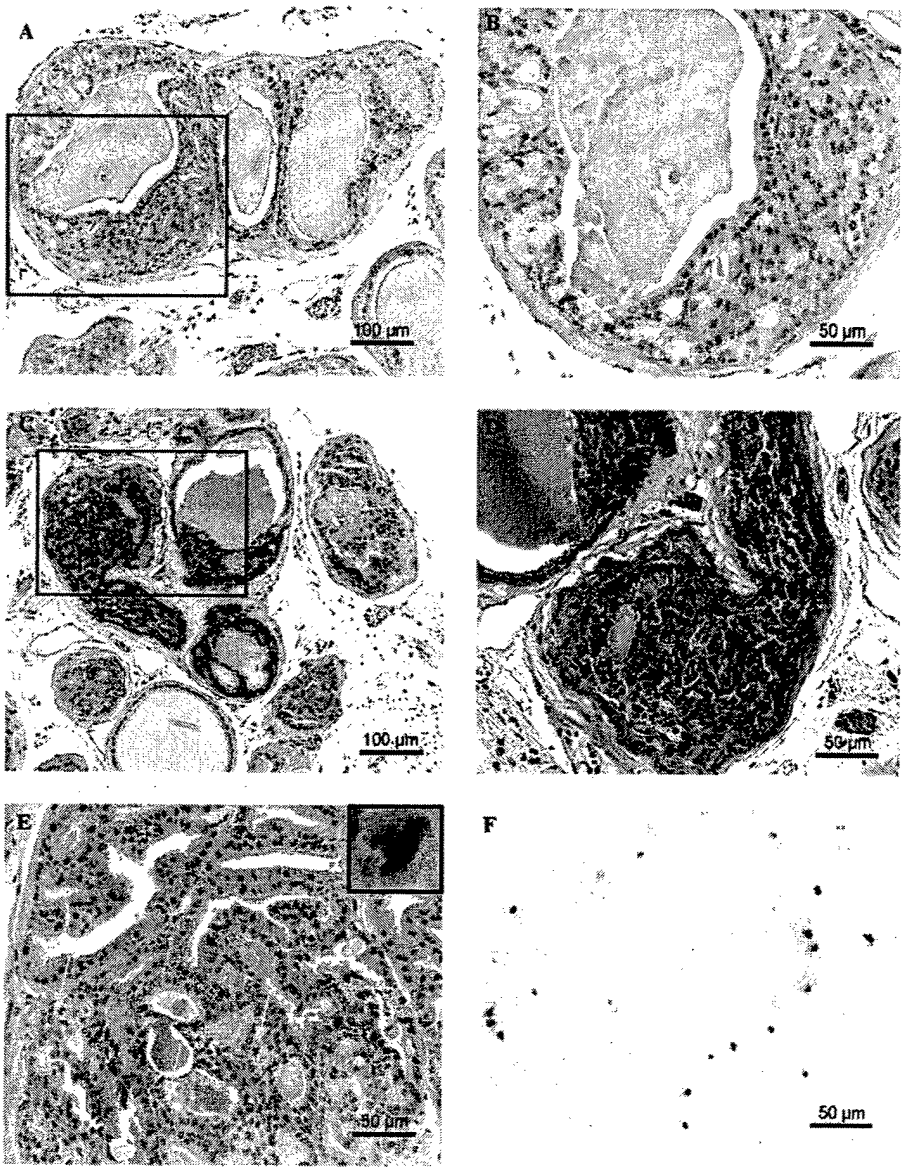


Fig. 6. Histopathology of *RXRα*-deficient prostates. *A* and *B*, LGPINs in DP from a $Cre^{+/-}$ $RXR\alpha^{floxed/floxed}$ male animal 12 months of age (H&E). Pleomorphic atypical cells filling prostatic duct stood out from adjacent normal glands. Lesions with lesser extent were also present. *C* and *D*, HGPINs in DP from a $Cre^{+/-}RXR\alpha^{floxed/floxed}$ animal 10 months of age (H&E). Cells with sparse cytoplasm almost filled the lumen of a bulging prostate gland, and the nucleus showed hyperchromatism, pleomorphism, and prominent nucleoi. Areas of LGPINs and normal glands existed on the same section. *E*, HGPINs in anterior prostate from a $Cre^{+/-}RXR\alpha^{wt/floxed}$ animal 18 months of age (H&E). Pleomorphic atypical cells were arranged in a cribiform pattern to fill the lumen of the prostate gland. Three mitotic figures were indicated by *arrows* with one abnormal tripolar mitotic figure (*inset*). *F*, the high proliferation index demonstrated by BrdUrd immunohistochemistry on lesions shown in *E*.

were clearly illustrated. In HGPINs, cells with sparse cytoplasm almost filled the lumen of prostate glands, and the nucleus showed hyperchromatism, pleomorphism, and prominent nucleoi. Along with aging, the incidence of LGPINs and HGPINs increased to 62 and 17%, respectively, at age groups from 10 to 15 months, which represented the oldest animals examined to date for homozygous *RXRα* mutant mice (Fig. 7*A*). For heterozygous *RXRα*-deficient mice, hyperplasia and LGPINs were demonstrated starting at the age of 11 and 14 months, respectively. HGPINs occurred after 18 months (Fig. 7*B*). In an example shown in Fig. 6*E*, lesions demonstrated different nuclear characteristics compared with normal prostatic epithelial cells: dense nucleus and prominent nucleoi. Moreover, three mitotic figures were prominent, including one abnormal tripolar mitotic figure in the field. These data supported the notion that RXRα might be involved in preventing initiation of abnormalities in the prostatic epithelium.

We also attempted to determine whether the rate of cell proliferation could be correlated with the development of hyperplasia and PINs seen in prostatic tissues lacking *RXRα*. For this purpose, we used the procedure of short-term exposure to BrdUrd *in vivo* followed by immunohistochemical detection of cells with BrdUrd incorporation. In control mice, all lobes were mostly unlabelled, with rare incorporation into scattered epithelial cells. In contrast, in the *RXRα*-deficient prostate, there was a pronounced increase in the percentage of labeled nuclei as shown in Fig. 6*F*. Thus, a normal function of RXRα appeared to be to maintain growth regulation in prostatic epithelium, and loss of RXRα resulted in an elevated proliferation rate, and presumably as a consequence, led to PINs.

## DISCUSSION

Dysfunctions of retinoid receptors have been implicated in multiple systems of carcinogenesis, especially in promyelocytic leukemia, and in carcinomas of breast, esophagus, lung, and skin (37–41). The human chromosomal region 9q34.3, in which the *RXRα* gene is mapped, is characterized by a high rate of recombination (42), and the

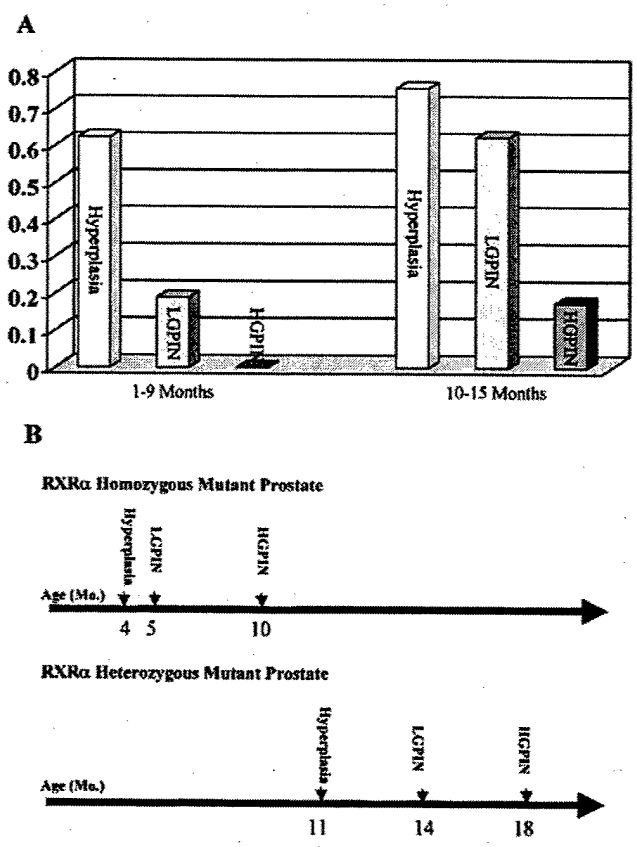


Fig. 7. Frequency of detection of phenotypic changes in *RXRα* mutant prostates. *A*, incidence of lesions in homozygous *RXRα* mutant prostate. Between 1 and 9 months, 63% (10 of 16) animals developed hyperplasia, and 19% (3 of 16) developed LGPINs. No HGPINs were detected. From 10 to 15 months, 76% (22 of 29) animals demonstrated hyperplasia, 62% (18 of 29) developed LGPINs, and 17% (5 of 29) developed HGPINs. *B*, comparison of the onset of premalignant lesions in *RXRα* homozygous and heterozygous mutant prostates. In homozygous *RXRα* mutant prostates, hyperplasia developed at the age of 4 months, LGPINs developed at 5 months, and HGPINs developed at 10 months. Heterozygous *RXRα* mutant prostates developed similar lesions in a delayed manner with hyperplasia starting from 11 months in 63% (10 of 16) of animals, 19% (3 of 16) LGPINs from 14 months, and 6% (1 of 16) HGPINs from 18 months.

incidence of loss of heterozygosity at this locus has been reported to be 20% in prostate cancer (43). Although absence of or loss of expression of RARβ is a common phenomenon in several types of cancer including prostate cancer (44–46), *RXRα* expression in prostate cancer remains largely unknown, and its investigation is further complicated by the recent finding that phosphorylation of RXRα can abolish its transactivation activity (47).

The investigations presented here address the role of loss of activity of RXRα specifically in the epithelium of the mouse prostate. The development of the PB-Cre4 transgenic mouse line with a robust and tissue-specific expression of Cre recombinase (30) allowed us to circumvent the embryonic lethality that is caused by conventional knockout of the *RXRα* gene in the mouse (28, 29). Our data from the *Cre-loxP* model that we developed demonstrate that the presence of *RXRα* is required for the normal control of prostate growth and differentiation. In its absence, *i.e.*, in the homozygous mutant animals, a substantial increase in ductal branching is induced in the prostate, most notably in the lateral and anterior lobes. Besides this aberrant ductal morphogenesis, there are a few other pronounced effects that could be directly attributed to loss of *RXRα* function in the prostatic epithelium. Evidence is also presented to support that there is no compensatory changes in the expression of any of the other *RXR* or *RAR* receptor family members in the prostate of these animals.

A deficiency in RXRα is sufficient to drive proliferation in the prostatic epithelium to produce multifocal hyperplasia as early as 4 months of age. Hyperplasia appears to precede the development of histopathologically identifiable lesions, many of which resemble human preneoplastic prostatic lesions. A stochastic pattern of increased degree of phenotypic abnormalities of lesions, beginning with epithelial hyperplasia followed by presentations of LGPINs and then by HGPINs is noted. For example, the incidence of hyperplasia, which is 63% during 1–9 months, increases to 76% by 10–15 months. The frequency of detection of LGPIN is only 19% at 1–9 months to increase to 62% at 10–15 months. Similarly, HGPIN, not detected up to 9 months, becomes 17% by 15 months. The development of progressive lesions is likely to be a multistep process that requires cumulative changes in gene expression. Thus, it seems that loss of RXRα function may make some of the affected cells escape negative growth control mechanisms, leading to hyperplasia. Increased proliferation is likely to enhance the probability to acquire additional genetic alterations to produce a higher degree of dysplasia. At this time, we have no direct evidence to support that LGPIN actually progresses to HGPIN, or even whether specific defined areas of hyperplasia turn to LGPIN, although detection of PINs, in general, is always associated with hyperplasia, as HGPINs with LGPINs but not *vice versa*. The lesions, however, do not progress to frank adenocarcinoma, at least during the 15 months of observation. This is not surprising because other genetic events necessary for progression from preneoplastic lesions to neoplasia may manifest only with further aging, a point that remains to be determined.

We also document reproducible changes in secretory protein profiles in the prostatic lobes, mainly LP, DP, and VP, attributable to *RXRα* gene inactivation, although the nature of the secreted proteins remains to be identified. Because some proteins are up-regulated and others are down-regulated, their characterization should be valuable in deriving clues for both positive and negative aspects of RXRα-mediated transcription control in the prostatic epithelium. In this regard, it is noteworthy that the prostatic spermine-binding protein, which is normally a major secretory protein in VP, is actually lost in the *Nkx3.1* mutant mice.

While studying biallelic inactivation of *RXRα* gene, we also accumulated animals with monoallelic deletion. Similar to homozygous mice, the monoallelic mice appear to develop hyperplasia, LGPIN, and HGPIN in a temporal fashion, except that the incidence is substantially delayed by several months. Haploinsufficiency at several gene loci, such as *Nkx3.1* (3, 48) and *p27* (49), leading to a dosage defect, has been observed in prostate tumorigenesis. We suggest that the RXRα protein is such a gene product, the reduced production and delayed accumulation of which might promote a positive environment for proliferation and transformation to preneoplastic lesions in the prostate. In this regard, a scrutiny of not only loss of heterozygosity at the *RXRα* gene locus but also of mutations of one or both *RXRα* alleles in human prostate cancer might be worthwhile.

Because RXRα is an obligatory heterodimeric partner for RARs, vitamin D receptor, PPARγ, thyroid hormone receptor, and some other nuclear receptors, it could be considered as a pivotal coordinating molecule in multiple signaling pathways. Retinoids, PPARγ-specific ligands, and vitamin D analogues have been shown to inhibit prostate cancer cell proliferation and clonal growth (16, 17, 27, 50–52). Retinoids are also the most investigated class of chemopreventive agents, and some promising results have been obtained on their utility in certain rodent models for prostate cancer (53, 54). Considering these issues, it seems that future studies on changes in gene expression in the prostatic epithelial cells of *RXRα*-inactivated mouse should help to elucidate the negative regulatory role of RXRα in normal prostatic epithelium and in the development of prostatic

preneoplastic lesions. Additionally, our results point to the potential value of testing RXRα-specific ligands in attempts to prevent development of prostate cancer.

In summary, our results demonstrate a functional role of RXRα in various aspects of prostate biology, including control of ductal branching, protein secretions, proliferation of epithelial cells, and then progression to premalignant phenotypes. The conditional *RXRα* mutant mice produced should be a valuable resource to examine RXRα signaling mechanisms in relation to the prostate, because they might be useful in studies of therapeutic regimens or chemoprevention of the beginning stages of prostate tumorigenesis.

## ACKNOWLEDGMENTS

We thank all members in Roy-Burman's laboratory for help during this work.

## REFERENCES

1. Coffey, D. S. Prostate cancer. An overview of an increasing dilemma. Cancer (Phila.), *71:* 880–886, 1993.
2. Abate-Shen, C., and Shen, M. M. Molecular genetics of prostate cancer. Genes Dev., *14:* 2410–2434, 2000.
3. Bhatia-Gaur, R., Donjacour, A. A., Sciavolino, P. J., Kim, M., Desai, N., Young, P., Norton, C. R., Gridley, T., Cardiff, R. D., Cunha, G. R., Abate-Shen, C., and Shen, M. M. Roles for Nkx3.1 in prostate development and cancer. Genes Dev., *13:* 966–977, 1999.
4. Podsypanina, K., Ellenson, L. H., Nemes, A., Gu, J., Tamura, M., Yamada, K. M., Cordon-Cardo, C., Catoretti, G., Fisher, P. E., and Parsons, R. Mutation of Pten/Mmac1 in mice causes neoplasia in multiple organ systems. Proc. Natl. Acad. Sci. USA, *96:* 1563–1568, 1999.
5. Roy-Burman, P., Zheng, J., and Miller, G. J. Molecular heterogeneity in prostate cancer: can TP53 mutation unravel tumorigenesis? Mol. Med. Today, *3:* 476–482, 1997.
6. Sporn, M. B., Roberts, A. B., and Goodman, D. S. The Retinoids, Second Edition, pp. 319–350. New York: Raven Press, 1994.
7. Wilson, J. G., Roth, C. B., and Warkany, J. An analysis of the syndrome of malformations induced by maternal vitamin A deficiency. Effects of restoration of vitamin A at various times during gestation. Am. J. Anat., *92:* 189–217, 1953.
8. Aboseif, S. R., Dahiya, R., Narayan, P., and Cunha, G. R. Effect of retinoic acid on prostatic development. Prostate, *31:* 161–167, 1997.
9. Seo, R., McGuire, M., Chung, M., and Bushman, W. Inhibition of prostate ductal morphogenesis by retinoic acid. J. Urol., *158:* 931–935, 1997.
10. Pasquali, D., Thaller, C., and Eichele, G. Abnormal level of retinoic acid in prostate cancer tissues. J. Clin. Endocrinol. Metab., *81:* 2186–2191, 1996.
11. Reichman, M. E., Hayes, R. B., Ziegler, R. G., Schatzkin, A., Taylor, P. R., Kahle, L. L., and Fraumeni, J. F. Serum vitamin A and subsequent development of prostate cancer in the first National Health and Nutrition Examination Survey Epidemiologic Follow-up Study. Cancer Res., *50:* 2311–2315, 1990.
12. Hayes, R. B., Bogdanovicz, J. F., Schroeder, F. H., De Bruijn, A., Raatgever, J. W., Van der Maas, P. J., Oishi, K., and Yoshida, O. Serum retinol and prostate cancer. Cancer (Phila.), *62:* 2021–2026, 1988.
13. Chopra, D. P., and Wilkoff, L. J. Reversal by vitamin A analogues (retinoids) of hyperplasia induced by *N*-methyl-*N'*-nitro-*N*-nitrosoguanidine in mouse prostate organ cultures. J. Natl. Cancer Inst., *58:* 923–930, 1977.
14. Lasnitzki, I., and Goodman, D. S. Inhibition of the effects of methylcholanthrene on mouse prostate in organ culture by vitamin A and its analogs. Cancer Res., *34:* 1564–1571, 1974.
15. Pollard, M., Luckert, P. H., and Sporn, M. B. Prevention of primary prostate cancer in Lobund-Wistar rats by *N*-(4-hydroxyphenyl)retinamide. Cancer Res., *51:* 3610–3611, 1991.
16. Dahiya, R., Park, H. D., Cusick, J., Vessella, R. L., Fournier, G., and Narayan, P. Inhibition of tumorigenic potential and prostate-specific antigen expression in LNCaP human prostate cancer cell line by 13-*cis*-retinoic acid. Int. J. Cancer, *59:* 126–132, 1994.
17. de Vos, S., Dawson, M. I., Holden, S., Le, T., Wang, A., Cho, S. K., Chen, D. L., and Koeffler, H. P. Effects of retinoid X receptor-selective ligands on proliferation of prostate cancer cells. Prostate, *32:* 115–121, 1997.
18. Culine, S., Kramar, A., Droz, J. P., and Theodore, C. Phase II study of all-*trans* retinoic acid administered intermittently for hormone refractory prostate cancer. J. Urol., *161:* 173–175, 1999.
19. Trump, D. L., Smith, D. C., Stiff, D., Adedoyin, A., Day, R., Bahnson, R. R., Hofacker, J., and Branch, R. A. A Phase II trial of all-*trans*-retinoic acid in hormone-refractory prostate cancer: a clinical trial with detailed pharmacokinetic analysis. Cancer Chemother. Pharmacol., *39:* 349–356, 1997.
20. DiPaola, R. S., Rafi, M. M., Vyas, V., Toppmeyer, D., Rubin, E., Patel, J., Goodin, S., Medina, M., Medina, P., Zarnek, R., Zhang, C., White, E., Gupta, E., and Hait, W. N. Phase I clinical and pharmacologic study of 13-*cis*-retinoic acid, interferon α, and paclitaxel in patients with prostate cancer and other advanced malignancies. J. Clin. Oncol., *17:* 2213–2218, 1999.
21. Kelly, W. K., Osman, I., Reuter, V. E., Curley, T., Heston, W. D., Nanus, D. M., and Scher, H. I. The development of biologic end points in patients treated with differentiation agents: an experience of retinoids in prostate cancer. Clin. Cancer Res., *6:* 838–846, 2000.
22. Leid, M., Kastner, P., and Chambon, P. Multiplicity generates diversity in the retinoic acid signalling pathways. Trends Biochem. Sci., *17:* 427–433, 1992.
23. Giguere, V. Retinoic acid receptors and cellular retinoid binding proteins: complex interplay in retinoid signaling. Endocr. Rev., *15:* 61–79, 1994.
24. Lohnes, D., Kastner, P., Dierich, A., Mark, M., LeMeur, M., and Chambon, P. Function of retinoic acid receptor γ in the mouse. Cell, *73:* 643–658, 1993.
25. Krezel, W., Dupe, V., Mark, M., Dierich, A., Kastner, P., and Chambon, P. *RXRγ* null mice are apparently normal and compound *RXRα* +/−/*RXRβ* −/−/*RXRγ* −/− mutant mice are viable. Proc. Natl. Acad. Sci. USA, *93:* 9010–9014, 1996.
26. Mangelsdorf, D. J., Umesono, K., and Evans, R. M. The retinoid receptors. *In:* M. B. Sporn and D. S. Goodman (eds.), The Retinoids, pp. 319–349. New York: Raven Press, 1994.
27. Kubota, T., Koshizuka, K., Williamson, E. A., Asou, H., Said, J. W., Holden, S., Miyoshi, I., and Koeffler, H. P. Ligand for peroxisome proliferator-activated receptor γ (troglitazone) has potent antitumor effect against human prostate cancer both *in vitro* and *in vivo*. Cancer Res., *58:* 3344–3352, 1998.
28. Kastner, P., Grondona, J. M., Mark, M., Gansmuller, A., LeMeur, M., Decimo, D., Vonesch, J. L., Dolle, P., and Chambon, P. Genetic analysis of *RXRα* developmental function: convergence of RXR and RAR signaling pathways in heart and eye morphogenesis. Cell, *78:* 987–1003, 1994.
29. Sucov, H. M., Dyson, E., Gumeringer, C. L., Price, J., Chien, K. R., and Evans, R. M. *RXRα* mutant mice establish a genetic basis for vitamin A signaling in heart morphogenesis. Genes Dev., *8:* 1007–1018, 1994.
30. Wu, X., Wu, J., Huang, J., Powell, W. C., Zhang, J., Matusik, R. J., Sangiorgi, F. O., Maxson, R. E., Sucov, H. M., and Roy-Burman, P. Generation of a prostate epithelial cell-specific *Cre* transgenic mouse model for tissue-specific gene ablation. Mech. Dev., *101:* 61–69, 2001.
31. Chen, J., Kubalak, S. W., and Chien, K. R. Ventricular muscle-restricted targeting of the *RXRα* gene reveals a non-cell-autonomous requirement in cardiac chamber morphogenesis. Development (Camb.), *125:* 1943–1949, 1998.
32. Makita, T., Hernandez-Hoyos, G., Chen, T. H., Wu, H., Rothenberg, E. V., and Sucov, H. M. A developmental transition in definitive erythropoiesis: erythropoietin expression is sequentially regulated by retinoic acid receptors and HNF4. Genes Dev., *15:* 889–901, 2001.
33. Ulven, S. M., Gundersen, T. E., Weedon, M. S., Landaas, V. O., Sakhi, A. K., Fromm, S. H., Geronimo, B. A., Moskaug, J. O., and Blomhoff, R. Identification of endogenous retinoids, enzymes, binding proteins, and receptors during early postimplantation development in mouse: important role of retinal dehydrogenase type 2 in synthesis of all-*trans*-retinoic acid. Dev. Biol., *220:* 379–391, 2000.
34. Li, J., Ning, G., and Duncan, S. A. Mammalian hepatocyte differentiation requires the transcription factor HNF-4α. Genes Dev., *14:* 464–474, 2000.
35. Cunha, G. R., Donjacour, A. A., Cooke, P. S., Mee, S., Bigsby, R. M., Higgins, S. J., and Sugimura, Y. The endocrinology and developmental biology of the prostate. Endocr. Rev., *8:* 338–362, 1987.
36. Podlasek, C. A., Duboule, D., and Bushman, W. Male accessory sex organ morphogenesis is altered by loss of function of Hoxd-13. Dev. Dyn., *208:* 454–465, 1997.
37. Kakizuka, A., Miller, W. H., Umesono, K., Warrell, R. P., Frankel, S. R., Murty, V. V., Dmitrovsky, E., and Evans, R. M. Chromosomal translocation t(15;17) in human acute promyelocytic leukemia fuses RAR α with a novel putative transcription factor, PML. Cell, *66:* 663–674, 1991.
38. Xu, X. C., Sneige, N., Liu, X., Nandagiri, R., Lee, J. J., Lukmanji, F., Hortobagyi, G., Lippman, S. M., Dhingra, K., and Lotan, R. Progressive decrease in nuclear retinoic acid receptor β messenger RNA level during breast carcinogenesis. Cancer Res., *57:* 4992–4996, 1997.
39. Qiu, H., Zhang, W., El-Naggar, A. K., Lippman, S. M., Lin, P., Lotan, R., and Xu, X. C. Loss of retinoic acid receptor-β expression is an early event during esophageal carcinogenesis. Am. J. Pathol., *155:* 1519–1523, 1999.
40. Gebert, J. F., Moghal, N., Frangioni, J. V., Sugarbaker, D. J., and Neel, B. G. High frequency of retinoic acid receptor β abnormalities in human lung cancer. Oncogene, *6:* 1859–1868, 1991.
41. Xu, X. C., Wong, W. Y., Goldberg, L., Baer, S. C., Wolf, J. E., Ramsdell, W. M., Alberts, D. S., Lippman, S. M., and Lotan, R. Progressive decreases in nuclear retinoid receptors during skin squamous carcinogenesis. Cancer Res., *61:* 4306–4310, 2001.
42. Almasan, A., Mangelsdorf, D. J., Ong, E. S., Wahl, G. M., and Evans, R. M. Chromosomal localization of the human retinoid X receptors. Genomics, *20:* 397–403, 1994.
43. Ruijter, E., van de Kaa, C., Miller, G., Ruiter, D., Debruyne, F., and Schalken, J. Molecular genetics and epidemiology of prostate carcinoma. Endocr. Rev., *20:* 22–45, 1999.
44. Faria, T. N., Mendelsohn, C., Chambon, P., and Gudas, L. J. The targeted disruption of both alleles of RARβ(2) in F9 cells results in the loss of retinoic acid-associated growth arrest. J. Biol. Chem., *274:* 26783–26788, 1999.
45. Liu, Y., Lee, M. O., Wang, H. G., Li, Y., Hashimoto, Y., Klaus, M., Reed, J. C., and Zhang, X. Retinoic acid receptor β mediates the growth-inhibitory effect of retinoic acid by promoting apoptosis in human breast cancer cells. Mol. Cell. Biol., *16:* 1138–1149, 1996.

46. Lotan, Y., Xu, X. C., Shalev, M., Lotan, R., Williams, R., Wheeler, T. M., Thompson, T. C., and Kadmon, D. Differential expression of nuclear retinoid receptors in normal and malignant prostates. J. Clin. Oncol., *18:* 116–121, 2000.
47. Matsushima-Nishiwaki, R., Okuno, M., Adachi, S., Sano, T., Akita, K., Moriwaki, H., Friedman, S. L., and Kojima, S. Phosphorylation of retinoid X receptor α at serine 260 impairs its metabolism and function in human hepatocellular carcinoma. Cancer Res., *61:* 7675–7682, 2001.
48. Abdulkadir, S. A., Magee, J. A., Peters, T. J., Kaleem, Z., Naughton, C. K., Humphrey, P. A., and Milbrandt, J. Conditional loss of nkx3.1 in adult mice induces prostatic intraepithelial neoplasia. Mol. Cell. Biol., *22:* 1495–1503, 2002.
49. Fero, M. L., Randel, E., Gurley, K. E., Roberts, J. M., and Kemp, C. J. The murine gene *p27Kip1* is haplo-insufficient for tumour suppression. Nature (Lond.), *396:* 177–180, 1998.
50. Campbell, M. J., Park, S., Uskokovic, M. R., Dawson, M. I., and Koeffler, H. P. Expression of retinoic acid receptor-β sensitizes prostate cancer cells to growth inhibition mediated by combinations of retinoids and a 19-nor hexafluoride vitamin D3 analog. Endocrinology, *139:* 1972–1980, 1998.
51. Elstner, E., Campbell, M. J., Munker, R., Shintaku, P., Binderup, L., Heber, D., Said, J., and Koeffler, H. P. Novel 20-epi-vitamin D3 analog combined with 9-*cis*-retinoic acid markedly inhibits colony growth of prostate cancer cells. Prostate, *40:* 141–149, 1999.
52. Blutt, S. E., Allegretto, E. A., Pike, J. W., and Weigel, N. L. 1,25-Dihydroxyvitamin D3 and 9-*cis*-retinoic acid act synergistically to inhibit the growth of LNCaP prostate cells and cause accumulation of cells in G1. Endocrinology, *138:* 1491–1497, 1997.
53. McCormick, D. L., Rao, K. V., Steele, V. E., Lubet, R. A., Kelloff, G. J., and Bosland, M. C. Chemoprevention of rat prostate carcinogenesis by 9-*cis*-retinoic acid. Cancer Res., *59:* 521–524, 1999.
54. Quader, S. T., Bello-DeOcampo, D., Williams, D. E., Kleinman, H. K., and Webber, M. M. Evaluation of the chemopreventive potential of retinoids using a novel *in vitro* human prostate carcinogenesis model. Mutat. Res., *496:* 153–161, 2001.

American Journal of Pathology, Vol. 161, No. 2, August 2002


# Animal Model

## Prostatic Intraepithelial Neoplasia in Genetically Engineered Mice

Jae-Hak Park,*† Judy E. Walls,* Jose J. Galvez,* Minjung Kim,‡ Cory Abate-Shen,‡ Michael M. Shen,‡ and Robert D. Cardiff*

*From the Center for Comparative Medicine and Department of Medical Pathology,* University of California, Davis, California; the Departments of Neuroscience and Pediatrics,‡ Center for Advanced Biotechnology and Medicine, UMDNJ-Robert Wood Johnson Medical School, Piscataway, New Jersey; and Laboratory Animal Medicine,† College of Veterinary Medicine, Seoul National University, Suwon, Korea*

**Several mouse models of human prostate cancer were studied to identify and characterize potential precursor lesions containing foci of atypical epithelial cells. These lesions exhibit a sequence of changes suggesting progressive evolution toward malignancy. Based on these observations, a grading system is proposed to classify prostatic intraepithelial neoplasia (PIN) in genetically engineered mice (GEM). Four grades of GEM PIN are proposed based on their architecture, differentiation pattern, and degree of cytological atypia. PIN I lesions have one or two layers of atypical cells. PIN II has two or more layers of atypical cells. PIN III has large, pleomorphic nuclei with prominent nucleoli and the cells tend to involve the entire lumen with expansion of the duct outlines. PIN IV lesions contain atypical cells that fill the lumen and bulge focally into, and frequently compromise, the fibromuscular sheath. Within the same cohorts, the lower grade PINs first appear earlier than the higher grades. Morphometric and immunohistochemical analyses confirm progressive change. Although the malignant potential of PIN IV in mice has not been proven, GEM PIN is similar to human PIN. This PIN classification system is a first step toward a systematic evaluation of the biological potential of these lesions in GEM.** ***(Am J Pathol 2002, 161:727–735)***

The frequency of prostate cancer has been increasing.[1] Afflicting 10% of men older than the age of 65, it represents the most frequently diagnosed cancer in American men, with an even higher incidence in the African-American population. Many investigators have tried to identify prognostic markers that distinguish indolent *versus* aggressive forms of prostate cancer, and to understand the genetic factors that evoke prostate cancer initiation and progression.[2] Animal models have been developed to study the potential relationship of molecular mechanisms and clinical progression.[3–5] The earlier models included xenograph and hormone induction models.[3,6,7] Recently, transgenic and knockout models have become available.[3–5,8] The most widely used models involve the SV40-Tag gene behind various types of prostate-targeting promoters.[9–17] These models involve a rapidly progressive, poorly differentiated, and metastatic neoplasm. The early lesions display varying degrees of epithelial atypia.[9–12] The later lesions in some models frequently involve the entire epithelium. These lesions have been characterized and a tentative grading system has been developed under the heading of prostatic intraepithelial neoplasia (PIN).[18]

More recently, other mouse models of human prostate cancers have been developed using knockouts or transgenes other than the SV40-Tag.[3] These models develop a more indolent proliferative disease that rarely progresses to invasive carcinoma.[19] They do, however, develop a variety of foci with atypical cells that are quite different from those observed in the SV40-Tag-based models.

We have studied the intraepithelial lesions occurring in nine of these models and have observed a continuum of structural and cytological changes that suggest increased severity and, thus, neoplastic progression. We have created a system to grade these lesions to assist others to evaluate their genetically engineered mice (GEM) models of prostate cancer. We describe and illustrate here, using examples from a single model (Nkx3.1−/− × PTEN+/−), our proposed grading system,

Supported by grants UO1 CA84294 from the National Cancer Institutes and U42-RR14905 from National Institutes of Health.

Accepted for publication April 29, 2002.

Address reprint requests to Robert D. Cardiff, M.D., Ph.D., Professor of Pathology, Center for Comparative Medicine, County Road 98 and Hutchison Dr., University of California, Davis, Davis, CA 95616. E-mail: rdcardiff@ucdavis.edu.

and the evidence to support progressive change as potentially useful guidelines for other investigators.

## Materials and Methods

### Prostatic Tissue

All samples were obtained from the University of California, Davis Center for Comparative Medicine Mutant Mouse Archives. The Mutant Mouse Archives contains a collection of paraffin blocks and slides cataloged, processed, and stored at the Center for Comparative Medicine. The samples were sent by our various collaborators either as wet tissues fixed in formalin or an alcohol-based fixative or as tissue blocks. The largest, most comprehensive collection involves studies of Nkx3.1,[19] PTEN,[20] p27[21] and p53 and hybrid crosses among these four genotypes. Samples of prostate from H-ras (N. Schreiber-Agus, unpublished data), Mxi,[22] PTEN,[20] p53 mutant, FGF8[23] and PyV-mT[24]mice were also available for examination. For consistency, we are illustrating the criteria using a single model system, the Nkx3.1−/− × PTEN +/− mice.[25]

### Whole Mounts

Whole mounts illustrated here were fresh dissections of mouse prostate were photographed using an Olympus S2410 steromicroscope and photo-controller (Melville, NY); images were input using a Kodak RFS 2035 (Rochester, NY) slide scanner and composited in Adobe Photoshop 6.0 (San Jose, CA).

### Immunohistochemical Staining

Immunohistochemistry was performed on 4-$\mu$m paraffin sections mounted on Superfrost/Plus slides (Fisher Scientific, Pittsburgh, PA), deparaffinized, and cleared. Endogenous peroxidase was blocked in a solution of 3% hydrogen peroxide ($H_2O_2$) in methanol. Antigen retrieval was performed by high-temperature (microwave) incubation in 0.01 mol/L of citric acid buffer (pH 6.0) for 3 × 4 minutes. Slides were cooled for 10 minutes in citric acid buffer then transferred to phosphate-buffered saline (pH 7.4). The sections were incubated 20 minutes in a humidified chamber in 10% normal horse serum (Vector Laboratories, Burlingame, CA). Slides were incubated in primary antibody solution and were incubated in a humidified chamber overnight at room temperature. Control slides were run without primary antibody. Immunohistochemistry for smooth muscle actin (SMA) was performed using a 1:1000 diluted mouse monoclonal primary antibody (A2537; Sigma, St. Louis, MO). The Animal Research Kit (DAKO, Carpinteria, CA) with peroxidase was used as amplification system according to manufacturer's instructions. The slides were stained for cytokeratin (CK) 8 and CK14 using 1:200 diluted polyclonal sheep primary antibody (PH182 and PH503; Binding Site, San Diego CA), E-cadherin 1:800 (c20820, Trand.), laminin 1:1000 (L9393, Sigma), Ki67 1:1800 (CLKi67, Novocastro, Newcastle, UK), androgen receptor 1:1000(06-686; Upstate Biotechnologies, Lake Placid, NY) were incubated as above. The Vectastain ABC Elite Kit (Vector Laboratories) was used as amplification system according to manufacturer's instructions. Slides were counterstained in Mayer's hematoxylin, dehydrated, cleared, and coverslipped.

### Morphometrics

Appropriate paraffin sections containing normal as well as abnormal prostate were stained for DNA using the standard Feulgen protocol.[26] Areas of interest were selected to exemplify the four grades of PIN, normal prostate luminal cells or normal lymphocytes. Images of area of interest were captured at ×40 using an Olympus BX45 microscope (Olympus, Melville, NY) equipped with a DVC digital color 1300C camera (DVC, Austin, TX) at a resolution of 1300 × 1030 pixels and 10 bits per color. Total samples of 329 normal, 205 PIN I, 305 PIN II, 220 PIN III, and 162 PIN IV nuclei were used. The images were acquired into Photoshop with the DVC Twain driver on a PC running Windows NT. The color depth was lowered from 10 bits/channel to 8 bits/channel for image analysis. The images were analyzed using Image Pro by Media Cybernetics (Carlsbad, CA). The selected areas of interest nuclei were measured for nuclear area, mean nuclear density, and the integrated optical density. The raw data were exported to Excel (Microsoft, Seattle, WA) for mathematical and statistical analysis. The relative DNA content was determined by multiplying the integrated optical density by the square root of the nuclear area[26] and all values were plotted using Excel's histogram function.

## Results

### Atypical Hyperplasia

Many mice, including some elderly wild-type male controls, have increased numbers of prostatic epithelial cells with scattered cells that have enlarged, hyperchromatic nuclei. However, they generally do not have the abundant cytoplasm and other cytoplasmic changes described below. Further, the scattered atypical cells do not stand out from the general population as discrete foci. These changes are referred to here as hyperplasia, with atypia or atypical hyperplasia.

### Prostate Intraepithelial Neoplasia (PIN)

Focal atypical lesions of the prostatic epithelium have been described in several models. As indicated, we have either developed or have access to at least nine mouse models of human prostate neoplasia and have studied others in slide sets developed for meeting workshops. These models include knockouts or transgenic mice from ras, Mxi, PTEN, p53 mutant, FGF8, and PyV-mT. Since detailed descriptions of some of these models are not yet published, we have chosen to illustrate the proposed criteria for GEM PIN using a single model system that we have thoroughly studied, the Nkx3.1−/− × PTEN+/− mutant mice.[25] These mice progress to a relatively more

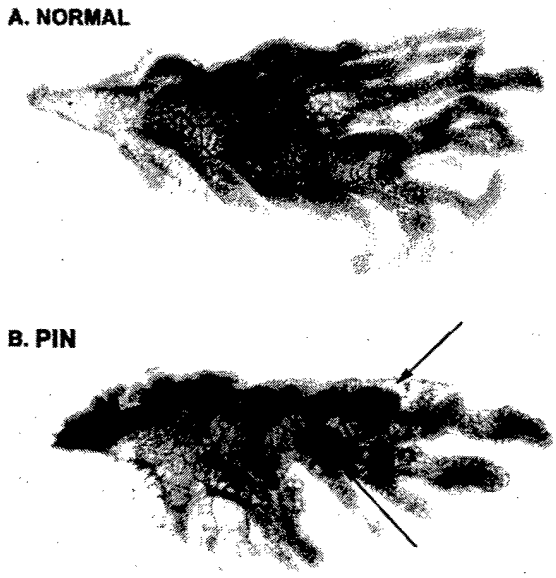


**Figure 1.** Whole mounts showing examples of dissected, unfixed, and unstained coagulating glands from a normal prostate from a 23-week-old GEM Nkx3.1+/− × PTEN+/− male (**A**) and a 23-week-old GEM Nkx3.1−/− × PTEN+/− male with nodular foci of PIN (**B**). Note the dark masses in **B** (**arrows**) that show the areas of cellular proliferation. The bulging profiles of the foci are consistent with GEM PIN III or IV. This type of visualization provides information about the number and volume of the lesions.

severe phenotype that has been described and illustrated in some detail.[25]

## Whole Mounts

Stained or unstained whole mount preparations can be used to visualize and enumerate the atypical lesions in the mouse prostate. Whole mounts of mice with PIN demonstrate small masses scattered in the different lobes (Figure 1). These masses varied in size. Microscopic examination verified that these masses were PIN lesions.

## Description of PIN

Foci of atypical cells were found in the prostatic lobes. However, in the models studied here, they were concentrated in the ducts of the coagulating gland and dorsolateral glands. The foci varied in the number of cell layers, the degree and pattern of atypia, and the relation to the fibromuscular stroma. The younger mice generally had fewer and less severe atypia. The low-grade lesions in younger mice did not necessarily occur in the context of more severe lesions. In contrast, prostate ducts with more severe atypia inevitably had less severe lesions. These observations implied a morphological continuum between the less and the more severe lesions. For the purpose of future studies, the lesions were classified into discrete classes fitting the criteria described below.

### *PIN I*

Relatively small foci with one or two layers of atypical cells. The fibromuscular stroma is intact and the duct profile is undisturbed. The cells are generally more columnar, larger, and taller than adjacent normal cells. They have abundant pale cytoplasm with hyperchromatic but minimally pleomorphic nuclei (Figure 2, A and B).

### *PIN II*

Larger foci with two or more layers of atypical cells that do not fill the lumen. The fibromuscular sheath is intact and the duct profile is undisturbed. The epithelial cells may have papillary, cribriform, or tufting patterns. The atypical cells are tall columnar with abundant pale pink cytoplasm with increasing but not severe nuclear pleomorphism and hyperchromasia. Increasing proportions of nuclei are larger and have vesicular chromatin patterns (Figure 2, C and D).

### *PIN III*

The foci of atypical cells fill, or almost fill, the lumen of the ducts. The diameter of the glands may be enlarged but the fibromuscular sheath is present and the gland outline is smooth. The epithelial cells may have papillary, cribriform, or tufting patterns that are frequently associated with small intraepithelial blood vessels. PIN III lesions may extend along the duct to involve adjacent ducts. The atypical cells are frequently poorly oriented with abundant relatively pale cytoplasm with increasingly severe nuclear pleomorphism and hyperchromasia. The nuclear to cytoplasmic ratio is inverted. Mitotic figures are present. Variable host responses are present with some inflammation and foamy macrophages (Figure 2, E and F).

### *PIN IV*

The foci of atypical cells fill the lumen of the ducts. The profiles of the ducts are distorted and irregular with bulging profiles. The fibromuscular sheath is irregular or absent in most areas. However, the epithelium continues to be surrounded by a layer of laminin. The epithelial cells may have solid, cribriform, or tufting patterns that are associated with small intraepithelial blood vessels. Central necrosis may also be present. PIN IV level lesions extend along the duct to involve adjacent ducts. The atypical cells are poorly oriented with abundant pale cytoplasm and with increasingly severe nuclear pleomorphism and hyperchromasia. The nuclear to cytoplasmic ratio is inverted. Mitotic figures are present. Host inflammatory responses are marked with lymphocytes and macrophages (Figure 2, G and H).

## Immunohistochemistry

The patterns of the immunohistochemical stains varied with the grade of PIN suggesting progressive cytoplasmic change.

### *SMA (Figure 3A)*

The SMA stain was most intense in the continuous fibromuscular layer surrounding the normal ducts. The staining was variable but continuous around areas with PIN I, II, or III lesions but became discontinuous or absent

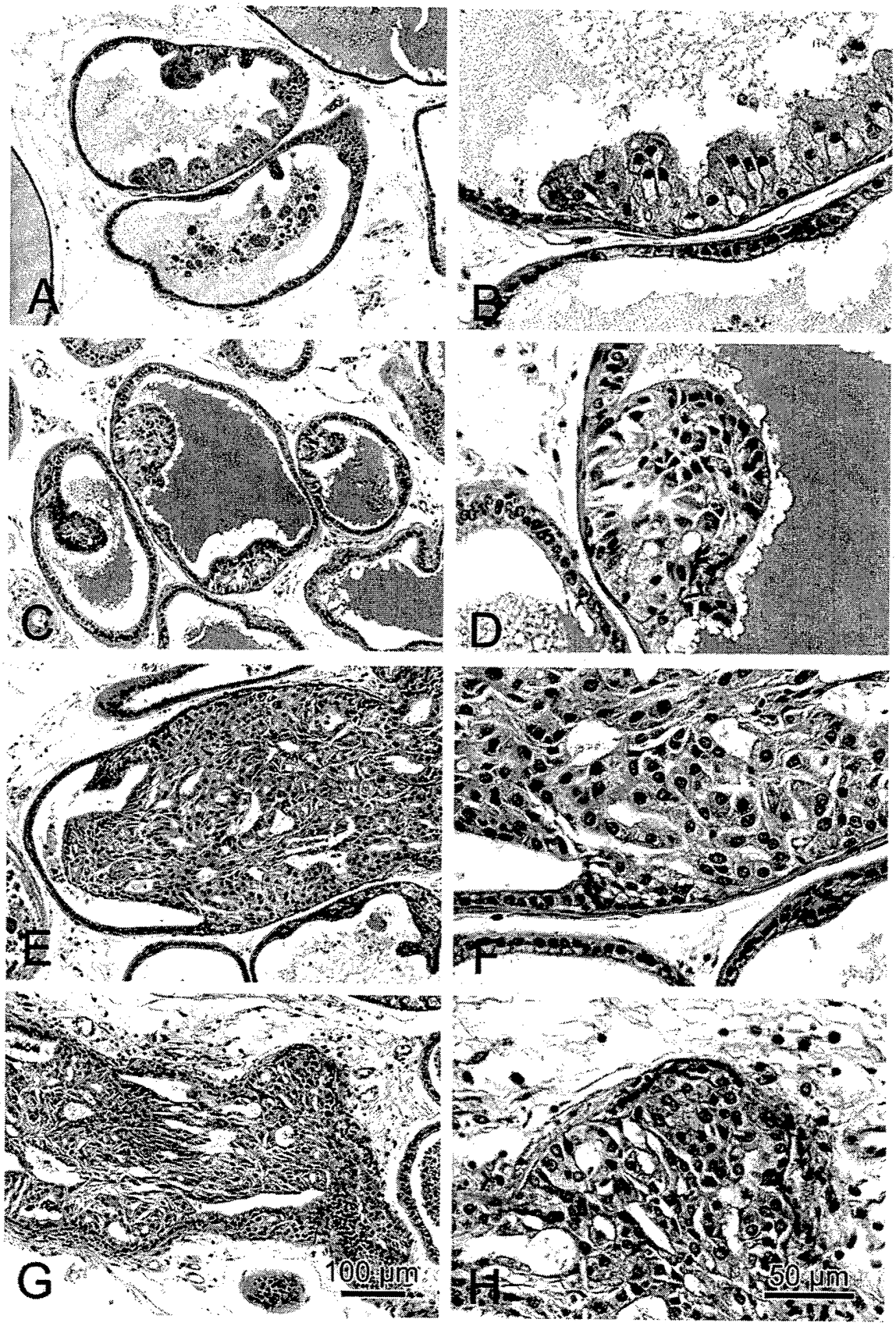
A
B
C
D
E
F
G
100 μm
H
50 μm

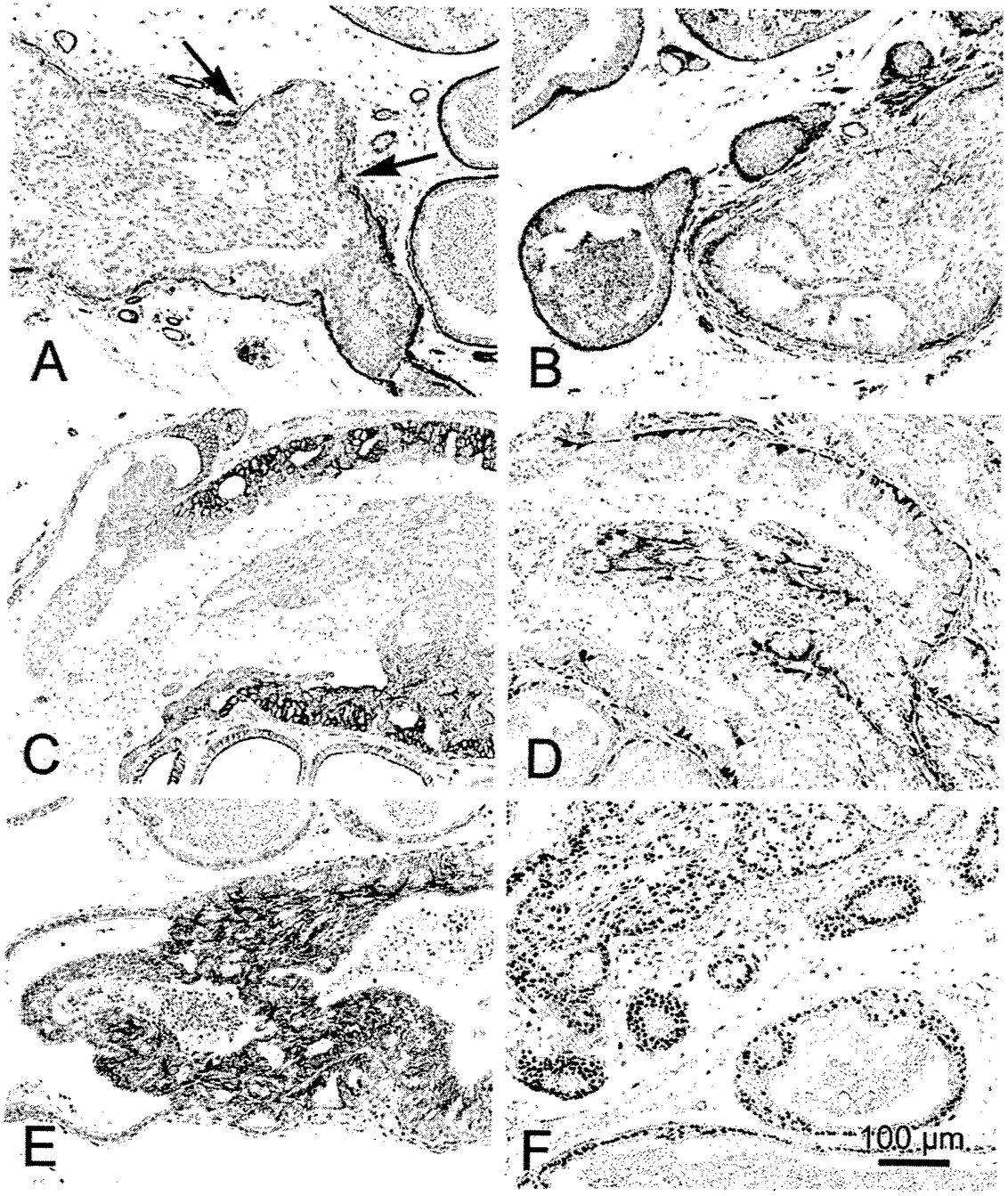


**Figure 3.** A panel of images from Nkx3.1−/− × PTEN+/− mice illustrating the immunohistochemical distribution of SMA (**A**), laminin (**B**), CK8 (**C**), CK14 (**D**), E-cadherin (**E**), and androgen receptors (**F**) in normal and PIN. The SMA (**A**) and laminin (**B**) are discontinuous or missing (**A**, **arrows**) around PIN IV lesions. The CK8 (**C**) is highly expressed in PIN III and PIN IV (**C**) with a displacement of the stain from the basolateral membranes in normal cell to a diffuse cytoplasmic stain in PIN III and IV. E-cadherin is also up-regulated in the higher grade PIN (**E**). The basal cells are identified by anti-CK14 (**D**). Note that they are increased in PIN lesions. Androgen receptors are also prominent in PIN (**F**).

**Figure 2.** A panel of H&E-stained slides from a Nkx3.1−/− × PTEN+/− mouse with low-magnification images (**A**, **C**, **E**, and **G**) and higher magnification images (**B**, **D**, **F**, and **H**) illustrating the histological and cytological patterns of PIN I (**A** and **B**), PIN II (**C** and **D**), PIN III (**E** and **F**), and PIN IV (**G** and **H**). These images show the details of the criteria for each grade described in the text. Scale bars document the magnification (**G** and **H**).

around PIN IV lesions. In addition, SMA identified small intraepithelial blood vessels in PIN III and PIN IV lesions.

*Laminin (Figure 3B)*

Basement membrane as identified by laminin staining was present around normal ducts and all grades of PIN but tended to be fragmented around PIN IV lesions.

*CK8 (Figure 3C)*

The luminal cells of the normal prostate had weak membrane stains with the anti-CK8 antibodies. All of the PIN cells had a much stronger, cytoplasmic CK8 stain. The intensity of the CK8 stain permitted the rapid identification of atypical foci.

*CK14 (Figure 3D)*

The basal cells are relatively sparse in the normal mouse prostate but can be identified by thin elongated, CK14-positive strands of cytoplasm. The CK14-positive basal cells did not increase in PIN I but were increased in number and size in all higher grades. The CD14-positive cells became haphazardly arranged in the PIN IV lesions that bulged into the stroma.

*E-Cadherin (Figure 3E)*

The luminal cells of the normal prostate reacted weakly along the lateral membranes with the anti-E-cadherin antibody. All PIN cells had a more intense stain. As with other reactions, the most intense reaction was observed in the bulging, PIN IV lesions.

*Androgen Receptors (Figure 3F)*

Many but not all normal cells had a nuclear reaction to the anti-androgen receptor antibody. In contrast, all PIN cells were strongly positive for androgen receptor. The nuclei with an open vesicular chromatin had the strongest reaction.

*Ki-67*

No Ki-67-positive cells were identified in the normal prostate cells (data not shown). This is consistent with the low-proliferative index of the normal mouse prostate. Scattered Ki-67-positive cells were found in PIN I and PIN II lesions. In contrast, eight to nine cells per high-powered field were Ki-67-positive in PIN III and PIN IV lesions, consistent with the observed increase in mitotic figures.

## Morphometric Analysis

A number of measurements of nuclear morphology and DNA content were taken from the same slides that are used to illustrate PIN in this manuscript. The goal was to determine whether the morphometric measurements could verify and extend our visual interpretations. Because the interpretation of morphometric differences between slides is compounded by differences in section thickness, fixation, stain intensity, and other factors, all analyses were performed on the same slide. The normal

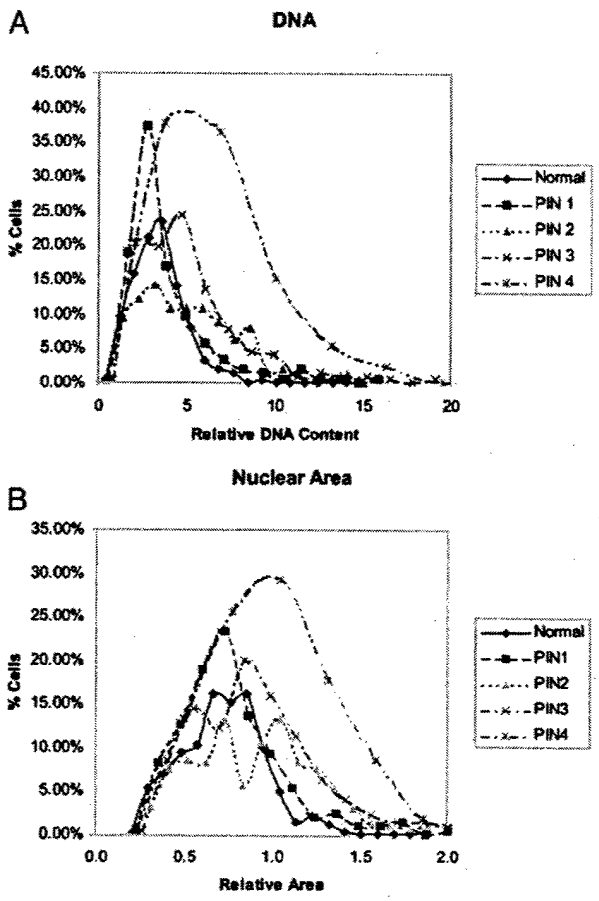


**Figure 4.** Graphs representing the results of the morphometric analysis of DNA content (**A**) and nuclear size (**B**). The DNA content is normalized for relative area using Bins formula.[26] Note that normal, PIN I, and PIN II have relatively similar nuclear size and DNA content. Also note that the relative DNA increases with the grade of PIN (**A**). The nuclear size also increases with the PIN grade (**B**). This analysis confirms the visual impressions and suggests that the grading system is consistent with the changes in the nuclear size and DNA content.

control values were also taken from morphologically normal luminal cells on the same slide.

In all cases, the nuclear area (Figure 4A) and the DNA content (Figure 4B) of normal prostatic epithelium and PIN I cells were indistinguishable even though the PIN I cells were larger and had cytoplasmic immunohistochemistry stains that identified them as atypical. The nuclear area of PIN II cells had distinctive bimodal peaks. The first peak had basically the same area as the PIN I and normal cells. The second peak and its extension had areas covered by the majority of the cells in the PIN IV population. PIN III also exhibited two peaks of nuclear area. The nuclear area of PIN IV cells was distinctly shifted to the right with the majority of cells having a nuclear area well outside the normal range. The range of nuclear area of the PIN IV cells matched those of adenocarcinoma (data not shown).

The DNA content, adjusted for nuclear area, exhibited similar properties with the PIN I and normal cells having similar DNA content with PIN II, PIN III, and PIN IV having increasing DNA content, well outside the range of normal.

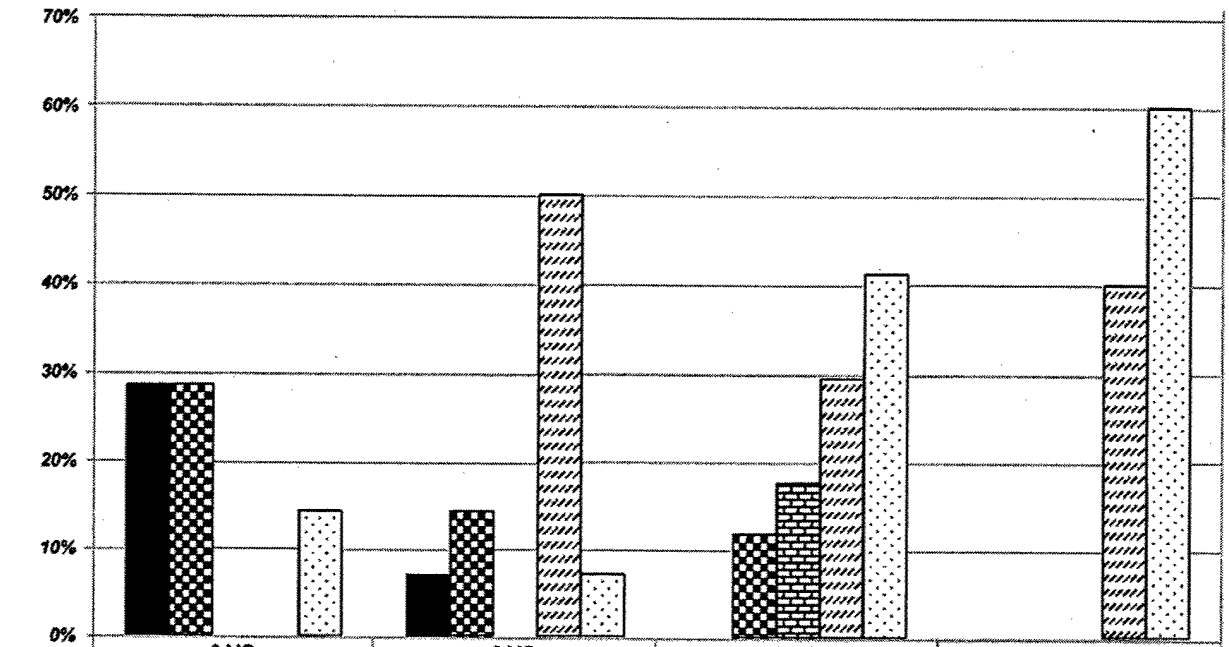


| | 3 MO | 6 MO | 9 MO | 12 MO |
|---|---|---|---|---|
| AH | 29% | 7% | | |
| PIN I | 29% | 14% | 12% | |
| PIN II | | | 18% | |
| PIN III | | 50% | 29% | 40% |
| PIN IV | 14% | 7% | 41% | 60% |

**Figure 5.** Histograms representing the relative proportions of diffuse atypical hyperplasia (AH) and PIN I to PIN IV in a single cohort of 43 Nkx3.1−/− × PTEN+/− males sacrificed at different ages. Note the relative increases in the higher grade PIN with age.

## *Biological Evolution*

Because the atypical foci are only sporadically associated with invasion, biological progression to malignancy is difficult to document. However, it was noted that the lesions in younger animals in these cohorts of animals are first associated with hyperplasia with scattered atypical cells. The smaller PIN I and PIN II lesions appear in the prostates of younger at-risk mice before the first PIN III or PIN IV lesions appear. The PIN III and PIN IV lesions rarely appear in animals that do not have PIN I or PIN II lesions (Figure 5).

An analysis of the GEM PIN kinetics from a single 43 animal cohort of Nkx3.1−/− × PTEN+/− males is shown in Figure 5. Young mice (>3 months) had few PIN lesions ($n$ = 7). Note that in this example all of the mice had abnormalities of their prostate after 6 months of age ($n$ = 14). By 9 months of age ($n$ = 17), an increasing percentage of the prostates had PIN III and PIN IV and at 12 months of age ($n$ = 5), all of the samples from the cohort had at least PIN III. This cohort has been previously presented in the context of a larger experimental group.[25]

## *Discussion*

PIN is thought to be a precursor to invasive carcinoma in humans because it is strongly associated with the malignant disease.[27,28] Evidence linking PIN to cancer is several fold. First, PIN lesions are primarily found in the peripheral zone, in proximity to the invasive carcinoma.[29] Second, the appearance of high-grade PIN lesions generally precedes the appearance of carcinoma by at least 10 years, consistent with the concept of neoplastic progression.[30] Third, allelic imbalance analysis has shown that PIN lesions are oligoclonal and multifocal. Moreover, the chromosomal abnormalities found in PIN resemble those found in early invasive carcinoma, although they are less prevalent.[31,32] Fourth, the architectural and cytological features of PIN resemble those of invasive carcinoma, including the progressive loss of the basal cell layer.[33] The basement membrane is normally intact in PIN and in well-differentiated adenocarcinoma.

The purpose of this study is to define a set of criteria for classifying GEM PIN in those GEM models of human prostate cancer that are not related to the SV40-Tag. We emphasize that the criteria illustrated here using one model can, in our experience, be applied to similar prostatic lesions in a wide variety of non-SV40-Tag mouse models. We further suggest these recommended criteria be tested in all non-SV40-Tag models.

Potential precursor lesions for the SV40-Tag models have been previously described.[9–12,18] The criteria presented here are based on our studies of more than nine GEM models that included Nkx3.1+/−, Nkx3.1−/−, PTEN+/−, p27−/−, p53−/−, and hybrid crosses among these five genotypes. Samples of prostate from H-ras,

p53 mutant, FGF8, and PyV-mT mice were also available for examination. In addition, the study slide set assembled for the recent Mouse Models of Human Prostate Cancer at the Jackson Laboratory was also available for examination. In our experience, all of the current non-Tag models present with very similar atypical morphological lesions. We have, however, chosen to illustrate our criteria using samples from a single model (Nkx3.1−/− × PTEN+/−) for consistent and reproducible examples.[25] The most complete and extensive collection of samples was available in this model and the Nkx3.1−/− × PTEN+/− animals displayed the highest number of the most severe lesions in our collection.

One of the critical issues is that, in contrast to the SV40-Tag models, the non-Tag models rarely progress to invasive carcinoma. Without definitive evidence of progression to invasive behavior, the use of the term PIN might be questioned. However, the evidence offered here suggests that these lesions undergo measurable and progressive changes in their architecture, nuclei, and cytoplasm. Because these atypical lesions either express a transgene or are the result of allelic insufficiency, they must also be regarded as genetically altered foci. Although the incidence of invasive neoplasms is low, it is much higher than in the background strains. These structural and genetic changes suggest that these lesions are autonomous new growths, that is, neoplasms. The current evidence, therefore, supports the notion that they are compatible with an intraepithelial neoplasm of the prostate. Thus, the use of the term PIN is justified until further evidence is accumulated.

If, as suggested here and in the discussion of the pathology workshop at the Jackson Meeting, GEM PIN is defined as any foci of atypical cells within the prostate that have evidence of neoplastic progression, the evidence for neoplastic progression must be explicit. The atypical foci described here differ from normal in their morphological appearance, the organization of the nuclear and cytoplasmic markers, the amount of cell proliferation, the size of the nuclei, the amount of DNA, and relationship with the stroma. Further, the atypical changes fit a morphological, morphometric and chronological continuum that implies progressive neoplastic changes. This combination of morphological atypia and biological progression fulfills the criteria of PIN.

The lack of progression to invasive neoplasia makes it difficult to prove that the atypical lesions are progressive or have malignant potential. It is possible, however, that the environment of the mouse prostate, with its low rate of proliferation, suppresses progression in all but the most aggressive models. However, the ultimate documentation of malignant potential might be transplantation beneath the renal capsule allowing progression to malignancy.[34] Similar studies have been done to demonstrate the malignant potential of Nkx3.1−/− × PTEN+/− cells.[35]

We have, however, attempted to use and illustrate another approach to documenting progressive changes in model systems that have little or no evidence of progression to invasive disease within the animal. For simplicity of communication, a simplified grading system has been proposed that correlates with objective morphological and cytological changes suggesting progression. This approach is offered in hope that it might assist others in their model evaluation, introduce a standard approach, present a controlled vocabulary, and allow comparisons with other models. This, in our opinion, is an initial step in defining rigorous criteria for GEM PIN. As the biological information evolves, the criteria recommended here may be modified to more accurately reflect the biology of the model systems.

The lesions described here are quite different from those observed by us and by others[9–12,15,18] in the SV40-Tag mice. The PIN lesions in SV40-Tag are much more diffuse with more compact, hyperchromatic nuclei and an inverted nuclear/cytoplasmic ratio. The non-Tag PINs are, in our experience, far less aggressive and have larger nuclei with a more open, vesicular chromatin and more abundant cytoplasm. The prominent nucleoli in these cells are reminiscent of the prominent nucleoli in human PIN and adenocarcinoma. Like the human disease the lesions in GEM PIN show evidence of progressive morphological disease suggesting that, under appropriate conditions, they will evolve into malignant neoplasms. However, in the models described here, these conditions for full malignancy have not been met. Because the mouse prostate glands are structurally and cytologically quite different from the human prostate, it is not surprising that the neoplasms in the two species would be structurally different. We hope that the description and classification provided here will assist others with the classification and study of their own GEM models.

## Acknowledgments

We thank Mr. Robert Munn for the image capture and processing, and the many collaborators who have generously provided the UCD Mutant Mouse Archives with their samples for analysis, including, in part, samples provided by Drs. Philip Leder, Nicole Agus-Schreiber, Pradip Roy-Burman, Pier Paolo-Pandolfi, Peter Barry, and David Morris. We appreciate the opportunity to study the mouse prostate slide set developed by Dr. Scott Shappell for The National Cancer Institute's Mouse Models of Human Cancer Consortium Workshop on Mouse Models of Human Prostate Cancer. We also appreciate insights provided by the workshop participants during the discussions of GEM PIN led by Dr. Scott Shappell.

## References

1. Coffey DS: Prostate cancer. An overview of an increasing dilemma. Cancer 1993, 71:880–886
2. Gopalkrishnan RV, Kang DC, Fisher PB: Molecular markers and determinants of prostate cancer metastasis. J Cell Physiol 2001, 189: 245–256
3. Abate-Shen C, Shen MM: Molecular genetics of prostate cancer. Genes Dev 2000, 14:2410–2434
4. Castrillon DH, DePinho RA: Modeling prostate cancer in the mouse. Adv Cancer Res 2001, 82:187–204
5. Huss WJ, Hanrahan CF, Barrios RJ, Simons JW, Greenberg NM:

Angiogenesis and prostate cancer: identification of a molecular progression switch. Cancer Res 2001, 61:2736–2743
6. van Weerden WM, Romijn JC: Use of nude mouse xenograft models in prostate cancer research. Prostate 2000, 43:263–271
7. Thompson TC, Timme TL, Park SH, Yang G, Ren C: Mouse prostate reconstitution model system: a series of in vivo and in vitro models for benign and malignant prostatic disease. Prostate 2000, 43:248–254
8. Sharma P, Schreiber-Agus N: Mouse models of prostate cancer. Oncogene 1999, 18:5349–5355
9. Yoshidome K, Shibata MA, Maroulakou IG, Liu ML, Jorcyk CL, Gold LG, Welch VN, Green JE: Genetic alterations in the development of mammary and prostate cancer in the C3(1)/Tag transgenic mouse model. Int J Oncol 1998, 12:449–453
10. Shibata MA, Ward JM, Devor DE, Liu ML, Green JE: Progression of prostatic intraepithelial neoplasia to invasive carcinoma in C3(1)/SV40 large T antigen transgenic mice: histopathological and molecular biological alterations. Cancer Res 1996, 56:4894–4903
11. Shibata MA, Jorcyk CL, Liu ML, Yoshidome K, Gold LG, Green JE: The C3(1)/SV40 T antigen transgenic mouse model of prostate and mammary cancer. Toxicol Pathol 1998, 26:177–182
12. Maroulakou IG, Anver M, Garrett L, Green JE: Prostate and mammary adenocarcinoma in transgenic mice carrying a rat C3(1) simian virus 40 large tumor antigen fusion gene. Proc Natl Acad Sci USA 1994, 91:11236–11240
13. Greenberg NM, DeMayo F, Finegold MJ, Medina D, Tilley WD, Aspinall JO, Cunha GR, Donjacour AA, Matusik RJ, Rosen JM: Prostate cancer in a transgenic mouse. Proc Natl Acad Sci USA 1995, 92: 3439–3443
14. Green JE, Shibata MA, Yoshidome K, Liu ML, Jorcyk C, Anver MR, Wigginton J, Wiltrout R, Shibata E, Kaczmarczyk S, Wang W, Liu ZY, Calvo A, Couldrey C: The C3(1)/SV40 T-antigen transgenic mouse model of mammary cancer: ductal epithelial cell targeting with multistage progression to carcinoma. Oncogene 2000, 19:1020–1027
15. Garabedian EM, Humphrey PA, Gordon JI: A transgenic mouse model of metastatic prostate cancer originating from neuroendocrine cells. Proc Natl Acad Sci USA 1998, 95:15382–15387
16. Masumori N, Thomas TZ, Chaurand P, Case T, Paul M, Kasper S, Caprioli RM, Tsukamoto T, Shappell SB, Matusik RJ: A probasin-large T antigen transgenic mouse line develops prostate adenocarcinoma and neuroendocrine carcinoma with metastatic potential. Cancer Res 2001, 61:2239–2249
17. Kasper S, Sheppard PC, Yan Y, Pettigrew N, Borowsky AD, Prins GS, Dodd JG, Duckworth ML, Matusik RJ: Development, progression, and androgen-dependence of prostate tumors in probasin-large T antigen transgenic mice: a model for prostate cancer. Lab Invest 1998, 78:i-xv
18. Gingrich J, Barrios R, Foster BA, Greenberg NM: Pathologic progression of autochthonous prostate cancer in the TRAMP. Prostate Cancer Prostatic Dis 1999, 2:70–75
19. Bhatia-Gaur R, Donjacour AA, Sciavolino PJ, Kim M, Desai N, Young P, Norton CR, Gridley T, Cardiff RD, Cunha GR, Abate-Shen C, Shen MM: Roles for Nkx3.1 in prostate development and cancer. Genes Dev 1999, 13:966–977
20. Di Cristofano A, Pesce B, Cordon-Cardo C, Pandolfi PP: Pten is essential for embryonic development and tumour suppression. Nat Genet 1998, 19:348–355
21. Di Cristofano A, De Acetis M, Koff A, Cordon-Cardo C, Pandolfi PP: Pten and p27KIP1 cooperate in prostate cancer tumor suppression in the mouse. Nat Genet 2001, 27:222–224
22. Schreiber-Agus N, Meng Y, Hoang T, Hou Jr H, Chen K, Greenberg R, Cordon-Cardo C, Lee HW, DePinho RA: Role of Mxi1 in ageing organ systems and the regulation of normal and neoplastic growth. Nature 1998, 393:483–487
23. Wu X, Wu J, Huang J, Powell WC, Zhang J, Matusik RJ, Sangiorgi FO, Maxson RE, Sucov HM, Roy-Burman P: Generation of a prostate epithelial cell-specific Cre transgenic mouse model for tissue-specific gene ablation. Mech Dev 2001, 101:61–69
24. Tehranian A, Morris DW, Min BH, Bird DJ, Cardiff RD, Barry PA: Neoplastic transformation of prostatic and urogenital epithelium by the polyoma virus middle T gene. Am J Pathol 1996, 149:1177–1191
25. Kim MJ, Cardiff RD, Desai N, Banach-Petrosky WA, Parsons R, Shen MM, Abate-Shen C: Cooperativity of Nkx3.1 and Pten loss of function in a mouse model of prostate carcinogenesis. Proc Natl Acad Sci USA 2002, 99:2884–2889
26. Bins M, Takens F: A method to estimate the DNA content of whole nuclei from measurements made on thin tissue sections. Cytometry 1985, 6:234–237
27. Montironi R, Mazzucchelli R, Algaba F, Lopez-Beltran A: Morphological identification of the patterns of prostatic intraepithelial neoplasia and their importance. J Clin Pathol 2000, 53:655–665
28. Bostwick DG, Montironi R, Sesterhenn IA: Diagnosis of prostatic intraepithelial neoplasia: Prostate Working Group/consensus report. Scand J Urol Nephrol Suppl 2000, 3–10
29. Bostwick DG, Brawer MK: Prostatic intra-epithelial neoplasia and early invasion in prostate cancer. Cancer 1987, 59:788–794
30. Sakr WA, Haas GP, Cassin BF, Pontes JE, Crissman JD: The frequency of carcinoma and intraepithelial neoplasia of the prostate in young male patients. J Urol 1993, 150:379–385
31. Matsuyama H, Pan Y, Oba K, Yoshihiro S, Matsuda K, Hagarth L, Kudren D, Naito K, Bergerheim US, Ekman P: Deletions on chromosome 8p22 may predict disease progression as well as pathological staging in prostate cancer. Clin Cancer Res 2001, 7:3139–3143
32. Haggman MJ, Macoska JA, Wojno KJ, Oesterling JE: The relationship between prostatic intraepithelial neoplasia and prostate cancer: critical issues. J Urol 1997, 158:12–22
33. Bostwick DG, Amin MB, Dundore P, Marsh W, Schultz DS: Architectural patterns of high-grade prostatic intraepithelial neoplasia. Hum Pathol 1993, 24:298–310
34. Wang Y, Hayward SW, Donjacour AA, Young P, Jacks T, Sage J, Dahiya R, Cardiff RD, Day ML, Cunha GR: Sex hormone-induced carcinogenesis in Rb-deficient prostate tissue. Cancer Res 2000, 60:6008–6017
35. Kim MJ, Bhatia-Gaur R, Banach-Petrosky W, Desai N, Wang Y, Hayward SW, Cunha GR, Cardiff RD, Shen MM, Abate-Shen C: Nkx3.1 mutant mice recapitulate early stages of prostate carcinogenesis. Cancer Res 2002, 62:2999–3004

[CANCER RESEARCH 62, 2999–3004, June 1, 2002]

*Advances in Brief*

# *Nkx3.1* Mutant Mice Recapitulate Early Stages of Prostate Carcinogenesis[1]

**Minjung J. Kim, Rajula Bhatia-Gaur,[2] Whitney A. Banach-Petrosky, Nishita Desai, Yuzhuo Wang,[3] Simon W. Hayward,[4] Gerald R. Cunha, Robert D. Cardiff, Michael M. Shen,[5] and Cory Abate-Shen[5]**

*Center for Advanced Biotechnology and Medicine [M. J. K., R. B-G., W. A. B-P., N. D., M. M. S., C. A-S.]. Departments of Neuroscience [M. J. K., R. B-G., W. A. B-P., C. A-S.], Medicine [C. A-S.], and Pediatrics [N. D., M. M. S.], The Cancer Institute of New Jersey [M. M. S., C. A-S.], University of Medicine and Dentistry of New Jersey, Robert Wood Johnson Medical School, Piscataway, New Jersey 08854; Department of Anatomy, University of California, San Francisco, California 94143 [Y. W., S. W. H., G. R. C.]; and Center for Comparative Medicine, University of California, Davis, California 95616 [R. D. C.]*

## Abstract

**Recent studies of human cancers and mutant mouse models have implicated the *Nkx3.1* homeobox gene as having a key role in prostate carcinogenesis. Consistent with such a role, here we show that *Nkx3.1* displays growth-suppressing activities in cell culture, and that aged *Nkx3.1* mutant mice display histopathological defects resembling prostatic intraepithelial neoplasia (PIN), the presumed precursor of human prostate cancer. Using a tissue recombination approach, we found that PIN-like lesions from *Nkx3.1* mutants can undergo progressively severe histopathological alterations after serial transplantation in *nude* mice. Our findings indicate that *Nkx3.1* loss-of-function is a critical event in prostate cancer initiation, and that *Nkx3.1* mutant mice accurately model early stages of prostate carcinogenesis. More generally, our tissue recombination assay provides an empirical test to examine the relationship of PIN to prostate carcinoma.**

## Introduction

During prostate carcinogenesis in humans, clinically undetectable precursor lesions progress to locally confined carcinoma and ultimately to life-threatening metastatic disease (1, 2). At the histopathological level, it is generally presumed that the precursor of human prostate cancer is PIN,[6] which can be readily distinguished from nonneoplastic abnormalities such as benign prostatic hyperplasia (3, 4). Indeed, PIN lesions display similar histopathological characteristics as prostate cancer and are often found in close proximity to overt carcinoma (3, 4). Despite compelling circumstantial evidence, however, it has been difficult to establish an experimental paradigm to examine the precursor-product relationship of PIN to prostate carcinoma.

The *Nkx3.1* homeobox gene is a key regulator of prostatic epithelial differentiation, while its loss-of-function in mice has been implicated in prostate cancer initiation (5–7). In particular, *Nkx3.1* null mutant mice display abnormal prostatic differentiation as well as epithelial hyperplasia and dysplasia prior to 1 year of age (6). Human *NKX3.1* maps to chromosome 8p21 (8, 9), which frequently undergoes loss of heterozygosity at early stages of prostate carcinogenesis (10, 11). Although *NKX3.1* is not mutated in prostate cancer (9), it undergoes epigenetic inactivation through loss of protein expression in human prostate cancer and in mouse models (7, 12). Here we demonstrate that *Nkx3.1* mutant mice develop lesions that histopathologically resemble human PIN, consistent with a key role for *Nkx3.1* inactivation in prostate cancer initiation. Furthermore, the susceptibility of *Nkx3.1* mutant mice to PIN formation has facilitated our development of a tissue recombination assay to explore the relationship of PIN to prostate cancer.

## Materials and Methods

**Retroviral Gene Transfer and Tumorigenicity Assays.** Sequences corresponding to the coding region of *Nkx3.1* (5) were subcloned into *pLZRSΔ-IRES-GFP*, a derivative of *LZRSpBMN-Z* (13). The *Nkx3.1(L140S)* mutant contains a substitution of leucine 140 to serine (position 16 of the homeodomain). Production of replication-defective mammalian retroviruses and infection of target cells has been described (14). Expression of Nkx3.1 protein was verified at the initiation and termination of each assay by Western blot analysis (Fig. 1*A* and data not shown). After retroviral infection, PC3 (15) or AT6 (AT6.3; Ref. 16) cells were seeded in triplicate at a density of $5 \times 10^3/cm^2$ or $1 \times 10^3/cm^2$, respectively, in low-serum medium (0.5 or 0.25%, respectively); medium was replenished every second day. At the indicated days, cell number was determined by absorbance after staining with Napthol blue black (Sigma). Anchorage-independent growth was monitored by seeding AT6 cells in triplicate at a density of $1 \times 10^3/cm^2$ in medium containing 0.35% agarose layered over 0.5% agar. After growth for 14 days, the number of GFP-expressing colonies was determined by counting under a fluorescence microscope. Tumor growth in *nude* mice (Taconic) was initiated by s.c. injection of AT6 ($1 \times 10^4$ in serum-free medium) or PC3 ($1 \times 10^6$ in 50% Matrigel) cells. Tumor size was monitored once per week for 4 (AT6) or 6 (PC3) weeks by caliper measurement, followed by determination of tumor weights at necropsy. Statistical analyses were performed using a two-sample *t* test for independent samples with unequal variances (Satterthwaite's method).

**Analysis of *Nkx3.1* Mutant Mice.** *Nkx3.1* mutant mice have been described (6). Unless otherwise indicated, analyses were performed on virgin male mice (birth to 24 months) in a hybrid 129/SvImJ and C57Bl/6J strain background. Congenic C57Bl/6J and FVB/N *Nkx3.1* strains were produced by 10 generations of sequential back-crosses; the resulting congenic mice were analyzed at 12 months. Histological analyses were performed on formalin-fixed paraffin tissues on a nonblinded basis by R. D. C.; M. M. S. independently reviewed the histological data on a blinded basis, reaching similar conclusions. Immunohistochemical analyses were performed on formalin-fixed paraffin sections after antigen retrieval. Monoclonal antibodies were: anti-smooth muscle actin (Sigma), anti-cytokeratin 14 (Biogenex), anti-p63 (Santa Cruz Biotechnology, Inc.), and anti-E-cadherin (Transduction Laboratories). Immunodetection was performed using the Vector M.O.M. (Mouse on Mouse) kit with Vector *NovaRED* for substrate detection (Vector Laboratories).

Received 3/14/02; accepted 4/16/02.

The costs of publication of this article were defrayed in part by the payment of page charges. This article must therefore be hereby marked *advertisement* in accordance with 18 U.S.C. Section 1734 solely to indicate this fact.

[1] This work was supported by Grants UO1 CA84294 (to C. A-S., M. M. S., R. D. C., and G. R. C.), CA76501 (to C. A-S., M. M. S.), and CA64872, CA59831, and CA89520 (to G. R. C.) from the National Cancer Institute; Grants DK60887 (to M. M. S.) and DK52708 (to G. R. C.) from the National Institute of Diabetes and Digestive and Kidney Diseases; Grants DAMD17-00-1-0091 (to C. A-S.); Grant DAMD17-98-1-8532 (to M. M. S.) from the United States Army Prostate Cancer Research Program; and Grant 5JB-0014 from the University of California Breast Cancer Research Program (to R. D. C.). C. A-S., M. M. S., R. D. C., and G. R. C. are members of the Mouse Models of Human Cancer Consortium (National Cancer Institute).

[2] Present address: Molecular Pathology/Functional Genomics, Aventis Pharmaceuticals, Bridgewater, NJ 08807.

[3] Present address: Department of Cancer Endocrinology, BC Cancer Agency, Vancouver, British Columbia, V5Z 1L3 Canada.

[4] Present address: Department of Urologic Surgery, Vanderbilt University Medical Center, Nashville, TN 37232.

[5] To whom requests for reprints should be addressed, at CABM, 679 Hoes Lane, Piscataway, NJ 08854. Phone: (732) 235-5161 (C. A-S.) or (732) 235-5645 (M. M. S.); Fax: (732) 235-5789 (C. A-S.) or (732) 235-5373 (M. M. .S.); E-mail: abate@cabm.rutgers.edu (C. A-S.) or mschen@cabm.rutgers.edu (M. M. S.).

[6] The abbreviations used are: PIN, prostatic intraepithelial neoplasia; GFP, green fluorescent protein.

**Tissue Recombination Assays.** Tissue recombination assays were performed using prostatic epithelium from *Nkx3.1* homozygous mutant mice or wild-type littermates from ages 10 to 15 months. Regions of PIN-like lesions were identified by bright-field illumination under a dissecting microscope as hyperplastic ductal densities; ~300-μm segments of the hyperplastic prostatic ducts were isolated by microdissection. We confirmed that these hyperplastic ducts were enriched for PIN-like lesions by histological analyses (data not shown). These ducts (or normal ducts from wild-type littermates) were recombined with fetal rat or mouse urogenital sinus mesenchyme essentially as described (17). The tissue recombinants were incubated overnight at 37°C, followed by surgical implantation under the kidney capsule of male *nude* mouse hosts. After growth for 1–2 months, the tissue recombinants were processed for histological and immunohistochemical analyses. For serial transplantation, an ~300-μm segment of the dissected tissue graft was recombined with fresh urogenital sinus mesenchyme and grafted in *nude* mice as before. Rat urogenital sinus mesenchyme was used for all recombinants used to calculate wet weights. In Fig. 3, the recombinants shown in panels *N, D, H, L, P,* and *T* were made with rat urogenital sinus mesenchyme and the others with mouse; similar findings were obtained regardless of whether mouse or rat urogenital sinus mesenchyme was used (data not shown).

## Results

**Growth-suppressing Activities of *Nkx3.1*.** Because several lines of evidence have implicated *Nkx3.1* loss-of-function as a contributing factor for prostate carcinogenesis, we examined whether its overexpression would suppress growth and tumorigenicity of prostate carcinoma cells. We expressed exogenous *Nkx3.1* by retroviral gene transfer using a vector containing IRES-GFP sequences, so that the infected GFP-expressing cells could be enriched by flow cytometry. After cell sorting, >95% of the recovered cells expressed GFP and high levels of Nkx3.1 protein (Fig. 1*A* and data not shown). As a control, we compared the activity of Nkx3.1 to that of a mutated derivative [Nkx3.1(L140S)] that contains a substitution of a conserved homeodomain residue, which renders the protein inactive in DNA-binding and transcription assays.[7]

For these assays, we used a human (PC3) and rodent (AT6) prostate carcinoma cell line, neither of which expresses the endogenous *Nkx3.1* gene (Fig. 1*A*). We found that overexpression of exogenous *Nkx3.1*, but not the mutated gene [*Nkx3.1(L140S)*], resulted in an ~70% reduction in cellular proliferation in AT6 cells and 60% reduction in PC3 cells (Fig. 1*A*). In addition, *Nkx3.1*-expressing AT6 cells displayed an ~60% reduction in anchorage-independent growth compared with those expressing the vector control, whereas the *Nkx3.1(L140S)*-expressing cells produced a modest increase (~25%) in anchorage-independent growth (Fig. 1*A*). Moreover, *Nkx3.1*-expressing AT6 and PC3 cells displayed an approximately 50 or 60% decrease, respectively, in tumor growth in *nude* mice relative to the control vector and/or *Nkx3.1(L140S)* (Fig. 1*C*). Similar results were obtained in all assays using a human *NKX3.1* retrovirus, as well as stable tetracycline-inducible cell lines expressing mouse or human *NKX3.1* (data not shown). Notably, these growth-suppressive activities of *Nkx3.1* in cell culture and *nude* mice are consistent with the increased proliferation of prostatic epithelium observed for *Nkx3.1* mutant mice (6).

**Formation of PIN-like Lesions in *Nkx3.1* Mutant Mice.** Following an initial observation that homozygous and heterozygous *Nkx3.1* mutant mice develop prostatic epithelial hyperplasia and dysplasia prior to 1 year of age (6), we have now found that prostate glands from older *Nkx3.1* mutants display successively more severe histopathological alterations in both the epithelium and the stroma (Fig. 2). These morphological alterations represent a continuum of changes ranging from an increase in the number of luminal epithelial cells with crowded papillae to more complex and severe forms, such as the formation of crowded, multilayered epithelium (Fig. 2, *B, D, F,* and *H*). The epithelial nuclei of *Nkx3.1* mutants are larger with a more open chromatin and prominent nucleoli but lack extensive pleomorphism (Fig. 2, *D, H,* and *insets*). Accompanying these changes in the epithelium, the smooth muscle of the fibromuscular sheath becomes attenuated and is occasionally discontinuous (Fig. 2, *M* and *N*). Despite these extensive histopathological alterations, however, no cases of overt carcinoma have been observed to date, even in the oldest *Nkx3.1* mutant mice (data not shown).

Notably, a majority (70%; $n = 16$) of homozygous mutants between 1 and 2 years of age developed histological features resembling human PIN, including cribriform or papillary architecture of epithelial cells, accompanied by atypical nuclei, enlarged nucleoli, and frequent mitotic figures (Fig. 2, *A–H*; Table 1A). Consistent with our previous findings indicating *Nkx3.1* haploinsufficiency (6), an intermediate number of *Nkx3.1* heterozygotes (36%; $n = 11$) developed PIN-like lesions with histopathological features indistinguishable from those in homozygotes (Table 1A, data not shown). In addition to these findings for mice in a mixed C57Bl/6J-129/SvImJ strain background, we found that the *Nkx3.1* prostatic phenotype was similar in three inbred backgrounds (C57Bl/6J, 129/SvImJ, and FVB/N); however, the occurrence of PIN-like lesions was more frequent in C57Bl/6J and FVB/N congenic mice but less frequent in the 129/SvImJ mice (Table 1B).

Immunohistochemical analyses demonstrated that the PIN-like lesions of *Nkx3.1* mutant prostates displayed several features consistent with human PIN (Fig. 2, *I–P*):

(*a*) Using two distinct basal cell markers, cytokeratin 14 and p63, we observed an increased ratio of luminal to basal cells in PIN-like lesions; the multilayered epithelium in the interior of these lesions lacked staining for these markers (Fig. 2, *I–L*). These findings are

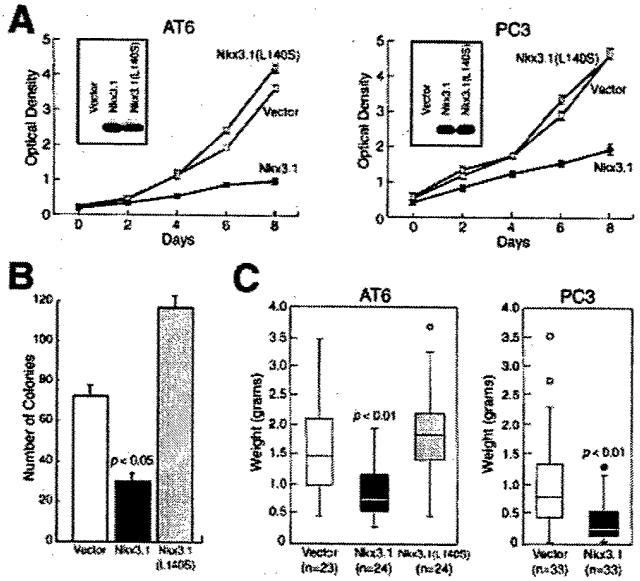


Fig. 1. Growth-suppressing activities of *Nkx3.1*. *A*, cellular proliferation assays performed with AT6 or PC3 cells infected with a control retrovirus (*Vector*) or retroviruses expressing *Nkx3.1* or *Nkx3.1(L140S)*. Assays were performed in triplicate; *bars*, 1 SD. *Insets*, Western blot assays showing expression of Nkx3.1 or Nkx3.1(L140S). *B*, anchorage-independent growth assays performed after retroviral infection of AT6 cells. Quantitation of assays performed in triplicate are shown; *bars*, 1 SD. Similar results were obtained in three independent experiments. *C*, tumor growth in *nude* mice after injection of retrovirally infected AT6 or PC3 cells. In the box plot, the *horizontal line* within the *box* represents the median tumor weight; the *box* represents 1 SD, the *vertical lines* show 2 SDs, and the *circles* represent outliers. *P* compares *Nkx3.1* with the vector control.

[7] P. Sciavolino and C. A-S., unpublished observations.

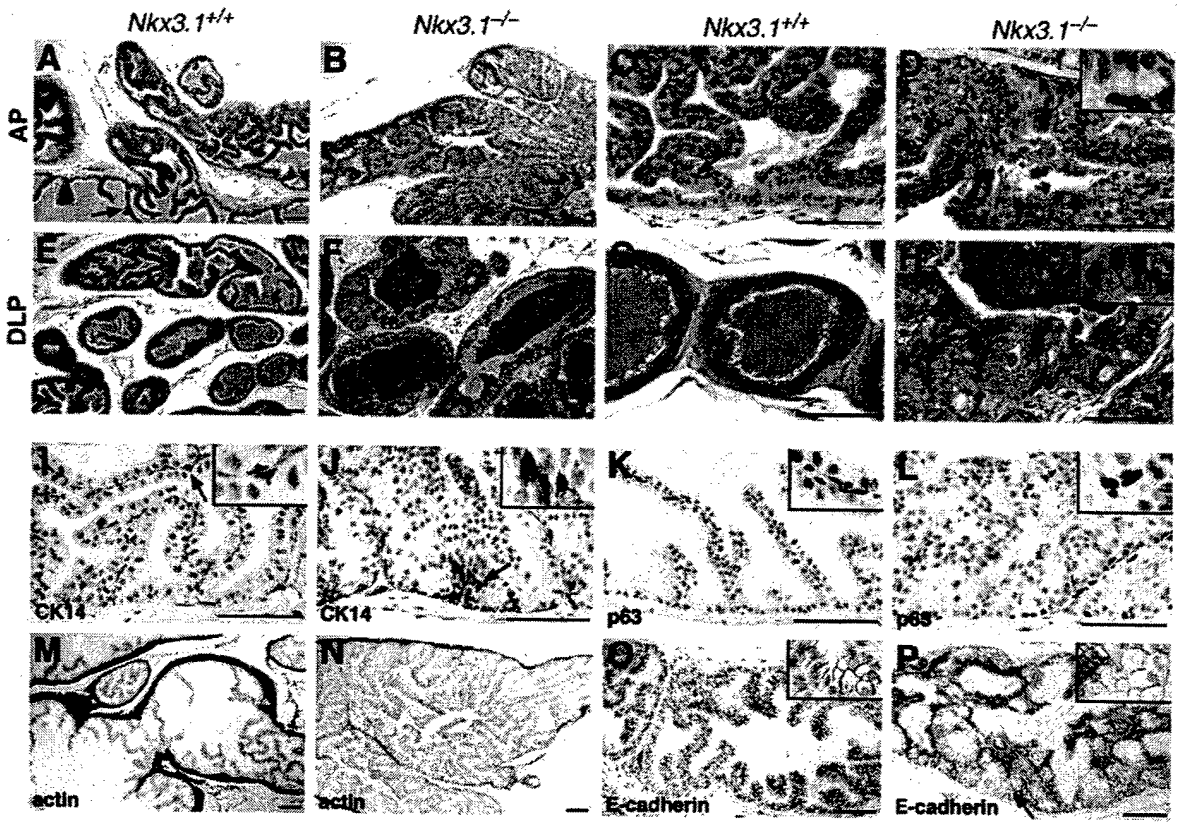


Fig. 2. Histopathology of PIN-like lesions in *Nkx3.1* mutant mice. *A–H*, H&E staining of formalin-fixed paraffin sections of anterior (*A–D*) or dorsolateral (*E–H*) prostate in wild-type ($Nkx3.1^{+/+}$) and homozygous mutant ($Nkx3.1^{-/-}$) mice at 19 months of age. *A*, *C*, *E*, and *G*, low and high-power views of wild-type ($Nkx3.1^{+/+}$) prostate lobes. In the anterior and dorsolateral prostate, well-differentiated columnar epithelial cells are arranged in papillary tufts (*arrow* in *A*), basal cells are evident (*arrow* in *C*), and luminal spaces are filled with secretions (lightly staining eosinophilic material). *B*, *D*, *F*, and *H*, the $Nkx3.1^{-/-}$ mutant prostates display multilayered hyperplastic and severely dysplastic epithelium, with little luminal space or secretory material. *Insets* in *D* and *H* show nuclear atypia with prominent and multiple nucleoli. As reported previously in younger *Nkx3.1* mutant mice (6), little or no phenotype was observed in the ventral prostate (data not shown). *I–L*, immunohistochemical analyses of $Nkx3.1^{+/+}$ and $Nkx3.1^{-/-}$ anterior prostate. *I* and *K*, immunodetection of basal epithelium with anti-cytokeratin 14 antibody (CK14) and anti-p63 shows an intact basal layer in the $Nkx3.1^{+/+}$ prostate (*arrow* in *I*). *J* and *L*, in PIN-like lesions of $Nkx3.1^{-/-}$ mutants, disorganized basal cells are often found at the margins (*arrow* in *J*), whereas the interior lacks basal cells. *M* and *N*, immunodetection of stroma with an anti-smooth muscle actin antiserum shows reduction of the fibromuscular sheath and an increased epithelial:stromal ratio in the $Nkx3.1^{-/-}$ prostates relative to wild-type controls. *O* and *P*, E-cadherin staining is relatively heterogeneous (*arrow* in *P*) but not absent in $Nkx3.1^{-/-}$ prostates relative to wild-type. Similar findings to those shown in panels *J*, *L*, *N*, and *P* were observed in PIN-like lesions of the dorsolateral prostate (data not shown). *Scale bars*, 100 μm.

consistent with the nonuniform basal cell layer that is a cardinal feature of human PIN (3, 4).

(*b*) We observed that the stromal layer was significantly attenuated in *Nkx3.1* mutants, as visualized by staining with anti-smooth muscle actin (Fig. 2, *M* and *N*), indicating an increased epithelial:stromal ratio that presumably reflects a decreased dependence of epithelial cells on the stromal layer.

(*c*) Expression of the luminal epithelial cell marker E-cadherin was increasingly heterogeneous in the PIN-like regions of *Nkx3.1* mutants (Fig. 2, *O* and *P*), consistent with its altered expression in human prostate cancers (18, 19).

(*d*) We noted that *Nkx3.1* mutant mice displayed no increase in neuroendocrine cells, as assessed by immunostaining with anti-chromogranin A or synaptophysin (data not shown); generally, these cells are not up-regulated in PIN (20).

Taken together, these findings demonstrate that *Nkx3.1* mutant mice develop lesions that strongly resemble human PIN but do not display invasive carcinoma.

**A Tissue Recombination Assay for Neoplastic Progression.** The susceptibility of *Nkx3.1* mutant mice to develop PIN-like lesions, but not carcinoma, prompted us to establish an experimental model system to test the capability of PIN to undergo neoplastic progression. For this purpose, we used a tissue recombination approach that circumvents the normal growth control of the prostatic epithelium. The rationale for this approach is based on our observations that although the prostatic epithelium is relatively growth quiescent in the context of the intact gland (even in *Nkx3.1* mutants), such epithelium displays robust proliferation in the presence of embryonic urogenital sinus mesenchyme (17). Specifically, we have found that embryonic mesenchyme can induce a relatively small (~300 μm) segment of an adult prostatic duct, composed of ~5000 epithelial cells (<1 mg), to generate several million epithelial cells in 1 month after grafting in male *nude* mouse hosts (wet weight of recovered recombinant at round 1, 39.5 ± 11.7 mg, $n = 8$). When wild-type prostatic tissue is used, the resulting tissue recombinants have prostatic ducts that are histologically normal in appearance and produce secretory proteins (Ref. 17 and Fig. 3, *A* and *E*). Serial transplantation of such tissue recombinants leads to their continued expansion and proliferation for two additional transplant generations, but not further (wet weight at round 2, 19.3 ± 5.3 mg, $n = 8$; at round 3, 18.5 ± 5.5 mg, $n = 8$; round 4, none recovered, $n = 8$). Thus, we reasoned that the robust stimulation of epithelial proliferation after serial transplantation of tissue recombinants would provide an ideal model system to test whether the PIN-like lesions of *Nkx3.1* mutants could undergo increasingly severe histopathological alterations.

Using this approach, we found that the initial round and serially

Table 1 *Summary of prostatic epithelial defects in Nkx3.1 mutant mice*

A. Analysis of mice from 1–24 months in a mixed strain background (C57Bl/6J/129/SvImJ)[a]

| Genotype | Total | Normal | Hyperplasia | PIN |
|---|---|---|---|---|
| +/+ | | | | |
| 1–6 month | 11 | 11 | 0 | 0 |
| 6–12 month | 6 | 4 | 1 | 1 |
| 12–24 month | 11 | 9 | 2 | 0 |
| | 28 | 24 | 3 | 1 |
| +/− | | | | |
| 1–6 month | 12 | 9 | 3 | 0 |
| 6–12 month | 7 | 2 | 2 | 3 |
| 12–24 month | 11 | 3 | 4 | 4 |
| | 30 | 14 | 9 | 7 |
| −/− | | | | |
| 1–6 months | 13 | 2 | 5 | 6 |
| 6–12 month | 9 | 3 | 1 | 5 |
| 12–24 month | 16 | 0 | 5 | 11 |
| | 38 | 5 | 11 | 22 |

B. Analysis of mice at 12–15 months in four strain backgrounds

| Strain and genoptype | Total | Normal | Hyperplasia | PIN |
|---|---|---|---|---|
| C57Bl/6J/129/SvImJ | | | | |
| +/+ | 3 | 3 | 0 | 0 |
| +/− | 3 | 2 | 1 | 0 |
| −/− | 3 | 0 | 0 | 3 |
| C57Bl/6J | | | | |
| +/+ | 5 | 5 | 0 | 0 |
| +/− | 5 | 2 | 3 | 0 |
| −/− | 6 | 0 | 1 | 5 |
| FVB/N | | | | |
| +/+ | 5 | 5 | 0 | 0 |
| +/− | 12 | 4 | 5 | 3 |
| −/− | 5 | 0 | 1 | 4 |
| 129/SvImJ | | | | |
| +/+ | 3 | 3 | 0 | 0 |
| +/− | 4 | 1 | 3 | 0 |
| −/− | 4 | 0 | 3 | 1 |

[a] Data for the mice at 1–12 months include data reported previously by Bhatia-Gaur *et al.* (6).

transplanted tissue recombinants of prostatic epithelium from wild-type (*Nkx3.1*$^{+/+}$) mice retained a recognizable papillary architecture surrounded by an organized fibromuscular stroma ($n$ = 13; Fig. 3, *A* and *E*, and data not shown). The papillary fronds were lined by a single layer of columnar epithelium with a normal distribution of basal cells, uniform expression of markers such as E-cadherin, and copious production of secretory fluids (Fig. 3, *A, E, I, M,* and *Q*). Notably, the pattern of the round 1 (initial) transplant did not change upon serial transplantation, although the size of the transplants diminished in serial passages (compare wet weights from initial with rounds 2 and 3 above).

In contrast, serial passage of prostatic tissue recombinants from *Nkx3.1* mutant mice resulted in a progressive loss of organized ductal architecture that is far more severe than the histopathological defects observed in mutant mice (compare Figs. 2 and 3). Although round 1 transplants retained a papillary architecture with columnar epithelium and a relatively unaltered relationship between the epithelium and stroma ($n$ = 14; Fig. 3, *B* and *F*), similar to the intact mutant prostate (Fig. 2), round 2 and 3 recombinants displayed a dramatically increased disorganization of the prostatic ducts and the surrounding stroma ($n$ = 14; Fig. 3, *C, D, G,* and *H*). These serially transplanted recombinants contained glandular epithelium that lost the papillary pattern and became subdivided into smaller glands with a variety of abnormal growth patterns, including solid masses, cribriform, and poorly differentiated (basalar or embryoid). This severely disorganized growth was also reflected by alterations in the basal cell layer (Fig. 3, *O* and *P*) and by the heterogeneous expression of E-cadherin (Fig. 3, *S* and *T*). Furthermore, the relationship between the epithelium and stroma was drastically altered, such that the fibromuscular stroma did not form a uniform sheath around the glands, leaving gaps in the smooth muscle layer (Fig. 3, *K* and *L*). Notably, masses of smooth muscle appear in some transplants that had no apparent relationship with epithelium (Fig. 3, *K* and *L*), with frequent extensions into the renal parenchyma as "tongues" of smooth muscle (Fig. 3, *K, inset*); this invasive behavior of the stroma was characteristic of the round 2 and 3 recombinants from the *Nkx3.1* mutants but was never observed in wild-type recombinants. Taken together, these findings provide experimental evidence supporting the potential for mouse PIN-like lesions to undergo successive stages of neoplastic progression.

## Discussion

Our study demonstrates the relevance of *Nkx3.1* mutant mice for studying early stages of prostate carcinogenesis, which are otherwise nearly inaccessible in humans. On the basis of the resemblance of the PIN-like lesions in *Nkx3.1* mutant mice to human PIN, we conclude that the lesions in this mouse model are indeed representative of the disease in humans. Furthermore, these PIN lesions display increasingly severe histopathological alterations after serial transplantation of tissue recombinants, consistent with their potential precursor relationship to prostate carcinoma.

Our findings that *NKX3.1* suppresses growth and tumorigenicity complement our previous observations that *Nkx3.1* mutant prostates exhibit increased cellular proliferation (6). Despite these activities, *NKX3.1* differs from classical tumor suppressor genes such as *RB, p53,* or *Pten*, because it does not undergo mutational inactivation but instead is inactivated through loss of protein expression (7, 12). Moreover, unlike classical tumor suppressors, which have broad functions in many types of cancers, the consequences of *Nkx3.1* loss-of-function are largely restricted to the prostate, in accordance with its tissue-specific expression pattern (6). Instead, *Nkx3.1* shares features in common with another homeobox gene, *Cdx2*, which displays gastrointestinal-specific expression in adults and whose loss-of-function results in epithelial dysplasia in mutant mice (21). Similar to *Nkx3.1*, *Cdx2* displays haploinsufficiency in mice, is inactivated by down-regulation of protein expression (21), and displays growth-suppressing activities in cell culture (22). These striking parallels suggest that *Nkx3.1* and *Cdx2* may represent a new class of growth-regulatory genes that display some features of classical tumor suppressors in experimental assays but are essentially mediators of tissue-specific differentiation *in vivo*. We propose that such growth-regulatory genes normally function to establish and/or maintain tissue-specific differentiation states but result in epithelial dedifferentiation and consequent predisposition to neoplasia when inactivated.

In recent years, the generation and analysis of mutant mouse models has demonstrated the validity of the mouse for studying human prostate carcinogenesis, as shown by the fundamental similarities in their histopathological characteristics as well as underlying molecular pathways (this work and reviewed in Refs. 1, 23, 24). However, unlike SV40-based gain-of-function transgenic mice (23, 25), loss-of-function mouse models are prone to develop PIN but rarely develop carcinoma (24). Nonetheless, in the tissue recombination assay, we found that PIN lesions from *Nkx3.1* mutants undergo increasingly severe histopathological changes consistent with neoplastic progression, although these recombinants have yet to display overt invasive carcinoma. These findings are consistent with our interpretation that *Nkx3.1* is a regulator of terminal differentiation of luminal epithelial cells, and that loss of *Nkx3.1* function requires additional cooperating events to result in overt carcinoma. Indeed, we have shown that mutant mice lacking both *Nkx3.1* and the *Pten* tumor suppressor develop high-grade PIN/carcinoma *in situ* lesions (7); thus, we anticipate that tissue recombinants from *Nkx3.1; Pten* compound

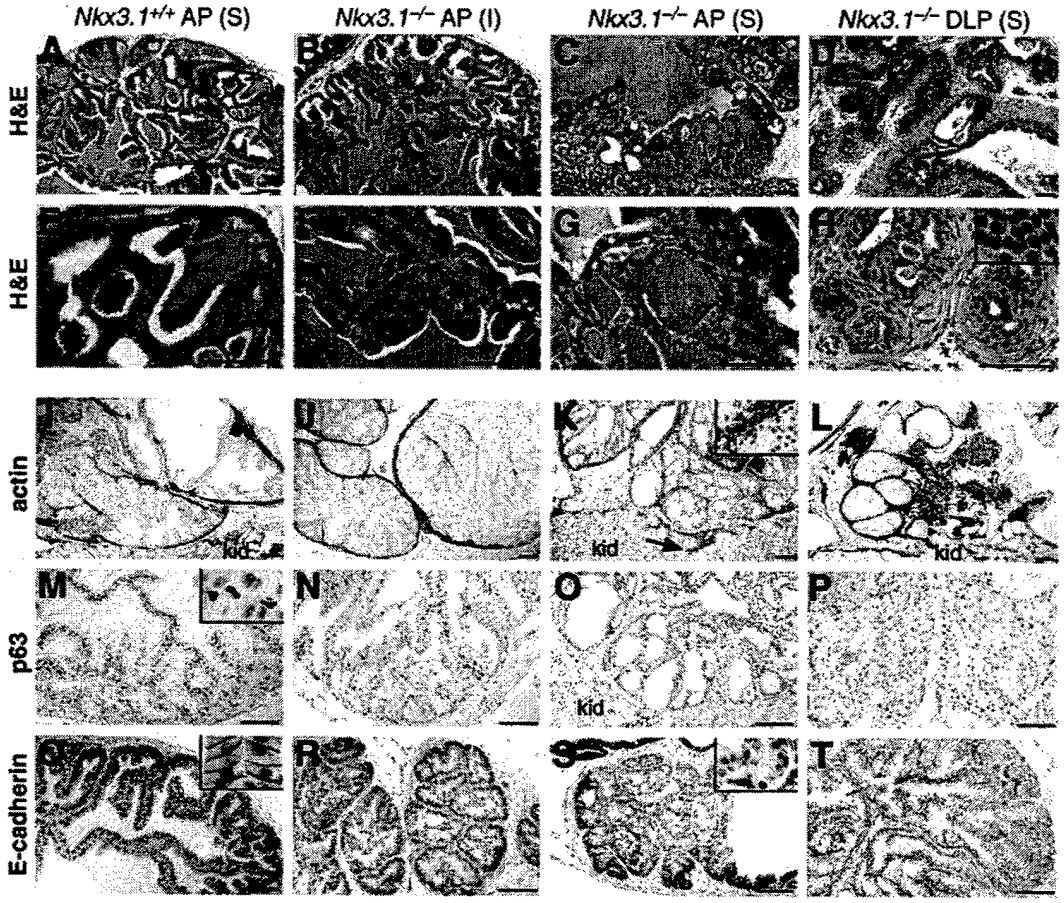


Fig. 3. Histopathology of *Nkx3.1* tissue recombinants. Sections of tissue recombinants grown in male *nude* mice from anterior (*AP*) or dorsolateral (*DLP*) prostates of wild-type ($Nkx3.1^{+/+}$) and homozygous ($Nkx3.1^{-/-}$) mice. Shown are examples from the initial round of transplants (*I*; round 1) or after serial transplantation (*S*) for one or two additional generations (rounds 2 or 3). *A–H*, low and high power views of H&E-stained paraffin sections. *A, B, E,* and *F,* recombinants of serially transplanted wild-type (*A* and *E*) and initial round (*B* and *F*) *Nkx3.1* mutants display recognizable papillary architecture. *C, D, G,* and *H,* prostatic ducts from serially transplanted *Nkx3.1* mutant recombinants display cribriform architecture (*G*) or solid masses of epithelial cells (*H*); nuclei display multiple prominent nucleoli but not extreme pleomorphism (*inset* in *H*). *I–T,* immunohistochemical analysis of tissue recombinants from anterior or dorsolateral prostate. *I* and *J,* anti-smooth muscle actin staining shows that serially transplanted wild-type and initial round *Nkx3.1* mutant recombinants have relatively normal association of stromal and epithelial layers. *K* and *L,* serially transplanted *Nkx3.1* mutant recombinants display abundant masses of smooth muscle stroma and frequent extensions into the kidney parenchyma (*arrow* and *inset* in *K*). *M* and *N,* basal cells detected by anti-p63 staining are distributed in normal fashion along the basement membrane and in papillary tufts of serially transplanted wild-type and initial round *Nkx3.1* mutant recombinants. *O* and *P,* basal cells in serially transplanted *Nkx3.1* mutant recombinants are distributed aberrantly or are limited to margins of large masses of epithelial cells. *Q–T,* E-cadherin localization in luminal cells is increasingly heterogeneous in serially transplanted mutant recombinants (*inset* in *S*). *kid,* kidney. *Scale bars,* 100 μm.

mutants may display histopathological changes consistent with carcinoma.

In conclusion, mouse models can overcome many inherent difficulties associated with studying human prostate carcinogenesis, including limitations of tissue availability and the characteristic heterogeneity of human prostate cancer. In particular, the prevalence of PIN in *Nkx3.1* mutants has enabled our initial examination of the precursor relationship of PIN to prostate carcinoma. We envision that the tissue recombination assay described herein will ultimately provide valuable insights into the contributions of individual genes for each stage of prostate carcinogenesis.

## Acknowledgments

We acknowledge Xiaohui Sun and Judy E. Walls for excellent technical assistance.

## References

1. Abate-Shen, C., and Shen, M. M. Molecular genetics of prostate cancer. Genes Dev., *14:* 2410–2434, 2000.
2. Dong, J. T., Isaacs, W. B., and Isaacs, J. T. Molecular advances in prostate cancer. Curr. Opin. Oncol., *9:* 101–107, 1997.
3. Bostwick, D. G., and Brawer, M. K. Prostatic intra-epithelial neoplasia and early invasion in prostate cancer. Cancer (Phila.), *59:* 788–794, 1987.
4. Bostwick, D. G. Prospective origins of prostate carcinoma. Prostatic intraepithelial neoplasia and atypical adenomatous hyperplasia. Cancer (Phila.), *78:* 330–336, 1996.
5. Sciavolino, P. J., Abrams, E. W., Yang, L., Austenberg, L. P., Shen, M. M., and Abate-Shen, C. Tissue-specific expression of murine Nkx3.1 in the male urogenital system. Dev. Dyn., *209:* 127–138, 1997.
6. Bhatia-Gaur, R., Donjacour, A. A., Sciavolino, P. J., Kim, M., Desai, N., Young, P., Norton, C. R., Gridley, T., Cardiff, R. D., Cunha, G. R., Abate-Shen, C., and Shen, M. M. Roles for Nkx3.1 in prostate development and cancer. Genes Dev., *13:* 966–977, 1999.
7. Kim, M. J., Cardiff, R. D., Desai, N., Banach-Petrosky, W. A., Parsons, R., Shen, M. M., and Abate-Shen, C. Cooperativity of Nkx3.1 and Pten loss of function in a mouse model of prostate carcinogenesis. Proc. Natl. Acad. Sci. USA, *99:* 2884–2889, 2002.
8. He, W. W., Sciavolino, P. J., Wing, J., Augustus, M., Hudson, P., Meissner, P. S., Curtis, R. T., Shell, B. K., Bostwick, D. G., Tindall, D. J., Gelmann, E. P., Abate-Shen, C., and Carter, K. C. A novel human prostate-specific, androgen-regulated homeobox gene (*NKX3.1*) that maps to 8p21, a region frequently deleted in prostate cancer. Genomics, *43:* 69–77, 1997.
9. Voeller, H. J., Augustus, M., Madike, V., Bova, G. S., Carter, K. C., and Gelmann, E. P. Coding region of NKX3.1, a prostate-specific homeobox gene on 8p21, is not mutated in human prostate cancers. Cancer Res., *57:* 4455–4459, 1997.
10. Emmert-Buck, M. R., Vocke, C. D., Pozzatti, R. O., Duray, P. H., Jennings, S. B., Florence, C. D., Zhuang, Z., Bostwick, D. G., Liotta, L. A., and Linehan, W. M. Allelic loss on chromosome 8p12–21 in microdissected prostatic intraepithelial neoplasia. Cancer Res., *55:* 2959–2962, 1995.

11. Vocke, C. D., Pozzatti, R. O., Bostwick, D. G., Florence, C. D., Jennings, S. B., Strup, S. E., Duray, P. H., Liotta, L. A., Emmert-Buck, M. R., and Linehan, W. M. Analysis of 99 microdissected prostate carcinomas reveals a high frequency of allelic loss on chromosome 8p12–21. Cancer Res., *56:* 2411–2416, 1996.
12. Bowen, C., Bubendorf, L., Voeller, H. J., Slack, R., Willi, N., Sauter, G., Gasser, T. C., Koivisto, P., Lack, E. E., Kononen, J., Kallioniemi, O. P., and Gelmann, E. P. Loss of NKX3.1 expression in human prostate cancers correlates with tumor progression. Cancer Res., *60:* 6111–6115, 2000.
13. Kinsella, T. M., and Nolan, G. P. Episomal vectors rapidly and stably produce high-titer recombinant retrovirus. Hum. Gene Ther., *7:* 1405–1413, 1996.
14. Hu, G., Lee, H., Price, S. M., Shen, M. M., and Abate-Shen, C. Msx homeobox genes inhibit differentiation through upregulation of cyclin D1. Development (Camb.), *128:* 2373–2384, 2001.
15. Kaighn, M. E., Shanker, N., Ohnuki, Y., Lechner, J. F., and Jones, L. W. Establishment and characterization of a human prostatic carcinoma cell line (PC-3). Investig. Urol., *17:* 16–23, 1979.
16. Isaacs, J. T., Isaacs, W. B., Feitz, W. F., and Scheres, J. Establishment and characterization of seven Dunning rat prostatic cancer cell lines and their use in developing methods for predicting metastatic abilities of prostatic cancers. Prostate, *9:* 261–281, 1986.
17. Norman, J. T., Cunha, G. R., and Sugimura, Y. The induction of new ductal growth in adult prostatic epithelium in response to an embryonic prostatic inductor. Prostate, *8:* 209–220, 1986.
18. Morton, R. A., Ewing, C. M., Nagafuchi, A., Tsukita, S., and Isaacs, W. B. Reduction of E-cadherin levels and deletion of the α-catenin gene in human prostate cancer cells. Cancer Res., *53:* 3585–3590, 1993.
19. Umbas, R., Isaacs, W. B., Bringuier, P. P., Schaafsma, H. E., Karthaus, H. F., Oosterhof, G. O., Debruyne, F. M., and Schalken, J. A. Decreased E-cadherin expression is associated with poor prognosis in patients with prostate cancer. Cancer Res., *54:* 3929–3933, 1994.
20. Abrahamsson, P. A. Neuroendocrine differentiation in prostatic carcinoma. Prostate, *39:* 135–148, 1999.
21. Chawengsaksophak, K., James, R., Hammond, V. E., Kontgen, F., and Beck, F. Homeosis and intestinal tumours in Cdx2 mutant mice. Nature (Lond.), *386:* 84–87, 1997.
22. Mallo, G. V., Soubeyran, P., Lissitzky, J. C., Andre, F., Farnarier, C., Marvaldi, J., Dagorn, J. C., and Iovanna, J. L. Expression of the *Cdx1* and *Cdx2* homeotic genes leads to reduced malignancy in colon cancer-derived cells. J. Biol. Chem., *273:* 14030–14036, 1998.
23. Huss, W. J., Maddison, L. A., and Greenberg, N. M. Autochthonous mouse models for prostate cancer: past, present and future. Semin. Cancer Biol., *11:* 245–260, 2001.
24. Abate-Shen, C., and Shen, M. M. Mouse models of prostate carcinogenesis. Biomednet. Trends Genet., *18:* 51–55, 2002.
25. Matusik, R., Masumori, M., Thomas, T., Case, T., Paul, M., Kasper, S., and Shappell, S. Transgenic mouse models of prostate cancer. *In:* M. Matzuk, C. Brown, and T. Kumar (eds.), Transgenics in Endocrinology, pp. 401–425. Totowa, NJ: The Humana Press, Inc., 2001.

# Cooperativity of *Nkx3.1* and *Pten* loss of function in a mouse model of prostate carcinogenesis

Minjung J. Kim*†, Robert D. Cardiff‡, Nishita Desai*†, Whitney A. Banach-Petrosky*†, Ramon Parsons§, Michael M. Shen*¶‖, and Cory Abate-Shen*†‖

*Center for Advanced Biotechnology and Medicine and Departments of †Neuroscience and ¶Pediatrics, University of Medicine and Dentistry of New Jersey–Robert Wood Johnson Medical School, Piscataway, NJ 08854; ‡Center for Comparative Medicine, University of California, Davis, CA 95616; and §Department of Pathology, College of Physicians and Surgeons, Columbia University, New York, NY 10032

Communicated by Aaron J. Shatkin, Center for Advanced Biotechnology and Medicine, Piscataway, NJ, December 20, 2001 (received for review November 6, 2001)

**Mouse models have provided significant insights into the molecular mechanisms of tumor suppressor gene function. Here we use mouse models of prostate carcinogenesis to demonstrate that the *Nkx3.1* homeobox gene undergoes epigenetic inactivation through loss of protein expression. Loss of function of *Nkx3.1* in mice cooperates with loss of function of the *Pten* tumor suppressor gene in cancer progression. This cooperativity results in the synergistic activation of Akt (protein kinase B), a key modulator of cell growth and survival. Our findings underscore the significance of interactions between tissue-specific regulators such as *Nkx3.1* and broad-spectrum tumor suppressors such as *Pten* in contributing to the distinct phenotypes of different cancers.**

Molecular investigations of the functions of oncogenes and tumor suppressor genes have been facilitated by analysis of mouse models (1, 2). With respect to prostate carcinogenesis, mouse models potentially can overcome inherent difficulties in studying the molecular genetics of this disease in humans (3–5). Human prostate cancer is characterized by the long latency between the appearance of precursor lesions, termed prostatic intraepithelial neoplasia (PIN), which can appear in men as early as in their twenties, and the manifestation of clinically detectable carcinomas that generally arise late in life. Thus, mouse models can provide insight into the molecular mechanisms involved in prostate cancer initiation and early steps of progression, which otherwise are nearly inaccessible in humans.

We have been using mouse models to investigate the individual and collaborative roles of candidate tumor suppressor genes for prostate carcinogenesis. Our work has focused on the *Nkx3.1* homeobox gene because of its restricted expression in the prostate and essential role in prostate differentiation and function (6, 7). Loss of function of *Nkx3.1* in mice results in prostatic epithelial hyperplasia and dysplasia as a correlate of aging (7), and *Nkx3.1* heterozygotes display a similar although less severe phenotype than homozygotes, indicating haploinsufficiency (7). The relevance of *NKX3.1* for human prostate cancer has been suggested by its localization to chromosomal region 8p21 (8, 9), which undergoes loss of heterozygosity (LOH) in ≈80% of prostate cancers (10–13). Notably, 8p21 LOH represents an early event in prostate carcinogenesis, because it occurs at high frequency in PIN (11, 12), suggesting that genes within this region are involved in cancer initiation. However, the role of *NKX3.1* in human prostate carcinogenesis has been unclear, because it is not mutated in prostate cancer specimens (9). Thus, although one allele of *NKX3.1* is presumed to be lost at high frequency in human prostate cancer because of its localization to 8p21, the remaining allele does not undergo mutational inactivation.

*Pten* encodes a lipid phosphatase that functions as an inhibitor of the phosphatidylinositol 3-kinase/Akt pathway (14–17), and its essential function is evident from the early embryonic lethality of homozygous mutants (18–20). In humans, *PTEN* maps to chromosomal region 10q23, which undergoes LOH at relatively advanced stages in many cancers (16, 17), suggesting that genes within this region are important for progression. *PTEN* represents a frequent target of mutational inactivation in human cancers (16, 17), and *Pten* heterozygous mutant mice develop cancers or dysplasias of multiple tissues including prostate (18, 20–22).

Our current investigations demonstrate that loss of function of *Nkx3.1* and *Pten* cooperate in prostate carcinogenesis in mice. *Nkx3.1;Pten* compound mutant mice display an increased incidence of high-grade PIN (HGPIN)/early carcinoma lesions, which resemble early stages of human prostate carcinogenesis. A hallmark of these lesions in mutant mice as well as human prostate cancer is the loss of Nkx3.1 protein expression without LOH. Finally, our analysis reveals the unexpected convergence of *Nkx3.1* and *Pten* in negative regulation of Akt activity.

## Experimental Procedures

The *Nkx3.1* and *Pten* mutant mice have been described (7, 20). Analyses were performed on a hybrid 129/SvImJ and C57BL/6J strain background by using virgin males. The primary histological analysis was performed on a nonblinded basis by R.D.C.; M.M.S. independently reviewed the histological data on a blinded basis. The scheme for histopathological grading will be described elsewhere (J.-H. Park, M.J.K., C.A.-S., M.M.S., and R.D.C., unpublished data). The human prostate tumor specimens were paraffin-embedded samples retrieved from the surgical pathology files at the University of California Davis Medical Center (generously supplied by Regina Gandour-Edwards). The histological diagnosis and Gleason grade were verified by independently R.D.C. and Regina Gandour-Edwards; no relationship between NKX3.1 protein loss and Gleason grade was observed.

Immunohistochemical analysis was performed on 4% paraformaldehyde-fixed cryosections (for anti-P-Akt) or formalin-fixed paraffin sections after antigen retrieval (for all other antibodies). The antibodies used were anti-cytokeratin 14 (monoclonal, BioGenex Laboratories, San Ramon, CA), anti-CD105/endoglin (monoclonal, Dako), anti-polycytokeratins (polyclonal, CK-P, Dako), anti-Ki67 antigen (polyclonal, NovoCastra Laboratories, Newcastle, U.K.), PTEN/MMAC1 (polyclonal, Ab-2, NeoMarkers, Fremont, CA), and anti-Akt and anti-P-Akt (Ser 473) (polyclonal, Cell Signaling Technology, Beverly, MA). Anti-mouse and anti-human Nkx3.1 antisera were generated by using as antigens the full-length proteins purified from *Escherichia coli* by hexahistidine affinity chromatography. Immunodetection was performed by using the Vector M.O.M. kit for monoclonal antibodies, the Vector Elite ABC kit for rabbit IgG for polyclonal antisera, and a Vector NovaRED kit for substrate detection. The data in Fig. 4 were

Abbreviations: PIN, prostatic intraepithelial neoplasia; LOH, loss of heterozygosity; HGPIN, high-grade PIN; LGPIN, low-grade PIN; LCM, laser-capture microdissection.

‖To whom reprint requests may be addressed at: Center for Advanced Biotechnology and Medicine, 679 Hoes Lane, Piscataway, NJ 08854. E-mail: mshen@cabm.rutgers.edu or abate@cabm.rutgers.edu.

The publication costs of this article were defrayed in part by page charge payment. This article must therefore be hereby marked "*advertisement*" in accordance with 18 U.S.C. §1734 solely to indicate this fact.



www.pnas.org/cgi/doi/10.1073/pnas.042688999

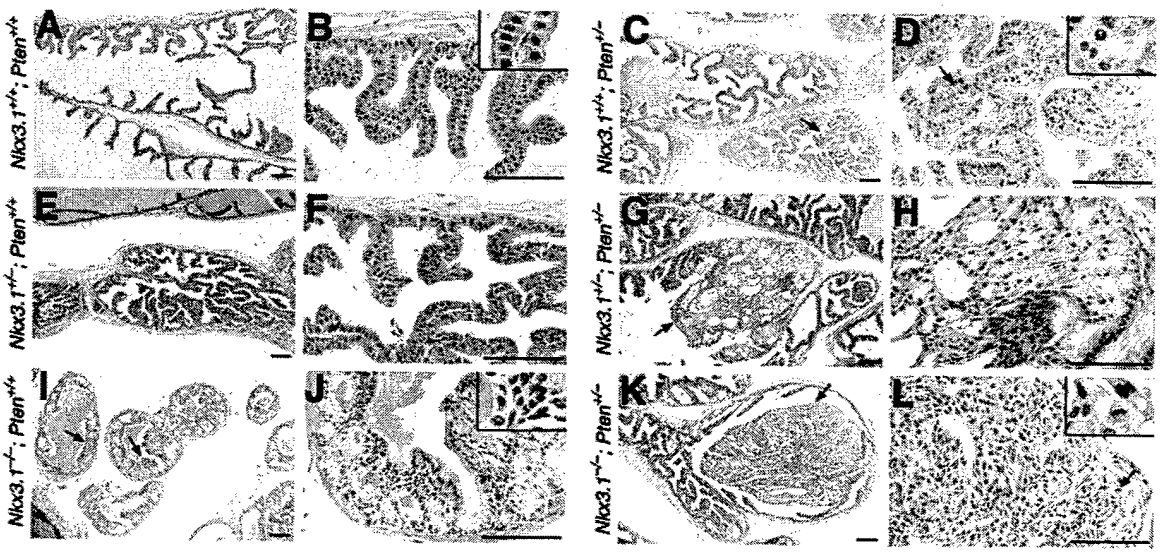


**Fig. 1.** HGPIN/early carcinoma lesions in *Nkx3.1;Pten* compound mutant prostates. Hematoxylin and eosin staining of anterior prostates of *Nkx3.1;Pten* compound mutants at 6 months is shown. (*A* and *B*) Well differentiated columnar epithelium. (*Inset*) High-power view. (*C* and *D*) Localized region of severely dysplastic epithelium (arrows) surrounded by well differentiated columnar epithelium. (*Inset*) Example of nuclear atypia. (*E* and *F*) Moderately hyperplastic epithelium. (*G* and *H*) HGPIN/early carcinoma lesion (arrow) surrounded by relatively unaffected epithelium. (*I* and *J*) Extensive low-grade PIN (LGPIN, arrows). (*Inset*) Example of nuclear atypia. (*K* and *L*) HGPIN/early carcinoma lesion surrounded by relatively unaffected epithelium. (*Inset*) Atypical nuclei with mitotic figure. (Scale bars, 100 microns.)

obtained with polyclonal antisera against mouse or human Nkx3.1; similar results were obtained with other anti-Nkx3.1 antisera. Ki67-labeled nuclei were quantitated as reported in ref. 7. Western blot analysis was done with extracts prepared from anterior prostates by sonication in 20 mM Hepes (pH 7.4)/450 mM NaCl/0.2 mM EDTA/0.5 mM DTT/25% glycerol and protease inhibitor and phosphatase inhibitor cocktails (Sigma p2714 and p2850, respectively). Laser-capture microdissection (LCM) of immunostained sections was performed by using a PixCell apparatus (Arcturus Engineering, Mountain View, CA).

## Results

**Loss of Function of *Nkx3.1* and *Pten* Cooperate in Prostate Cancer Progression.** To examine whether loss of function of *Nkx3.1* and *Pten* collaborate in prostate carcinogenesis, we intercrossed compound heterozygotes ($Nkx3.1^{+/-}$;$Pten^{+/-}$) in a mixed C57BL/6J-129/SvJ strain background to produce cohort groups comprised of all six viable genotypes (Fig. 1). Interestingly, our comparison of the prostatic phenotype of *Nkx3.1* and *Pten* single mutant mice ($Nkx3.1^{-/-}$;$Pten^{+/+}$, $Nkx3.1^{+/-}$;$Pten^{+/+}$, and $Nkx3.1^{+/+}$;$Pten^{+/-}$) at 6 months of age revealed notable histological differences. At this age, the *Pten* mutant prostates displayed localized regions of severely dysplastic epithelium, unlike *Nkx3.1* mutants in which the prostatic epithelium was more broadly hyperplastic but less severely dysplastic (Fig. 1 *C–F*, *I*, and *J*).

Our analysis of the compound mutants revealed that loss of function of *Nkx3.1* and *Pten* displayed striking cooperativity in the anterior and dorsolateral prostatic lobes by 6 months of age (Figs. 1 and 2). In particular, $Nkx3.1^{+/-}$;$Pten^{+/-}$ and $Nkx3.1^{-/-}$;$Pten^{+/-}$ mice developed extensive multifocal lesions comprised of poorly differentiated cells with prominent and multiple nucleoli, an increased nuclear/cytoplasmic ratio, and frequent mitotic figures (Fig. 1 *G*, *H*, *K*, and *L*). These lesions were readily discernible as light-dense regions within the normally transparent prostatic ducts, usually filled the affected ducts, and were highly vascularized (Fig. 3 *A–D*, *I*, and *J*). Among the histopathological features that distinguished these lesions from the relatively normal ("unaffected") adjacent epithelium were a marked elevation of wide-spectrum cytokeratins and an absence of basal epithelium (Fig. 3 *E–H*). In addition, the lesions displayed a high proliferative index (≈15%) relative to the adjacent unaffected epithelium, as indicated by the prevalence of mitotic figures and the abundance of Ki67-labeled nuclei (Figs. 1*L* and 3 *K* and *L*). Based on their undifferentiated cytology, microvascularization, and high proliferative index, we have defined these multifocal lesions as HGPIN/early carcinoma in accordance with terminology used to describe human prostate cancer precursors (23).

The cooperativity of loss of function of *Nkx3.1* and *Pten* in prostate carcinogenesis was apparent from the increased incidence of HGPIN/early carcinoma lesions in the $Nkx3.1^{-/-}$;$Pten^{+/-}$ and $Nkx3.1^{+/-}$;$Pten^{+/-}$ prostates relative to $Nkx3.1^{+/+}$;$Pten^{+/-}$ pros-

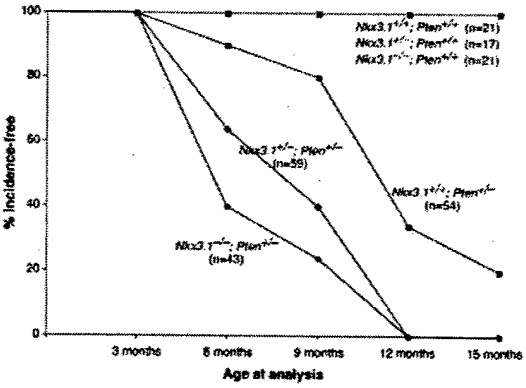


**Fig. 2.** Loss of function of *Nkx3.1* and *Pten* cooperate in prostate cancer progression. A graphical representation of the percentage of mice lacking HGPIN/early carcinoma lesions in the dorsolateral prostate at the indicated ages is shown. Incidence corresponds to the occurrence of HGPIN/early carcinoma lesions, which is defined by using the histopathological and morphological criteria described in the text. The percentage incidence-free was calculated by dividing the number of unaffected mice by the total number of mice analyzed for each age group.

DEVELOPMENTAL BIOLOGY

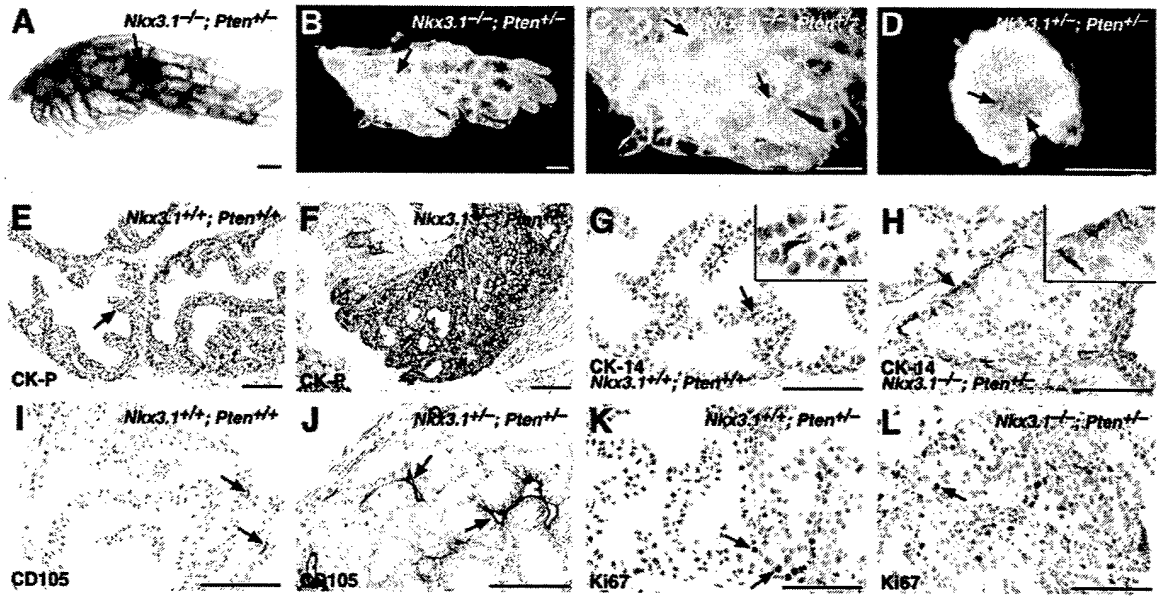


**Fig. 3.** Analysis of HGPIN/early carcinoma lesions. (*A–D*) Bright-field (*A*) and dark-field (*B–D*) images of anterior prostates at 6 months. (*A–C*) Whole mounts show light dense masses corresponding to the HGPIN/early carcinoma lesions (arrows). (*D*) Microdissected lesion containing numerous blood vessels (arrows). (Scale bars, 500 microns.) (*E–L*) Immunohistochemical analysis of the anterior prostate at 6 months. (*E* and *F*) Robust staining of wide-spectrum cytokeratins (CK-P) in HGPIN/early carcinoma lesions. (*G* and *H*) Immunodetection with anti-CK14 (arrows) shows an absence of basal cells in lesion. (*Insets*) High-power views. (*I* and *J*) Anti-CD105 (endoglin) shows increased microvascularization (*J*, arrows) of lesions. (*K* and *L*) Ki67 antibody shows increased cellular proliferation in lesions. (Scale bars, 100 microns.)

tates (Fig. 2). Notably, at 6 months of age these lesions were observed in 60% of the *Nkx3.1*$^{-/-}$;*Pten*$^{+/-}$ prostates and 36% of the *Nkx3.1*$^{+/-}$;*Pten*$^{+/-}$ prostates, in contrast to only 10% of *Nkx3.1*$^{+/+}$;*Pten*$^{+/-}$ prostates. By 12 months, all the *Nkx3.1*$^{-/-}$;*Pten*$^{+/-}$ and *Nkx3.1*$^{+/-}$;*Pten*$^{+/-}$ prostates displayed lesions, whereas 34% of *Nkx3.1*$^{+/+}$;*Pten*$^{+/-}$ prostates remained lesion-free. When found, however, the HGPIN/early carcinoma lesions of the *Nkx3.1*$^{+/+}$;*Pten*$^{+/-}$ prostates were indistinguishable morphologically and immunohistochemically from those of the *Nkx3.1*;*Pten* compound mutants. Therefore, the cooperativity of *Nkx3.1* and *Pten* loss of function reflects the decreased latency of HGPIN/early carcinoma lesion formation in compound mutants. In contrast, we observed no increase in the occurrence of LGPIN in compound mutants (data not shown), suggesting that cooperativity of *Nkx3.1* and *Pten* loss of function occurs at the level of cancer progression.

Aside from the development of these HGPIN/early carcinoma lesions, the compound mutants displayed no additional phenotypes compared with the single mutants. In particular, the compound mutants displayed a similar survival profile to the *Pten* single mutants (data not shown), which generally succumb to lymphomas and other nonprostate tumors (18, 20, 22). These observations are consistent with the prostate-specific phenotype of *Nkx3.1*, which does not have an impact on survival rate, and emphasize the prostate specificity of the cooperativity between loss of function of *Nkx3.1* and *Pten*.

**Absence of Nkx3.1 Protein Expression in Mouse and Human Prostate Cancer.** Because the HGPIN/early carcinoma lesions occurred frequently in *Nkx3.1*$^{+/-}$;*Pten*$^{+/-}$ compound mutants, which are heterozygous for *Nkx3.1*, we examined the status of *Nkx3.1* expression in these lesions (Fig. 4). Strikingly, Nkx3.1 immunostaining was invariably absent from lesions of the compound heterozygotes (100%; $n = 25$; Fig. 4*D*) but displayed robust nuclear staining in the unaffected regions adjacent to the lesions. In some cases, we observed mislocalization of Nkx3.1 protein to the cytoplasm (Fig. 4*F*), which may provide an alternative means for inactivating *Nkx3.1* function. In contrast to alterations of Nkx3.1 protein, *Nkx3.1* mRNA was readily detected in these HGPIN/early carcinoma lesions as well as the adjacent unaffected epithelium by reverse transcriptase–PCR (Fig. 4*P*).

More generally, we have observed the absence of Nkx3.1 protein expression in regions of atypical hyperplasia, LGPIN, and HGPIN occurring in both single and compound mutant mice ($n = 20$). For example, Nkx3.1 protein was absent in HGPIN regions in *Pten* single mutants, which are genotypically wild type for *Nkx3.1* (Fig. 4*C*). Loss of Nkx3.1 protein was common also in LGPIN of *Nkx3.1* heterozygotes, which are wild type for *Pten* (Fig. 4*B*). Finally, we have observed the absence of Nkx3.1 immunostaining in small clusters of atypical hyperplastic cells in both *Nkx3.1* heterozygotes and *Nkx3.1*;*Pten* compound heterozygotes (Fig. 4*E*), suggesting that Nkx3.1 protein loss may precede formation of PIN during cancer progression.

In a parallel analysis of human prostate cancer, we observed that NKX3.1 protein expression was reduced significantly or absent (56 or 26%, respectively; $n = 27$) in a majority of cancer specimens, with an occasional shift from nuclear to cytoplasmic subcellular localization (11%; $n = 27$; Fig. 4 *G–I*). These findings are in accordance with a recent report demonstrating the frequent reduction or absence of NKX3.1 protein expression in a large-scale tissue array analysis of human PIN and prostate cancer specimens (24). Thus, loss and/or mislocalization of NKX3.1 protein expression is characteristic of prostate carcinogenesis in the mouse model as well as in human cancer.

***Pten* but Not *Nkx3.1* Undergoes Allelic Loss in HGPIN/Early Carcinoma Lesions of Compound Mutants.** To examine the status of the wild-type *Nkx3.1* and *Pten* alleles in the HGPIN/early carcinoma lesions of compound heterozygotes, we performed LCM on Nkx3.1-immunostained sections to recover genomic DNA from lesions (Nkx3.1-nonexpressing) and adjacent unaffected regions (Nkx3.1-expressing controls; Fig. 4*M*). In all cases analyzed, the wild-type

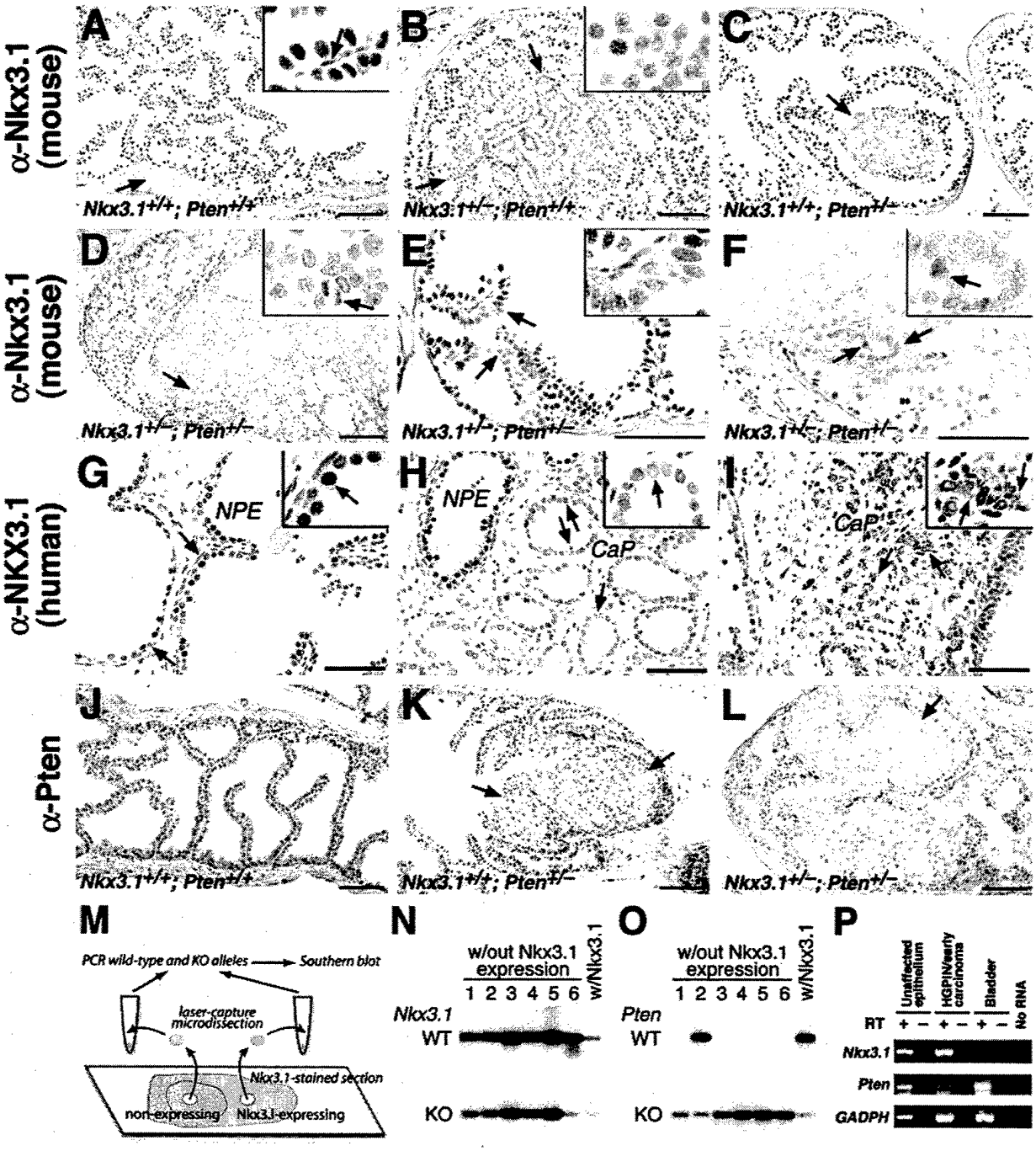


**Fig. 4.** Absence of Nkx3.1 protein expression in mouse and human prostate cancer. (*A–F*) Immunohistochemical analysis of the anterior prostate of *Nkx3.1* and *Pten* mutants with an anti-mouse Nkx3.1 polyclonal antisera. (*A*) Uniform immunostaining of luminal epithelium with adjacent stroma unstained (arrow). (*Inset*) Nuclear staining of secretory cells and absence of staining of basal cells (arrow). (*B*) Absence of staining in LGPIN in a 12-month prostate. (*Inset*) Unstained and stained nuclei at the margin of the PIN (arrow). (*C* and *D*) Lack of staining in HGPIN in a 6-month prostate (*C*, arrow) and in an HGPIN/early carcinoma lesion of an 8-month prostate (*D*, arrow). Note the uniform staining of adjacent unaffected regions (*C*). (*Inset*) Unstained nuclei with atypia and mitotic figure (arrow). (*E*) Heterogeneity of staining (arrows) in a cluster of hyperplastic cells in an 8-month prostate. (*Inset*) Juxtaposition of stained, unstained, and lightly stained nuclei. (*F*) Example of cytoplasmic immunostaining (arrows and *inset*) at the margins of an HGPIN/early carcinoma lesion in a 12-month prostate. (*G–I*) Immunohistochemical analysis of human prostatectomy specimens using a polyclonal anti-human NKX3.1 antisera. (*G*) Immunostaining of normal prostate epithelium (NPE). Note absence of staining in basal cells (arrows) and stroma. (*Inset*) Nuclear staining of secretory cells (arrow). (*H*) Absent or heterogeneous staining in well differentiated cancer (CaP) compared with adjacent normal prostate epithelium. (*Inset*) Lack of staining in cancer cells (arrow). (*I*) Predominantly cytoplasmic immunostaining of a poorly differentiated cancer (arrows and *Inset*). (*J–L*) Immunohistochemical analysis of the anterior prostate using anti-Pten antisera. (*J*) Uniform staining in the epithelium and stroma. (*K*)

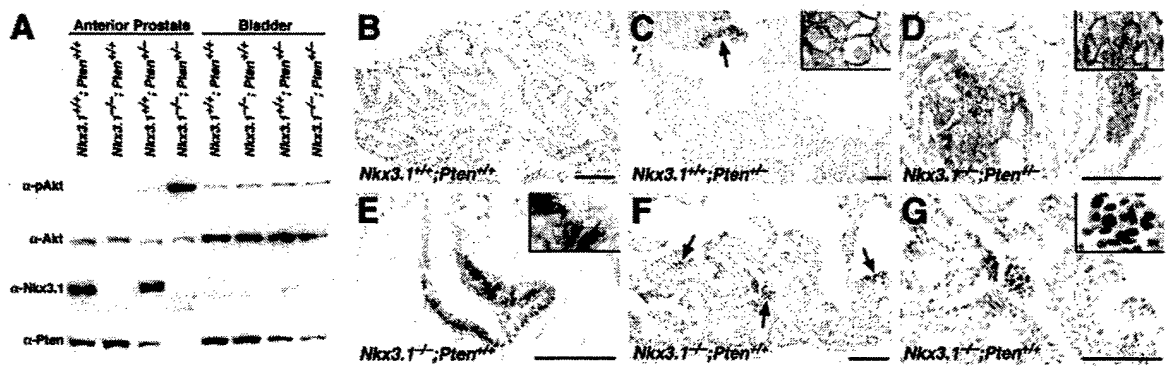


**Fig. 5.** Synergistic activation of Akt in *Nkx3.1;Pten* compound mutant prostates. (*A*) Western blot analysis shows high levels of activated Akt in protein extracts from the anterior prostate but not the bladder of *Nkx3.1;Pten* compound mutants at 8 months. Protein lysates (20 μg) were resolved by SDS/PAGE and probed with antisera to detect P-Akt, total Akt, Pten, or Nkx3.1. Note the reduced levels of Pten in the $Nkx3.1^{-/-};Pten^{+/-}$ compound mutants relative to the *Pten* single mutants. (*B–G*) Immunohistochemical analysis of P-Akt in the anterior prostates of *Nkx3.1* and *Pten* mutants. (*B*) Absence of staining in wild-type mice. (*C*) Staining in a cluster of hyperplastic cells (arrows and *Inset*). (*D*) Robust staining of HGPIN/early carcinoma lesion (*Inset*). (*E–G*) P-Akt immunostaining in clusters of cells in the $Nkx3.1^{-/-}$ prostates shows nuclear and cell surface staining (*E*, *Inset*) and primarily nuclear staining (*G*, *Inset*).

*Nkx3.1* allele was retained ($n = 20$); moreover, no mutations were detected in the *Nkx3.1* coding region (Fig. 4*N* and data not shown).

In contrast, *Pten* sustained allelic loss in 9 of 10 lesions from *Nkx3.1;Pten* compound heterozygotes (Fig. 4*O*); this was accompanied by a loss of Pten protein expression, which was apparent both by immunohistochemistry and Western blotting (Figs. 4*L* and 5*A*). Interestingly, *Pten* did not undergo allelic loss in adjacent unaffected regions, and Pten protein expression was reduced but not absent in regions of HGPIN in *Pten* single mutants (Fig. 4 *K*, *L*, and *O*). Thus, our findings using LCM demonstrate that *Pten* undergoes LOH within HGPIN/early carcinoma lesions and help to reconcile discrepancies in the literature regarding the allelic status of *Pten* in mouse models (21, 22, 25).

**Synergistic Activation of Akt in *Nkx3.1; Pten* Compound Mutant Mice.** Because *Pten* is known to inhibit activation of the Akt kinase (refs. 26–28 and reviewed in refs. 17, 29, and 30), we examined the expression levels and distribution of activated Akt in single and compound mutant prostates by using an antibody specific for the activated (phosphorylated) form (P-Akt; Fig. 5). By Western blot analysis, we observed a synergistic increase in P-Akt in the $Nkx3.1^{-/-};Pten^{+/-}$ prostates relative to wild-type or single mutants, although the level of total Akt protein was equivalent in all genotypes ($n = 9$ cohorts; Fig. 5*A*). Moreover, Akt activation was restricted to the prostate and was not observed in tissues that do not express *Nkx3.1* such as the bladder (Fig. 5*A*). Elevated P-Akt was detected in compound mutants as early as 2 months of age (data not shown), which precedes lesion formation (Fig. 2).

Immunohistochemical analysis revealed robust P-Akt staining in the HGPIN/early carcinoma lesions of *Nkx3.1;Pten* mice ($n = 30$; Fig. 5*D*). These P-Akt-positive regions correspond to those lacking Pten immunostaining and have undergone *Pten* LOH (Fig. 4 *L* and *O* and data not shown). In addition, we detected P-Akt staining in PIN regions of *Pten* single mutants as well as in small clusters of hyperplastic cells in both *Pten* single and *Nkx3.1;Pten* compound mutants (Fig. 5*C* and data not shown).

We also observed P-Akt staining in the prostatic epithelium of *Nkx3.1* single mutants, suggesting that loss of function of *Nkx3.1* can affect Akt activation in the context of wild-type *Pten* function ($n = 13$; Fig. 5 *E–G* and data not shown). P-Akt was relatively restricted in its distribution and detected typically in isolated clusters of cells within regions of LGPIN in $Nkx3.1^{+/-}$ and $Nkx3.1^{-/-}$ mice. Although P-Akt-positive clusters were prevalent in the prostate, they were not found in non-*Nkx3.1*-expressing tissues such as bladder and intestine, and Pten protein expression was unaffected in the *Nkx3.1* mutant prostates (data not shown). Although we occasionally detected P-Akt staining associated with the cell surface in *Nkx3.1* mutant prostates, we more frequently observed nuclear distribution of phospho-Akt (Fig. 5 *E–G*). In summary, our findings demonstrate synergistic activation of Akt in compound mutant prostates, suggesting a potential molecular basis for the observed cooperativity of *Nkx3.1* and *Pten* loss of function.

## Discussion

Until recently, the validity of the mouse as a model for human prostate cancer has been controversial because of the anatomical and histological differences between mouse and human prostate and the absence of spontaneous prostate cancer in mice (3–5). Our findings demonstrate the utility of mutant mouse models for recapitulating early stages of human prostate carcinogenesis and for providing novel mechanistic insights into this process.

Several lines of evidence implicate *NKX3.1* as a tumor suppressor gene, the loss of function of which represents a critical step in prostate cancer initiation. First, *NKX3.1* displays tumor suppressor activities in cell culture and in *nude* mice (M.J.K., M.M.S., and C.A.-S., unpublished data). Second, *Nkx3.1* mutant mice develop PIN, paralleling the predicted consequences of chromosome 8p21 LOH in human prostate carcinogenesis. Finally, the *NKX3.1* locus is contained within a minimal deletion interval (≈1,500 kb) of human chromosome 8p21 that has been defined by allelotyping

Moderate reduction of Pten staining in a region of HGPIN in a 5-month prostate (arrows). (*L*) Absence of Pten staining in an HGPIN/early carcinoma lesion of a 12-month prostate. Note that in *K* and *L* the staining of adjacent unaffected regions is similar to wild type (*J*). (*M–O*) Analysis of allelic status of *Nkx3.1* and *Pten* in HGPIN/early carcinoma lesions. (*M*) LCM was performed on Nkx3.1-immunostained sections to isolate genomic DNA from lesions ($n = 20$, Nkx3.1-nonexpressing) and adjacent unaffected regions ($n = 8$, Nkx3.1-expressing); representative data are shown. (*N* and *O*) Southern blot analysis to detect the wild-type (WT) alleles for *Nkx3.1* and *Pten*; detection of the targeted allele (KO) serves as an internal control. (*P*) Reverse transcriptase–PCR analysis showing robust expression of *Nkx3.1* and reduced expression of *Pten* in HGPIN/early carcinoma lesion of $Nkx3.1^{+/-};Pten^{+/-}$ mutant relative to the adjacent unaffected epithelium. cDNA was prepared in the absence (−) or presence (+) of reverse transcriptase (RT). Note that *Nkx3.1* is not expressed in bladder; glyceraldehyde-3-phosphate dehydrogenase is the positive control.

studies of prostate carcinomas (C. Vocke and M. Emmert-Buck, personal communication).

Furthermore, the epigenetic inactivation of *NKX3.1* function through loss of protein expression is a hallmark of prostate cancer in humans and mutant mouse models (ref. 24 and M.J.K., M.M.S., and C.A.-S., unpublished observations). Notably, this loss of protein expression occurs without an accompanying loss of mRNA expression or mutational inactivation of the *NKX3.1* locus (refs. 9, 31, and 32 and this work). One possible mechanism for the loss of NKX3.1 protein is altered translational or posttranslational control, potentially involving the unusually long (≈4-kb) *NKX3.1* 3′ untranslated region (6); an alternative possibility is deregulated intracellular transport and/or degradation, which would account for the cytoplasmic localization of NKX3.1 protein. Regardless of the mechanism, the observed absence of Nkx3.1 protein provides an explanation for the haploinsufficient phenotype of *Nkx3.1* heterozygotes and reconciles a crucial role for *NKX3.1* in human prostate cancer with the failure to detect inactivating mutations.

In our studies of compound mutant mice, we have observed that the loss of function of *Nkx3.1* and *Pten* cooperates in prostate cancer progression, as shown by the increased incidence of HGPIN/early carcinoma lesions in the *Nkx3.1;Pten* compound mutants relative to the *Pten* single mutants. These HGPIN/early carcinoma lesions can be distinguished from the surrounding epithelium by their (*i*) high mitotic index, (*ii*) increased microvessel density, (*iii*) absence of the basal epithelial layer, (*iv*) altered wide-spectrum cytokeratin expression, (*v*) absence of Nkx3.1 protein expression without corresponding LOH or loss of *Nkx3.1* mRNA expression, (*vi*) *Pten* LOH and corresponding absence of Pten protein expression, and (*vii*) elevated P-Akt.

Despite the extensive morphological changes observed in *Nkx3.1;Pten* compound mutant prostates, these mice rarely develop invasive prostatic adenocarcinoma. Notably, these findings contrast with the reported consequences of loss of function of *Pten* and the cyclin-dependent kinase inhibitor $p27^{KIP1}$ (21). However, we have found that *Pten;*$p27^{KIP1}$ compound mutants as well as *Nkx3.1;Pten;*$p27^{KIP1}$ triple mutants develop HGPIN/early carcinoma lesions resembling those of *Nkx3.1;Pten* compound mutants with respect to their histopathological and immunohistochemical features (M.J.K., M.M.S., C.A.-S., unpublished observations).

These findings highlight the significance and potential synergies of *Nkx3.1*, *Pten*, and $p27^{KIP1}$ in prostate cancer progression. Although the cumulative data from human studies indicate that loss of function of *NKX3.1* corresponds to an initiation event, whereas loss of function of *PTEN* and $p27^{KIP1}$ correspond to progression events, a limitation of these mutant mouse models is their inability to provide insight into the sequential order of events. Thus, although these studies have elucidated genetic components of a prostate cancer progression pathway, future studies using inducible targeting strategies or similar approaches will be necessary to explore the physiological sequence of events.

The synergistic activation of Akt in *Nkx3.1;Pten* compound mutant prostates suggests that deregulation of Akt activity is a critical event in prostate carcinogenesis, consistent with the recent observation of elevated phospho-Akt levels in human PIN (33). Interestingly, we have observed nonuniform activation of Akt in the prostatic epithelium of *Nkx3.1* single mutants, suggesting that *Nkx3.1* loss of function also affects Akt activation, albeit indirectly. Moreover, *Nkx3.1* seems to affect the nuclear-cytoplasmic distribution of Akt protein (Fig. 5 and M.J.K., M.M.S., and C.A.-S., unpublished observations), which is noteworthy because Akt is activated at the cell membrane and subsequently translocated to the nucleus, where it has been proposed to phosphorylate regulatory targets (34–36).

In conclusion, we have shown that collaboration between a tissue-specific modulator of prostatic epithelial differentiation and a broad-spectrum tumor suppressor can contribute to cancer progression. These observations raise the possibility that the apparent tissue selectivity of broad-spectrum tumor suppressors (1, 2) may be generated through their synergy with tissue-specific genes to affect common signaling pathways such as what we have observed for *Pten* and *Nkx3.1* for Akt activation in the prostate. Thus, we propose that these collaborative interactions contribute to the distinguishing features of prostate carcinoma and that similar interactions may generally explain the tissue-specific phenotypes of cancers.

We are indebted to Dr. Regina Gandour-Edwards for the human prostate cancer specimens. We acknowledge April Graham and Judy E. Walls for excellent technical assistance. We thank David Ornstein and Michael Emmert-Buck for assistance with LCM and discussions. We are grateful to David Berman, Diego Castrillon, Ron DePinho, Simon Hayward, and Danny Reinberg for comments on the manuscript. This work was supported by National Cancer Institute Grants UO1 CA84294 (to C.A.-S., M.M.S., and R.D.C) and CA76501 (to C.A.-S. and M.M.S.), National Institute of Diabetes and Digestive and Kidney Diseases Grant DK60887 (to M.M.S.), U.S. Army Prostate Cancer Research Program Grants DAMD17-00-1-0091 (to C.A.-S.) and DAMD17-98-1-8532 (to M.M.S.), and University of California Breast Cancer Research Program Grant 5JB-0014 (to R.D.C.).

1. Jacks, T. (1996) *Annu. Rev. Genet.* **30**, 603–636.
2. Macleod, K. F. & Jacks, T. (1999) *J. Pathol.* **187**, 43–60.
3. Abate-Shen, C. & Shen, M. M. (2000) *Genes Dev.* **14**, 2410–2434.
4. Matusik, R., Masumori, M., Thomas, T., Case, T., Paul, M., Kasper, S. & Shappell, S. B. (2002) in *Transgenics in Endocrinology*, eds. Matzuk, M., Brown, C. & Kumar, T. (Humana, Totowa, NJ), pp. 401–425.
5. Green, J. E., Greenberg, N. M., Ashendel, C. L., Barrett, J. C., Boone, C., Getzenberg, R. H., Henkin, J., Matusik, R., Janus, T. J. & Scher, H. I. (1998) *Prostate* **36**, 59–63.
6. Sciavolino, P. J., Abrams, E. W., Yang, L., Austenberg, L. P., Shen, M. M. & Abate-Shen, C. (1997) *Dev. Dyn.* **209**, 127–138.
7. Bhatia-Gaur, R., Donjacour, A. A., Sciavolino, P. J., Kim, M., Desai, N., Young, P., Norton, C. R., Gridley, T., Cardiff, R. D., Cunha, G. R., *et al.* (1999) *Genes Dev.* **13**, 966–977.
8. He, W. W., Sciavolino, P. J., Wing, J., Augustus, M., Hudson, P., Meissner, P. S., Curtis, R. T., Shell, B. K., Bostwick, D. G., Tindall, D. J., *et al.* (1997) *Genomics* **43**, 69–77.
9. Voeller, H. J., Augustus, M., Madike, V., Bova, G. S., Carter, K. C. & Gelmann, E. P. (1997) *Cancer Res.* **57**, 4455–4459.
10. Bergerheim, U. S., Kunimi, K., Collins, V. P. & Ekman, P. (1991) *Genes Chromosomes Cancer* **3**, 215–220.
11. Emmert-Buck, M. R., Vocke, C. D., Pozzatti, R. O., Duray, P. H., Jennings, S. B., Florence, C. D., Zhuang, Z., Bostwick, D. G., Liotta, L. A. & Linehan, W. M. (1995) *Cancer Res.* **55**, 2959–2962.
12. Haggman, M. J., Wojno, K. J., Pearsall, C. P. & Macoska, J. A. (1997) *Urology* **50**, 643–647.
13. Vocke, C. D., Pozzatti, R. O., Bostwick, D. G., Florence, C. D., Jennings, S. B., Strup, S. E., Duray, P. H., Liotta, L. A., Emmert-Buck, M. R. & Linehan, W. M. (1996) *Cancer Res.* **56**, 2411–2416.
14. Machama, T. & Dixon, J. E. (1998) *J. Biol. Chem.* **273**, 13375–13378.
15. Myers, M. P., Pass, I., Batty, I. H., Van der Kaay, J., Stolarov, J. P., Hemmings, B. A., Wigler, M. H., Downes, C. P. & Tonks, N. K. (1998) *Proc. Natl. Acad. Sci. USA* **95**, 13513–13518.
16. Cantley, L. C. & Neel, B. G. (1999) *Proc. Natl. Acad. Sci. USA* **96**, 4240–4245.
17. Di Cristofano, A. & Pandolfi, P. P. (2000) *Cell* **100**, 387–390.
18. Di Cristofano, A., Pesce, B., Cordon-Cardo, C. & Pandolfi, P. P. (1998) *Nat. Genet.* **19**, 348–355.
19. Suzuki, A., de la Pompa, J. L., Stambolic, V., Elia, A. J., Sasaki, T., del Barco Barrantes, I., Ho, A., Wakeham, A., Itie, A., Khoo, W., Fukumoto, M. & Mak, T. W. (1998) *Curr. Biol.* **8**, 1169–1178.
20. Podsypanina, K., Ellenson, L. H., Nemes, A., Gu, J., Tamura, M., Yamada, K. M., Cordon-Cardo, C., Catoretti, G., Fisher, P. E. & Parsons, R. (1999) *Proc. Natl. Acad. Sci. USA* **96**, 1563–1568.
21. Di Cristofano, A., De Acetis, M., Koff, A., Cordon-Cardo, C. & Pandolfi, P. P. (2001) *Nat. Genet.* **27**, 222–224.
22. Stambolic, V., Tsao, M. S., Macpherson, D., Suzuki, A., Chapman, W. B. & Mak, T. W. (2000) *Cancer Res.* **60**, 3605–3611.
23. Bostwick, D. G. & Brawer, M. K. (1987) *Cancer* **59**, 788–794.
24. Bowen, C., Bubendorf, L., Voeller, H. J., Slack, R., Willi, N., Sauter, G., Gasser, T. C., Koivisto, P., Lack, E. E., Kononen, J., Kallioniemi, O. P. & Gelmann, E. P. (2000) *Cancer Res.* **60**, 6111–6115.
25. Kwabi-Addo, B., Giri, D., Schmidt, K., Podsypanina, K., Parsons, R., Greenberg, N. & Ittmann, M. (2001) *Proc. Natl. Acad. Sci. USA* **98**, 11563–11568.
26. Stambolic, V., Suzuki, A., de la Pompa, J. L., Brothers, G. M., Mirtsos, C., Sasaki, T., Ruland, J., Penninger, J. M., Siderovski, D. P. & Mak, T. W. (1998) *Cell* **95**, 29–39.
27. Wu, X., Senechal, K., Neshat, M. S., Whang, Y. E. & Sawyers, C. L. (1998) *Proc. Natl. Acad. Sci. USA* **95**, 15587–15591.
28. Sun, H., Lesche, R., Li, D. M., Liliental, J., Zhang, H., Gao, J., Gavrilova, N., Mueller, B., Liu, X. & Wu, H. (1999) *Proc. Natl. Acad. Sci. USA* **96**, 6199–6204.
29. Coffer, P. J., Jin, J. & Woodgett, J. R. (1998) *Biochem. J.* **335**, 1–13.
30. Datta, S. R., Brunet, A. & Greenberg, M. E. (1999) *Genes Dev.* **13**, 2905–2927.
31. Ornstein, D. K., Cinquanta, M., Weiler, S., Duray, P. H., Emmert-Buck, M. R., Vocke, C. D., Linehan, W. M. & Ferretti, J. A. (2001) *J. Urol.* **165**, 1329–1334.
32. Xu, L. L., Srikantan, V., Sesterhenn, I. A., Augustus, M., Dean, R., Moul, J. W., Carter, K. C. & Srivastava, S. (2000) *J. Urol.* **163**, 972–979.
33. Paweletz, C. P., Charboneau, L., Bichsel, V. E., Simone, N. L., Chen, T., Gillespie, J. W., Emmert-Buck, M. R., Roth, M. J., Petricoin, I. E. & Liotta, L. A. (2001) *Oncogene* **20**, 1981–1989.
34. Meier, R., Alessi, D. R., Cron, P., Andjelkovic, M. & Hemmings, B. A. (1997) *J. Biol. Chem.* **272**, 30491–30497.
35. Andjelkovic, M., Alessi, D. R., Meier, R., Fernandez, A., Lamb, N. J., Frech, M., Cron, P., Cohen, P., Lucocq, J. M. & Hemmings, B. A. (1997) *J. Biol. Chem.* **272**, 31515–31524.
36. Brunet, A., Bonni, A., Zigmond, M. J., Lin, M. Z., Juo, P., Hu, L. S., Anderson, M. J., Arden, K. C., Blenis, J. & Greenberg, M. E. (1999) *Cell* **96**, 857–868.

**Reprint of this paper is forthcoming:**

**Rego E.M. and Pandolfi PP. Reciprocal products of chromosomal translocations in human cancer pathogenesis: key players or innocent bystanders? Trends Mol Med. 2002 Aug;8(8):396-405.**

# Pten and p27$^{KIP1}$ cooperate in prostate cancer tumor suppression in the mouse

Antonio Di Cristofano[1,2], Marika De Acetis[1,2], Andrew Koff[2], Carlos Cordon-Cardo[3] & Pier Paolo Pandolfi[1,2]

**The genetic bases underlying prostate tumorigenesis are poorly understood. Inactivation of the tumor-suppressor gene *PTEN* and lack of p27$^{KIP1}$ expression have been detected in most advanced prostate cancers[1,2]. But mice deficient for *Cdkn1b* (encoding p27$^{Kip1}$) do not develop prostate cancer[3–5]. PTEN activity leads to the induction of p27$^{KIP1}$ expression, which in turn can negatively regulate the transition through the cell cycle[6]. Thus, the inactivation of p27$^{KIP1}$ may be epistatic to PTEN in the control of the cell cycle. Here we show that the concomitant inactivation of one *Pten* allele and one or both *Cdkn1b* alleles accelerates spontaneous neoplastic transformation and incidence of tumors of various histological origins. Cell proliferation, but not cell survival, is increased in *Pten*$^{+/-}$/*Cdkn1b*$^{-/-}$ mice. Moreover, *Pten*$^{+/-}$/*Cdkn1b*$^{-/-}$ mice develop prostate carcinoma at complete penetrance within three months from birth. These cancers recapitulate the natural history and pathological features of human prostate cancer. Our findings reveal the crucial relevance of the combined tumor-suppressive activity of Pten and p27$^{Kip1}$ through the control of cell-cycle progression.**

Adenocarcinoma of the prostate is the most common cancer in men and the second leading cause of cancer death in males[7]. The long arm of chromosome 10 shows loss of heterozygosity in sporadic prostate cancer[8]. Biallelic inactivation of *PTEN*, at 10q23, is a frequent event in metastatic prostate cancer[1] and *Pten*$^{+/-}$ mice display hyperplastic-dysplastic features in the prostate at young age[9,10]. Expression levels of the cyclin-dependent kinase inhibitor p27$^{KIP1}$ have been shown to be a reliable prognostic marker in prostate cancer, as low or absent expression of p27$^{KIP1}$ correlates with poor prognosis[2]. Targeted disruption of *Cdkn1b* in the mouse, however, only results in a mild hyperplasia of the prostate at advanced age[11].

We have previously reported that *Pten*$^{+/-}$ mice often die within eight months because of massive lympho-splenomegaly[12]. Here, we examined long-term survivors to determine the spectrum of spontaneous tumorigenesis. *Pten*$^{+/-}$ mice were extremely susceptible to developing epithelial tumors (Fig. 1*a–f* and Table 1). All *Pten*$^{+/-}$ mutants analyzed developed bilateral adrenal medullary tumors between 9 and 16 months of age, whereas 60–70% of the mice developed thyroid follicular carcinoma and endometrial atypical complex hyperplasia, which is considered a precursor of endometrial carcinoma[13]. We also observed, albeit less frequently, small intestine, large intestine and lung adenocarcinomas characterized by cellular dysplasia (based on their nuclear-cytoplasmic ratios), prominent nucleoli, and abundant, irregular, ring-like mitotic figures (Fig. 1 and Table 1). In contrast, none of the wild-type control mice analyzed developed tumors. In all cases, these carcinomas were well differentiated, did not show major invasion in the surrounding tissue and did not metastasize. Approximately 50% of *Pten*$^{+/-}$ mice developed prostatic intraepithelial neoplasia (PIN). Multiple PINs were often observed in the same prostate lobe. PINs were never observed before nine months (Fig. 1*a*). The Pten protein was found to be expressed in both normal and neoplastic tissue (n=5; Fig. 1*g*).

*In vitro* studies have shown that PTEN can exert its tumor suppressive function through different mechanisms, including regulation of cell death and cell proliferation[14]. It is still unclear, however, which pathways are critical for the *in vivo* tumor-suppressive function of PTEN. Regulation of p27$^{KIP1}$ levels through the control of Akt kinase activity has been proposed as one mechanism through which PTEN might control cell-cycle progression[6]. Inactivation of *Cdkn1b* in the mouse does not result in enhanced spontaneous tumorigenesis, with the exception of pituitary adenomas[3–5]; how-

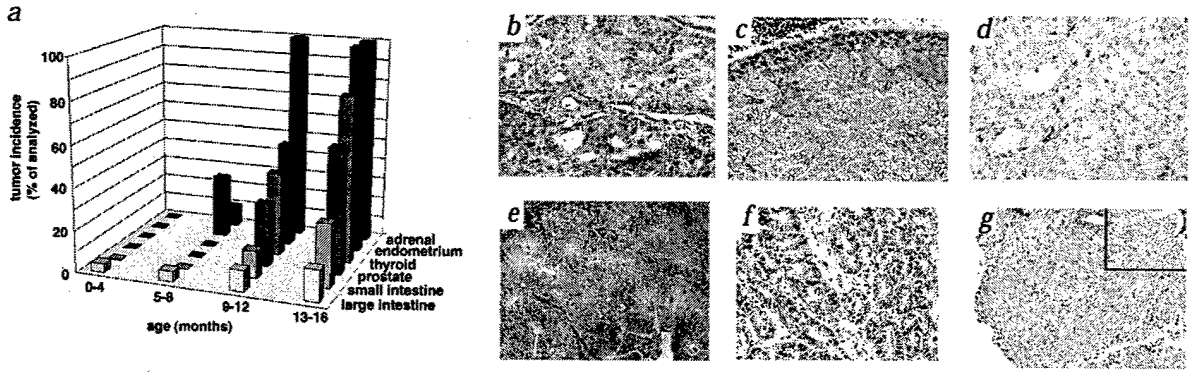


**Fig. 1** *Pten*$^{+/-}$ mice are highly susceptible to developing epithelial tumors. ***a***, Tumor incidence in *Pten*$^{+/-}$ mice. ***b***, Hematoxylin and eosin-stained dorsolateral prostate showing prostatic intraepithelial neoplasia (PIN). ***c***, Adrenal medullary tumor (pheochromocytoma). ***d***, Thyroid follicular carcinoma. ***e***, Endometrial complex atypical hyperplasia. ***f***, Colon adenocarcinoma. ***g***, Immunodetection of Pten expression in a PIN-like lesion. Inset, the negative control, in which the primary antibody has been omitted. Original magnifications, ×400.

[1]*Department of Human Genetics and* [2]*Molecular Biology Program, and* [3]*Department of Pathology, Memorial Sloan-Kettering Cancer Center, Sloan-Kettering Institute, New York, New York, USA. Correspondence should be addressed to P.P.P. (e-mail: p-pandolfi@ski.mskcc.org).*

**Table 1 • Tumorigenesis in *Pten*$^{+/-}$ and *Pten*$^{+/-}$/*Cdkn1b*$^{-/-}$ mice**

| Tissue of origin | Tumors observed | |
|---|---|---|
| | *Pten*$^{+/-}$ (9–16 months) | *Pten*$^{+/-}$/*Cdkn1b*$^{-/-}$ (3–5 months) |
| prostate | 9/18[a] | 13/13[a] |
| adrenal medulla | 34/34 | 26/26 |
| thyroid | 14/24[b] | 23/23[b] |
| endometrium | 11/16[c] | 12/12[c] |
| small intestine | 8/35[d] | 13/25[d] |
| large intestine | 4/35 | 4/25 |
| lung | 2/35 | 0/26 |

Analysis of *Pten*$^{+/-}$ long-term survivors (that is, mice older than 9 months) and of all the *Pten*$^{+/-}$/*Cdkn1b*$^{-/-}$ mutants studied is shown. [a]$P$=0.003, [b]$P$=0.0006, [c]$P$=0.05, [d]$P$=0.028 (Fisher's exact $P$ value).

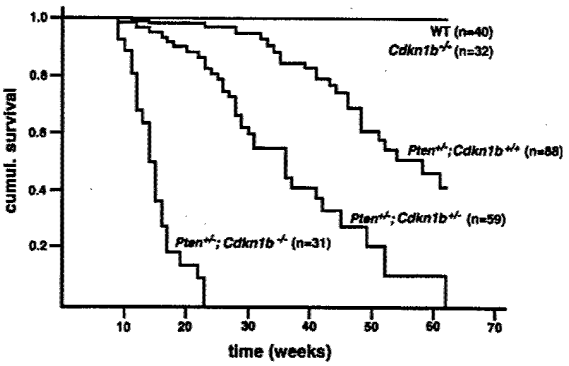


**Fig. 2** Reduction of the *Cdkn1b* gene dose accelerates tumorigenesis in *Pten*$^{+/-}$ mice. Kaplan–Meier survival analysis of *Pten*$^{+/-}$ mice with different *Cdkn1b* genotypes ($P$<0.0001).

ever, expression levels of p27$^{KIP1}$ have been shown to inversely correlate with the aggressiveness of tumors of various histological origins and patient overall survival[2]. To investigate the functional relationship between the loss of *Pten* and the loss of *Cdkn1b* in prostate cancer etiopathogenesis, we crossed the *Pten*$^{+/-}$ mice with *Cdkn1b*$^{-/-}$ mice in a C57BL/6 genetic background. Reduction of the copy number of *Cdkn1b* in *Pten*$^{+/-}$ mice resulted in a progressive decrease in the survival of the double-mutant mice (Fig. 2). The mean survival for *Pten*$^{+/-}$ mice was 51.01±1.48 weeks, whereas this value decreased to 35.9±2.05 weeks for the double-heterozygous mutants. The mean survival for the *Pten*$^{+/-}$/*Cdkn1b*$^{-/-}$ mice was 15.06±0.18 weeks (100% of the mutants died within 5 months of birth). In all cases postmortem analysis of *Pten*$^{+/-}$/*Cdkn1b*$^{-/-}$ mice revealed an intestinal occlusion (ileus) due to extensive polypoid outgrowths in the small intestine (data not shown), which was the probable cause of death. Histopathological analysis demonstrated that each *Pten*$^{+/-}$/*Cdkn1b*$^{-/-}$ mouse had multiple tumors in several different organs, and that *Cdkn1b* inactivation increased the penetrance and reduced the latency of the tumors observed in *Pten*$^{+/-}$ mutants (Fig. 1*a* and Table 1). All of the *Pten*$^{+/-}$/*Cdkn1b*$^{-/-}$ double mutants analyzed had developed prostate cancer.

The specific localization of the neoplastic lesion in the mouse prostate is particularly important because not all the lobes of this organ have an analogous counterpart in the human gland. For example, the mouse ventral lobe does not have an analogous structure in the human prostate, whereas the dorsolateral lobe corresponds to the peripheral zone in the human gland[15]. The peripheral zone is the area undergoing transformation in approximately 80% of human prostate cancers[16]. The dorsolateral prostate was involved in 100% of cases both in *Pten*$^{+/-}$ and in *Pten*$^{+/-}$/*Cdkn1b*$^{-/-}$ mice, as also observed in human prostate cancers (Fig. 3*a*). Focal areas of the anterior prostate displayed lesions in approximately 85% of cases, whereas the ventral lobe and the seminal vesicles were found to be free of tumors, contrary to what is commonly seen in transgenic mouse models of prostate cancer[17] (Fig. 3*a*). Moreover, these prostate cancers were invasive, as rupture of the basal membrane of the epithelium by the tumor was found in 25% of *Pten*$^{+/-}$/*Cdkn1b*$^{-/-}$ mutants (Fig. 3*b–e*).

The reduction of *Pten* and *Cdkn1b* gene dose may influence both cell survival and cell proliferation in the prostate. To determine the relative relevance of these two processes in prostate cancer pathogenesis, we analyzed in a comparative manner the apoptotic and proliferation indexes in the prostates from 8–12-week tumor-free *Pten*$^{+/-}$, wild-type, *Cdkn1b*$^{-/-}$ and double-mutant mice. We did not detect differences in the rate of apoptosis between the various genotypes, as determined by scoring the percentage of TUNEL-positive nuclei (data not shown). But the analysis of the expression of the proliferation marker Ki-67 revealed an increase in the proliferative index of the prostatic epithelium in the *Pten*$^{+/-}$/*Cdkn1b*$^{-/-}$ mice (Fig. 4*a,b*).

Our analysis leads to two major conclusions. First, Pten and p27$^{Kip1}$ have a pivotal, cooperative role in tumor suppression in epithelial tissues, and combined loss of Pten and p27$^{Kip1}$ are key events in the pathogenesis of epithelial cancers as indicated by the short latency and complete penetrance of these tumors in *Pten*/*Cdkn1b* double-mutant mice. Second, Pten and p27$^{Kip1}$ negatively control in a cooperative manner the proliferative rate in prostate epithelial cells. Thus, monoallelic mutations in *PTEN*, in combination with the reduction of p27$^{KIP1}$ expression levels, may have prognostic value in human prostate cancer. Moreover, our findings demonstrate the critical relevance of these two 'hits' for prostate cancer pathogenesis in a mouse model that parallels the human disease.

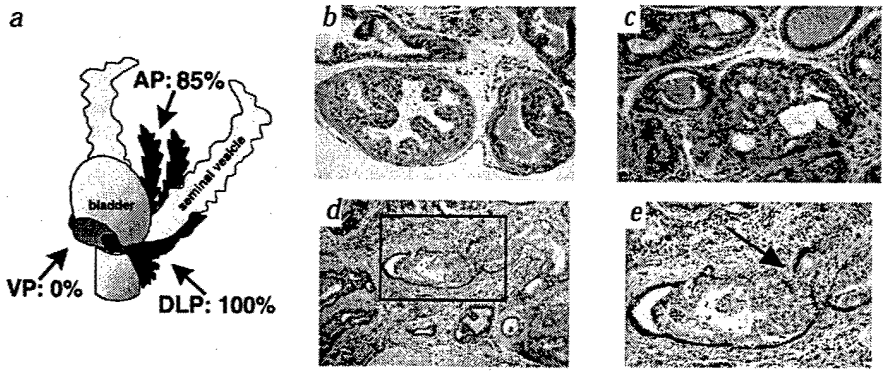


**Fig. 3** Prostate tumorigenesis in *Pten*$^{+/-}$/*Cdkn1b*$^{-/-}$ mice. ***a***, Schematic representation of the mouse genitourinary structures showing the lobular nature of the prostate and the incidence of neoplastic lesions in each of the three lobes of *Pten*$^{+/-}$/*Cdkn1b*$^{-/-}$ mice. AP, anterior prostate; VP, ventral prostate; DLP, dorsolateral prostate. ***b***, Normal appearance of the dorsolateral prostate in a wild-type mouse. ***c***, PIN-like lesion in a *Pten*$^{+/-}$/*Cdkn1b*$^{-/-}$ mouse. ***d***, Invasive carcinoma in a *Pten*$^{+/-}$/*Cdkn1b*$^{-/-}$ mouse. The area in the inset is magnified in (***e***). The arrow indicates the area of invasion. Original magnifications: *b,c,e*, ×400; *d*, ×200.

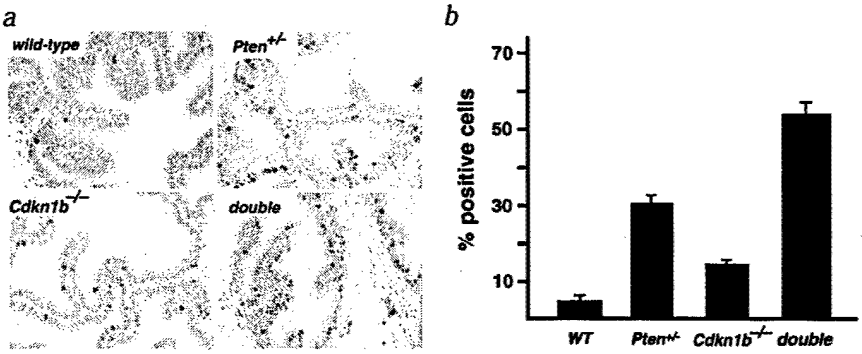


**Fig. 4** Increased proliferation of prostate epithelial cells in *Pten*$^{+/-}$/*Cdkn1b*$^{-/-}$ mice. ***a,b***, Prior tumor onset (8 weeks) prostates from wild-type, *Pten*$^{+/-}$, *Cdkn1b*$^{-/-}$ and double mutant (*Pten*$^{+/-}$/*Cdkn1b*$^{-/-}$) mice were stained with antibodies specific for the Ki-67 proliferation marker. Positive nuclei were counted in several randomly chosen fields.

## Methods

Mice. Generation and characterization of *Pten*$^{+/-}$ and *Cdkn1b*$^{-/-}$ mice have been described[4,9]. We genotyped the mice by PCR on tail DNA. Oligonucleotide sequences are available on request.

Follow-up design. *Pten*$^{+/-}$ mice older than 9 months and all the *Pten*$^{+/-}$/*Cdkn1b*$^{-/-}$ mice were analyzed when found dead or when killed because they were moribund. Tumorigenesis in mice younger than 9 months was analyzed as follows: 20 animals were killed between 1 and 4 months of age and 20 animals between 5 and 9 months. A control group of over 50 wild-type mice did not show signs of illness during the 16 months follow-up. Of these animals, 10 were killed between 9 and 16 months of age.

Histopathology and immunohistochemistry. Animals were autopsied and all tissues were examined regardless of their pathological status. We fixed normal and tumor tissue samples in 10% buffered formalin and embedded them in paraffin. Sections (4–5 μm) were stained with hematoxylin and eosin according to standard protocols. For Pten detection, immunohistochemistry was performed on representative sections using a rabbit polyclonal antibody (Zymed) following the manufacturer's instructions.

Proliferation and apoptosis. We analyzed consecutive sections of prostates from 8-week-old wild-type, *Pten*$^{+/-}$, *Cdkn1b*$^{-/-}$ and double-mutant mice for proliferation and apoptosis. Immunodetection of the proliferation marker Ki-67 and analysis of the apoptotic rate by TUNEL assay were carried out according to published protocols[18].

### Acknowledgments

*We thank C. Abate-Shen, M. Shen, P. Scardino and H.I. Scher for advice and discussions; M. Jiao for the preparation of pathological samples; and S. Kim for critical suggestions concerning the Pten immunohistochemical analysis. P.P.P. is a Scholar of the Leukemia & Lymphoma Society of America (formerly known as the Leukemia Society of America). This work was supported by the NCI and by the I.T. Hirschl/M. Weill-Caulier Foundation to P.P.P.*

Received 8 September; accepted 19 December 2000.

1. Cairns, P. *et al.* Frequent inactivation of PTEN/MMAC1 in primary prostate cancer. *Cancer Res.* **57**, 4997–5000 (1997).
2. Macri, E. & Loda, M. Role of p27 in prostate carcinogenesis. *Cancer Metastasis Rev.* **17**, 337–344 (1998).
3. Fero, M.L. *et al.* A syndrome of multiorgan hyperplasia with features of gigantism, tumorigenesis, and female sterility in p27(Kip1)-deficient mice. *Cell* **85**, 733–744 (1996).
4. Kiyokawa, H. *et al.* Enhanced growth of mice lacking the cyclin-dependent kinase inhibitor function of p27(Kip1). *Cell* **85**, 721–732 (1996).
5. Nakayama, K. *et al.* Mice lacking p27(Kip1) display increased body size, multiple organ hyperplasia, retinal dysplasia, and pituitary tumors. *Cell* **85**, 707–720 (1996).
6. Li, D.M. & Sun, H. PTEN/MMAC1/TEP1 suppresses the tumorigenicity and induces G1 cell cycle arrest in human glioblastoma cells. *Proc. Natl. Acad. Sci. USA* **95**, 15406–15411 (1998).
7. Landis, S.H., Murray, T., Bolden, S. & Wingo, P.A. Cancer statistics, 1998. *CA Cancer J. Clin.* **48**, 6–29 (1998).
8. Verma, R.S., Manikal, M., Conte, R.A. & Godec, C.J. Chromosomal basis of adenocarcinoma of the prostate. *Cancer Invest.* **17**, 441–447 (1999).
9. Di Cristofano, A., Pesce, B., Cordon-Cardo, C. & Pandolfi, P.P. Pten is essential for embryonic development and tumour suppression. *Nature Genet.* **19**, 348–355 (1998).
10. Podsypanina, K. *et al.* Mutation of Pten/Mmac1 in mice causes neoplasia in multiple organ systems. *Proc. Natl. Acad. Sci. USA* **96**, 1563–1568 (1999).
11. Cordon-Cardo, C. *et al.* Distinct altered patterns of p27KIP1 gene expression in benign prostatic hyperplasia and prostatic carcinoma. *J. Natl. Cancer Inst.* **90**, 1284–1291 (1998).
12. Di Cristofano, A. *et al.* Impaired Fas response and autoimmunity in Pten+/– mice. *Science* **285**, 2122–2125 (1999).
13. Kurman, R.J., Kaminski, P.F. & Norris, H.J. The behavior of endometrial hyperplasia. A long-term study of "untreated" hyperplasia in 170 patients. *Cancer* **56**, 403–412 (1985).
14. Di Cristofano, A. & Pandolfi, P.P. The multiple roles of PTEN in tumor suppression. *Cell* **100**, 387–390 (2000).
15. Price, D. Comparative aspects of development and structure in the prostate. in *Biology of the Prostate and Related Tissues* (eds. Vollmer, E.P. & Kauffman, G.) 1–28 (US Government Printing Office, Washington, DC, 1963).
16. McNeal, J.E. Origin and development of carcinoma in the prostate. *Cancer* **23**, 24–34 (1969).
17. Green, J.E. *et al.* Workgroup 3: transgenic and reconstitution models of prostate cancer. *Prostate* **36**, 59–63 (1998).
18. Osman, I. *et al.* Alterations affecting the p53 control pathway in bilharzial-related bladder cancer. *Clin. Cancer Res.* **3**, 531–536 (1997).

# Prostatic intraepithelial neoplasia in mice expressing an androgen receptor transgene in prostate epithelium

Michael Stanbrough*, Irwin Leav†, Paul W. L. Kwan†, Glenn J. Bubley*, and Steven P. Balk*‡

*Cancer Biology Program, Hematology–Oncology Division, Department of Medicine, Beth Israel Deaconess Medical Center and Harvard Medical School, 330 Brookline Avenue, Boston, MA 02215; and †Department of Pathology and Biomedical Sciences, Tufts University Schools of Medicine and Veterinary Medicine, Boston, MA 02111

Edited by Arthur B. Pardee, Dana–Farber Cancer Institute, Boston, MA, and approved July 16, 2001 (received for review May 11, 2001)

**Prostate cancer (PCa) is an androgen dependent disease that can be treated by androgen ablation therapy, and clinical trials are under way to prevent PCa through the reduction of androgen receptor (AR) activity. However, there are no animal models of AR-mediated prostatic neoplasia, and it remains unclear whether the AR is a positive or negative regulator of cell growth in normal prostate secretory epithelium. To assess the direct effects of the AR in prostate epithelium, a murine AR transgene regulated by the rat probasin promoter (Pb) was used to generate transgenic mice expressing increased levels of AR protein in prostate secretory epithelium. The prostates in younger (<1 year) Pb-mAR transgenic mice were histologically normal, but Ki-67 immunostaining revealed marked increases in epithelial proliferation in ventral prostate and dorsolateral prostate. Older (>1 year) transgenic mice developed focal areas of intraepithelial neoplasia strongly resembling human high-grade prostatic intraepithelial neoplasia (PIN), a precursor to PCa. These results demonstrate that the AR is a positive regulator of cell growth in normal prostate epithelium and provide a model system of AR-stimulated PIN that can be used for assessing preventative hormonal therapies and for identifying secondary transforming events relevant to human PCa.**

Prostate cancer (PCa) is an androgen-dependent disease and a leading cause of cancer morbidity and mortality in men (1, 2). The androgen receptor (AR) is a steroid hormone receptor member of the larger nuclear receptor superfamily of ligand-activated transcription factors (3–5). The vast majority of prostate cancers express the AR, are androgen dependent for their growth, and initially respond to androgen ablation therapy (6, 7). PCa that recurs after androgen ablation therapy also expresses the AR, and AR gene amplification and mutations contribute to disease progression (8–12). Epidemiological data further suggest a role for increased AR activity in stimulating PCa development, as higher testosterone levels and lower levels of sex steroid binding globulin are associated with an increased risk of PCa (13, 14). Increased PCa risk is also associated with ARs containing shorter polyglutamine (CAG) repeats in exon 1 (15–20), which are transcriptionally more active or may be more highly expressed *in vivo* (21–23). Taken together, these observations support a role for the AR in PCa development and progression.

AR protein is highly expressed in normal prostate by secretory epithelial cells and to a lesser extent by a subset of stromal smooth muscle cells (24, 25). However, in contrast to the direct stimulation of PCa growth by androgens, *in vitro* studies have shown that androgens do not stimulate the growth of normal prostate epithelial cells (26–28). Moreover, the AR can induce cell cycle arrest or apoptosis when transfected into AR-negative PCa cell lines or when stimulated in PCa cell lines adapted to grow at low androgen levels (29–34). AR expressed by prostate stromal cells can also induce the production of growth factors that indirectly stimulate the development and growth of prostate epithelial cells (35–37). Therefore, whether the AR can stimulate prostate epithelial cell growth *in vivo* and the relative role of AR in epithelium versus stroma are uncertain.

The important role of the AR in PCa has stimulated efforts to model PCa in animals through administration of exogenous androgens. Chronic administration of high dose testosterone to some strains of rats has been reported to cause prostatic neoplasms, but these appear to originate in seminal vesicle (38). Combined treatments with testosterone, and a mutagen (39) or estradiol (40, 41), are generally required to develop PCa in rat models, and androgen-induced PCa in mice has not been reported. Further insight into the role of the AR in regulating prostate growth was obtained from the classic studies of Bruchovsky *et al.* on castrated rats (42). They demonstrated that AR levels decreased immediately after castration and that readministration of androgen increased epithelial AR levels, with a concomitant dramatic proliferative effect on prostate epithelium. However, AR levels and the rate of DNA synthesis declined to normal levels once the differentiated epithelial cell population achieved precastration levels, and continued androgen supplementation did not increase cell numbers. These results demonstrate that androgen-mediated cell proliferation and AR levels are tightly controlled in the prostate and suggest that the respective regulatory processes may be coupled. Indeed, the AR can positively and negatively regulate AR mRNA levels via response elements in the promoter and coding region (43, 44).

Based on these observations, we speculated that AR levels in prostate epithelium might be an important factor regulating proliferation and that increased AR expression might result in a higher proliferative rate and increased PCa risk. This hypothesis was tested by selectively augmenting AR expression in prostate epithelium, by using a fragment (−426 to +28) of the rat probasin (Pb) promoter to target a murine AR (mAR) transgene to prostate secretory epithelium in sexually mature mice (45, 46). The Pb-mAR transgene was transcribed specifically in prostate and caused increased AR expression in the epithelium, but not the stroma. A marked increase in proliferation was demonstrated in secretory epithelium in histologically normal ventral prostate (VP) and dorsolateral prostate (DLP) glands from all Pb-mAR transgenic mice when compared with wild-type littermate controls. Aged Pb-mAR transgenic mice developed moderate to severe intraepithelial dysplasias with the histological



This paper was submitted directly (Track II) to the PNAS office.

Abbreviations: PCa, prostate cancer; AR, androgen receptor; mAR, murine AR; Pb, probasin; PIN, prostatic intraepithelial neoplasia; VP, ventral prostate; DLP, dorsolateral prostate; RT-PCR, reverse transcription–PCR; PAS, periodic acid/Schiff.

‡To whom reprint requests should be addressed at: Hematology–Oncology Division, Beth Israel Deaconess Medical Center, HIM Building, Room 1050, 330 Brookline Avenue, Boston, MA 02215. E-mail: sbalk@caregroup.harvard.edu.

The publication costs of this article were defrayed in part by page charge payment. This article must therefore be hereby marked "*advertisement*" in accordance with 18 U.S.C. §1734 solely to indicate this fact.

features of human high-grade prostatic intraepithelial neoplasia (PIN), believed to be a precursor to PCa (47). These results support a role for increased AR activity in stimulating epithelial proliferation and provide a murine model of AR-mediated prostatic neoplasia.

## Materials and Methods

**Pb-mAR Transgene Construction.** Mouse AR has only an eight-residue CAG (glutamine) repeat in exon 1 (48), so no effort was made to further decrease this repeat. A promoterless 3.6-kb *Sal*I fragment containing the complete mAR cDNA and a rabbit β-globin polyadenylation site from $pmAR_0$ (48) was subcloned into the *Sal*I site of pBlueScriptSK+ (pSKmAR) (Stratagene). The −426 to +28 probasin promoter was excised from pBH500 (49) as a *Hin*dIII-*Bam*HI fragment and was blunt ligated to *Xho*I-cut pSKmAR to give the probasin-mouse androgen receptor vector Pb-mAR (pMS501–9F). The 4.0-kb Pb-mAR was excised with *Kpn*I and *Xba*I digestion, and pronuclear microinjection was performed at the Beth Israel Deaconess Medical Center Transgenic Facility in the FVB strain. Transgenic mice were identified by PCR of tail DNA with the use of probasin promoter 5′-AATCCACAGTTCAGGTTCAATG-3′ (−384 to −363) and mAR 5′-AGCTGAGTCATCCTGATCTG-3′ (534 to 515) or mAR 5′-CTCCTCGATAGGTCTTGGATG-3′ (193 to 173). All procedures were in accordance with institutional protocols.

**Histology.** Prostates were harvested by removing the bladder–urethra–prostate complex in one piece, with or without attached seminal vesicles, placed directly in 50 ml of neutral buffered 10% formalin at room temperature for 4 to 6 h, and machine dehydrated to paraffin immediately after fixation. Specimens were embedded to obtain sagittal sections of the urethra such that VP and DLP were in the same plane.

**Immunohistology.** Fresh 5-μm paraffin sections were baked at 60°C for 1 h just before processing, then brought to water and antigen retrieved by boiling in 10 mM sodium citrate (pH 6.2) for 20 min and cooling for 2 h. Blocking steps were with 1× PowerBlock and 1× Protein Block, each for 10 min at 25°C (BioGenex Laboratories, San Ramon, CA). Ab was diluted in Common Ab Diluent (BioGenex Laboratories) at 1:50 for the Ki-67 Ab (Immunotech, Westbrook, ME) and at 1:50 for AR Ab (Upstate Biotechnology, Lake Placid, NY). Primary Abs were incubated overnight at 5° followed by a biotinylated anti-IgG linking Ab (Multilink; BioGenex Laboratories) at 1:50 for 30 min at 25°C, and then a horseradish peroxidase–streptavidin conjugate (BioGenex) at 1:50 for 30 min at 25°C. Color was developed with 50 mM Tris·Cl (pH 7.6), 0.06% hydrogen peroxide, and 0.5 mg/ml diaminobenzidine for 1 min to 5 min, and nuclei were counterstained with hematoxylin.

**Reverse Transcription–PCR (RT-PCR).** Anterior prostate, DLP, and VP were dissected and processed separately and were substantially freed of extraneous fatty and connective tissues. RNA was extracted in RNAzol B (Tel-Test, Friendswood, TX), and reverse transcription was with 1 μg of RNA and an oligo-dT primer. PCR was with a common 5′ sense primer in exon 7 of the mAR: (2594–2613) 5′-AAGAAAGAATCCCACATCC-3′ (no. 5722), in conjunction with antisense primers on distinct exons to prevent amplification from any contaminating genomic DNA. The endogenous mAR was detected with an antisense exon 8 primer in the 3′ untranslated region, 5′-CAGAGAAGTAGTGCAGAGTT-3′ (no. 6417). The transgene transcript was detected with an antisense primer in the 3′ exon encoding the rabbit β-globin polyadenylation signal, 5′-CCACACCAGCCACCACCTTC-3′ (no. 5711).

**AR Immunoblotting.** Frozen VP and DLP samples were ground with a micropestle in 1% SDS, heated to 100°C for 15 min, and centrifuged at 45,000 rpm for 25 min in a Beckman TLA 45 rotor. The protein content of the lysates was assayed with bicinchoninic acid reagent (Pierce), and 40 μg was run reduced on SDS/PAGE and transferred to nitrocellulose membranes. Blots were blocked in 5% nonfat dry milk, then incubated with AR Abs (Santa Cruz Biotechnology SC-816 and SC-815, each at 1:2,000) overnight at 5°C. Washed blots were then incubated with horseradish peroxidase-conjugated goat anti-rabbit IgG (Promega) at 1:5,000, washed extensively, and developed with Renaissance chemiluminescence reagent (NEN).

**Terminal Deoxynucleotidyltransferase-Mediated UTP End-Labeling Assays.** Formalin-fixed paraffin sections were brought to water and antigen retrieved as above. Terminal deoxynucleotidyltransferase-mediated UTP end labeling assays were carried out with an *In Situ* Cell Death Detection Kit, TMR Red (Roche Pharmaceuticals, Nutley, NJ), according to the manufacturer's directions. Slides were mounted with Fluoromount-G (Southern Biotechnology Associates).

## Results

**Generation of Transgenic Mice.** The rat probasin promoter (−426 to +28), which is positively regulated by the AR and expressed specifically in the prostate epithelium of sexually mature mice (45, 46), was used to target a mAR transgene to prostate. Transgenic mice were generated by pronuclear injection in FVB mice, and founders were identified that transmitted the Pb-mAR transgene to their progeny. RT-PCR was used to identify founder lines expressing the mAR transgene in prostate. Wild-type and transgenic AR cDNA were coamplified with the use of a common exon 7 sense primer and antisense primers on distinct exons specific to the unique 3′ untranslated regions of the endogenous and transgenic ARs, yielding a slightly larger product from the transgenic AR. Transgene expression was detected in prostates from three of four founder lines examined (Fig. 1*A* and data not shown).

Consistent with previous studies of this probasin promoter, the transgene was expressed in prostate (anterior prostate, VP, and DLP) but was not detected in kidney, liver, or testis (Fig. 1*B*). Whereas the Pb promoter is targeted selectively to prostate secretory epithelium, the endogenous AR transcript is also expressed in prostate by stromal and basal cells (24, 25). Therefore, the RT-PCR compared endogenous AR transcripts in multiple cell types with transgenic AR transcripts in secretory epithelium and provided only a qualitative assessment of transgenic versus wild-type AR expression. Nonetheless, the amount of amplified transgenic AR message was comparable to or greater than that of the wild-type AR.

**AR Protein Expression in Transgenic Versus Wild-Type Prostate.** The levels of AR protein in prostate tissues were determined by immunoblotting samples from transgenic and wild-type littermate siblings in the initially established 2R1 line. Higher AR levels were detected in transgenic VP versus wild-type VP (Fig. 2*A*, lanes 1 and 2) and in transgenic DLP versus wild-type DLP (Fig. 2*A*, lanes 3 and 4). Interestingly, more AR protein was detected in VP than in DLP, regardless of the source. Because immunoblots were normalized for protein content, this higher level of AR protein may reflect the higher stromal content in DLP (see below). The distribution and level of AR protein in prostates from wild-type littermate controls versus transgenic mice were also assessed by immunohistochemistry in the 2R1 line. As in wild-type mice (Fig. 2 *B* and *C*), the AR in transgenic mice was located in the nuclei of secretory epithelial cells and in scattered stromal cells in VP (Fig. 2*D*) and DLP (Fig. 2*E*). However, the epithelial expression in wild-type glands was

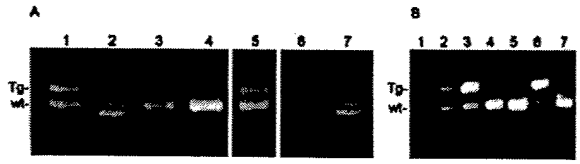


**Fig. 1.** RT-PCR analysis of Pb-mAR and wild-type tissue RNAs. (*A*) Comparison of endogenous and transgenic AR transcript levels in transgenic founders. Lane 1, 2R1 DLP; lane 2, markers; lane 3, 9R1 DLP; lane 4, 9R1 VP; lane 5, 23R1 VP; lane 6, $H_2O$ negative control; lane 7, markers. (*B*) Comparison of endogenous and transgenic AR transcript levels among tissues in the transgenic lineage 2R1. Lane 1, marker; lane 2, VP; lane 3, DLP; lane 4, liver; lane 5, kidney; lane 6, anterior prostate; lane 7, testis. Positions of the transgenic (Tg) and wild-type (wt) transcripts are indicated. Samples in *A* and *B* were amplified independently under the same conditions. Prostatic and other tissues were dissected and processed separately.

heterogeneous, with many nuclei exhibiting low or undetectable levels of AR immunostaining. In contrast, there was uniform high-level AR expression in transgenic glands. These findings were consistent with the RT-PCR and immunoblotting results and demonstrated that the Pb-mAR transgene augmented AR protein expression in VP and DLP epithelium.

**Histological Analysis of mAR Transgenic Mice.** Prostates from mice in each of the three founder lines expressing the mAR transgene (2R1, 23R1, and 2R2) were collected for histological study. Mice with dysplastic glands in the VP or DPL were found in all three lineages (see below), whereas dysplasia was not found in any age-matched wild-type littermate controls. This difference in the presence of dysplasia between the transgenic and wild-type mice indicated that the dysplastic lesions were because of the expressed AR and were not the result of insertional mutagenesis. Results from the initially established 2R1 line versus wild-type littermate controls are summarized in Table 1, and examples are shown in Fig. 3. Statistical analysis indicated that the development of dysplasia was significantly greater in the transgenic mice versus wild-type littermate controls (one-tailed Student's $t$ test, $P = 0.0023$), as was the development of severe dysplasia (one-tailed Student's $t$ test, $P = 0.0062$). The development of dysplasia was strongly age-dependent, as it was not found in mice younger than 12 months.

An example of a moderate to severely dysplastic lesion in the DLP of a 2R1 founder line mouse is illustrated in Fig. 3*A*. Fig. 3*B* is a low-power micrograph of several severely dysplastic lesions in the DLP, some showing a cribriform growth pattern in which intraluminal glands appear to form within the original gland. At higher power the severely dysplastic lesions were further characterized by pronounced epithelial cell crowding, enlarged vesicular nuclei that often contained one or more prominent nucleoli, and apoptotic cells (Fig. 3*C*). These lesions shared the cytological and histological features that characterize high-grade dysplastic lesions in human prostate, generally referred to as high-grade prostatic intraepithelial neoplasia (PIN), which appear to be precursor lesions to PCa (47).

Changes suggestive of the initial stages of microinvasive carcinoma were found arising in a PIN lesion in the DLP of one animal. Because penetration of the basement membrane is a histological hallmark of early invasion, periodic acid/Schiff (PAS) staining was used to assess this feature in high-grade PIN lesions. In Fig. 3*D*, a PAS-stained PIN lesion shows an intact basement membrane that is of uniform thickness in areas with only moderate dysplasia. In contrast, in the center right of this figure there are cells impinging on the basement membrane, possibly in the initial stages of cribriform gland formation, with thinning of the adjacent basement membrane. At the bottom of this figure (higher power in Fig. 3*E*), a cribriform gland is seen protruding into, but not completely penetrating, the basement membrane. This cribriform gland is associated with a marked thinning of the basement membrane. In other PAS-stained PIN lesions, many dysplastic cells with prominent nucleoli appear to be impinging on or embedded in the basement membrane (Fig. 3*F*, arrow). AR immunohistochemistry of replicate sections, as shown in Fig. 3*G*, demonstrated that these cells were strongly AR-positive (arrow). Finally, Fig. 3*H* shows a gland from the 2R2 lineage with hyperplasia and cribriform growth similar to that seen in the 2R1 line.

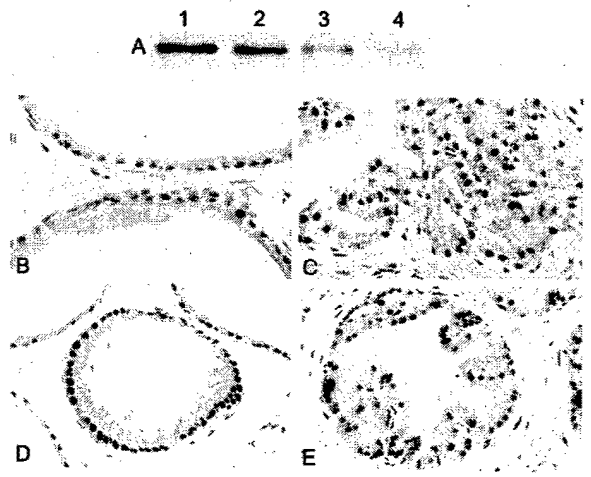


**Fig. 2.** AR immunoblot and immunohistochemistry in prostate from transgenic and wild-type mice. (*A*) Anti-AR immunoblot. Lanes 1 and 2, VP from transgenic and wild-type, respectively; lanes 3 and 4, DLP from transgenic and wild-type, respectively. (*B–E*) Anti-AR immunohistochemistry. (*B*) Wild-type VP (×500). (*C*) Wild-type DLP (×400). (*D*) 2R1 transgenic VP (×330). (*E*) 2R1 transgenic DLP (×400).

**Increased Proliferation in mAR Transgenic Mice.** AR expression in the transgenic mice was relatively uniform by immunohistochemistry, but PIN lesions in these mice were focal and occurred in aged mice. This lack of correspondence between AR expression and PIN lesions indicated that these lesions were likely a result of sporadic secondary genetic or epigenetic events, rather than a primary result of the AR transgene. To identify primary effects of the AR transgene, proliferation of prostate epithelium from Pb-mAR mice was assessed by immunostaining for the Ki-67 proliferation antigen. Ki-67-positive cells (identified by the MIB1 mAb) were rare in prostate epithelium from wild-type mice, with most glands having no positive cells and occasional glands having a single Ki-67-positive cell (not shown). This finding was consistent with a previous report showing an extremely low rate of proliferation (about 0.1%) in normal mouse

**Table 1. Histological outcomes of 2R1 lineage Pb-mAR versus wild-type littermate control mice**

| Lineage | No. | Average age, mo | No dysplasia | Mild/moderate dysplasia | Severe dysplasia |
|---|---|---|---|---|---|
| 2 R1 | | | | | |
| <12 mos | 20 | 5.9 | 20 | 0 | 0 |
| >12 mos | 11 | 16.8 | 6 | 1 | 4 |
| Wild type | | | | | |
| <12 mos | 16 | 5.1 | 16 | 0 | 0 |
| >12 mos | 14 | 14.6 | 14 | 0 | 0 |

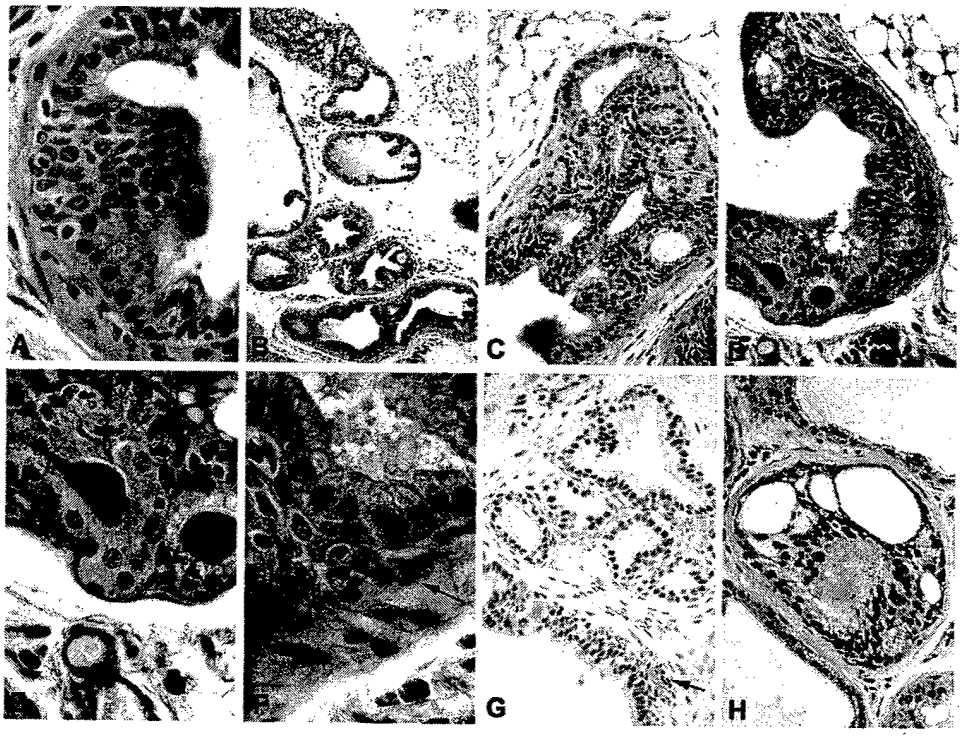


**Fig. 3.** PIN in prostates from aged Pb-mAR transgenic mice. (*A*) Moderate grade PIN in DLP (hematoxylin/eosin, ×600). (*B*) High-grade PIN in DLP among normal glands (hematoxylin/eosin, ×60). (*C*) High-grade PIN in DLP (hematoxylin/eosin, ×400). (*D*) High-grade PIN in DLP with focal thinning of basement membrane (PAS stain, ×290). (*E*) Higher magnification of sample in *D* (×600). (*F*) High-grade PIN in DLP. The arrow indicates an epithelial nucleus with prominent nucleoli in basement membrane (PAS stain, ×600). (*G*) AR immunohistochemistry of DLP with arrow showing AR-stained epithelial nuclei within or through the basement membrane (×250). (*H*) 2R2 lineage DLP (×330).

prostate epithelium (50). In contrast, glands containing Ki-67-positive cells were frequent in histologically normal VP and DLP from Pb-mAR mice, with one or two positive cells in a gland being common (Fig. 4*A*, arrow), and with some glands having three or more positive cells. Ki-67 staining was particularly high in the ventral prostate from one Pb-mAR mouse (4.5 months old), despite the absence of histologically apparent lesions (Fig. 4*B*). Not surprisingly, dysplastic glands in Pb-mAR mice contained large numbers of Ki-67-positive cells (Fig. 4*C*). Adjacent histologically normal glands also contained large numbers of positive cells, which were possibly because of paracrine factors secreted by the dysplastic gland.

The Ki-67 staining results were quantified in VP and DLP to obtain a proliferative index in prostate glands from wild-type littermate control mice versus histologically normal glands from Pb-mAR transgenic mice that did not have PIN. This quantification was achieved by tabulation of the percentage of total VP or DLP secretory epithelial cells that were Ki-67-positive in a representative group of normal-appearing glands from a series of wild-type and Pb-mAR transgenic mice. Six hundred to 4,000 secretory epithelial cells were typically counted per VP or DLP. Mice with PIN were excluded from this analysis to avoid concerns about paracrine factors from PIN lesions stimulating growth of adjacent glands. Prostates with areas of focal hyperplasia were included in this analysis, but only the histologically normal areas, and not the hyperplastic areas, were counted.

In VP from wild-type littermate control mice, the percentage of Ki-67-positive epithelial cells averaged 0.39% and ranged from 0.36% to 0.44% (Fig. 5, wt VP). In contrast, Pb-mAR transgenic VP averaged 1.76% Ki-67-positive cells and ranged from 0.5% to 8.98%. In DLP, the percentage of Ki-67-positive cells in the wild-type mice averaged 0.21% (Fig. 5, wt DLP). Ki-67-positive cells in DLP from Pb-mAR mice averaged 1.14% and ranged from 0.75% to 2.0%. Therefore, there was a statistically significant increase in epithelial cell proliferation in both the VP and DLP in the Pb-mAR mice relative to wild-type (≈5-fold, one-tailed *t* test: dorsolateral, $P = 0.0007$; ventral, $P = 0.033$). This consistent result in histologically normal-appearing glands indicated that a direct effect of the mAR transgene was to stimulate proliferation of secretory epithelial cells.

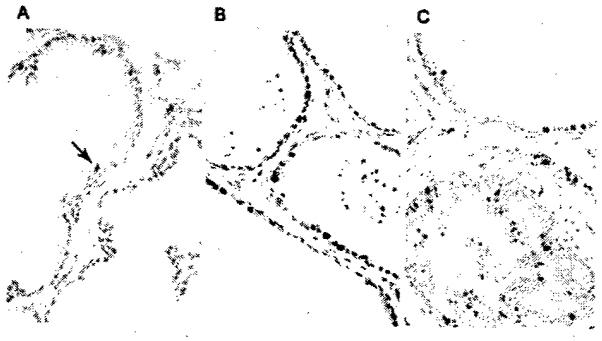


**Fig. 4.** Higher frequency of expression of the proliferation marker Ki-67 in transgenic mouse prostates. (*A*) Typical view of Ki-67 staining in VP from a transgenic mouse, with a single Ki-67 reactive nucleus (arrow, center) in this specimen with 1.67% Ki-67-positive epithelial cells (×90). (*B*) High Ki-67 staining in histologically normal VP from a 4.5-month-old transgenic mouse (×180). (*C*) High Ki-67 staining in DLP PIN lesion from a transgenic mouse (×100). Wild-type prostate with very rare positive cells is not shown.

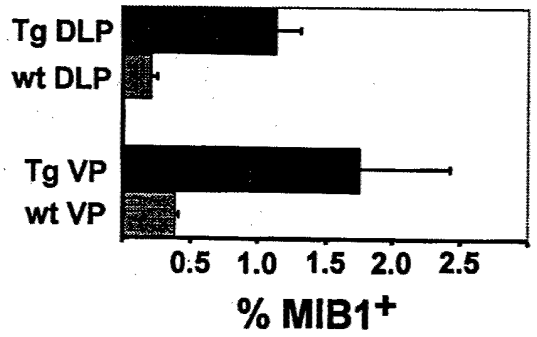


Fig. 5. Comparison of Ki-67 (MIB1)-positive percentages in transgenic versus wild-type prostates.

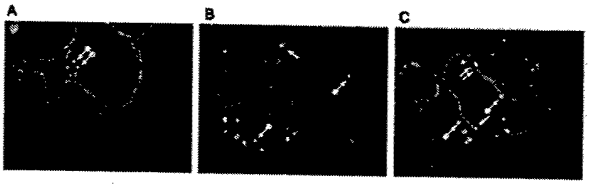


Fig. 6. Higher frequency of apoptosis in VP with higher proliferative index. (*A*) Wild-type VP. (*B*) Transgenic VP with 1.67% Ki-67-positive cells. (*C*) Transgenic VP with 8.98% Ki-67-positive cells. All apoptotic cells located within the prostatic epithelium are indicated by simple arrows, and representative sloughed apoptotic cells are indicated by arrows with asterisks (×125).

**Apoptosis in Pb-mAR Prostate Epithelium.** Apoptosis was next examined to determine whether the increased proliferation in otherwise normal-appearing prostate epithelium might be balanced by increased apoptosis. Apoptosis was assessed *in situ* by terminal deoxynucleotidyltransferase-mediated UTP end labeling assays and was undetectable in wild-type DLP (not shown) and VP epithelium (Fig. 6*A*). In contrast, apoptotic cells were detected in transgenic DLP (not shown) and VP (Fig. 6*B*, simple arrow, prostate with 1.57% Ki-67-positive cells). More frequent apoptotic cells were seen in a transgenic VP with an extremely high proliferative index (8.98% Ki-67-positive cells) (Fig. 6*C*). There were also sloughed, apoptotic cells in the lumens of glands from all specimens (arrows with asterisks). These were more frequent in the samples with higher proliferation, but whether these primarily represented epithelial cells was not determined. These data indicated that the increased proliferation driven by expression of the mAR transgene was balanced by increased apoptosis in tissue that had normal histology.

## Discussion

The majority of prostate cancers are androgen dependent, but androgens have a limited ability to stimulate growth of normal prostate epithelium, and the mechanisms by which AR might contribute to PCa development have not been clear. This study demonstrated that a mAR transgene targeted selectively to prostate secretory epithelium in transgenic mice stimulated proliferation of the epithelium, with the subsequent development of PIN in aged, but otherwise unmanipulated mice. These results provide direct evidence that the AR can function as a positive regulator of proliferation in normal prostate secretory epithelium and stimulate the development of neoplasia. In conjunction with epidemiological data linking increased AR activity and PCa risk, these findings indicate a direct role for the AR in promoting PCa development in humans.

The earliest alteration observed in Pb-mAR mouse prostates was a substantial 5-fold increase in the proliferation of secretory epithelial cells, as evidenced by Ki-67 immunostaining, in the absence of histological abnormalities. This pattern was seen throughout the VP and DLP in all Pb-mAR mice examined and occurred in young and old mice, indicating that it was a direct effect of the transgene. Proliferation in these glands was associated with increased apoptosis, accounting for the absence of hyperplasia. In contrast, PIN lesions were focal and increased with age, indicating that they reflected the occurrence of additional secondary genetic or epigenetic events. Taken together, these findings suggest that the PCa susceptibility associated with increased AR expression is because of a balanced increase in proliferation and apoptosis, with a resultant increase in the frequency of secondary transforming events. It is not yet clear whether these secondary events involve changes in proliferation, apoptosis, or both, but studies in human PCa have found that increased rates of both proliferation and apoptosis correlate with increased malignant potential (51, 52).

The AR has been shown to regulate or interact with a number of proteins that control cell growth. The growth-inhibitory effects of the AR may reflect its ability to stimulate the p21 cyclin-dependent kinase promoter (53) or bind cyclins D or E (54–56). In contrast, the reported interaction between AR and retinoblastoma protein (Rb) could stimulate growth by decreasing the inhibition of E2F (57, 58). The AR may also interact with or regulate multiple other proteins that can affect cell growth (59–64). Therefore, as indicated by the Pb-mAR mice, the level of AR expression and/or activity may be an important determinant of its effects on cell growth. The relative increase in AR activity in the Pb-mAR mice is likely greater than what occurs in men at high risk versus low risk for PCa, accounting for the large effects on proliferation and development of PIN in these mice. Nonetheless, the results indicate that modest prolonged increases in AR activity because of androgen levels or AR polymorphisms can account for an increased lifetime risk for PCa. Moreover, the results provide support for PCa prevention therapies such as finasteride that are designed to decrease AR activity in prostate epithelium.

AR expression is not increased in human high-grade PIN or primary PCa (25, 65–67). This finding is consistent with the interpretation that the increased AR expression in the Pb-mAR mice is not by itself a transforming event, and that PIN in these mice is the result of additional steps. Such a multistep process is certainly consistent with our current understanding of how PCa develops in humans. Analyses of human prostate cancers have suggested multiple possible secondary genetic or epigenetic events that could further increase cell proliferation and/or increase cell survival (68). It will clearly be of interest to identify such additional changes in this Pb-mAR model.

There are now multiple murine transgenic and knockout models that develop varying degrees of prostate hyperplasia, dysplasia, or cancer (69, 70). In some cases these models reflect events that appear to contribute to human PCa, such as stimulation of the insulin-like growth factor-1 axis (71) or loss of PTEN and p27 (50, 72), although PTEN and p27 loss may be late events in human PCa development. Other models introduce potent oncogenes, in particular, the simian virus 40 TAg (46), but do not reflect mechanisms that occur commonly in PCa as primary events. We propose that like the adult human male, Pb-mAR transgenic mice represent a model that is genetically susceptible to androgen-dependent PCa, but which has not acquired secondary transforming events. Therefore, this may be a biologically relevant model in which to identify AR functions that contribute to PCa and to identify secondary transforming genetic and epigenetic events. Furthermore, this model may prove useful for the testing of drugs, diet, or other therapies designed for the prevention of PCa.

We thank Joel Lawitts for the generation of transgenic mice, Suzanne Lee and Suzanne White for technical assistance, and J. Trapman and R. Matusik for reagents. This work was supported by the National Institutes of Health (R01-CA65647, P01-CA89021, and T32-AI07542), the Massachusetts Cancer Research Grants Program, and the Hershey Family Prostate Cancer Research Fund at the Beth Israel Deaconess Medical Center.

1. Catalona, W. J. (1994) *N. Engl. J. Med.* **331,** 996–1004.
2. Bubley, G. J. & Balk, S. P. (1996) *Hematol. Oncol. Clin. North Am.* **10,** 713–725.
3. Mangelsdorf, D. J., Thummel, C., Beato, M., Herrlich, P., Schutz, G., Umesono, K., Blumberg, B., Kastner, P., Mark, M. & Chambon, P. (1995) *Cell* **83,** 835–839.
4. Brinkmann, A. O., Blok, L. J., de Ruiter, P. E., Doesburg, P., Steketee, K., Berrevoets, C. A. & Trapman, J. (1999) *J. Steroid Biochem. Mol. Biol.* **69,** 307–313.
5. Quigley, C. A., De Bellis, A., Marschke, K. B., el Awady, M. K., Wilson, E. M. & French, F. S. (1995) *Endocr. Rev.* **16,** 271–321.
6. Huggins, C. & Hodges, C. V. (1972) *CA Cancer J. Clin.* **22,** 232–240.
7. Jenster, G. (1999) *Semin. Oncol.* **26,** 407–421.
8. Culig, Z., Hobisch, A., Cronauer, M. V., Cato, A. C., Hittmair, A., Radmayr, C., Eberle, J., Bartsch, G. & Klocker, H. (1993) *Mol. Endocrinol.* **7,** 1541–1550.
9. Suzuki, H., Sato, N., Watabe, Y., Masai, M., Seino, S. & Shimazaki, J. (1993) *J. Steroid Biochem. Mol. Biol.* **46,** 759–765.
10. Taplin, M. E., Bubley, G. J., Shuster, T. D., Frantz, M. E., Spooner, A. E., Ogata, G. K., Keer, H. N. & Balk, S. P. (1995) *N. Engl. J. Med.* **332,** 1393–1398.
11. Visakorpi, T., Hyytinen, E., Koivisto, P., Tanner, M., Keinanen, R., Palmberg, C., Palotie, A., Tammela, T., Isola, J. & Kallioniemi, O. P. (1995) *Nat. Genet.* **9,** 401–406.
12. Taplin, M. E., Bubley, G. J., Ko, Y. J., Small, E. J., Upton, M., Rajeshkumar, B. & Balk, S. P. (1999) *Cancer Res.* **59,** 2511–2515.
13. Gann, P. H., Hennekens, C. H., Ma, J., Longcope, C. & Stampfer, M. J. (1996) *J. Natl. Cancer Inst.* **88,** 1118–1126.
14. Shaneyfelt, T., Husein, R., Bubley, G. & Mantzoros, C. S. (2000) *J. Clin. Oncol.* **18,** 847–853.
15. Hardy, D. O., Scher, H. I., Bogenreider, T., Sabbatini, P., Zhang, Z. F., Nanus, D. M. & Catterall, J. F. (1996) *J. Clin. Endocrinol. Metab.* **81,** 4400–4405.
16. Giovannucci, E., Stampfer, M. J., Krithivas, K., Brown, M., Dahl, D., Brufsky, A., Talcott, J., Hennekens, C. H. & Kantoff, P. W. (1997) *Proc. Natl. Acad. Sci. USA* **94,** 3320–3323.
17. Stanford, J. L., Just, J. J., Gibbs, M., Wicklund, K. G., Neal, C. L., Blumenstein, B. A. & Ostrander, E. A. (1997) *Cancer Res.* **57,** 1194–1198.
18. Hakimi, J. M., Schoenberg, M. P., Rondinelli, R. H., Piantadosi, S. & Barrack, E. R. (1997) *Clin. Cancer Res.* **3,** 1599–1608.
19. Nam, R. K., Elhaji, Y., Krahn, M. D., Hakimi, J., Ho, M., Chu, W., Sweet, J., Trachtenberg, J., Jewett, M. A. & Narod, S. A. (2000) *J. Urol.* **164,** 567–572.
20. Hsing, A. W., Gao, Y. T., Wu, G., Wang, X., Deng, J., Chen, Y. L., Sesterhenn, I. A., Mostofi, F. K., Benichou, J. & Chang, C. (2000) *Cancer Res.* **60,** 5111–5116.
21. Chamberlain, N. L., Driver, E. D. & Miesfeld, R. L. (1994) *Nucleic Acids Res.* **22,** 3181–3186.
22. Choong, C. S., Kemppainen, J. A., Zhou, Z. X. & Wilson, E. M. (1996) *Mol. Endocrinol.* **10,** 1527–1535.
23. Irvine, R. A., Ma, H., Yu, M. C., Ross, R. K., Stallcup, M. R. & Coetzee, G. A. (2000) *Hum. Mol. Genet.* **9,** 267–274.
24. Cussenot, O., Berthon, P., Cochand-Priollet, B., Maitland, N. J. & Le Duc, A. (1994) *Exp. Cell Res.* **214,** 83–92.
25. Leav, I., McNeal, J. E., Kwan, P. W., Komminoth, P. & Merk, F. B. (1996) *Prostate* **29,** 137–145.
26. Peehl, D. M. & Stamey, T. A. (1986) *In Vitro Cell Dev. Biol.* **22,** 82–90.
27. Grant, E. S., Batchelor, K. W. & Habib, F. K. (1996) *Prostate* **29,** 339–349.
28. Berthon, P., Waller, A. S., Villette, J. M., Loridon, L., Cussenot, O. & Maitland, N. J. (1997) *Int. J. Cancer* **73,** 910–916.
29. Marcelli, M., Haidacher, S. J., Plymate, S. R. & Birnbaum, R. S. (1995) *Endocrinology* **136,** 1040–1048.
30. Heisler, L. E., Evangelou, A., Lew, A. M., Trachtenberg, J., Elsholtz, H. P. & Brown, T. J. (1997) *Mol. Cell. Endocrinol.* **126,** 59–73.
31. Shen, R., Sumitomo, M., Dai, J., Harris, A., Kaminetzky, D., Gao, M., Burnstein, K. L. & Nanus, D. M. (2000) *Endocrinology* **141,** 1699–1704.
32. Wu, H. C., Hsieh, J. T., Gleave, M. E., Brown, N. M., Pathak, S. & Chung, L. W. (1994) *Int. J. Cancer* **57,** 406–412.
33. Kokontis, J. M., Hay, N. & Liao, S. (1998) *Mol. Endocrinol.* **12,** 941–953.
34. Culig, Z., Hoffmann, J., Erdel, M., Eder, I. E., Hobisch, A., Hittmair, A., Bartsch, G., Utermann, G., Schneider, M. R., Parczyk, K., *et al.* (1999) *Br. J. Cancer* **81,** 242–251.
35. Cunha, G. R. (1984) *Prog. Clin. Biol. Res.* **145,** 81–102.
36. Yan, G., Fukabori, Y., Nikolaropoulos, S., Wang, F. & McKeehan, W. L. (1992) *Mol. Endocrinol.* **6,** 2123–2128.
37. Peehl, D. M. & Rubin, J. S. (1995) *World J. Urol.* **13,** 312–317.
38. Lucia, M. S., Bostwick, D. G., Bosland, M., Cockett, A. T., Knapp, D. W., Leav, I., Pollard, M., Rinker-Schaeffer, C., Shirai, T. & Watkins, B. A. (1998) *Prostate* **36,** 49–55.
39. McCormick, D. L., Rao, K. V., Dooley, L., Steele, V. E., Lubet, R. A., Kelloff, G. J. & Bosland, M. C. (1998) *Cancer Res.* **58,** 3282–3288.
40. Noble, R. L. (1982) *Int. Rev. Exp. Pathol.* **23,** 113–159.
41. Leav, I., Merk, F. B., Kwan, P. W. & Ho, S. M. (1989) *Prostate* **15,** 23–40.
42. Bruchovsky, N., Lesser, B., Van Doorn, E. & Craven, S. (1975) *Vitam. Horm.* **33,** 61–102.
43. Quarmby, V. E., Yarbrough, W. G., Lubahn, D. B., French, F. S. & Wilson, E. M. (1990) *Mol. Endocrinol.* **4,** 22–28.
44. Dai, J. L. & Burnstein, K. L. (1996) *Mol. Endocrinol.* **10,** 1582–1594.
45. Greenberg, N. M., DeMayo, F. J., Sheppard, P. C., Barrios, R., Lebovitz, R., Finegold, M., Angelopoulou, R., Dodd, J. G., Duckworth, M. L., Rosen, J. M., *et al.* (1994) *Mol. Endocrinol.* **8,** 230–239.
46. Greenberg, N. M., DeMayo, F., Finegold, M. J., Medina, D., Tilley, W. D., Aspinall, J. O., Cunha, G. R., Donjacour, A. A., Matusik, R. J. & Rosen, J. M. (1995) *Proc. Natl. Acad. Sci. USA* **92,** 3439–3443.
47. Bostwick, D. G., Pacelli, A. & Lopez-Beltran, A. (1996) *Prostate* **29,** 117–134.
48. Faber, P. W., King, A., van Rooij, H. C., Brinkmann, A. O., de Both, N. J. & Trapman, J. (1991) *Biochem. J.* **278,** Part 1, 269–278.
49. Rennie, P. S., Bruchovsky, N., Leco, K. J., Sheppard, P. C., McQueen, S. A., Cheng, H., Snoek, R., Hamel, A., Bock, M. E., MacDonald, B. S., *et al.* (1993) *Mol. Endocrinol.* **7,** 23–36.
50. Di Cristofano, A., Pesce, B., Cordon-Cardo, C. & Pandolfi, P. P. (1998) *Nat. Genet.* **19,** 348–355.
51. Wheeler, T. M., Rogers, E., Aihara, M., Scardino, P. T. & Thompson, T. C. (1994) *J. Cell Biochem. Suppl.* **19,** 202–207.
52. Aihara, M., Scardino, P. T., Truong, L. D., Wheeler, T. M., Goad, J. R., Yang, G. & Thompson, T. C. (1995) *Cancer (Philadelphia)* **75,** 522–529.
53. Lu, S., Liu, M., Epner, D. E., Tsai, S. Y. & Tsai, M. J. (1999) *Mol. Endocrinol.* **13,** 376–384.
54. Knudsen, K. E., Cavenee, W. K. & Arden, K. C. (1999) *Cancer Res.* **59,** 2297–2301.
55. Yamamoto, A., Hashimoto, Y., Kohri, K., Ogata, E., Kato, S., Ikeda, K. & Nakanishi, M. (2000) *J. Cell Biol.* **150,** 873–880.
56. Reutens, A. T., Fu, M., Wang, C., Albanese, C., McPhaul, M. J., Sun, Z., Balk, S. P., Janne, O. A., Palvimo, J. J. & Pestell, R. G. (2001) *Mol. Endocrinol.* **15,** 797–811.
57. Lu, J. & Danielsen, M. (1998) *J. Biol. Chem.* **273,** 31528–31533.
58. Yeh, S., Miyamoto, H., Nishimura, K., Kang, H., Ludlow, J., Hsiao, P., Wang, C., Su, C. & Chang, C. (1998) *Biochem. Biophys. Res. Commun.* **248,** 361–367.
59. Lu, S., Tsai, S. Y. & Tsai, M. J. (1997) *Cancer Res.* **57,** 4511–4516.
60. Chi, S. G., deVere White, R. W., Muenzer, J. T. & Gumerlock, P. H. (1997) *Clin. Cancer Res.* **3,** 1889–1897.
61. Gregory, C. W., Hamil, K. G., Kim, D., Hall, S. H., Pretlow, T. G., Mohler, J. L. & French, F. S. (1998) *Cancer Res.* **58,** 5718–5724.
62. Ye, D., Mendelsohn, J. & Fan, Z. (1999) *Clin. Cancer Res.* **5,** 2171–2177.
63. Lee, D. K., Duan, H. O. & Chang, C. (2000) *J. Biol. Chem.* **275,** 9308–9313.
64. Truica, C. I., Byers, S. & Gelmann, E. P. (2000) *Cancer Res.* **60,** 4709–4713.
65. Tsuji, M., Kanda, K., Murakami, Y., Kurokawa, Y., Kanayama, H., Sano, T. & Kagawa, S. (1999) *J. Med. Invest.* **46,** 35–41.
66. Harper, M. E., Glynne-Jones, E., Goddard, L., Mathews, P. & Nicholson, R. I. (1998) *J. Pathol.* **186,** 169–177.
67. Sweat, S. D., Pacelli, A., Bergstralh, E. J., Slezak, J. M. & Bostwick, D. G. (1999) *J. Urol.* **161,** 1229–1232.
68. Ozen, M. & Pathak, S. (2000) *Anticancer Res.* **20,** 1905–1912.
69. Green, J. E., Greenberg, N. M., Ashendel, C. L., Barrett, J. C., Boone, C., Getzenberg, R. H., Henkin, J., Matusik, R., Janus, T. J. & Scher, H. I. (1998) *Prostate* **36,** 59–63.
70. Sharma, P. & Schreiber-Agus, N. (1999) *Oncogene* **18,** 5349–5355.
71. DiGiovanni, J., Kiguchi, K., Frijhoff, A., Wilker, E., Bol, D. K., Beltran, L., Moats, S., Ramirez, A., Jorcano, J. & Conti, C. (2000) *Proc. Natl. Acad. Sci. USA* **97,** 3455–3460.
72. Di Cristofano, A., De Acetis, M., Koff, A., Cordon-Cardo, C. & Pandolfi, P. P. (2001) *Nat. Genet.* **27,** 222–224.

MOLECULAR AND CELLULAR BIOLOGY, May 2002, p. 3373–3388
0270-7306/02/$04.00+0 DOI: 10.1128/MCB.22.10.3373–3388.2002

Vol. 22, No. 10

# Androgen Receptor Acetylation Governs *trans* Activation and MEKK1-Induced Apoptosis without Affecting In Vitro Sumoylation and *trans*-Repression Function

Maofu Fu,[1] Chenguang Wang,[1] Jian Wang,[1] Xueping Zhang,[1] Toshiyuki Sakamaki,[1] Y. G. Yeung,[1] Chawnshang Chang,[2] Torsten Hopp,[3] Suzanne A. W. Fuqua,[3] Ellis Jaffray,[4] Ron T. Hay,[4] Jorma J. Palvimo,[5] Olli A. Jänne,[5] and Richard G. Pestell[1]*

*Department of Developmental and Molecular Biology and Medicine, The Albert Einstein Comprehensive Cancer Center, Albert Einstein College of Medicine, Bronx, New York 10461[1]; George Whipple Laboratory for Cancer Research, Departments of Urology, Pathology, Radiation Oncology, Biochemistry, and Toxicology, and The Cancer Center, University of Rochester, Rochester, New York 14642[2]; Baylor College of Medicine, Houston, Texas 77030[3]; School of Biology, University of St. Andrews, The North Haugh, St. Andrews KY16 9ST, Scotland[4]; and Biomedicum Helsinki, Institute of Biomedicine and Department of Clinical Chemistry, FIN-00014 University of Helsinki, Finland[5]*

Received 16 July 2001/Returned for modification 10 September 2001/Accepted 14 February 2002

**The androgen receptor (AR) is a nuclear hormone receptor superfamily member that conveys both *trans* repression and ligand-dependent *trans*-activation function. Activation of the AR by dihydrotestosterone (DHT) regulates diverse physiological functions including secondary sexual differentiation in the male and the induction of apoptosis by the JNK kinase, MEKK1. The AR is posttranslationally modified on lysine residues by acetylation and sumoylation. The histone acetylases p300 and P/CAF directly acetylate the AR in vitro at a conserved KLKK motif. To determine the functional properties governed by AR acetylation, point mutations of the KLKK motif that abrogated acetylation were engineered and examined in vitro and in vivo. The AR acetylation site point mutants showed wild-type *trans* repression of NF-κB, AP-1, and Sp1 activity; wild-type sumoylation in vitro; wild-type ligand binding; and ligand-induced conformational changes. However, acetylation-deficient AR mutants were selectively defective in DHT-induced *trans* activation of androgen-responsive reporter genes and coactivation by SRC1, Ubc9, TIP60, and p300. The AR acetylation site mutant showed 10-fold increased binding of the N-CoR corepressor compared with the AR wild type in the presence of ligand. Furthermore, histone deacetylase 1 (HDAC1) bound the AR both in vivo and in cultured cells and HDAC1 binding to the AR was disengaged in a DHT-dependent manner. MEKK1 induced AR-dependent apoptosis in prostate cancer cells. The AR acetylation mutant was defective in MEKK1-induced apoptosis, suggesting that the conserved AR acetylation site contributes to a pathway governing prostate cancer cellular survival. As AR lysine residue mutations that abrogate acetylation correlate with enhanced binding of the N-CoR repressor in cultured cells, the conserved AR motif may directly or indirectly regulate ligand-dependent corepressor disengagement and, thereby, ligand-dependent *trans* activation.**

Steroid receptors, including the androgen receptor (AR), are members of the nuclear receptor (NR) superfamily which generally function as ligand-dependent transcriptional regulators (9, 31, 84). The AR is expressed in a variety of cell types and plays an important role in development, male sexual differentiation, and prostate cellular proliferation. The functional domains of the AR (termed A to F) are conserved with other members of the classical receptor subclass. The C-terminal region of the AR, including the hinge region and ligand-binding domain (LBD), is responsible for ligand binding and dimerization. The well-conserved DNA binding domain consists of 68 amino acids with two zinc finger structures. The N-terminal region contributes to transcriptional activation through its activation function 1 (AF-1) (5). In contrast to several other hormone-regulated NRs, the AR lacks an intrinsic AF-2 function in the LBD. The LBD, which consists of 12 α helices projecting away from the hormone-binding pocket in the absence of ligand, undergoes substantial conformational changes in the presence of ligand. The folding of the most carboxyl-terminal helix 12 over the ligand-binding pocket in turn creates new structural surfaces that bind coactivators required for efficient transactivation.

Several AR coactivators have been identified, including the p160 proteins, the p300/CREB-binding protein (CBP) family, Ubc9, ARA70, ARA55, and TIP60 (1, 5, 15, 68, 92). The efficient recruitment of coactivators to the AR involves an association between both the AR amino terminus and the LBD (5, 34). The coactivator proteins regulate gene expression through several distinct mechanisms. CBP and the related functional homologue p300 (CBP/p300) convey a bridging function between the DNA-bound transcription factor and the basal apparatus and provide a scaffold to assemble high-molecular-weight enhanceosomes (reviewed in reference 26). In addition, the cointegrator proteins p300/CBP share the capacity to acetylate histones, which correlates, under certain circumstances, with their transcriptional coactivator function (54, 87). Acetylation facilitates binding of transcription factors to

* Corresponding author. Mailing address: The Albert Einstein Cancer Center, Department of Developmental and Molecular Biology, Albert Einstein College of Medicine, Chanin 302, 1300 Morris Park Ave., Bronx, NY 10461. Phone: (718) 430-8662. Fax: (718) 430-8674. E-mail: pestell@aecom.yu.edu.

specific target DNA sequences by destabilizing nucleosomes bound to the promoter region of a target gene (45, 61). Furthermore, cointegrators may directly acetylate nonhistone proteins, including transcription factor, to regulate their activity (reviewed in references 81 and 87). Acetylation of the tumor suppressor p53 (51), the transcription factor erythroid Kruppel-like factor (95), and the erythroid cell differentiation factor GATA-1 (33) enhanced their transactivation functions. More recently nuclear hormone receptors (NHR) and NR coactivators were shown to serve as targets of acetylation. Direct acetylation of the nuclear receptor coactivator ACTR (18) or estrogen receptor α (86) contributed to ligand-dependent transcriptional attenuation. The AR is acetylated in vitro and in cultured cells at a conserved KLKK motif (23). Mutation of the AR KLKK motif abrogated acetylation of the AR in cultured cells and reduced ligand-dependent activity (23). However, the role of the AR acetylation site in regulating the other diverse functions of the AR is not known.

The AR conveys both *trans* activation and *trans*-repression function. The mechanism by which the AR represses expression of other transcription factors is a relatively poorly understood process. The AR inhibits activity of both c-Jun and c-Fos through mechanisms that may involve direct protein-protein interaction or competition for limiting coactivators (62, 76). Several genes downregulated by androgens contain NF-κB binding sites in their promoters, and components of tumor necrosis factor alpha (TNF-α)-dependent antiproliferation required the AR, suggesting an important function for AR–NF-κB cross talk in prostate cancer cells. The AR binds to RelA and attenuates RelA-mediated *trans* activation at an NF-κB site, consistent with a role for direct physical binding of NF-κB proteins in AR *trans* repression (62).

The activity of several NHR, such as the thyroid hormone receptor and the retinoic acid receptor, is actively repressed in the absence of ligand by binding to the corepressor protein N-CoR or SMRT. N-CoR and SMRT are largely modular proteins that interact with NHR through their C termini. The N-terminal repression domain interacts with histone deacetylase (HDAC) complexes. Upon recognition of their substrates, acetylated lysine residues of histone, HDACs remove acetyl groups from lysine residues, resulting in a more compact chromatin structure, decreasing the accessibility of the chromatin for transcription factors. In the case of the Rev-erbβ NHR superfamily member, N-CoR contacts both the NHR and the basal transcription apparatus. As some components of the basal apparatus are acetylated, it has been proposed that deacetylation may also decrease transcriptional activity. The mechanisms responsible for repressing the activity of the AR are not well understood. The cell cycle regulatory protein cyclin D1 and an intracellular transducer of transforming growth factor β signaling, Smad3, are reported to inhibit the activity of the ligand-treated AR (29, 44, 73). Smad3 repression of other NRs involves, at least in part, hormone-sensitive interactions with the corepressors N-CoR, SMRT, and Alien, which bind to the SIN3 proteins and recruit HDAC activity (17, 43). The finding that coactivator and corepressor surfaces of NHR overlap substantially (32, 66) is compatible with a dynamic model in which enzymatic modifications of the NR coordinate sequential disengagement of corepressors followed by coactivator binding (56). Whether such processes regulate AR activity remains to be determined.

In addition to responding to ligands, the AR is modified by kinase signaling pathways. The mitogen-activated protein kinase (MAPK) kinase kinase 1 (MEKK1) leads to activation of MKK4 and JNK (46). Constitutively active alleles of *MEKK1* can induce cellular apoptosis (25, 89). Activity of the AR is enhanced by constitutively active MEKK1 expression that induces cellular apoptosis in an AR-dependent manner (2). The AR is also posttranslationally modified by sumoylation. The modification of proteins by SUMO-1 (sumoylation) is a reversible, conserved, enzymatic event targeted to a lysine within the motif ψKXE (where ψ represents a large hydrophobic amino acid and X represents any amino acid) within the protein target. Conjugation of the small ubiquitin-like modifier SUMO-1/SMT3C/Sentrin-1 to cellular substrates involves an E1-like enzyme known as SAE1/SAE2. SUMO-1 is transferred from the E1 to a cysteine within the SUMO-specific residue E2-conjugating enzyme (Ubc9). Ubc9 then catalyzes an isopeptide bond between SUMO-1 and the ε-amino group of lysine in the target protein. A proportion of the AR is sumoylated in cultured cells (70), and like sumoylation of c-Jun (57), sumoylation of the AR attenuates AR transactivation function (70). The specificity for the target protein of sumoylation is thought to reside with Ubc9 itself. Ubc9 binds the AR within the hinge region (68) that includes the site of direct acetylation, raising the possibility that AR acetylation may in turn affect modification by SUMO-1 and, thereby, transactivation.

The role of AR acetylation in AR *trans* repression and *trans* activation for specific target genes and the molecular mechanisms by which the AR acetylation site regulates transcriptional coregulator complex recruitment are unknown. Furthermore, the functional consequence of the AR acetylation site on cellular phenotype is unknown. As similar types of questions either remain to be addressed or are controversial with other transcription factors that are directly acetylated, such as p53 (72), it is likely that analysis of the AR acetylation site may provide insight into the function of other acetylated transcription factors. In this study, we investigated the functional significance of the conserved lysine residue motif within the AR hinge region that was previously shown to serve as a substrate for acetylation by the histone acetyltransferase (HAT) p300 and P/CAF (23). The AR mutations at the acetylation site maintained *trans*-repression function, bound ligands with wild-type affinity, were sumoylated, and conveyed 80 to 90% of the basal activity of the AR wild type (ARwt). The dihydrotestosterone (DHT)-induced activity of the androgen-responsive reporter genes, prostate-specific antigen (PSA), mouse mammary tumor virus (MMTV), and an androgen-responsive element (ARE) reporter was abrogated. Coactivation by SRC1, p300, Ubc9, and TIP60 was abolished. Binding of the AR mutant to the corepressor N-CoR in the presence of ligand was increased, suggesting a critical role for these lysine residues in ligand-dependent recruitment of N-CoR. Prostate cancer cell lines stably expressing either ARwt or AR acetylation mutants demonstrated a resistance of the AR acetylation site mutant lines to several apoptosis-inducing agents. Mutation of the AR acetylation site abrogated MEKK1-induced apoptosis. These studies indicate that the conserved AR lysine residues, which are acetylated in vitro and in cultured cells, play a role in

coordinating a subset of AR functions, including corepressor disengagement, ligand-induced transactivation, and cellular apoptosis.

## MATERIALS AND METHODS

**Reporter genes and expression vectors.** The expression vector pCMVHA-p300 (4) and the AR-regulated reporter genes PSA-LUC, a 600-bp fragment of the PSA promoter with an additional 2.4-kb enhancer sequence cloned upstream of luciferase (PSA P/E-luc), MMTV-LUC, and ARE-LUC were used (23, 93). The NF-κB-responsive reporter 3xRel-LUC (3), the AP-1-responsive promoter 3xAP-1-LUC, and the $(UAS)_5$-E1B-TATA-LUC reporter were as described previously (21). The wild-type human AR was subcloned from pARO into pcDNA3, and the AR acetylation site mutants $AR_{K630R}$, $AR_{K630A}$, $AR_{K(632/633)A}$, and $AR_{K(630/632/633)R}$ were derived by PCR with sequence-specific primers and cloned into pcDNA3. The integrity of all constructs was confirmed by sequence analysis. The expression vectors for Gal4-Sp1 (65), pCMVSRC1a (38), TIP60 (35), ARA70 (92), ARA55, Ubc9 (68), Smad3, Smad3ΔC (40), pCEP4-MEKK1wt (67), pCMV-FlagN-CoR (6), pCMV-HDAC1 (13), and pCMV-EGFP were previously described.

**Cell culture, DNA transfection, and luciferase assays.** Cell culture, DNA transfection, and luciferase assays were performed as previously described (16, 21). The prostate cancer cell line DU145 and the HEK293 cell line were cultured in Dulbecco's minimal essential medium (DMEM) supplemented with 10% fetal bovine serum (FBS), 1% penicillin, and 1% streptomycin. In studies of cellular apoptosis with MEKK1, transfections were performed exactly as previously described (2). Cells were plated at a density of $5 \times 10^5$ cells in a 60-mm-diameter dish on the day prior to transfection. For DU145 cells, Lipofectamine Plus (Gibco BRL) was used. The DNA-Lipofectamine mix was added to the cells in optimem. Cells were incubated in media containing 10% charcoal-stripped fetal bovine serum prior to experimentation with DHT (23). At least two different plasmid preparations of each construct were used. In cotransfection experiments, a dose response was determined in each experiment with 300 and 600 ng of expression vector and the promoter reporter plasmids (2.4 μg). Luciferase activity was normalized for transfection with β-galactosidase reporters as internal controls. Luciferase assays were performed at room temperature with an Autolumat LB 953 (EG&G Berthold) (88). The fold effect was determined for 300 to 600 ng of expression vector with comparison made to the effect of the empty expression vector cassette, and statistical analyses were performed by using the Mann-Whitney U test.

**In vitro SUMO conjugation assays.** SAE2/SAE1, Ubc9, and SUMO-1 were expressed in *Escherichia coli* B834 and purified as described previously (82). In vitro transcription-translation of proteins was performed by using 1 μg of plasmid DNA and a wheat germ coupled transcription-translation system according to the instructions provided by the manufacturer (Promega, Madison, Wis.). [$^{35}$S]methionine (Amersham) was used in the reactions to generate radiolabeled proteins. SUMO conjugation assays were performed in 10-μl volumes containing 1 μl of [$^{35}$S]methionine-labeled substrate (AR or promyelocytic leukemia [PML] protein), 10 μg of SUMO-1, 120 ng of SAE1/SAE2, and 650 ng of Ubc9 in 50 mM Tris (pH 7.5), 5 mM $MgCl_2$, 2 mM ATP, and 10 mM creatine phosphate (containing 3.5 U of creatine kinase/ml and 0.6 U of inorganic pyrophosphatase/ml). The reaction mixtures were incubated at 37°C for 120 min. After termination with sodium dodecyl sulfate (SDS) sample buffer containing β-mercaptoethanol, reaction products were fractionated by electrophoresis in 8% polyacrylamide gels containing SDS, stained, destained, and dried before analysis by phosphorimaging.

**Protease sensitivity and ligand-binding assays.** Protease sensitivity assays were performed as previously described (10), with minor modifications. In vitro [$^{35}$S]methionine-labeled ARwt and $AR_{K630A}$ proteins were prepared by coupled transcription-translation with a Promega TNT coupled reticulocyte lysate kit (Promega) with 1.0 μg of plasmid DNA in a total volume of 50 μl. The translated products were subsequently separated into 22.5-μl aliquots and treated with or without DHT (10 nM) for 20 min at 25°C. The mixtures were then separated into 4.5-μl aliquots and incubated with increasing amounts of trypsin as indicated for 10 min at 25°C. The digestion was terminated by the addition of 20 μl of denaturing gel loading buffer and boiling for 5 min. The products of the digestion were separated by SDS–12% polyacrylamide gel electrophoresis (PAGE) and visualized by autoradiography.

Ligand-binding assays were performed as described previously (79) with equal amounts of in vitro-translated recombinant wild-type AR and mutant ARs diluted to a total volume of 2 μl in ligand-binding buffer (50 mM Tris, 1 mM EDTA, 10% glycerol, 1 mM dithiothreitol [pH 7.5]). Fifty microliters of this dilution was mixed with 50 μl of different concentrations of [1,2,4,5,6,7-$^3$H]DHT (127 Ci/mmol) with or without a 200-fold excess of unlabeled DHT and incubated at 4°C for 2 h. Unbound steroids were removed with HAP (79), and counts per minute were determined by liquid scintillation counting.

**Western blots, IP, and electrophoretic mobility shift assays (EMSAs).** Western and immunoprecipitation (IP)-Western blotting were performed as previously described (73). The antibodies used in Western blot analysis were rabbit anti-AR antibody (N-20), the polyclonal p300 antibody (Santa Cruz Biotechnology, Santa Cruz, Calif.) (4), anti-Flag antibody (M2; Sigma) (73), and anti-HDAC1 antibody (Upstate Biotechnology, Lake Placid, N.Y.). The guanine nucleotide dissociation inhibitor antibody (a generous gift from Perry Bickel, Washington University, St. Louis, Mo.) was used as an internal control for protein abundance (47). For the detection of protein, the membrane was incubated with anti-AR (N-20) (1:1,000), anti-p300 (N-20) (1:1,000), anti-HDAC1, and anti-M2 Flag antibody for Flag N-CoR at room temperature for 2 h or at 4°C overnight. The blots were then washed three times with 0.5% Tween 20–phosphate-buffered saline and incubated with the appropriate horseradish peroxidase-conjugated secondary antibody. The proteins were visualized by the enhanced chemiluminescence system (Amersham Pharmacia Biotech). The abundance of immunoreactive protein was quantified by phosphorimaging with an Image Quant, version 1.11, computing densitometer (Molecular Dynamics, Sunnyvale, Calif.).

IP-Western blotting was performed as previously described (73) with the lysates from HEK293 cells transfected with pcDNA3AR, $pcDNA3AR_{K630A}$, $pcDNA3AR_{K(632/633)A}$, pCMVHA-p300, pCMV-FlagN-CoR, or an empty expression vector cassette as a control. The cells were treated for 24 h with 100 nM DHT or vehicle. Cells were rinsed with phosphate-buffered saline, harvested by scraping, pelleted, and lysed in buffer (50 mM HEPES [pH 7.2], 150 mM NaCl, 1 mM EDTA, 1 mM EGTA, 1 mM dithiothreitol, 0.1% Tween 20, 0.1 mM phenylmethylsulfonyl fluoride, 2.5 μg of leupeptin/ml, 0.1 mM sodium orthovanadate [Sigma]). The extracts were cleared by centrifugation and further precleared by rocking at 4°C with washed protein A-agarose beads (Roche Molecular Biochemicals, Indianapolis, Ind.). The precleared extracts were immunoprecipitated with 0.5 μg of AR antibody or equivalent amounts of the appropriate control immunoglobulin G and 50 μl of protein A-agarose for 8 to 12 h at 4°C. The beads were washed five times with lysis buffer and boiled in SDS sample buffer, and the released proteins were resolved by SDS-PAGE. The gels were transferred to nitrocellulose, and Western blotting was performed.

EMSAs were performed as previously described by using the ARE sequence (74). Oligonucleotides encoding the high-affinity androgen response element (74) (5′-ATG CAT TGG GTA CAT CTT GTT CAC ATA GAC A-3′) and its complementary strand were used for EMSAs as recently described (8). In vitro translation products of ARwt, $AR_{K630A}$, and $AR_{K630R}$ were generated by using the TNT T7/SP6 Coupled Reticulocyte Lysate system (Promega) and 1 μg of plasmid DNA for ARwt, $AR_{K630A}$, and $AR_{K630R}$. The level of the ARs synthesized was assessed by Western blot analysis and shown to be similar. The binding reaction was performed with 3 μl of in vitro-translated AR, 100 fmol of [γ-$^{32}$P]ATP-labeled probe, and 1.0 μg of poly[d(I-C)] in 20 mM Tris (pH 7.9), 0.5 mM EDTA, 2.5 mM $MgCl_2$, 1.5 mM dithiothreitol, 100 mg of Pefabloc SC/ml, 10% glycerin, 100 nM DHT, and 200 μM $ZnCl_2$. The reaction mixture was incubated on ice for 30 min. The complexes were separated on 5% polyacrylamide gels in 0.5× Tris-borate-EDTA. The gels were vacuum dried at 80°C for 2 h, and the protein-DNA complexes were visualized by autoradiography.

**Apoptosis assays.** The thiazolyl blue (MTT) assay, which is a quantitative colorimetric assay for mammalian cell survival and proliferation, was performed as previously described (93). Briefly, $2 \times 10^3$ cells of the DU145 stable cell lines for ARwt, $AR_{K630A}$, and $AR_{K(632/633)A}$ were grown in 96-well plates in 50 μl of DMEM with 10% charcoal-stripped FBS. After 24 h, the cells were treated with either vehicle or 10 nM DHT for approximately 20 to 30 min to engage the endogenous AR (71) and then treated with either cycloheximide (10 μg/ml), TNF-related apoptosis-inducing ligand (TRAIL) (10 ng/ml) (R&D Systems, Minneapolis, Minn.), TNF-α (10 ng/ml) (Promega), or tetradecanoyl phorbol acetate (TPA) (100 ng/ml). After 6 h, 20 μl of MTT (5 mg/ml; Sigma) was added to each plate for 3 h at 37°C. After incubation, 200 μl of 0.04 N HCl in isopropanol was added to each well. After several rounds of pipetting and 5 min of incubation at room temperature, the absorbency was read at a test wavelength of 490 nm. Comparisons were made within each cell line to the vehicle-treated standard (control), as it could not be assumed that cellular division rates were identical between the cell lines (78).

In separate experiments, the stable cell lines were treated as described above and then analyzed directly for morphological features of apoptosis after direct fixation of all cells with 10% paraformaldehyde. This procedure ensured fixation of both adherent and nonadherent cells that had undergone apoptosis. At least

three high-power fields chosen at random were assessed for each treatment to ensure the counting of at least 300 cells. The percent apoptotic cells was scored for blebbing and chromatin condensation. Data are shown as the relative change in apoptosis by the inducing agent in the presence of 10 nM DHT.

In studies with MEKK1, apoptosis was detected by morphological analysis of green fluorescent protein (GFP)-transfected cells (2). Equal amounts of GFP were transfected into the wells with either the ARwt or the AR mutants; thus, GFP itself was not an independent variable between the groups compared. At least 200 cells were counted by using a fluorescent microscope, and cells were scored for blebbing and chromatin condensation by an investigator blinded to the experimental condition. At 24 h posttransfection, cells were treated with either 100 nM DHT or vehicle, and at 48 h, the cells were rinsed with phosphate-buffered saline, fixed with 4% paraformaldehyde for 15 min, permeabilized with 0.5% Triton X-100, and stained for DNA with Hoechst 3325 dye (5 μg/ml).

## RESULTS

**DHT-induced AR activity involves lysine residues acetylated in vitro.** In previous studies, the AR was shown to be acetylated in cultured cells with anti-acetyl lysine antibodies (23). Either p300 or P/CAF was capable of acetylating the AR in vitro, and Edman degradation analysis of the acetylated AR products demonstrated that lysines 630, 632, and 633 were preferentially acetylated, constituting an acetylation motif that is conserved between species (Fig. 1A). Only monoacetylated lysine-containing peptides were detected in the samples by matrix-assisted laser desorption ionization–time of flight mass spectrometry, indicating that the product analyzed by Edman degradation was a heterogeneous population of peptides, each acetylated at a single site. We assessed the role of the in vitro AR acetylation sites in ligand sensitivity with point mutants of the AR acetylation sites and reporter genes encoding a specific ARE (ARE-LUC), an endogenous androgen-responsive gene (PSA-LUC), or the androgen-responsive MMTV-LUC.

In the presence of DHT, ARE-LUC activity was induced six- to sevenfold by the ARwt compared with the empty pcDNA3 vector but was induced less than 50% by either of the AR acetylation site mutants (Fig. 1A). We next assessed the role for the AR lysine residues in regulating basal and ligand-treated AR function with the androgen-responsive PSA gene promoter linked to the luciferase reporter gene in the prostate cancer cell line DU145 (Fig. 1B). The ARwt enhanced basal AR activity 2.5-fold. The addition of DHT ($10^{-6}$ M) induced AR activity 4.3-fold. The expression plasmid encoding the AR acetylation site mutant ($AR_{K630A}$) increased basal AR activity 1.5-fold compared with the empty expression vector cassette; however, there was no significant increase in DHT-induced activity of the PSA-LUC reporter. Expression of the $AR_{K(632/633)A}$ construction enhanced basal AR activity 1.7-fold; however, DHT-induced activity was reduced 50 to 60% compared with the wild type (Fig. 1B). To assess whether ligand sensitivity was affected at subphysiological concentrations, dose-response curves were examined. The androgen-responsive MMTV-LUC reporter was induced threefold by ARwt compared with the empty pcDNA3 vector with 1 to 10 nM DHT in DU145 cells; however, the AR acetylation mutants were not induced (Fig. 1C).

Similar studies were performed with point mutants in which the AR lysine residues were replaced with arginine (Fig. 1D and E). In HEK cells, the MMTV-LUC reporter was induced by ARwt four- to fivefold; however, the arginine substitution mutants were not induced by DHT. Similar observations were made in DU145 prostate cancer cells (Fig. 1E). In previous studies of DU145 cells, it has been shown that the ligand-treated AR does not induce either the $pA_3$LUC vector or several other luciferase reporter genes (RSV-LUC, *cyclin E*-LUC, and c-*Fos*-LUC) (73), suggesting that the induction of the PSA-LUC and MMTV-LUC reporters is promoter specific. The expression plasmids encoding point mutations of the AR acetylation site were shown to be expressed in numbers equal to those of the wild type in cultured cells (see Fig. 4G, left panel). Together these studies suggest that the AR acetylation sites reduce both basal and ligand-induced activity of androgen-responsive reporter genes.

**The AR acetylation site does not regulate AR *trans*-repression function.** The AR inhibits AP-1 activity in different cell types, which likely involves several different mechanisms (39, 76, 77). The ability of the AR to inhibit AP-1 activity was assessed by using the AP-1 site from the collagenase promoter. The ARwt and the AR acetylation mutants inhibited AP-1 activity approximately 60 to 75% (Fig. 2A). In the presence of DHT, ARwt repressed AP-1 activity by 80% and the AR mutants repressed AP-1 activity by 70% (Fig. 2B). Several genes downregulated by androgen contain NF-κB binding sites, and the AR attenuates NF-κB reporter activity in a dose-dependent manner (62). We assessed NF-κB activity with the well-characterized 3xRel-LUC reporter gene (3). The ARwt and the AR mutants inhibited 3xRel-LUC reporter activity 50% in the absence of ligand and 60 to 70% in the presence of DHT (Fig. 2C and D). The AR forms a physical interaction with Sp1 and shares a common coactivator, SNURF (52, 69). The ability of the ARwt to regulate Sp1 function was examined in DU145 cells with a heterologous reporter gene system. The Sp1 coding region was linked to the Gal4 DNA binding domain, and activity was assessed with a heterologous reporter consisting of multimerized Gal4 DNA binding sites linked to the luciferase reporter gene $(UAS)_5$-E1B-TATA-LUC (Fig. 2E). The ARwt repressed Sp1 activity 30 to 50%, and similar repression was observed with the AR acetylation mutant (Fig. 2E and F). Together these studies suggest that the ability of the AR to *trans* repress the activity of several distinct signaling pathways is not affected by the mutation of the AR acetylation site.

**In vitro sumoylation and DNA binding of the AR are not dependent upon the AR acetylation site.** In order to investigate the mechanisms responsible for the defect in ligand-dependent transactivation of the AR acetylation site mutants, we examined the possibility that the acetylation site may regulate AR sumoylation, AR gross structure in the presence of ligand, and DNA binding. Acceptors of SUMO-1 modification are not targeted for degradation, unlike the majority of ubiquitinated proteins; however, the transcriptional activity of specific proteins appears to be affected. The AR binds Ubc9 in a region that includes the AR acetylation motif (68), and Ubc9 has the capacity to serve as an E3 for sumoylation. The ligand-dependent transactivation of the AR is regulated by sumoylation (70); therefore, we investigated the possibility that the AR acetylation site may play a role in the defective ligand-dependent transactivation of the AR acetylation mutants. Modification of the PML protein by sumoylation targets it to distinct nuclear bodies (20), and $^{35}$S-labeled in vitro-translated PML serves as an ideal substrate for in vitro sumoylation assays with Ubc9 (82). As expected, PML was modified by SUMO-1 that

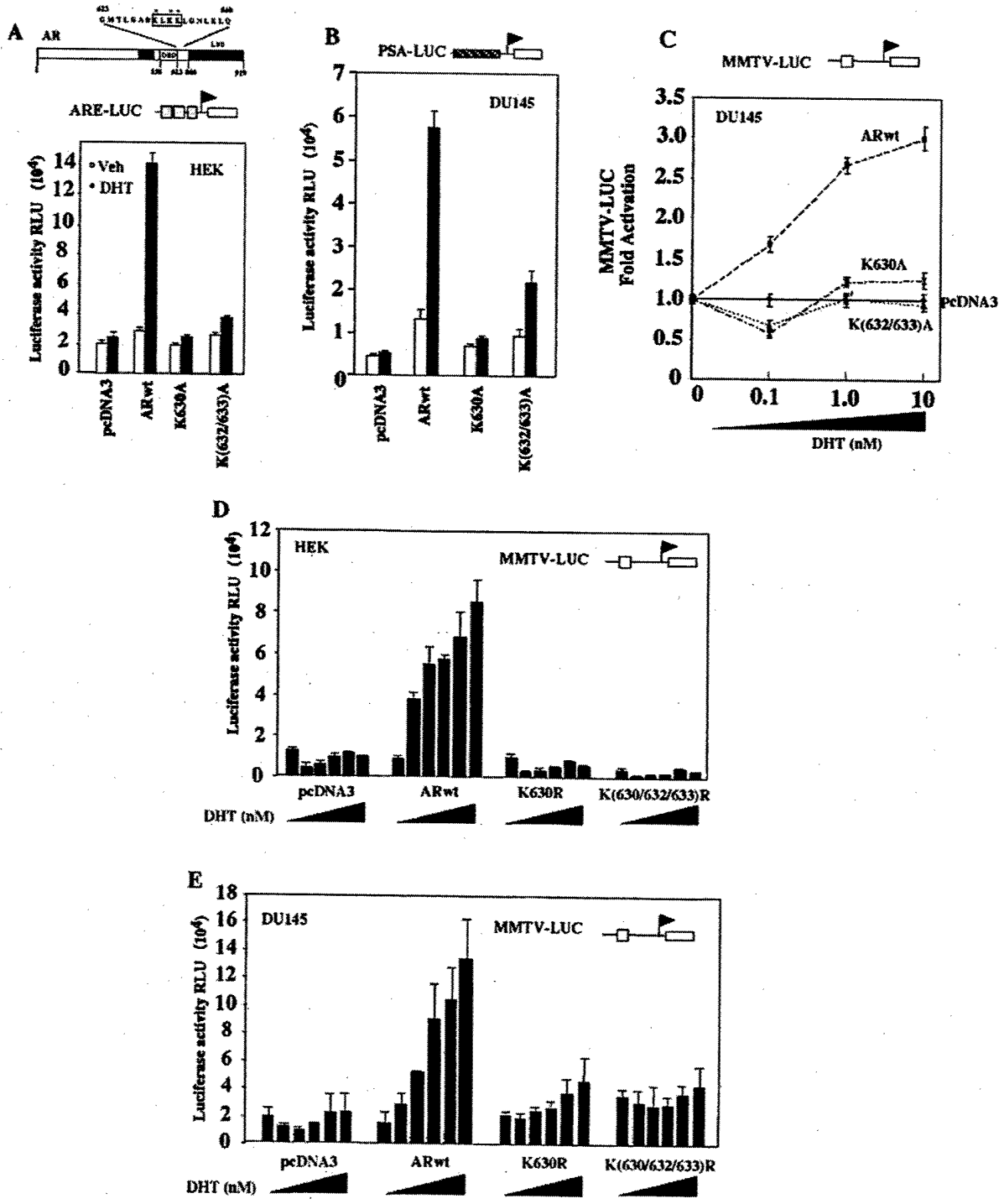


FIG. 1. The AR acetylation site is required for DHT-mediated activation of androgen-responsive reporter genes. (A) Schematic representation of the human AR indicating the DNA binding domain (DBD), the LBD, and the conserved KXKK motif (indicated by asterisks). The androgen-responsive reporter gene ARE-LUC (A), PSA-LUC (B), or MMTV-LUC (C) was transfected into DU145 cells with either the ARwt or AR acetylation site mutant expression plasmids. The cells were treated for 24 h with either vehicle, DHT ($10^{-7}$ M), or DHT at concentrations ranging from 0.1 to 10 nM (C) as indicated. Luciferase activity was determined, and the data are shown as means ± standard deviations for at least six separate transfections. The MMTV-LUC reporter was transfected into DU145 (D) or HEK293 (E) cells either alone or with the expression plasmid encoding ARwt or the AR acetylation site mutant (arginine substitution) expression plasmids. The cells were treated with either vehicle or DHT (0.01, 0.1, 1, 10, 100 nM) as indicated for 24 h, and luciferase activity was determined. RLU, relative luciferase units.

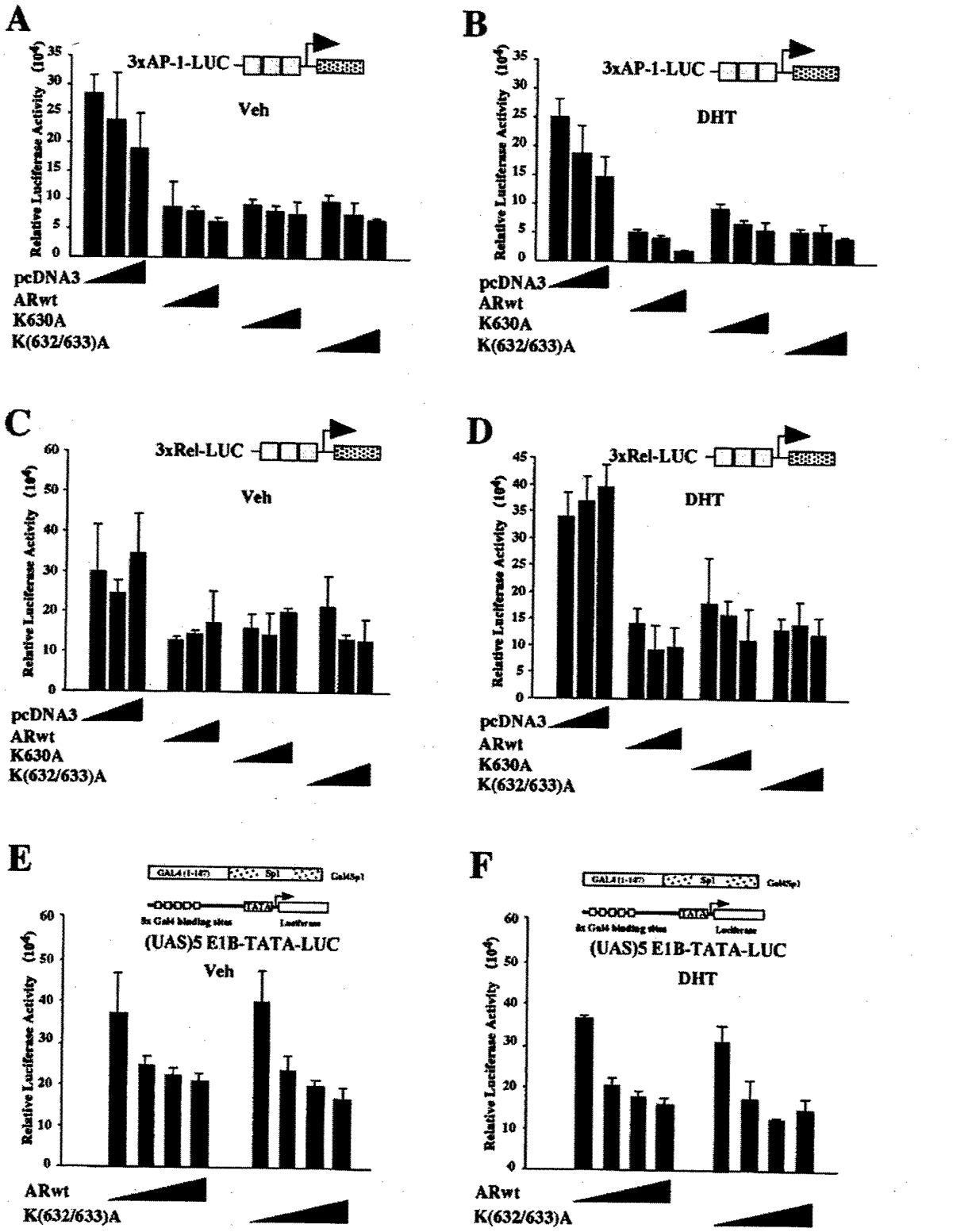


FIG. 2. The *trans*-repression function of the AR acetylation site mutants is preserved. The expression vectors for either the wild-type or mutant AR or equal amounts of the empty expression vector cassettes (pCMV) were cotransfected into HEK293 cells with the luciferase reporter genes for AP-1 (3xAP-1-LUC) (A and B), NF-κB activity (3xRel-LUC) (C and D), or the $(UAS)_5$-E1B-TATA-LUC heterologous reporter (E and F), and the chimeric transcription factor for Sp-1 was fused to the Gal4 DNA binding domain. The cells were treated with either DHT ($10^{-7}$ M) or vehicle (Veh) for 24 h, and luciferase activity was assessed. The data are shown as means ± standard deviations. The DHT treatment ($10^{-7}$ M) was for 24 h.

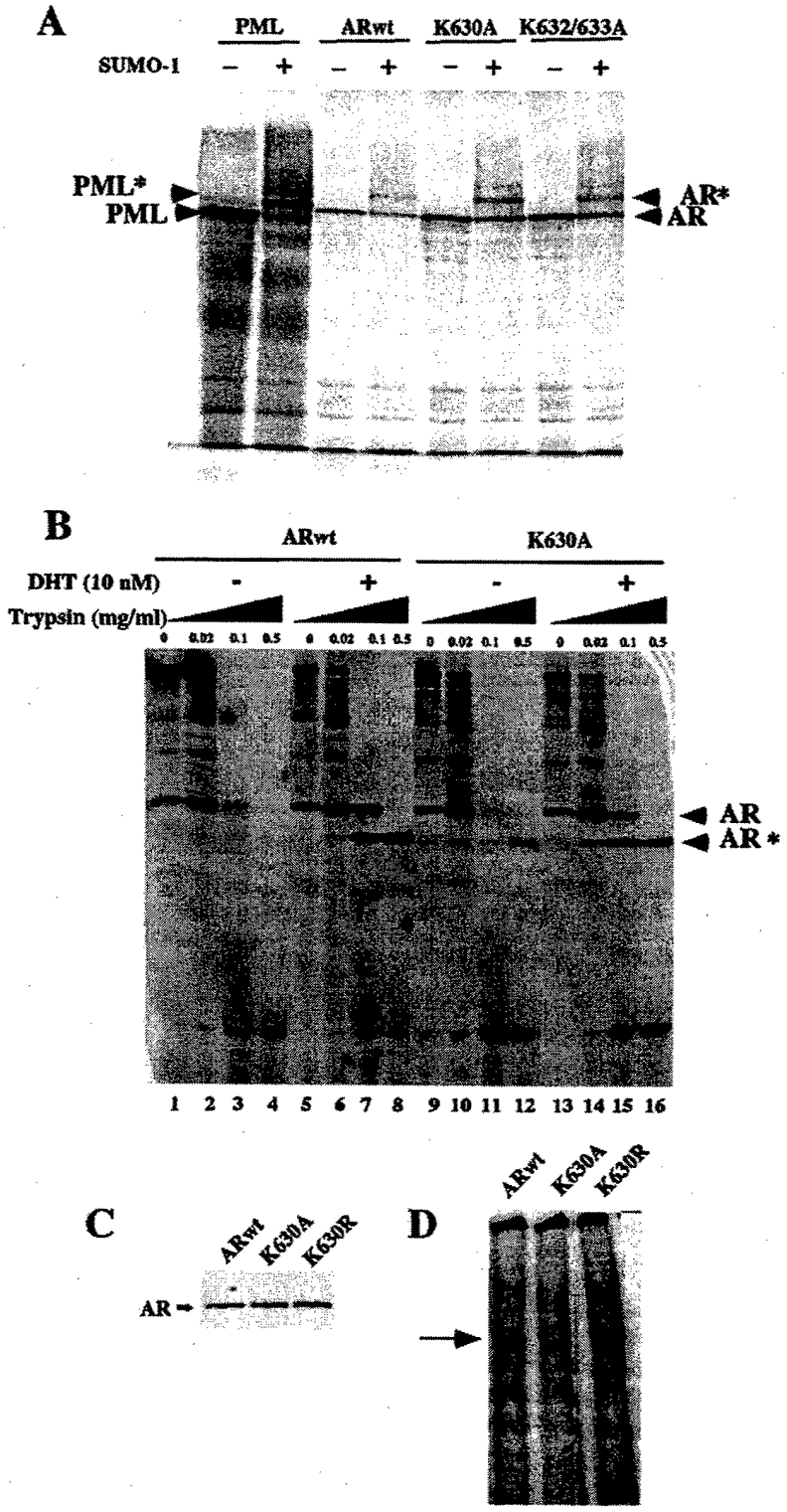


FIG. 3. AR in vitro sumoylation, protease cleavage pattern, and in vitro DNA binding are not affected by the AR acetylation site. (A) The in vitro SUMO-1 conjugation assays were conducted as described previously (82) with in vitro-translated $^{35}$S-labeled PML, ARwt, or AR acetylation mutants as indicated. The unconjugated proteins are indicated by arrows, and the SUMO-1-conjugated forms are indicated by asterisks. (B) Protease sensitivity assays were conducted with ARwt or AR mutants by using increasing concentrations of trypsin and either vehicle or DHT as indicated. The full-length in vitro-translated $^{35}$S-labeled AR and the major trypsin digestion products are shown. (C) Equal amounts of in vitro-translated $^{35}$S-labeled AR (shown by autoradiography) were used in an EMSA with a $^{32}$P-labeled high-affinity ARE (74). The DNA-protein complex of delayed migration is indicated by an arrow. +, present; −, absent.

occurred at several sites (Fig. 3A). The ARwt was also sumoylated, and there was no significant difference in the pattern or proportion of sumoylation of the AR acetylation mutants (Fig. 3A).

It is known that the addition of DHT induces a conformational change in the AR and that ligand-induced conformational changes of NHR can be assessed by limited proteolytic digestion (10). To determine whether the AR lysine substitution mutations altered conformation of the full-length AR protein in the presence of ligand, limited proteolytic digestion was performed comparing the ARwt and the $AR_{K630A}$. Trypsin addition induced a dose-dependent cleavage pattern, with a specific pattern induced in the presence of ligand (Fig. 3B, lanes 3 and 4 versus lanes 7 and 8). The proteolytic pattern of the $AR_{K630A}$ mutant in the presence or absence of ligand was similar to that of the ARwt (Fig. 3B, lanes 7 and 8 versus lanes 15 and 16). The induction of trypsin cleavage upon ligand addition was consistent with the similar in vitro ligand-binding properties of the ARwt and the AR mutant within the physiological range of the ligand (for ARwt, kDa = 0.84 nM; for $AR_{K630A}$, kDa = 1.3 nM). In addition, the DNA binding properties of the AR mutants were assayed. As several different cellular proteins have been proposed to regulate the DNA binding properties of the AR, we performed EMSAs with an ARE previously identified as a selective AR-binding site (74) and compared binding by using equal amounts of in vitro-translated full-length AR protein (Fig. 3C). A specific DNA-protein complex formed in the presence of the ARwt (Fig. 3D) that was competed by a specific cognate competitor (data not shown) and which was of mobility and intensity similar to those of the mutant ARs.

**Mutation of the conserved AR lysine residue abrogates coactivator-dependent induction.** Several distinct coactivators have been described which can enhance AR activity in either the presence or the absence of ligand. To investigate the possibility that reduced ligand-dependent transactivation of the AR acetylation mutants was due to a selective defect in activation of the AR by a previously described coactivator, transient expression studies were conducted in DU145 cells with the androgen-responsive MMTV-LUC reporter gene. TIP60 encodes an AR-interactive protein with a domain homologous to the HAT domain of p300 and conveys DNA-dependent ATPase activity that plays a role in DNA repair (35). The activity of the ARwt was augmented 4-fold by TIP60 in the absence of ligand and 12-fold in the presence of ligand (Fig. 4A). The basal activity of the AR mutant $AR_{K630A}$ was induced fourfold by TIP60; however, in the presence of ligand there was no significant additional induction (Fig. 4A). SRC1 binds the non-ligand-treated AR through AF-1 (12), recruits p300 (91), and is known to augment ligand-treated AR function in fibroblasts (12). Coexpression of SRC1 (38) increased the activity of the ligand-treated ARwt sixfold, whereas the $AR_{K630A}$ was not induced (Fig. 4B). The AR-binding proteins, ARA55 and ARA70, induced AR activity in some but not all studies (12, 92). In the present studies, neither ARA55 nor ARA70 induced either the ARwt or the AR mutants (Fig. 4C and D). The $AR_{K(632/633)A}$ mutant was also defective in ligand-induced activation by each of the coactivators (data not shown). We examined Ubc9, a homologue of the class E2 ubiquitin-conjugating enzymes, which is thought to function as an AR transactivator independently of its ubiquitin conjugation function (68). The AR 629 to 633 region was necessary for Ubc9-induced AR activity. Ubc9 augmented ligand-dependent activation of the ARwt three- to fourfold, whereas activity of $AR_{K630A}$ was not enhanced by coexpression of Ubc9 (Fig. 4E). Consistent with CBP induction of the AR in CV1 cells (1), coexpression of p300 increased DHT-induced activity three- to fourfold (Fig. 4F). In contrast, the $AR_{K630A}$ mutant was not significantly induced by p300 in the presence of ligand (Fig. 4F). Together, these studies suggest that the AR acetylation mutants are defective in transactivation by several distinct AR coactivators.

Several models have been proposed to explain the mechanisms by which p300 augments NR activity. p300 may augment ligand-treated AR activity either by bridging AF-1 and AF-2 (34) or by interacting with the AR N terminus and the LBD (22). Alternatively, p300 may, upon recruitment through SRC coactivators (83, 85), facilitate histone acetylation and basal machinery interactions to promote gene expression. To determine whether failed activation of the $AR_{K630A}$ by p300 was due to reduced binding in cultured cells, IP-Western blotting was performed. The ARwt and the AR mutants were transfected into AR-deficient HEK293 cells with the p300 expression vector. The ARwt and the mutants showed similar levels of expression by Western blotting, and p300 levels were also similar (Fig. 4G, left panel). IP showed equal amounts of the AR in the immunoprecipitate (Fig. 4G, right panel). The amount of p300 associated with AR was reduced in the $AR_{K630A}$ and $AR_{K(632/633)A}$ mutants compared with ARwt (Fig. 4G, lane 4 versus lanes 5 and 6).

**TSA induction and DHT-induced AR activity involve lysine residues acetylated in vitro.** In previous studies, the androgen-responsive synthetic reporter gene MMTV-LUC was shown to be induced in the presence of ARwt by the specific HDAC inhibitor trichostatin A (TSA) (23, 53). We therefore assessed the role of the in vitro AR acetylation sites on TSA sensitivity with point mutants of the AR acetylation sites and the androgen-responsive reporter gene MMTV-LUC in the human prostate cancer cell line DU145. Increasing concentrations of TSA induced the ARwt 2.5 to 3-fold at 10 to 20 nM compared with the empty vector (pcDNA3) (Fig. 5A). In contrast, neither of the AR acetylation site mutants, $AR_{K630A}$ and $AR_{K(632/633)A}$, was induced by TSA. TSA failed to augment ligand-treated AR activity (23), suggesting that the mechanisms governing ligand-treated activity and TSA sensitivity involve a common pathway. As TSA is a specific inhibitor of HDACs, we investigated the possibility that HDAC1 may physically associate with the AR in vivo. Cellular extracts from the murine liver, which expresses the AR (73), were immunoprecipitated with an AR-specific antibody (73). Western blotting of the AR with an HDAC1-specific antibody demonstrated the presence of HDAC1 in the AR IP (Fig. 5B). The addition of DHT ($10^{-7}$ M) reduced the abundance of HDAC1 in the AR IP (Fig. 5C, lane 1 versus lane 2). TSA treatment also reduced the amount of HDAC1 coprecipitated with the AR (Fig. 5C, lane 1 versus lane 3). The addition of TSA to DHT did not significantly alter the amount of HDAC1 bound to the AR (Fig. 5C, lane 3 versus lane 4). The treatment with DHT and TSA did not affect the abundance of HDAC1 in the cells (Fig. 5C, lane 6 versus lanes 7 and 8). Thus, HDAC1 coprecipitates with the AR in vivo and in

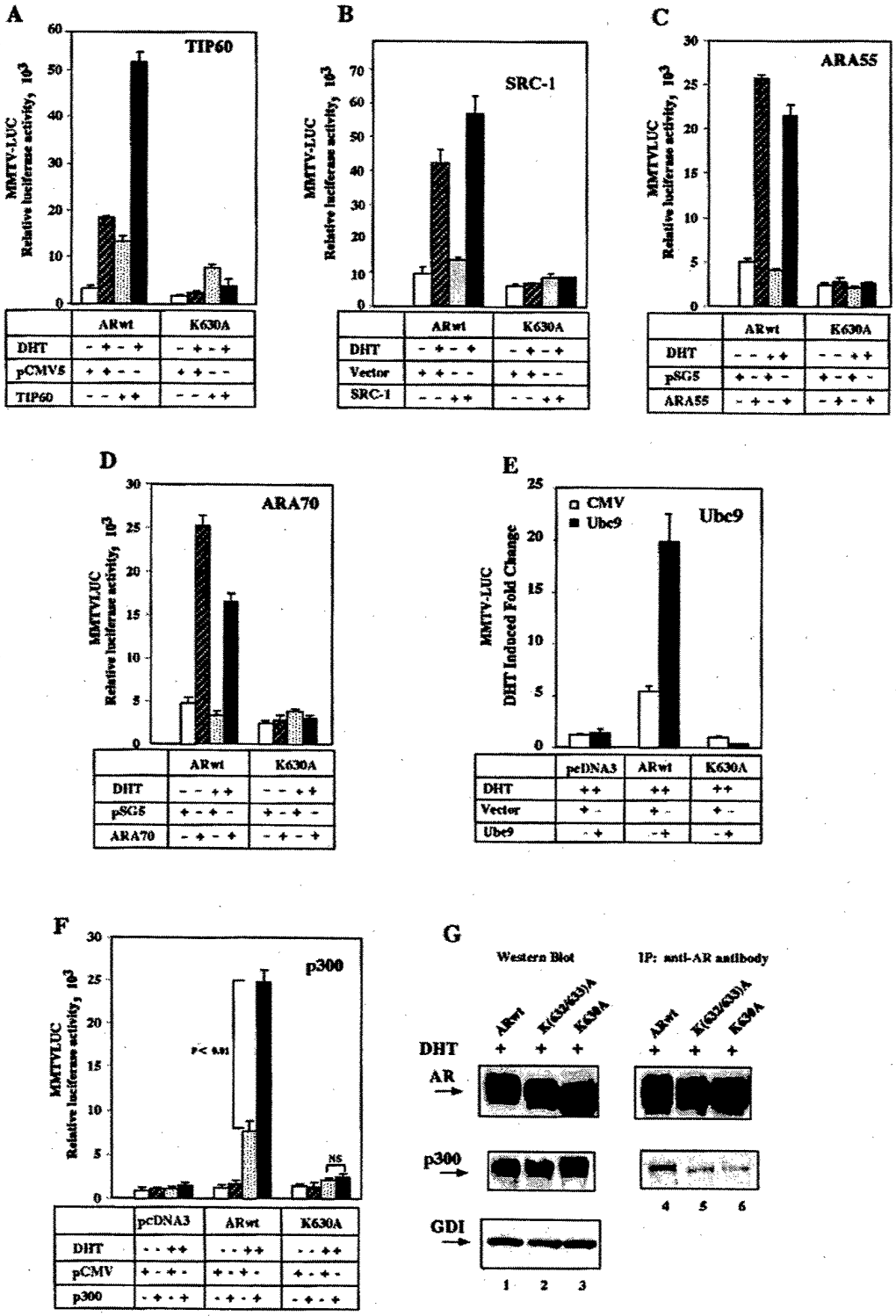


FIG. 4. The AR acetylation site regulates coactivator-mediated induction of ligand-treated AR. The MMTV-LUC reporter was cotransfected with expression vectors for either the wild-type or mutant AR and the candidate AR coactivators TIP60 (A), SRC1 (B), ARA55 (C), ARA70 (D), Ubc9 (E), and p300 (F) or equal amounts of the empty expression vector cassettes (pCMV). The cells were treated with either DHT ($10^{-7}$ M) or vehicle for 24 h, and luciferase activity was assessed. The data are shown as the means ± standard deviations for at least six separate transfections. DHT treatment ($10^{-7}$ M) was for 24 h. (G) The ARwt and AR acetylation site mutant were transfected into HEK293 cells, and Western blotting was performed for AR, p300, and the loading control guanine nucleotide dissociation inhibitor (GDI). In the right panel, equal amounts of the cellular extracts were immunoprecipitated with the AR antibody, and Western blotting was performed with either the AR or the p300 antibody. +, present; −, absent.

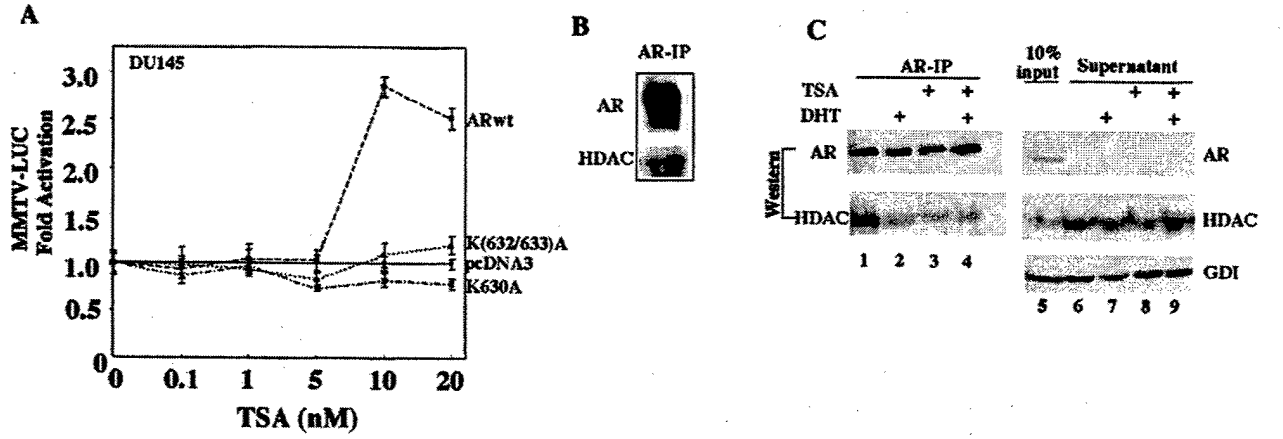


FIG. 5. TSA induction of the AR involves the AR acetylation site. (A) The expression plasmids encoding the wild-type and mutant AR were transfected into DU145 cells with the MMTV-LUC reporter. The cells were treated with either vehicle or TSA at the dose indicated for 24 h, and luciferase activity was determined. The data are means ± standard errors of the means for at least six separate transfections. (B) IP was performed with murine hepatic extracts with an AR-specific antibody, with sequential Western blotting for either AR or HDAC1. (C) Hepatocellular extracts were treated with either vehicle, TSA (30 nM), or DHT (100 nM) and subjected to IP with an AR-specific antibody. The AR IP was electrophoresed on an SDS-PAGE gel, and Western blotting was performed for AR or HDAC1 (lanes 1 to 4). In the right panel (lanes 5 to 9), the supernatant was analyzed by Western blotting. The absence of AR in the IP supernatant indicates that the IP is saturating. Similar levels of HDAC1 are seen in the supernatant treated with vehicle, TSA, or DHT. +, present; GDI, guanine nucleotide dissociation inhibitor.

cultured cells and the association between HDAC1 and the AR is regulated by DHT or TSA.

**Increased N-CoR binding of the AR acetylation mutant.** HDAC1 is found in a large transcriptional regulatory complex that includes the corepressors mSIN3 and N-CoR (6, 30, 59). In recent studies, N-CoR was shown to bind Smad3 (reviewed in reference 43) and Smad3 was shown to inhibit ligand-induced AR activity in CV1 cells (29). We therefore investigated the possibility that Smad3 may repress ligand-induced AR activity in prostate cancer cells. Cotransfection of the AR with Smad3 showed that the ligand-treated AR activity was repressed 70% by Smad3 (Fig. 6A). The carboxyl terminus of Smad3 was required for protein-protein interaction with the AR (29). The C-terminal deletion mutant of Smad3

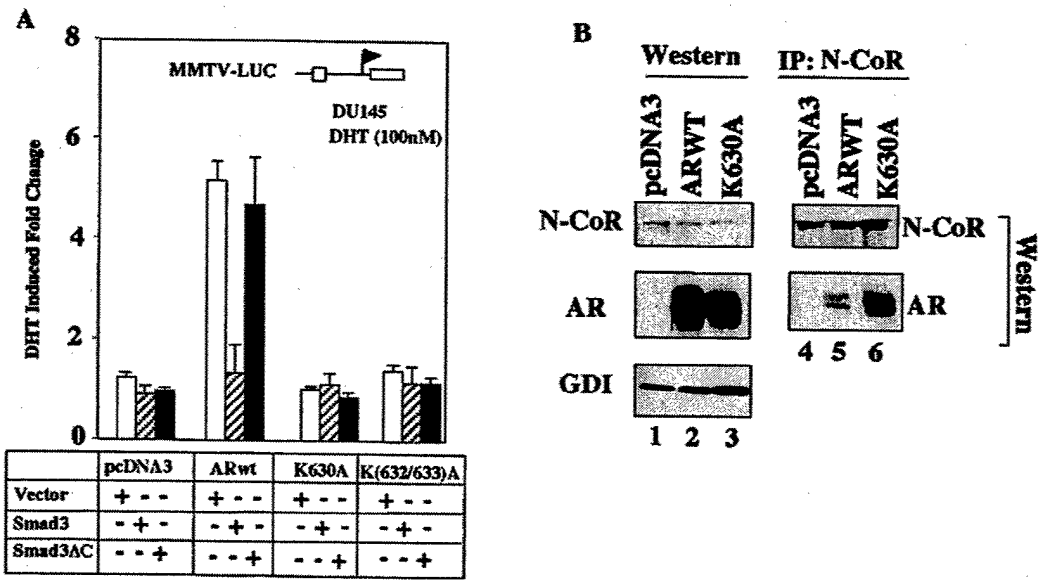


FIG. 6. Enhanced N-CoR binding of the AR acetylation site mutant in cultured cells. (A) Smad3 binds components of the HDAC regulatory complex (HDAC1, N-CoR). Smad3 or a Smad3 mutant with the carboxyl terminus deleted (Smad3ΔC) was transfected with the MMTV-LUC reporter into DU145 cells with either ARwt or the AR acetylation site mutant, and the cells were treated with DHT for 24 h. (B) The binding of N-CoR to the AR was determined by IP-Western blotting. HEK293 cells transfected with expression vectors for FlagN-CoR and either ARwt or the AR acetylation site mutant were assessed by Western blotting in the presence of DHT for expression levels. Similar levels of AR are shown by Western blotting. Equal amounts of cell extracts were subjected to IP with anti-Flag antibody (M2) to precipitate N-CoR and Western blotting performed for Flag (N-CoR) and the AR. AR immunoreactivity is detected in the N-CoR IP. +, present; −, absent; GDI, guanine nucleotide dissociation inhibitor.

(Smad3ΔC) failed to repress the activity of the ligand-treated AR. Smad3 had no effect on the activity of either $AR_{K630A}$ or $AR_{K(632/633)A}$ (Fig. 6A). Smad3 repression is thought to be mediated through N-CoR/HDAC1. As Smad3 repressed ARwt to the level of activity seen for $AR_{K630A}$ or $AR_{K(632/633)A}$, we considered the possibility that the reduced activity of the ligand-treated AR acetylation mutants may be a function of their enhanced binding to corepressors of the Smad3/N-CoR complex. As Smad3 repression is thought to involve N-CoR binding (29, 43), we examined the interaction between N-CoR and the AR. IP-Western blotting was performed with HEK293 cells transfected with equal amounts of Flag-tagged N-CoR and AR. Western blotting showed that similar levels of N-CoR were expressed in transfected cells and that the expression levels of the ARwt and AR mutant were similar (Fig. 6B, lanes 2 and 3). IP with the anti-Flag antibody showed similar amounts of N-CoR by IP (Fig. 6B, lanes 4 to 6). The amount of N-CoR bound to $AR_{K630A}$ was 10-fold higher than that with the ARwt in the presence of DHT (Fig. 6B, right panel, lane 5 versus lane 6).

**The AR acetylation site regulates AR function induced by JNK in prostate cancer cells.** It is known that the AR can induce cell cycle arrest or apoptosis when introduced into AR-negative cells and that overexpression of the AR in transgenic animals is associated with increased cellular apoptosis (11, 80). TRAIL and TNF-α in the presence of cycloheximide induce prostate cancer cellular apoptosis (7, 58, 60, 94). To further investigate the functional properties of the AR acetylation site, stable prostate cancer cell lines (DU145) expressing either ARwt, AR acetylation site mutant, or control vector pcDNA3 were made and examined for responses to cellular apoptosis-inducing agents. Analyses were performed with at least three separate experimental analyses of each line, and the findings were representative of at least three separate stable lines. Initial experiments were conducted with the MTT assay. The cells were treated with either vehicle or DHT (100 nM) for approximately 30 min to engage the AR with ligand (71), and then the cells were treated with apoptosis-inducing agents. Treatment of the ARwt DU145 cells with TRAIL (50 ng/ml) in the presence of cycloheximide (2 μM) inhibited MTT activity 55% compared with vehicle, and either TNF-α or TPA inhibited activity by 40 to 50% (Fig. 7A). In contrast, the AR acetylation mutant stable lines showed no change in activity with any of these treatments (Fig. 7A) ($n = 6$, $P < 0.01$).

Direct measurement of morphological features of apoptosis was also performed, as both cellular proliferation and apoptosis may affect activity in the MTT assay. Cells may become detached upon apoptosis and may become underrepresented in analysis; therefore, cells were fixed in a manner to include both adherent and nonadherent cells and scored for apoptosis by morphological features in separate experiments (48, 78). The cells were pretreated with vehicle or 100 nM DHT for 30 min and then treated with apoptosis-inducing agent for 6 h (Fig. 7B and C). At least 300 cells were scored in three independent high-power fields as described in Materials and Methods. The relative apoptosis rate of the ARwt-expressing stable DU145 cells was increased by either TRAIL or TRAIL with cycloheximide in the presence of ligand compared with the vehicle control. In contrast, the stable DU145 cell line expressing the AR acetylation mutants did not show the same induction of apoptosis in the presence of DHT (Fig. 7B and C).

Transient expression studies were also conducted to examine the role of the AR acetylation site in AR mutant proteins. To assess the role of the AR acetylation site in AR-mediated apoptosis, a previously described experimental approach was used (2). AR activity is induced by the MAPK kinase kinase, MEKK1, which induces phosphorylation of MKK4 (SEK1) and JNK as well as IκB kinase (37, 46). Activation of MEKK1 induces apoptosis of prostate cancer cells in an AR-dependent manner through the JNK pathway (2). To examine the functional significance of the AR acetylation site in MEKK1-induced prostate cellular apoptosis, studies were performed in DU145 cells exactly as previously described (2). Cells were cotransfected with either wild-type or mutant ARs and either the MEKK1 expression vector or control empty vector. A GFP expression vector was used to monitor the transfected cells. The cells were treated for 24 h with either DHT ($10^{-7}$ M) or control vehicle and scored for apoptosis with morphological markers of blebbing or nuclear condensation (Fig. 7D). The expression of either the ARwt or MEKK1 alone did not affect basal apoptosis compared with equal amounts of empty vector cassette (Fig. 7E). In contrast, the coexpression of MEKK1 and the ARwt in the presence of ligand induced apoptosis to approximately 30% as previously described (2). Coexpression of MEKK1 with either $AR_{K630A}$ or $AR_{K(632/633)A}$ resulted in an apoptosis rate similar to that of vector controls (Fig. 7E). These studies demonstrate an important function of the AR acetylation site in regulating MEKK1-dependent apoptosis in cultured human prostate cancer cells.

## DISCUSSION

The recent findings that nonhistone proteins serve as direct targets of histone acetylases have led to further mechanistic analysis of the substrate residues in transcription factor function (81, 86). The AR conveys both *trans*-repression and *trans*-activation function. In the present studies, the AR acetylation site selectively regulated the AR *trans* activation but not the *trans*-repression functions. The sumoylation of the AR was unaffected by the mutation of the AR acetylation site in vitro. Ligand-induced conformational changes, assessed by limited protease digestion, showed a similar pattern induced by the ligand in the ARwt and the AR acetylation mutant. Intriguingly, the AR acetylation mutants showed increased N-CoR binding and reduced p300 binding compared with the wild-type AR. As p300 and N-CoR regulate ligand-dependent gene expression of other NHR, these studies suggest that the AR lysine residues may play an important role in a subset of AR functions by regulating recruitment of hormone-dependent coregulators.

The role of direct transcription factor acetylation in hormone signaling to endogenous androgen-regulated target genes was largely unknown. In the present studies, point mutation of the AR lysine residues, which was previously shown to abrogate acetylation of the full-length AR protein (23), substantially reduced DHT-dependent activation of several androgen-responsive reporters, including the PSA promoter, the MMTV promoter, and a simple synthetic androgen response element. *PSA*, an endogenous androgen-regulated target gene,

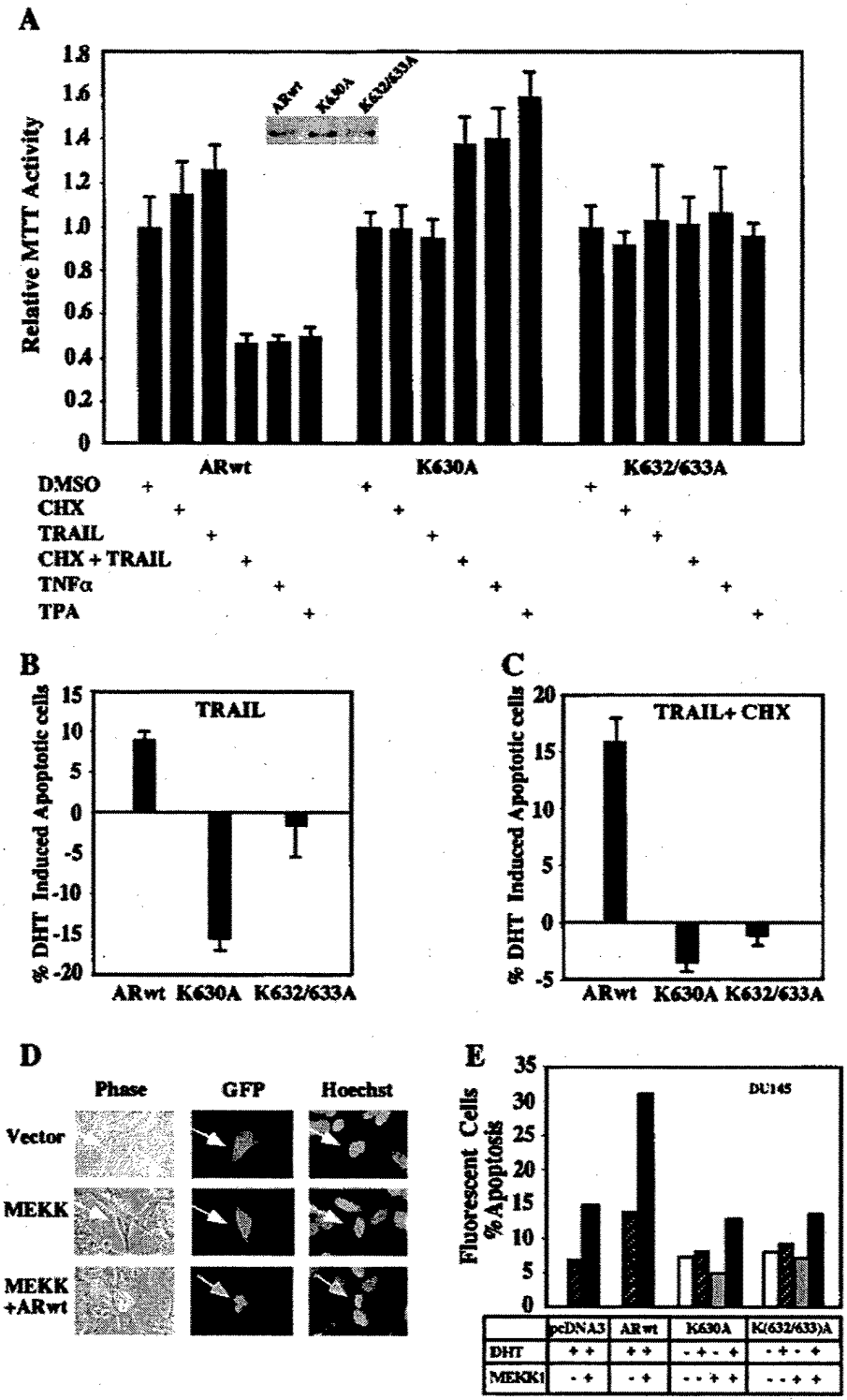


FIG. 7. Induction of apoptosis and the AR acetylation site. (A) Induction of apoptosis by TRAIL is reduced in stable cell lines expressing the AR acetylation site mutants. DU145 cells stably expressing either ARwt, $AR_{K630A}$, or $AR_{K(632/633)A}$ were grown in 96-well plates in 50 μl of DMEM with 10% charcoal-stripped FBS. After 24 h, the cells were treated with vehicle or 100 nM DHT and then treated with either cycloheximide (CHX; 10 μg/ml), TRAIL (10 ng/ml), TNF-α (10 ng/ml), or TPA (100 ng/ml) as indicated. The MTT assay was performed after 6 h. The data are shown as means ± standard deviations for six separate experiments. Vehicle-treated cells are established as 100%. (B and C) DU145 stable lines were treated with vehicle or 100 nM DHT for 30 min, and then apoptosis-inducing agents were added as indicated, and apoptotic cells were scored (see Materials and Methods). Data are shown as the relative change in apoptosis by the inducing agent in the presence of 100 nM DHT. A representative experiment is shown. (D) Induction of apoptosis by Jun kinase kinase (MEKK1) through the AR is abrogated by the mutation of

is a prostate-specific kallikrein, the expression of which is used to monitor patients with prostate cancer (24). The PSA promoter has been well characterized as an androgen-responsive gene. In the present studies, mutation of the AR acetylation site reduced the transcriptional activity of androgen-responsive reporter gene coactivation by several AR regulators (Ubc9, SRC1, TIP60). Ubc9 *trans* activation of the AR occurs independently of its ubiquitin-ligase function. The failure of Ubc9 to induce $AR_{K630A}$ activity is consistent with previous findings that the AR hinge region, which includes the lysine motif, is required for Ubc9 binding and activation (68). The interaction of SRC1 with the AR involves the glutamine-rich region of SRC1 and the AF-2 region of the AR. Coactivation of AR by SRC1 requires AD1 of SRC1, the same region responsible for recruitment of p300/CBP, and does not require the LXXLL motif that interacts with AF-2 (12). Thus, failed SRC1 coactivation of the acetylation site mutants is consistent with defective p300 coactivation. TIP60 binds the AR through a region which includes the acetylation site (15), conveys intrinsic HAT activity (15, 90), and regulates DNA repair and apoptosis (35). As TIP60 augmented the activity of the ligand-treated ARwt but not the AR mutant and MEKK1 augmented AR apoptosis in the presence of ligand, it will be of interest to further evaluate the role of TIP60 in AR-mediated apoptosis.

What common features shared by this subset of coactivators (SRC1, Ubc9, TIP60, and p300) might explain their reduced ligand-dependent coactivation of the AR acetylation site mutants? The bromodomains of several coactivators serve as recognition motifs providing recruitment to acetylated lysine residues (36), and it is feasible that one or more of the bromodomain-containing coactivators (p300, P/CAF) serves as a docking module through the AR-acetylated residues for sequential recruitment of other coactivators. P/CAF, which failed to activate the acetylation site mutants (23), is an important regulator of AR function in prostate cancer cells. P/CAF binds the AR in vivo (73), binds p300, and contains a bromodomain that is required for AR binding. p300 is viewed as a limiting coactivator for many NR, including the AR; therefore, although the reduction in p300 binding to the AR mutants was modest, reduced recruitment of coactivators may contribute to the defective *trans* activation of the AR acetylation mutants.

Transcriptional repression by N-CoR involves a multiprotein complex that includes HDAC complexes, chromatin remodeling proteins, and a transducin β-like protein that interacts with histones (41, 59). In the present studies, the nuclear corepressor N-CoR showed proportionally more binding to the AR lysine point mutants in cultured DU145 cells. The enhanced N-CoR binding to the AR lysine point mutants may provide an important mechanistic link to the reduced activity of the AR acetylation-defective mutants. The finding that coactivator and corepressor surfaces of NR overlap substantially (32, 66) is compatible with a dynamic model in which enzymatic modifications of the NR coordinate the sequential disengagement of corepressors followed by coactivator binding (56). Enhanced corepressor binding of the AR acetylation-defective mutants suggests a role for acetylation in the disengagement of corepressors. Acetylation of upstream binding factor also correlates with reduced transcriptional repression by the pRB-recruited HDAC (64). Together these studies provide evidence for a model in which acetylation disengages corepressors to sequentially recruit coactivators (45).

Several observations in the present studies suggest that the defective transactivation of the AR acetylation mutants may relate to altered coactivator-corepressor binding and does not result from reduced expression levels or ligand binding. Firstly, expression levels of the ARwt and the $AR_{K630A}$ or $AR_{K(632/633)A}$ mutant proteins were similar in cultured cells, suggesting that reduced transactivation was not due to reduced expression. The AR acetylation site does not fall within the ligand-binding pocket deduced from the crystal structure (55), the AR acetylation site mutants demonstrated wild-type ligand-induced protease sensitivity, and in vitro ligand-binding assays showed normal ligand-binding affinity at the physiological concentrations of ligand. Thus, the reduced ligand-induced transactivation of the AR acetylation mutants does not appear to be due to reduced expression or altered ligand binding. The recruitment of HDAC1/N-CoR-containing complexes to the promoters of target genes induces a repressive chromatin state through the functions of HDAC1 (19, 50). It has been proposed that ligand-dependent activation of NHR involves both recruitment of coactivators and disengagement of corepressors (27). The present studies of the AR are consistent with a model in which the selective defects in coactivation of the AR acetylation mutants may be due to increased binding of N-CoR regulated through the acetylation site.

The cellular phenotype regulated by direct acetylation of specific transcription factor events remains to be determined. Several studies have implicated direct transcription factor acetylation in regulating reporter gene expression (81, 87). Thus, acetylation regulates the transcriptional activity of p53 (28, 75), GATA-1 (14), erythroid Kruppel-like factor (95), *Xenopus* NF-Y (49), and the human immunodeficiency virus transactivator protein (Tat) (42) in reporter assays. Only recently has the functional cellular phenotype governed by transcription factor acetylation been examined (63). Acetylation site mutations of p53 were defective in repression of Ras-induced transformation, suggesting an important functional role for p53 acetylation in vivo (63). In previous studies, the AR KXKK motif was both necessary and sufficient for acetylation by either p300 or P/CAF (23). This motif resembles the C-terminal p53 acetylation motif and is highly conserved between NHR, suggesting an important biological function (86). Activation of the MEKK1 pathway enhances AR activity and induces cellular

the AR acetylation site. DU145 cells were transfected with expression vectors for the AR, MEKK1, and pCMV-GFP or equal amounts of empty vector control. The cells were treated for 24 h with DHT and scored for apoptosis 48 h posttransfection as previously described (2). The morphology of the transfected DU145 cells is shown, in phase contrast. White arrows indicate GFP-positive cells, and the yellow arrows indicate GFP-positive cells with chromatin condensation. (E) The graph represents independent experiments in which 200 green fluorescent cells were counted and scored for cytoplasmic blebbing and chromatin condensation. The results are representative of three separate experiments. +, present; −, absent; DMSO, dimethyl sulfoxide.

apoptosis in prostate cancer cells (2). In the present studies, AR acetylation was a critical determinant of the apoptotic response induced by MEKK1 in prostate cancer cells. Furthermore, stable cell lines expressing the AR acetylation mutants showed no enhancement of apoptosis by several agents in the presence of the ligand DHT. AR-dependent apoptosis has been observed in cultured cells and in transgenic mice in which the AR was targeted to the prostate by the probasin promoter (80). Several agents can induce apoptosis through AR-dependent and AR-independent pathways. Ligand-dependent events correlate with AR-mediated nuclear events, as the AR is thought to be required for nuclear DHT function. Therefore, in the present studies, comparison was made between the vehicle and the ligand to examine those apoptotic events most likely regulated by the AR in the stable cell lines. It remains possible, although unlikely, that DHT may govern non-AR-dependent apoptotic events that were selectively altered by the AR acetylation site, for example, through altered expression of a paracrine growth factor. The mechanisms by which the AR acetylation site regulates cellular apoptosis remain to be further explored. The evasion of cellular apoptosis contributes to aberrant growth control during tumorigenesis in multiple settings. The identification of acetylation as a key posttranslational modification required for activation of the AR by multiple distinct coactivators suggests that these residues may form an ideal target for AR inactivation and tumor therapies.

## ACKNOWLEDGMENTS

We thank R. Evans, E. Kalkhoven, J. Kyriakis, B. O'Malley, Y. Nakatani, N. Schreiber-Agus, and E. R. Stanley for plasmids and helpful discussions.

This work was supported by grants from the NIH (R01CA86072 to R.G.P. and R01CA72038-01 to S.A.W.F.) and The Susan Komen Breast Cancer Foundation (to R.G.P.). R.T.H. and E.J. were supported by the Medical Research Council. Y.-G.Y. is supported by grant CA26504 to E. R. Stanley. Work conducted at the Albert Einstein College of Medicine was supported by Cancer Center Core National Institutes of Health grant 5-P30-CA13330-26.

## REFERENCES

1. **Aarnisalo, P., J. J. Palvimo, and O. A. Janne.** 1998. CREB-binding protein in androgen receptor-mediated signaling. Proc. Natl. Acad. Sci. USA **95:** 2122–2127.
2. **Abreu-Martin, M. T., A. Chari, A. A. Palladino, N. A. Craft, and C. L. Sawyers.** 1999. Mitogen-activated protein kinase kinase kinase 1 activates androgen receptor-dependent transcription and apoptosis in prostate cancer. Mol. Cell. Biol. **19:**5143–5154.
3. **Akama, K. T., C. Albanese, R. G. Pestell, and L. J. Van Eldik.** 1998. Amyloid β-peptide stimulates nitric oxide production in astrocytes through an NFκB-dependent mechanism. Proc. Natl. Acad. Sci. USA **95:**5795–5800.
4. **Albanese, C., M. D'Amico, A. T. Reutens, M. Fu, G. Watanabe, R. J. Lee, R. N. Kitsis, B. Henglein, M. Avantaggiati, K. Somasundaram, B. Thimmapaya, and R. G. Pestell.** 1999. Activation of the *cyclin D1* gene by the E1A-associated protein p300 through AP-1 inhibits cellular apoptosis. J. Biol. Chem. **274:**34186–34195.
5. **Alen, P., F. Claessens, G. Verhoeven, W. Rombauts, and B. Peeters.** 1999. The androgen receptor amino-terminal domain plays a key role in p160 coactivator-stimulated gene transcription. Mol. Cell. Biol. **19:**6085–6097.
6. **Alland, L., R. Muhle, H. J. Hou, J. Potes, L. Chin, N. Schreiber-Agus, and R. A. DePinho.** 1997. Role for N-CoR and histone deacetylase in Sin3-mediated transcriptional repression. Nature **387:**49–55.
7. **Avdi, N. J., J. A. Nick, B. B. Whitlock, M. A. Billstrom, P. M. Henson, G. L. Johnson, and G. S. Worthen.** 2001. Tumor necrosis factor-alpha activation of the c-Jun N-terminal kinase pathway in human neutrophils. Integrin involvement in a pathway leading from cytoplasmic tyrosine kinases apoptosis. J. Biol. Chem. **276:**2189–2199.
8. **Barbulescu, K., C. Geserick, I. Schuttke, W. D. Schleuning, and B. Haendler.** 2001. New androgen response elements in the murine pem promoter mediate selective transactivation. Mol. Endocrinol. **15:**1803–1816.
9. **Beato, M., and A. Sanchez-Pacheco.** 1996. Interaction of steroid hormone receptors with the transcription initiation complex. Endocr. Rev. **17:**587–609.
10. **Berger, J., P. Bailey, C. Biswas, C. A. Cullinan, T. W. Doebber, N. S. Hayes, R. Saperstein, R. G. Smith, and M. D. Leibowitz.** 1996. Thiazolidinediones produce a conformational change in peroxisomal proliferator-activated receptor-gamma: binding and activation correlate with antidiabetic actions in db/db mice. Endocrinology **137:**4189–4195.
11. **Berthon, P., A. S. Waller, J. M. Villette, L. Loridon, O. Cussenot, and N. J. Maitland.** 1997. Androgens are not a direct requirement for the proliferation of human prostatic epithelium in vitro. Int. J. Cancer **73:**910–916.
12. **Bevan, C. L., S. Hoare, F. Claessens, D. M. Heery, and M. G. Parker.** 1999. The AF1 and AF2 domains of the androgen receptor interact with distinct regions of SRC1. Mol. Cell. Biol. **19:**8383–8392.
13. **Bouzahzah, B., M. Fu, A. Iavarone, V. M. Factor, S. S. Thorgeirsson, and R. G. Pestell.** 2000. Transforming growth factor β1 recruits histone deacetylase 1 to a p130 repressor complex in transgenic mice in vivo. Cancer Res. **60:**4531–4537.
14. **Boyes, J., P. Byfield, Y. Nakatani, and V. Ogryzko.** 1998. Regulation of activity of the transcription factor GATA-1 by acetylation. Nature **396:**594–598.
15. **Brady, M. E., D. M. Ozanne, L. Gaughan, I. Waite, S. Cook, D. E. Neal, and C. N. Robson.** 1999. Tip60 is a nuclear hormone receptor coactivator. J. Biol. Chem. **274:**17599–17604.
16. **Bromberg, J. F., M. H. Wrzeszczynska, G. Devgan, Y. Zhao, R. G. Pestell, C. Albanese, and J. E. Darnell.** 1999. Stat3 as an oncogene. Cell **98:**295–303.
17. **Burke, L. J., and A. Baniahmad.** 2000. Co-repressors 2000. FASEB J. **14:** 1876–1888.
18. **Chen, H., R. J. Lin, W. Xie, D. Wilpitz, and R. M. Evans.** 1999. Regulation of hormone-induced histone hyperacetylation and gene activation via acetylation of an acetylase. Cell **98:**675–686.
19. **David, G., L. Alland, S. H. Hong, C. W. Wong, R. A. DePinho, and A. Dejean.** 1998. Histone deacetylase associated with mSin3A mediates repression by the acute promyelocytic leukemia-associated PLZF protein. Oncogene **16:** 2549–2556.
20. **Duprez, E., A. J. Saurin, J. M. Desterro, V. Lallemand-Breitenbach, K. Howe, M. N. Boddy, E. Solomon, H. de The, R. T. Hay, and P. S. Freemont.** 1999. SUMO-1 modification of the acute promyelocytic leukaemia protein PML: implications for nuclear localisation. J. Cell Sci. **112:**381–393.
21. **Fan, S., J.-A. Wang., R. Yuan, Y. Ma, Q. Meng, M. R. Erdos, R. G. Pestell, F. Yuan, K. J. Auborn, I. D. Goldberg, and E. M. Rosen.** 1999. BRCA1 inhibition of estrogen receptor signaling in transfected cells. Science **284:** 1354–1356.
22. **Fronsdal, K., N. Engedal, T. Slagsvold, and F. Saatcioglu.** 1998. CREB binding protein is a coactivator for the androgen receptor and mediates cross-talk with AP-1. J. Biol. Chem. **273:**31853–31859.
23. **Fu, M., C. Wang, A. T. Reutens, R. Angelletti, L. Siconolfi-Baez, V. Ogryzko, M. L. Avantaggiati, and R. G. Pestell.** 2000. p300 and P/CAF acetylate the androgen receptor at sites governing hormone-dependent transactivation. J. Biol. Chem. **275:**20853–20860.
24. **Garnick, M., and W. Fair.** 1996. Prostate cancer: emerging concepts. Part II. Ann. Intern. Med. **125:**205–212.
25. **Gibson, S., C. Widmann, and G. L. Johnson.** 1999. Differential involvement of MEK kinase 1 (MEKK1) in the induction of apoptosis in response to microtubule-targeted drugs versus DNA damaging agents. J. Biol. Chem. **274:**10916–10922.
26. **Giordano, A., and M. L. Avantaggiati.** 1999. p300 and CBP: partners for life and death. J. Cell. Physiol. **181:**218–230.
27. **Glass, C. K., and M. G. Rosenfeld.** 2000. The coregulator exchange in transcriptional functions of nuclear receptors. Genes Dev. **14:**121–141.
28. **Gu, W., and R. G. Roeder.** 1997. Activation of p53 sequence-specific DNA binding by acetylation of the p53 C-terminal domain. Cell **90:**595–606.
29. **Hayes, S., M. Zarnegar, M. Sharma, F. Yang, D. M. Peehl, P. ten Dijke, and Z. Sun.** 2001. SMAD3 represses androgen receptor-mediated transcription. Cancer Res. **61:**2112–2118.
30. **Heinzel, T., R. M. Lavinsky, T. M. Mullen, M. Soderstrom, C. D. Laherty, J. Torchia, W. M. Yang, G. Brard, S. D. Ngo, J. R. Davie, E. Seto, R. N. Eisenman, D. W. Rose, C. K. Glass, and M. G. Rosenfeld.** 1997. A complex containing N-CoR, mSin3 and histone deacetylase mediates transcriptional repression. Nature **387:**43–48.
31. **Horwitz, K. B., T. A. Jackson, D. L. Bain, J. K. Richer, G. S. Takimoto, and L. Tung.** 1996. Nuclear receptor coactivators and corepressors. Mol. Endocrinol. **10:**1167–1177.
32. **Hu, X., Y. Li, and M. Lazar.** 2001. Determinants of CoRNR-dependent repression complex assembly on nuclear hormone receptors. Mol. Cell. Biol. **21:**1747–1758.
33. **Hung, H. L., J. Lau, A. Y. Kim, M. J. Weiss, and G. A. Blobel.** 1999. CREB-binding protein acetylates hematopoietic transcription factor GATA-1 at functionally important sites. Mol. Cell. Biol. **19:**3496–3505.
34. **Ikonen, T., J. J. Palvimo, and O. A. Janne.** 1997. Interaction between the amino- and carboxyl-terminal regions of the rat androgen receptor modulates transcriptional activity and is influenced by nuclear receptor coactivators. J. Biol. Chem. **272:**29821–29828.

35. **Ikura, T., V. V. Ogryzko, M. Grigoriev, R. Groisman, J. Wang, M. Horikoshi, R. Scully, J. Qin, and Y. Nakatani.** 2000. Involvement of the TIP60 histone acetylase complex in DNA repair and apoptosis. Cell **102**:463–473.
36. **Jackson, R. H., A. G. Ladurner, D. S. King, and R. Tjian.** 2000. Structure and function of a human TAFII250 double bromodomain module. Science **288**: 1422–1425.
37. **Joyce, D., C. Albanese, J. Steer, M. Fu, B. Bouzahzah, and R. G. Pestell.** 2001. NF-kB and cell-cycle regulation: the cyclin connection. Cytokine Growth Factor Rev. **12**:73–90.
38. **Kalkhoven, E., J. E. Valentine, D. M. Heery, and M. G. Parker.** 1998. Isoforms of steroid receptor co-activator 1 differ in their ability to potentiate transcription by the oestrogen receptor. EMBO J. **17**:232–243.
39. **Kallio, P. J., H. Poukka, A. Moilanen, O. A. Janne, and J. J. Palvimo.** 1995. Androgen receptor-mediated transcriptional regulation in the absence of direct interaction with a specific DNA element. Mol. Endocrinol. **9**:1017–1028.
40. **Kang, H.-Y., H.-K. Lin, Y.-C. Hu, K.-E. Huang, and C. Chang.** 2001. From transforming growth factor-b signaling to androgen action: identification of Smad3 as an androgen receptor coregulator in prostate cancer cells. Proc. Natl. Acad. Sci. USA **98**:3018–3023.
41. **Kao, H. Y., M. Downes, P. Ordentlich, and R. M. Evans.** 2000. Isolation of a novel histone deacetylase reveals that class I and class II deacetylases promote SMRT-mediated repression. Genes Dev. **14**:55–66.
42. **Kiernan, R., C. Vanhulle, L. Schiltz, E. Adam, H. Xiao, F. Maudoux, C. Calomne, A. Burny, Y. Nakatani, K.-T. Jeang, M. Benkirane, and C. Van Lint.** 1999. HIV Tat transcriptional activity is regulated by acetylation. EMBO J. **18**:6106–6118.
43. **Knoepfler, P. S., and R. N. Eisenman.** 1999. Sin meets NuRD and other tails of repression. Cell **99**:447–450.
44. **Knudson, K. E., W. K. Cavenee, and K. C. Arden.** 1999. D-type cyclins complex with the androgen receptor and inhibit its transcriptional transactivation ability. Cancer Res. **59**:2297–2301.
45. **Kouzarides, T.** 2000. Acetylation: a regulatory modification to rival phosphorylation. EMBO J. **19**:1176–1179.
46. **Kyriakis, J. M., and J. Avruch.** 1996. Sounding the alarm: protein kinase cascades activated by stress and inflammation. J. Biol. Chem. **271**:24313–24316.
47. **Lee, R. J., C. Albanese, M. Fu, M. D'Amico, B. Lin, G. Watanabe, G. K. Haines III, P. M. Siegel, M.-C. Hung, Y. Yarden, J. M. Horowitz, W. J. Muller, and R. G. Pestell.** 2000. Cyclin D1 is required for transformation by activated Neu and is induced through an E2F-dependent signaling pathway. Mol. Cell. Biol. **20**:672–683.
48. **Levkau, B., H. Koyama, E. W. Raines, B. E. Clurman, B. Herren, K. Orth, J. M. Roberts, and R. Ross.** 1998. Cleavage of $p21^{Cip1/Waf1}$ and $p27^{Kip1}$ mediates apoptosis in endothelial cells through activation of cdk2: role of a caspase cascade. Mol. Cell **1**:553–563.
49. **Li, Q., M. Herrler, N. Landsberger, N. Kaludov, V. V. Ogryzko, Y. Nakatani, and A. P. Wolffe.** 1998. Xenopus NF-Y pre-sets chromatin to potentiate p300 and acetylation-responsive transcription from the Xenopus hsp70 promoter in vivo. EMBO J. **17**:6300–6315.
50. **Lin, R. J., L. Nagy, S. Inoue, W. Shao, W. H. Miller, Jr., and R. M. Evans.** 1998. Role of the histone deacetylase complex in acute promyelocytic leukaemia. Nature **391**:811–814.
51. **Liu, L., D. M. Scolnick, R. C. Trievel, H. B. Zhang, R. Marmorstein, T. D. Halazonetis, and S. L. Berger.** 1999. p53 sites acetylated in vitro by PCAF and p300 are acetylated in vivo in response to DNA damage. Mol. Cell. Biol. **19**:1202–1209.
52. **Lu, S., G. Jenster, and D. E. Epner.** 2000. Androgen induction of cyclin-dependent kinase inhibitor p21 gene: role of androgen receptor and transcription factor Sp1 complex. Mol. Endocrinol. **14**:753–760.
53. **Luo, R. X., A. A. Postigo, and D. C. Dean.** 1998. Rb interacts with histone deacetylase to repress transcription. Cell **92**:463–473.
54. **Martinez-Balbas, M. A., A. J. Bannister, K. Martin, P. Haus-Seuffert, M. Meisterernst, and T. Kouzarides.** 1998. The acetyltransferase activity of CBP stimulates transcription. EMBO J. **17**:2886–2893.
55. **Matias, P. M., P. Donner, R. Coelho, M. Thomaz, C. Peixoto, S. Macedo, N. Otto, S. Joschko, P. Scholz, A. Wegg, S. Basler, M. Schafers, U. Egner, and M. A. Carrondo.** 2000. Structural evidence for ligand specificity in the binding domain of the human androgen receptor. J. Biol. Chem. **275**:26164–26171.
56. **McKenna, J., R. B. Lanz, and B. W. O'Malley.** 1999. Nuclear receptor co-regulators: cellular and molecular biology. Endocr. Rev. **20**:321–344.
57. **Muller, S., M. Berger, F. Lehembre, J. S. Seeler, Y. Haupt, and A. Dejean.** 2000. c-Jun and p53 activity is modulated by SUMO-1 modification. J. Biol. Chem. **275**:13321–13329.
58. **Munshi, A., G. Pappas, T. Honda, T. J. McDonnell, A. Younes, Y. Li, and R. E. Meyn.** 2001. TRAIL (APO-2L) induces apoptosis in human prostate cancer cells that is inhibitable by Bcl-2. Oncogene **20**:3757–3765.
59. **Nagy, L., H. Y. Kao, D. Chakravarti, R. J. Lin, C. A. Hassig, D. E. Ayer, S. L. Schreiber, and R. M. Evans.** 1997. Nuclear receptor repression mediated by a complex containing SMRT, mSin3A and histone deacetylase. Cell **89**:373–380.
60. **Nimmanapalli, R., C. L. Perkins, M. Orlando, E. O'Bryan, D. Nguyen, and K. N. Bhalla.** 2001. Pretreatment with paclitaxel enhances apo-2 ligand/tumor necrosis factor-related apoptosis-inducing ligand-induced apoptosis of prostate cancer cells by inducing death receptors 4 and 5 protein levels. Cancer Res. **61**:759–763.
61. **Ogryzko, V. V., R. L. Schiltz, V. Russanova, B. H. Howard, and Y. Nakatani.** 1996. The transcriptional coactivators p300 and CBP are histone acetyltransferases. Cell **87**:953–959.
62. **Palvimo, J. J., P. Reinikainen, T. Ikonen, P. J. Kallio, A. Moilanen, and O. A. Jänne.** 1996. Mutual transcriptional interference between RelA and androgen receptor. J. Biol. Chem. **271**:24151–24156.
63. **Pearson, M., R. Carbone, C. Sebastiani, M. Cioce, M. Fagioli, S. Saito, Y. Higashimoto, E. Appella, S. Minucci, P. P. Pandolfi, and P. G. Pelicci.** 2000. PML regulates p53 acetylation and premature senescence induced by oncogenic Ras. Nature **406**:207–210.
64. **Pelletier, G., V. Y. Stefanovsky, M. Faubladier, I. Hirschler-Laszkiewicz, J. Savard, L. I. Rothblum, J. Cote, and T. Moss.** 2000. Competitive recruitment of CBP and Rb-HDAC regulates UBF acetylation and ribosomal transcription. Mol. Cell **6**:1059–1066.
65. **Pena, P., A. T. Reutens, M. D'Amico, C. Albanese, G. Watanabe, A. Donner, I.-W. Shu, T. Williams, and R. G. Pestell.** 1999. Activator protein-2 mediates transcriptional activation of the CYP11A1 gene by interaction with Sp1 rather than binding to DNA. Mol. Endocrinol. **13**:1402–1416.
66. **Perissi, V., L. M. Staszewski, E. M. McInerney, R. Kurokawa, A. Krones, D. W. Rose, M. H. Lambert, M. V. Milburn, C. K. Glass, and M. G. Rosenfeld.** 1999. Molecular determinants of nuclear receptor-corepressor interaction. Genes Dev. **13**:3198–3208.
67. **Pombo, C. M., J. H. Kehrl, I. Sanchez, P. Katz, J. Avruch, L. I. Zon, J. R. Woodgett, T. Force, and J. M. Kyriakis.** 1995. Activation of the SAPK pathway by the human STE20 homologue germinal centre kinase. Nature **377**:750–754.
68. **Poukka, H., P. Aarnisalo, U. Karvonen, J. J. Palvimo, and O. A. Janne.** 1999. Ubc9 interacts with the androgen receptor and activates receptor-dependent transcription. J. Biol. Chem. **274**:19441–19446.
69. **Poukka, H., P. Aarnisalo, H. Santti, O. A. Janne, and J. J. Palvimo.** 2000. Coregulator small nuclear RING finger protein (SNURF) enhances Sp1- and steroid receptor-mediated transcription by different mechanisms. J. Biol. Chem. **275**:571–579.
70. **Poukka, H., U. Karvonen, O. A. Janne, and J. J. Palvimo.** 2000. Covalent modification of the androgen receptor by small ubiquitin-like modifier 1 (SUMO-1). Proc. Natl. Acad. Sci. USA **97**:14145–14150.
71. **Poukka, H., U. Karvonen, N. Yoshikawa, H. Tanaka, J. J. Palvimo, and O. A. Jänne.** 2000. The RING finger protein SNURF modulates nuclear trafficking of the androgen receptor. J. Cell Sci. **113**:2991–3001.
72. **Prives, C., and J. L. Manley.** 2001. Why is p53 acetylated? Cell **107**:815–818.
73. **Reutens, A. T., M. Fu, G. Watanabe, C. Albanese, M. J. McPhaul, S. P. Balk, O. A. Janne, J. J. Palvimo, and R. G. Pestell.** 2001. Cyclin D1 governs androgen receptor function by ligand-dependent regulation of P/CAF. Mol. Endocrinol. **15**:797–811.
74. **Roche, P. J., S. A. Hoare, and M. G. Parker.** 1992. A consensus DNA-binding site for the androgen receptor. Mol. Endocrinol. **6**:2229–2235.
75. **Sakaguchi, K., J. E. Herrera, S. Saito, T. Miki, M. Bustin, A. Vassilev, C. W. Anderson, and E. Appella.** 1998. DNA damage activates p53 through a phosphorylation-acetylation cascade. Genes Dev. **12**:2831–2841.
76. **Sato, N., M. D. Sadar, N. Bruchovsky, F. Saatcioglu, P. S. Rennie, S. Sato, P. H. Lange, and M. E. Gleave.** 1997. Androgenic induction of prostate-specific antigen gene is repressed by protein-protein interaction between the androgen receptor and AP-1/c-Jun in the human prostate cancer cell line LNCaP. J. Biol. Chem. **272**:17485–17494.
77. **Shemshedini, L., R. Knauthe, P. Sassone-Corsi, A. Pornon, and H. Gronemeyer.** 1992. Cell-specific inhibitory and stimulatory effects of Fos and Jun on transcription activation by nuclear receptors. EMBO J. **11**:167–175.
78. **Soengas, M. S., R. M. Alarcon, H. Yoshida, A. J. Giaccia, R. Hakem, T. W. Mak, and S. W. Lowe.** 1999. Apaf-1 and caspase-9 in p53-dependent apoptosis and tumor inhibition. Science **284**:156–159.
79. **Sperry, T. S., and P. Thomas.** 1999. Characterization of two nuclear androgen receptors in Atlantic croaker: comparison of their biochemical properties and binding specificities. Endocrinology **140**:1602–1611.
80. **Stanbrough, M., I. Leav, P. W. L. Kwan, G. J. Bubley, and S. P. Balk.** 2001. Prostatic intraepithelial neoplasia in mice expressing an androgen receptor transgene in prostate epithelium. Proc. Natl. Acad. Sci. USA **98**:10823–10828.
81. **Sterner, D. E., and S. L. Berger.** 2000. Acetylation of histones and transcription-related factors. Microbiol. Mol. Biol. Rev. **64**:435–459.
82. **Tatham, M. H., E. Jaffray, O. A. Vaughan, J. M. Desterro, C. H. Botting, J. H. Naismith, and R. T. Hay.** 2001. Polymeric chains of SUMO-2 and SUMO-3 are conjugated to protein substrates by SAE1/SAE2 and Ubc9. J. Biol. Chem. **276**:35368–35374.
83. **Torchia, J., D. W. Rose, J. Inostroza, Y. Kamei, S. Westin, C. K. Glass, and M. G. Rosenfeld.** 1997. The transcriptional co-activator p/CIP binds CBP and mediates nuclear-receptor function. Nature **387**:677–684.
84. **Tsai, M. J., and B. W. O'Malley.** 1994. Molecular mechanisms of action of

steroid/thyroid receptor superfamily members. Annu. Rev. Biochem. **63:** 451–486.

85. **Voegel, J. J., M. J. S. Heine, M. Tini, V. Vivat, P. Chambon, and H. Gronemeyer.** 1998. The co-activator TIF2 contains three nuclear receptor binding motifs and mediates transactivation through CBP binding-dependent and -independent pathways. EMBO J. **17:**507–519.
86. **Wang, C., M. Fu, R. Angeletti, L. Siconolfi-Baez, A. Reutens, M. P. Lisanti, B. Katzenellenbogen, S. Kato, T. Hopp, S. A. W. Fuqua, P. J. Kushner, and R. G. Pestell.** 2001. Direct acetylation of the estrogen receptor α hinge region by p300 regulates transactivation and hormone sensitivity. J. Biol. Chem. **276:**18375–18383.
87. **Wang, C., M. Fu, S. Mani, S. Wadler, A. M. Senderowicz, and R. G. Pestell.** 2001. Histone acetylation and the cell-cycle in cancer. Front. Biosci. **6:**D610–D629.
88. **Watanabe, G., C. Albanese, R. J. Lee, A. Reutens, G. Vairo, B. Henglein, and R. G. Pestell.** 1998. Inhibition of cyclin D1 kinase activity is associated with E2F-mediated inhibition of cyclin D1 promoter activity through E2F and Sp1. Mol. Cell. Biol. **18:**3212–3222.
89. **Widmann, C., P. Gerwins, N. L. Johnson, M. B. Jarpe, and G. L. Johnson.** 1998. MEK kinase 1, a substrate for DEVD-directed caspases, is involved in genotoxin-induced apoptosis. Mol. Cell. Biol. **18:**2416–2429.
90. **Yamamoto, T., and M. Horikoshi.** 1997. Novel substrate specificity of the histone acetyltransferase activity of HIV-1-Tat interactive protein Tip60. J. Biol. Chem. **272:**30595–30598.
91. **Yao, T. P., G. Ku, N. Zhou, R. Scully, and D. M. Livingston.** 1996. The nuclear hormone receptor coactivator SRC-1 is a specific target of p300. Proc. Natl. Acad. Sci. USA **93:**10626–10631.
92. **Yeh, S., and C. Chang.** 1996. Cloning and characterization of a specific coactivator, ARA70, for the androgen receptor in human prostate cells. Proc. Natl. Acad. Sci. USA **93:**5517–5521.
93. **Yeh, S., Y.-C. Hu, M. Rahman, H.-K. Lin, C.-L. Hsu, H.-J. Ting, H.-Y. Kang, and C. Chang.** 2000. Increase of androgen-induced cell death and androgen receptor transactivation by BRCA1 in prostate cancer cells. Proc. Natl. Acad. Sci. USA **97:**11256–11261.
94. **Yu, R., S. Mandlekar, S. Ruben, J. Ni, and A. N. Kong.** 2000. Tumor necrosis factor-related apoptosis-inducing ligand-mediated apoptosis in androgen-independent prostate cancer cells. Cancer Res. **60:**2384–2389.
95. **Zhang, W., and J. J. Bieker.** 1998. Acetylation and modulation of erythroid Kruppel-like factor (EKLF) activity by interaction with histone acetyltransferases. Proc. Natl. Acad. Sci. USA **95:**9855–9860.